Optimization of Vertical Greenery Systems for Noise Mitigation in Urban Environments

Sofia Markson

This page is intentionally left blank

Optimization of Vertical Greenery Systems for Noise Mitigation in Urban Environments

Thesis report

by

Sofia Markson

to obtain the degree of Master of Science
at the Delft University of Technology
to be defended publicly on July 3rd, 2024 at 09:00

Author: S. (Sofia) Markson
                           Master track Building Technology
                           Student number 5691362

                           Dr. Ir. M. (Martijn) C. Lugten
Supervisors: Environmental Technology and Design
                           Faculty of Architecture and the Built Environment

                           Dr. Ir. M. (Marc) Ottelé
                           Material, Mechanics, Management & Design
                           Faculty of Civil Engineering & Geosciences

                           Ir. A. (Alvaro) Balderrama
                           Architectural Technology
                           Faculty of Architecture and the Built Environment

                           Delft University of Technology
Place: Faculty of Architecture and the Built Environment
                           Julianalaan 134
                           2628 BL Delft

Project Duration: November 2023 – July 2024

Faculty of Architecture and the Built Environment · Delft University of Technology

Acknowledgements

Abstract

Environmental noise is a pervasive and significant issue in urban areas, negatively affecting the health and well-being of both residents and wildlife. Despite efforts under the European Noise Directive to reduce noise from sources such as road, rail, air traffic, and industrial activities, around 20% of the EU population still lives in areas where noise levels exceed health-based guidelines. The dense infrastructure and reflective surfaces in urban environments amplify noise levels, highlighting the urgent need for effective noise reduction strategies.

Vertical Greenery Systems (VGSs) can effectively reduce urban noise pollution when implemented thoughtfully. State-of-the-art VGS designs commonly incorporate multi-layer structures comprising a bearing wall, substrate layer, and foliage layer. This research aimed to optimize such VGSs in the early design stages to enhance their noise mitigation capabilities. Among the available generic models, the Transfer Matrix Method (TMM) offers the most comprehensive approach for modelling the acoustic characteristics of these structures. TMM allows for the modelling of acoustic properties on both sides of a one-dimensional fluid-like layer using effective, frequency-dependent parameters encapsulated within a 2×2 matrix. The total transfer matrix of the VGS results from the product of its individual layer transfer matrices.

It was established that to accurately evaluate the acoustic effectiveness of multi-layered VGSs, it is imperative to concentrate on the performance resulting from the superposition of layers under specific boundary conditions, rather than analysing individual layer parameters in isolation. This approach recognizes that there is no definitive answer regarding which specific components demonstrate superior performance. Instead, the intricate nature of superposition underscores the necessity for systematic experimentation with various component combinations and the manipulation of extrinsic variables, such as layer thicknesses, to optimize VGS performance.

In this research, the TMM was utilized to develop a tool for evaluating the acoustic performance of VGS designs, suitable for deployment during the early phase of the design process. The tool includes a comprehensive material library that allows stakeholders to explore various design options, making the approach more adaptable. It enables the evaluation of VGS design feasibility by examining the normal incidence weighted sound absorption coefficient and its corresponding absorption class. Additionally, the tool serves as a framework for conducting further analysis on the long-term environmental impact and economic viability of VGSs.

Comprehensive access and operational instructions for the tool can be found in the repository:

GitHub Repository
https://github.com/smrksn/Optimization-of-the-Vertical-Greenery-Systems

Contents

III Developmental Study: Optimization Tool 99

10 Performance Metric 100

11 Backend Development of the Tool 102

12 User Guide 104

13 Discussion 107

IV Closure 112

14 Conclusion 113

15 Reflection 117

References 120

A Data Processing Procedure 129

Nomenclature

List of Abbreviations

ASTM	American Society for Testing and Materials
CBA	Cost Benefit Analysis
DALY	Disability-Adjusted Life Years
END	European Noise Directive
GF	Green Facade
GUI	Graphical User Interface
ISO	International Organization for Standardization
LCA	Life Cycle Assessment
LWS	Living Wall System
NPV	Net Present Value
RL	Return Loss
TMM	Transfer Matrix Method
UHI	Urban Heat Island
VGS	Vertical Greenery System
WHO	World Health Organization

List of Main Symbols

α	Absorption
λ	Wavelength

$\mathbf{T}$	Transfer matrix
$\mathcal{R}$	Reflection power
ω	Angular frequency
ϕ	Phase
ρ	Density
A	Amplitude
c	Speed of sound
d	Thickness
f	Frequency
j	Imaginary unit
k	Wavenumber
p	Pressure
R	Resistance
r	Pressure reflection coefficient
RL	Return loss
t	Time
u	Particle velocity
X	Reactance
z_c	Characteristic impedance
z_s	Surface impedance

List of Figures

List of Tables

Introduction

1.1. Problem Statement

Environmental noise is a pervasive pollutant that negatively impacts the health and well-being of European citizens and wildlife (Peris & et al., 2020). According to the European Noise Directive (END), environmental noise is defined as any unwanted or harmful outdoor sound produced by human activities, including noise from road traffic, rail traffic, air traffic, and industrial activities (European Parliament and Council, 2002). While various human activities contribute to environmental noise, transport-related sources, particularly road traffic, are the most significant contributors (Peris & et al., 2020).

Environmental noise remains a significant issue in Europe, with at least 20% of the European Union population living in areas where noise levels are harmful to health (Peris & et al., 2020). Most of the affected population resides in urban areas. With the rapid expansion of urban areas (Alberti et al., 2019) and the increasing demand for transportation (European Environmental Agency, 2022), noise exposure is expected to increase, leading to more adverse health effects. The World Health Organization (WHO) emphasizes that prolonged exposure to environmental noise is associated with a higher risk of both short- and long-term health issues, such as sleep disturbances, cardiovascular effects, poorer work and school performance, and hearing impairment (WHO, 2010).

Addressing and finding solutions for this environmental issue requires a thorough understanding of the current situation to effectively reduce noise pollution where necessary (Morillas, Gozalo, González, Moraga, & Vílchez-Gómez, 2018). To address the need for understanding, the European Commission and the Joint Research Centre, in collaboration with numerous noise experts across Europe, have been developing a standardized assessment method for noise mapping called CNOSSOS-EU (Kephalopoulos, Paviotti, & Anfosso-Lédée, 2012; Peris & et al., 2020). Environmental noise maps serve the purpose of quantifying and visually representing noise pollution levels across different geographical areas (Peris & et al., 2020).

For example, Figure 1.1 depicts the traffic noise map of Amsterdam for the year 2021. The noise data represented in the figure is based on the parameters L_{den} and L_{night}, as stipulated in the END (European Parliament and Council, 2002). Noise levels are considered high when $L_{den} \leq 55$ dB and $L_{night} \leq 50$ dB (Peris & et al., 2020). The levels of environmental noise vary depending on factors such as the location of the noise source, the receiver position, and any intervening obstacles like terrain, buildings, or barriers. Hence, noise mapping serves as a valuable tool for stakeholders, aiding them in identifying regions where noise levels surpass acceptable thresholds. This empowers them to integrate these findings into their decision-making processes aimed at improving the environmental quality and overall living conditions.

In urban environments, stakeholders have predominantly focused on addressing noise at its source, which accounts for over 50% of noise management efforts (Peris & et al., 2020). Strategies aimed at managing and reducing noise through urban planning and land use constitute a smaller proportion of the approaches employed to tackle noise pollution. However, urban design has a major influence on the perceived sound levels. In urban environments, buildings, typically constructed with acoustically rigid materials, are situated on both sides of the street. Incident noise is reflected from the facades of buildings, leading to a multiplicity of re-reflected noise paths, which increases overall sound levels (Lyon, 1974). Therefore, in addition to concentrating on reducing road traffic noise by altering sources, such as

(a) L_den   **(b)** L_night
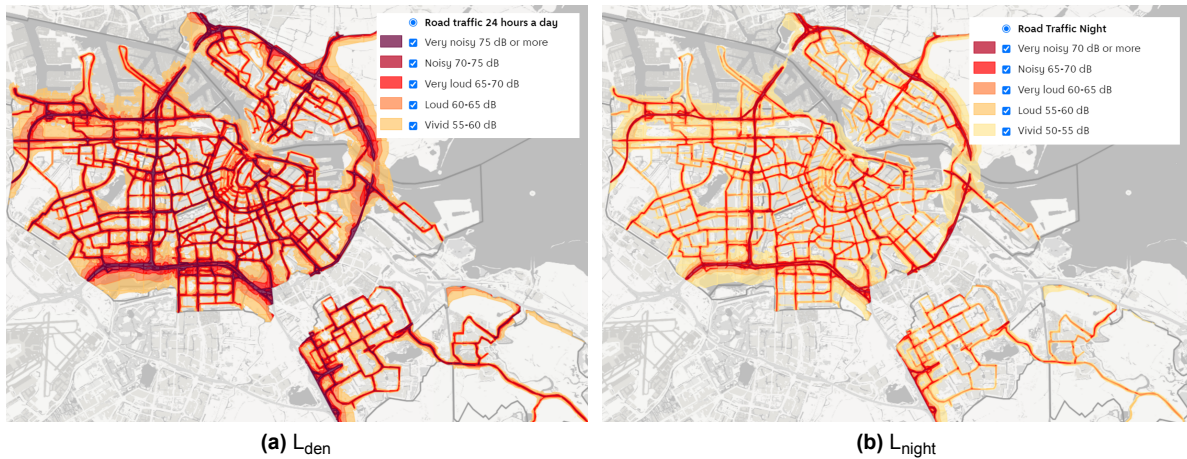
Figure 1.1: Noise map for Amsterdam, the Netherlands
Note. Adapted from "Geluidskaart 2021," by Gemeente Amsterdam (2021)
(`https://maps.amsterdam.nl/geluid/`). Copyright 2024 by Municipality of Amsterdam.

introducing quieter vehicles or implementing traffic measures like speed reduction, there is an increasing acknowledgement that interventions aimed at the infrastructure itself could gain more traction.

Nature-based solutions, which provide multiple ecosystem services, should be prioritized over conventional infrastructure modifications that use artificial elements for scattering or absorption. For example, introducing greenery is an effective way to reduce overall noise levels in reverberant spaces, such as streets (Lacasta, Peñaranda, & Cantalapiedra, 2018). Recognizing the potential of vegetation to mitigate urban noise, the European project HOSANNA (2009-2013) was launched to explore the impacts of using greenery and recycled materials to reduce noise levels (Alves, Scheuren, & Altreuther, 2016). It has been demonstrated that among potential green interventions, the introduction of Vertical Greenery Systems (VGSs) can lead to improvements not only in noise reduction but also in urban appearance and the reduction of air pollution (Nilsson et al., 2013).

Following the conclusion of the HOSANNA project, further research has been conducted to explore VGSs benefits. Cardinali, Balderrama, Arztmann, and Pottgiesser (2023) analyzed 30 review publications published between 2014 and 2022, with a significant emphasis on discussing the potential mechanisms of VGSs in providing ecosystem services. The analysis provided positive associations that VGSs can mitigate Urban Heat Island (UHI) effects by reducing the surface temperature of bare walls, as well as decrease air pollution by lowering levels of $PM_{2.5}$, PM_{10}, NO_2, and SO_2. Additionally, VGSs, especially Living Wall Systems (LWSs), have demonstrated significant potential in reducing noise pollution, likely attributable to their porous structures, akin to sound-absorbing facade materials. While the potential of VGSs in providing ecosystem services, particularly noise reduction in urban environments, is acknowledged, the current body of evidence remains limited. A lack of quantitative data contributes to uncertainties regarding the true benefits that VGSs can offer.

Cardinali et al. (2023) hypothesized that properly designed LWSs could potentially outperform traditional acoustic facade materials, as they offer greater depth, layering, and variations in material densities. However, variability in noise attenuation efficiency among different VGS types complicates efforts to determine the most effective designs. To address this, a concise quantitative assessment method is essential. However, quantitatively evaluating VGSs, particularly LWSs, poses challenges due to their complex multilayer structures, typically composed of a bearing wall, substrate layer, and foliage layer. Understanding how the foliage layer interacts with the substrate layer against rigid materials like concrete or bricks is crucial. While in-situ measurements offer direct insights, they are impractical during the initial design stages. Hence, there is a pressing need for alternative tools to aid decision-making in these early design phases.

However, there remains a notable absence of accessible generic engineering models to predict the acoustical impact of VGS, considering the combined effects of its various layers. Addressing this gap,

Attal, Dubus, Leblois, and Cretin (2021) have pioneered a novel methodology, utilizing the theoretical model - Transfer Matrix Method (TMM) - to optimize VGSs for urban applications. Their research effectively validated the proposed theoretical approach by demonstrating a strong correlation between experimental measurements and model predictions. Therefore, there is a compelling need to further explore the TMM, and investigate ways to enhance its adoption in the industry to improve its applicability in early-stage design decisions.

Additionally, expanding TMM's framework could facilitate the evaluation of the broader benefits of VGSs, including their contributions to environmental sustainability and economic viability. This expansion would help recognize the significant influence of VGSs' acoustic performance on these broader contexts, making them more relevant and beneficial across different applications. However, a significant challenge hindering the widespread adoption of TMM lies in its requirement for precise knowledge of the acoustic properties of the materials used in VGS design (Attal, Dubus, et al., 2021). This limitation is particularly critical due to the current lack of reference data, especially regarding materials suitable for implementation in VGS designs in the Dutch climate.

1.2. Research Objectives

Primary Research Objective

The primary objective of this study is to develop a decision-support tool for stakeholders to assess the acoustical performance of arbitrary VGS designs using a multi-layered approach.

The secondary objectives include:

- Creating a framework for quantifying the broader environmental and monetary impacts of VGSs.
- Developing a material library containing information about the acoustic properties of various VGS components.
- Leveraging the power of TMM to accelerate the implementation and enhance the effectiveness of VGS designs.

1.3. Research Questions

In pursuit of the main objective established, the primary research question to be addressed is:

Main Research Question

How does the TMM facilitate the quantification of the acoustic performance of VGSs?

However, to arrive at a comprehensive answer to this overarching question, a series of sub-questions must first be explored. These sub-questions are categorized based on the literature, empirical and developmental studies.

Sub-questions related to the literature study:

Sub-Question 1

How are VGSs classified, and which factors shape the selection of their components?

Sub-Question 2

What are the key sustainability challenges in the widespread adoption of VGSs, and how can these challenges be addressed?

Sub-Question 3
What mechanisms define the acoustic performance of VGSs?

Sub-question related to the empirical study:

Sub-Question 4
How do the proposed VGS components perform acoustically?

Sub-question related to the developmental study:

Sub-Question 5
What key metrics are essential for stakeholders to effectively assess VGS design effectiveness and make informed implementation decisions?

1.4. Research Framework

As shown in Figure 1.2, the framework of the current research comprises three primary study components:

1. **Literature Study:** Establishes the theoretical foundation for the research objectives.

2. **Empirical Study:** Transitions from theoretical constructs to practical applications through empirical research, aimed at achieving secondary objectives.

3. **Developmental Study:** Integrates theory with practice by implementing empirical findings. This phase directly addresses the primary objective.

1.5. Methodology

The methodology employed in this project adheres to a framework of **linearly applied research**, which involves a systematic progression through distinct phases. This structured approach ensures that the research moves coherently from theory development to practical application, thereby enhancing both theoretical insights and real-world outcomes.

In the context of linearly applied research (Figure 1.3), the following reasoning processes play pivotal roles in shaping the research phases:

- **Induction:** The initial phase serves as the bedrock of the research, where a theoretical framework is established based on a comprehensive review of existing knowledge. Through an extensive literature study, key concepts and theoretical constructs are identified.

- **Deduction:** Building upon the theoretical foundation laid out during induction, the deductive phase focuses on quantitive research, involving the collection and analysis of empirical data. This step aims to test and validate the theories derived from the induction phase through systematic experimentation and data processing methods.

- **Abduction:** The final phase of abduction focuses on translating the validated theories and empirical findings into practical applications. This step bridges the gap between theory and practice by deriving actionable insights that can inform decision-making or lead to the development of new methods.
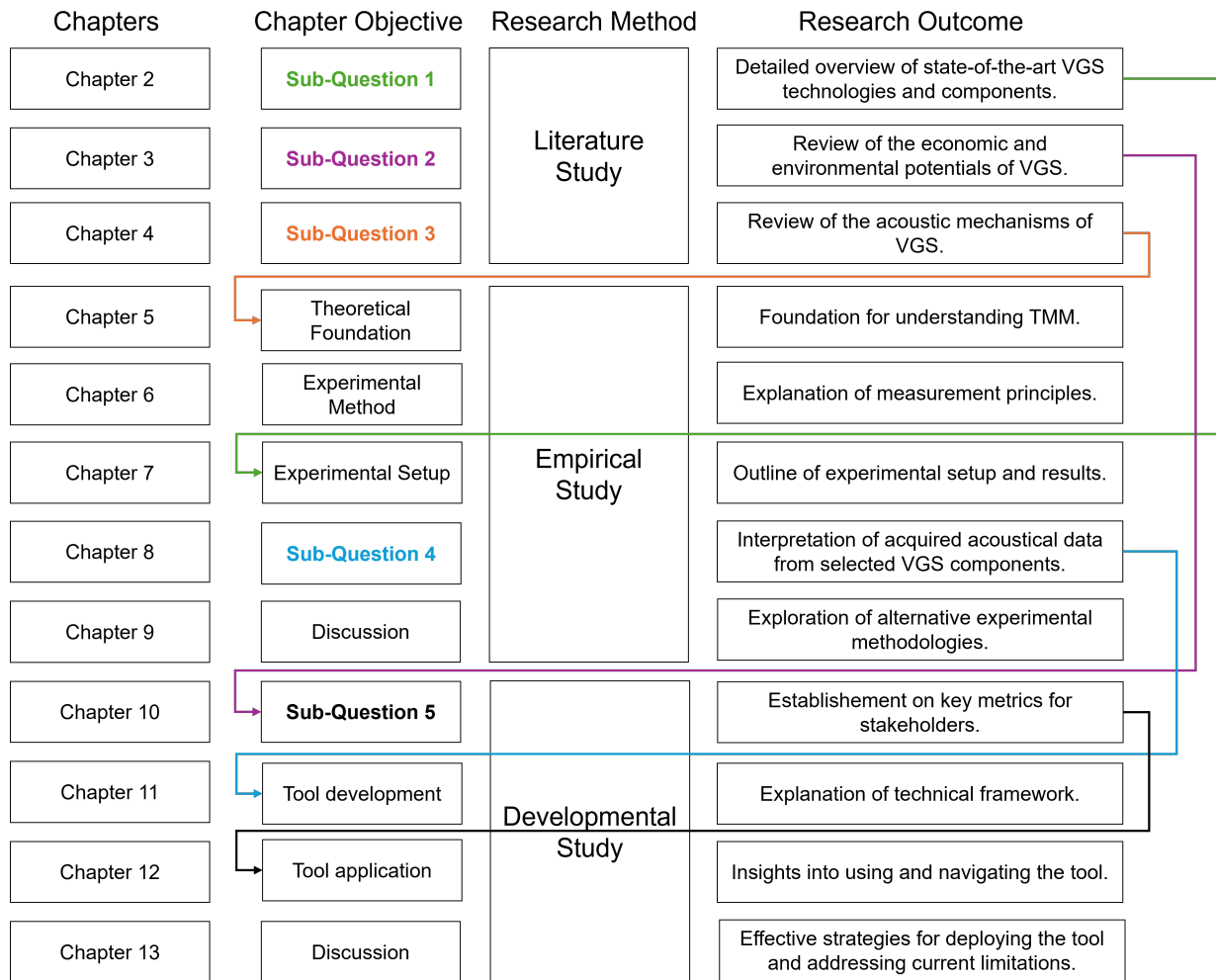
Figure 1.2: Research framework
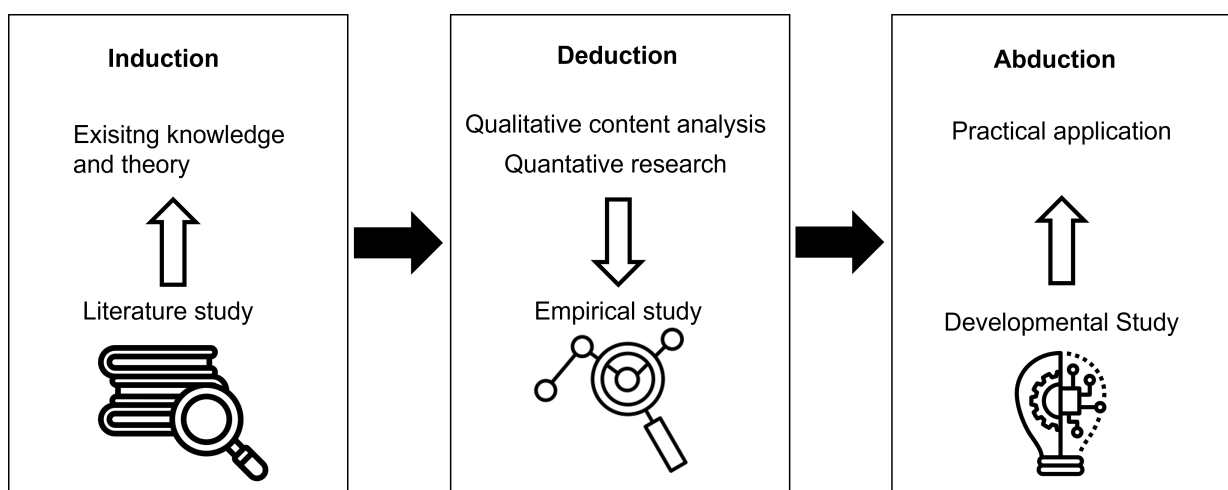
Figure 1.3: Research methodology

1.5.1. Induction

Relevant literature is reviewed throughout the induction process. The literature study focuses on three main sub-research questions, thus three domains, that aid in defining the foundation for the empirical study.

The inclusion criteria for selected literature are:

- **Relevance**: Direct relevance to the identified domains of the study.
- **Recency**: Preference for recent publications to ensure up-to-date information, ideally not older than 2010, with a preference for publications post-2015.
- **Credibility**: Prioritizing peer-reviewed articles, followed by credible books and non-peer-reviewed sources with significant contributions to the topic.

The first domain helps to identify state-of-the-art VGS technologies discussed in the literature. Subsequently, commonly used components in VGS designs, such as various types of plants and growing media, are explored. This exploration aims to provide insights into the strategic selection of these components, thereby facilitating the development of optimized VGS designs with enhanced acoustic performance in urban noise mitigation.

The second domain focuses on the commonly cited criticisms regarding the integration of VGSs, particularly LWSs, into urban environments, as highlighted by Riley (2016):

- VGSs (mostly LWSs) being perceived as too expensive and unsustainable.
- Concerns about the complexity of LWSs and their susceptibility to failure.
- Criticisms regarding the decorative nature of VGSs.

These criticisms are addressed by focusing on the economic and environmental performance of state-of-the-art VGSs. Firstly, a review of the economic and environmental factors crucial for assessing the feasibility of VGSs is conducted. Subsequently, key ecosystem services provided by VGSs are addressed. A discussion of the main challenges in the widespread adaptation of VGSs is provided, aiming to uncover the conditions under which they can be considered feasible for implementation.

Lastly, the third domain examines current knowledge and available data on the acoustic performance of various VGS configurations and their components. It delves into the mechanisms influencing the acoustic effectiveness of VGSs, providing a comprehensive exploration and elaboration on these aspects.

1.5.2. Deduction

In the pursuit of understanding the effectiveness of VGSs in noise reduction, a modelling approach is explored that accurately predicts their quantitative performance. Among various available empirical models (e.g., Delany-Bazley, Miki, Johnson-Champoux-Allard, etc.), the TMM is identified as powerful, simple, and expedient (Jiménez, Groby, & Romero-García, 2021). A versatile framework is offered by the TMM for investigating various one-dimensional wave-motion phenomena, encompassing reflection, transmission, absorption, attenuation, and dispersion. Here, "one-dimensional" refers to the assumption that only longitudinal plane waves propagate within the medium under scrutiny.

A distinctive advantage of the TMM is found in its applicability to complex structures, such as configurations involving multiple layers, which are common in VGSs. The total transfer matrix of the multi-layered VGS is derived as the product of individual transfer matrices corresponding to the layers constituting the system. This property makes the method particularly well-suited for analysing VGS configurations, where each layer can be modelled as an equivalent fluid model with complex and frequency-dependent effective parameters across a wide frequency range. Hence, the theoretical foundation elaborates on sound propagation through equivalent fluid mediums and elucidates the underlying principles of the TMM.

To employ the TMM for predicting wave propagation within an equivalent fluid medium, it is essential to ascertain the frequency-dependent complex effective impedance and complex wavenumber. Therefore, the methodology for deriving these crucial parameters is established. This entails an exhaustive exploration of the principles governing impedance tube measurements according to NEN-EN-ISO 10534-2:2023 (2023). This is followed by the elucidation of mathematical models tailored to derive these parameters from the measurement data gathered according to specified measurement protocols.

An analysis of the effective properties derived from the selected plants and substrates in the study is conducted. Its primary goal is to discern patterns and insights from the obtained data, shedding light on the significance of these properties within the context of VGS components. Through meticulous examination, key trends and phenomena within the dataset are identified and elucidated. The subsequent discussion evaluates the implications of these findings, contextualizing their relevance to the study's objectives.

1.5.3. Abduction

Central to abduction is the adoption of a generalized framework established during the deduction phase. Efficient and robust optimization of arbitrary VGS designs relies on a specialized tool designed to integrate empirical study findings. This tool plays a critical role in popularizing VGSs and facilitating widespread integration, thereby making the application of the TMM accessible across diverse stakeholders involved in VGSs development and implementation. Once a design is configured, the tool provides performance metrics crucial for decision-making in the early design phases to assess VGS implementation feasibility.

The tool is developed using the Python programming language. Python is chosen for its extensive libraries, cross-platform compatibility, and the possibility of incorporating a Graphical User Interface (GUI). Applications developed in Python run on Windows, macOS, and Linux without significant modifications. Additionally, Python's open-source nature makes it accessible to a wider audience, including individual developers, startups, educational institutions, and various other stakeholders.

Part I

Literature Study: Vertical Greenery Systems

<div align="right">

2

</div>

Technology and Components

2.1. Historical Retreat

Vertical greening has ancient origins, seen in wonders like the Hanging Gardens of Babylon, dating back to the 7th century BC (Martins & de Campos, 2019). Throughout history, civilizations such as Egypt, Greece, Roman and medieval Europe employed vertical gardening techniques, utilizing climbing plants to adorn structures like pergolas and lattice fences. The Renaissance and Baroque periods further refined these practices, introducing elaborate trellises and green corridors to enhance garden aesthetics and functionality. However, it was the groundbreaking Art Nouveau movement in the early 20th century that truly championed vertical greening (Pudelska & Miroslaw, 2015). Embracing nature as an integral part of architecture, Art Nouveau architects ingeniously incorporated climbing plants to seamlessly merge buildings with gardens, creating a harmonious and organic environment.

The foundation for modern green wall technologies was laid by historical precedents in vertical greening. The first patented interpretation of modern green walls was proposed by Stanley Hart White, a professor of landscape architecture at the University of Illinois (Hindle, 2012). White's invention, titled "Vegetation-Bearing Architectonic Structure and System," was patented in 1938. However, despite his groundbreaking invention, White did not popularize his invention, and it remained largely unrecognized until after his death.

It was not until half a century later that green walls started to gain prominence. In 1986, French biologist-inventor Patrick Blanc presented the first implementation of his idea at a landscape design festival in Paris (Bianchini, 2016). Blanc advocated for placing green plant coverings on vertical surfaces, thereby introducing the concept of "vertical gardens" (fre. *Mur Végétal*). Blanc's pioneering work was highly regarded in design circles, marking a significant shift in landscape creativity. However, it was not until the early 2000s that his ideas reached a broader audience. Blanc's approach transcended merely placing pots in vertical space; he developed a technology that allows plants to be directly attached to wall surfaces.

According to the design specifications, a metal frame is affixed to the building facade. This frame incorporates a waterproof plastic casing, specifically 10 mm thick expanded PVC, which is then layered with polymer felt and pockets composed of nonwoven felt and polypropylene raffia for planting (Fernández-Cañero, Pérez Urrestarazu, & Perini, 2018). The primary reason for using synthetic materials in construction was that natural fibers like wool and cotton, as well as organic materials like wood, deteriorate and break down when exposed to constant moisture. The vertical garden receives a nutrient-rich mineral solution for soilless plant cultivation through special tubes and filters. Blanc's pioneering and subsequent work laid the foundation for modern living wall systems, particularly in the realm of hydroponic systems.

2.2. Terminology

The challenge stems from the diverse terminology used to depict vertical greenery on building facades. Terms like 'green walls,' 'green facades,' 'living walls,' and 'vertical gardens' are often used interchangeably, causing confusion. Radić, Brković Dodig, and Auer (2019) clarified that 'living walls' are synonymous with 'green walls,' distinct from 'green facades.' Perini, Ottelé, Haas, and Raiteri (2011) also distinguished 'living wall systems' as either 'green walls' or 'vertical gardens'. On the other hand, Teotónio, Silva, and Cruz (2021) used the term 'green wall systems' to encompass both 'green facades' and standalone 'green walls,' while other authors view the latter rather as 'living walls.'

Manso and Castro-Gomes (2015) pioneered efforts to classify vertical greenery typologies and emphasized that the term 'green walls' encompasses any system facilitating the greening of a vertical surface, including facades, walls, blind walls, and partition walls. Besir and Cuce (2018) supported this notion, equating 'green walls' with 'vertical greenery systems', which comprise green facades and living walls.

Hence, it can be asserted that the widely-used term 'green wall' is prevalent both in scientific literature and commercial contexts, appealing to a broad audience. However, Bustami, Belusko, Ward, and Beecham (2018) noted that the term 'green wall' is sometimes used for projects unrelated to vertical greening on the building facades, like Great Green Wall projects or studies on green-coloured walls, *etc*.

> Consequently, due to the lack of clearly defined nomenclature, it was decided that, in the current research, the term 'vertical greenery system' (VGS) must be used to encompass greening systems as further defined.

2.3. Taxonomy

VGSs are subdivided into two main systems: green facades (GFs) and living wall systems (LWSs). There is an evident distinction between GF, where usually climbing plants grow along the wall covering it, and the most recent concepts of LWS, which include materials and technology to support a wider variety of plants, creating a uniform growth along the surface. The challenge is that many same-type VGSs, mostly LWSs, keep appearing under different names (Radić et al., 2019), though design principles and constructive solutions are similar. There is evident growth in the VGSs market day by day (Ogut, Tzortzi, & Bertolin, 2022), and different manufacturers present their products with a focus on their exceptional features and uniqueness, often employing varied names for systems that essentially belong to the same typology. Consequently, many VGSs of the same type appear under different names in manufacturers' catalogues, also affecting the names appearing in various research studies (Radić et al., 2019).

Therefore, it was necessary to create a categorization of modern VGS typologies to understand their design and construction principles, highlight existing systems' characteristics in terms of components and materials, and underline their similarities and differences. Manso and Castro-Gomes (2015) proposed a general classification where GFs can be distinguished by direct or indirect typologies, and LWSs by continuous or modular systems (Figure 2.1). Radić et al. (2019) developed an identification of various VGS types based on the extensive review, suggesting common names for similar systems; thus contributing to the schematic classification of different VGSs, as depicted in Figure 2.2.

(a) Direct GF   **(b)** Indirect GF

(c) Continuous LWS   **(d)** Modular LWS
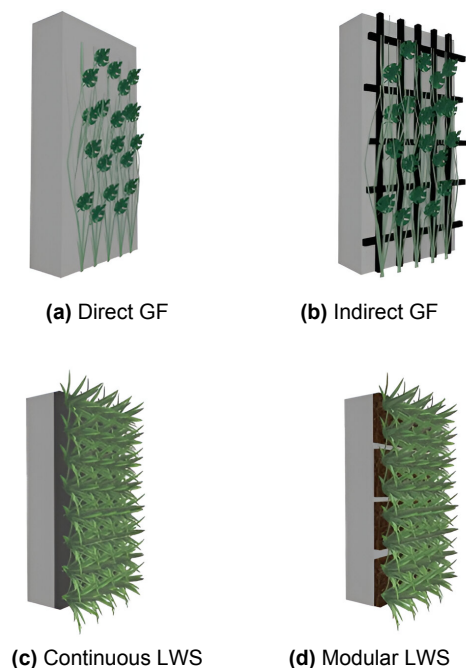
Figure 2.1: VGS typologies
Note. From "Innovative module of expanded cork agglomerate for green vertical systems," by Cortês, Tadeu, Santos, de Brito, and Almeida (2021), *Building and Environment*, p. 2. Copyright 2020 by Elsevier Ltd.

```
                                        ┌──────────────┐      ┌──────────────────┐
                                        │    Direct    │─────▶│   Climber GF     │
                                        └──────────────┘      ├──────────────────┤
                 ┌─────────────────┐                          │    Moss Wall     │
                 │  Green Facade   │                          └──────────────────┘
                 │      (GF)       │                          ┌──────────────────┐
                 └─────────────────┘                          │ Cable Wire System│
                                        ┌──────────────┐      ├──────────────────┤
                                        │   Indirect   │─────▶│   Grid System    │
                                        └──────────────┘      ├──────────────────┤
┌─────────────────────┐                                       │   Mesh System    │
│ Vertical Greenery   │                                       ├──────────────────┤
│   System (VGS)      │                                       │Double-Skin System│
└─────────────────────┘                                       └──────────────────┘
                                        ┌──────────────┐      ┌──────────────────┐
                                        │  Continuous  │─────▶│Geotextile Felt Sys│
                 ┌─────────────────┐    └──────────────┘      └──────────────────┘
                 │  Living Wall    │                          ┌──────────────────┐
                 │  System (LWS)   │                          │   Panel System   │
                 └─────────────────┘                          ├──────────────────┤
                                        ┌──────────────┐      │Vegetated Mat Sys │
                                        │   Modular    │─────▶├──────────────────┤
                                        └──────────────┘      │ Framed Box System│
                                                              ├──────────────────┤
                                                              │   Tray System    │
                                                              ├──────────────────┤
                                                              │  Plug-in System  │
                                                              └──────────────────┘
```
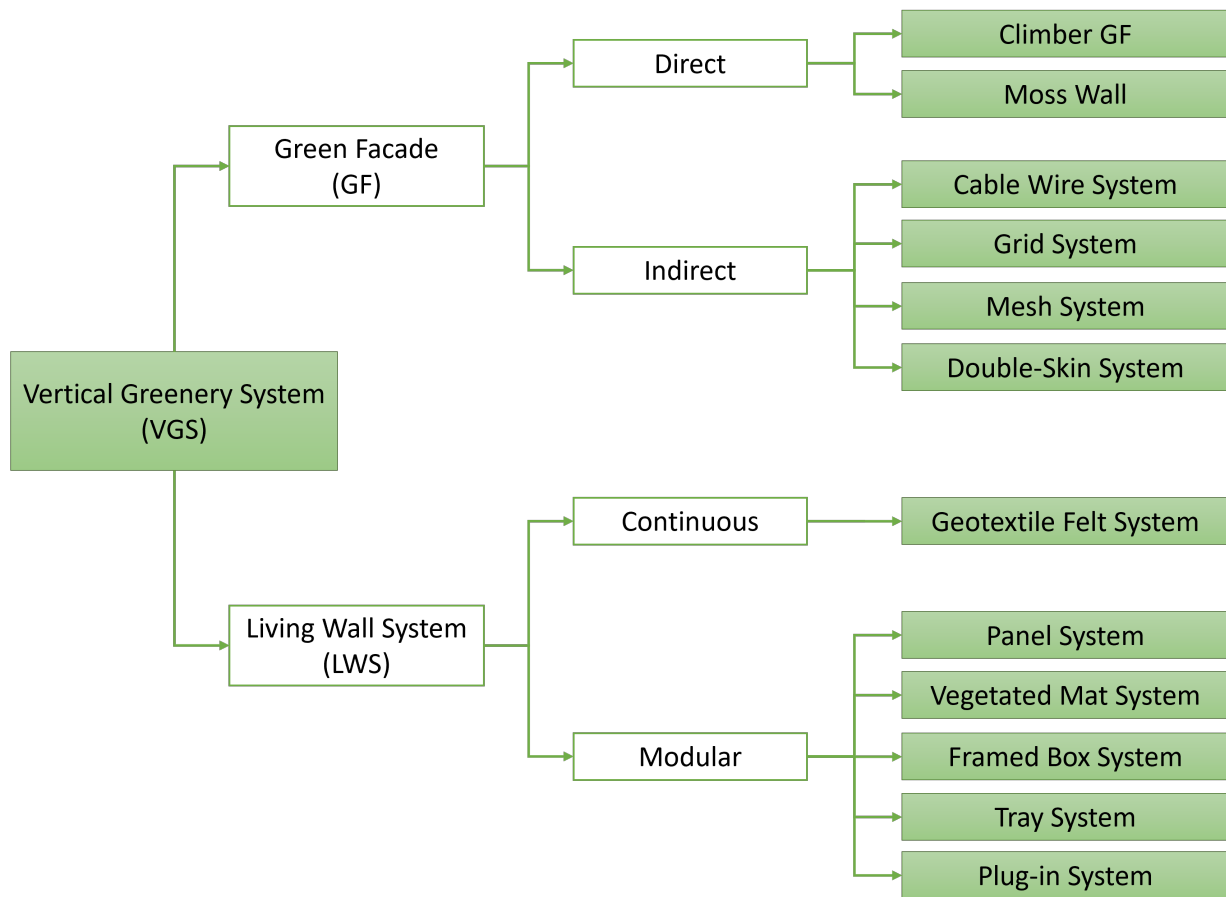
Figure 2.2: Classification of VGSs based on construction characteristics

2.3.1. Green Facades

GFs offer an aesthetically pleasing and environmentally beneficial solution for integrating vegetation into urban environments. GFs are classic methods of incorporating vegetation vertically onto structures. They typically involve climbing and self-clinging species, which are rooted in the ground at the base of the structure. Alternatively, when the height of the facade is substantial, plants are often introduced in tiers or levels, typically using containers or planter boxes (Fernández-Cañero et al., 2018). Understanding the distinction between direct and indirect GFs is crucial for selecting appropriate plant species and ensuring the structural integrity of buildings.

Direct GF entails the attachment of plants directly to a building's surface without the need for a separate supporting structure (Susorova, 2015). Within typology categorization, these conventional direct green facades are often termed **climber GFs**. This category encompasses both self-clinging climbers, as depicted in Figure 2.3a, and self-supporting woody plants. In Wall-climbing GF installations, climbing plants and vines typically originate from the ground soil, planters positioned either at ground level or at various intervals along the height of the facade.

Living moss walls, although not widely recognized compared to walls featuring flowering or vascular plants, can be considered as an unconventional type of GF and offer unique benefits (Julinova & Beckovsky, 2019). Living moss walls are typically installed using pre-grown moss mats, as depicted in Figure 2.3b, ensuring live moss without preservation or dormancy. These mats can be attached to the building facade directly provided that the necessary assets such as proper shade and misting are available. Living moss walls offer buildings a resilient, evergreen exterior with minimal maintenance. Mosses, lacking roots, seeds, and flowers, derive nutrients from the substrate, precipitation, and dust, eliminating the need for chemical fertilizers and pesticides. Achieving optimal moss growth requires balancing factors like humidity, light, nutrients, and temperature, with varying adaptability among moss species. Most mosses thrive in acidic conditions, which are commonly encountered in urban environments.

(a) Climber GF
Note. Adapted from Natuur & Milieuteam Zuid (2017)
(`https://nmtzuid.nl/album/verkiezing-fraaiste
-groene-gevels-in-zuid-2017/`). Copyright 2024 by
Natuur & Milieuteam Zuid.

(b) Living Moss Wall
Note. Adapted from Greenworks (2016)
(`https://greenworks.se/variety-of-vertical-gardens/`).
Copyright 2024 by Greenworks.

Figure 2.3: Direct GFs

(a) Cable Wire System
Note. Adapted from Carl Stahl
ARC GmbH (2023)
(`https://greencable.eu/
en/greencable-light/`).
Copyright 2024 by Carl Stahl
ARC GmbH.

(b) Grid System
Note. Adapted from MMA
Architectural Systems Ltd
(2021)
(`https://greencable.eu/
en/greencable-light/`).
Copyright 2021 by MMA
Architectural Systems Limited.

(c) Mesh System
Note. Adapted from MMA
Architectural Systems Ltd
(2020) (`https://
jakob.co.uk/projects/
view/the-shires/`).
Copyright 2021 by MMA
Architectural Systems Limited.

(d) Double-Skin System
Note. Adapted from Green
Wall SG (2018)
(`https://www.facebook
.com/photo/?fbid=
494667257611024&set=pb
.100063650810262.
-2207520000`). Copyright 2018
by Green Wall SG.

Figure 2.4: Indirect GFs

Indirect GF, on the other hand, utilizes a separate supporting structure to which climbing plants are attached. Plants in indirect systems can be rooted directly in the ground or planters, with their growth guided along the support structure (Manso & Castro-Gomes, 2015). Guides, such as **wire cables, wire grids, meshes or trellis** are common solutions for indirect GF, providing individual support structures for

plant development.

Wire cables and grids, often with smaller intervals, are commonly used to support slow-growing plants. The cable system involves tightly drawn wire ropes mounted vertically, usually in a parallel array on the wall (Jim, 2015), as shown in Figure 2.4a. This method facilitates the twining of climbers, which ascend by clockwise or anticlockwise spiral wrapping of stems around the wire rope. The grid system utilizes flexible wire ropes to weave a web, which may feature square or other aperture shapes (Jim, 2015), as depicted in Figure 2.4b. This flexible netting offers advantages over rigid trellises, particularly in green wall design, due to its ability to accommodate various geometrical shaping requirements.

Meshes (Figure 2.4c) and trellises (Figure 2.4d) serve as effective structures for holding climbing plants with dense foliage, providing support for their weight. The trellis system is commonly referred to as a 'double-skin system' because it has a significant air cavity between the wall and the vertical support structure. The air cavity must be sufficiently wide to avoid constraining the growth of species with thick stems, thus preventing stem deformation, injuries, decay, poor performance, and damage to the training system (Jim, 2015). The primary advantage of a trellis system for heavy plants is that it effectively absorbs and dissipates energy, particularly when the climber faces strong winds, thereby enhancing stability and resilience.

2.3.2. Living Wall Systems

LWSs involve fully integrating plants and planting media onto exterior walls, forming a cohesive facade construction. Typically, these systems are comprised of pre-vegetated plants and cladding structures, offering plenty of vegetated designs for coating the building facade uniformly (Besir & Cuce, 2018). LWS requires some essential materials such as supporting elements, growing substrate and irrigation system to maintain various plants. The vegetation comprises a diverse array of plant species, including grasses, perennial plants, shrubs, succulents, herbs, and vegetables (Ogut et al., 2022). However, there is a preference for evergreen plants such as small shrubs, as well as those that do not naturally grow vertically (Perini et al., 2011). The plants acquire water and nutrients from the vertical support structure instead of from the ground. Hence, a system is typically categorized as LWS if it necessitates nutrient provision and integration of an irrigation system. A waterproof membrane separates the plants and planting media from the facade surface to shield the structure from moisture.

The LWSs can be divided into continuous and modular systems (Manso & Castro-Gomes, 2015). Continuous LWSs employ lightweight layers of permeable, flexible, and root-proof screens that are stapled to the base panels attached to the frame. Typically, plants are inserted individually into prepared pockets in the external layer. Owing to their layered structure, continuous LWSs are generally lighter than modular systems and accommodate a broader range of plant species, as they lack physical constraints for root development. While, modular LWSs consist of structured elements with precise dimensions, fostering plant growth within compartments of the growing medium organized into individual cells. These cells are then assembled into panels that securely attach to a frame. The classification of modular LWSs can vary based on the type of growing medium used, whether hydroponic or substrate-based, and the design of the cells within the panels. The installation of plants within modular LWSs can be conducted directly at the location by inserting small-calibre plants into perforations within the cells, or alternatively, pre-planted modules can be employed.

Continuous systems

Geotextile Felt Systems, frequently labelled as hydroponic systems, embody a distinct form of continuous VGSs. However, it is crucial to recognize that while often linked with hydroponics, this designation predominantly refers to the irrigation method utilized rather than the construction type (Radić et al., 2019). Hydroponic refers to a method of cultivation that does not rely on soil but on the constant supply of nutrient-enriched solutions to plants. As a result, geotextile felt systems utilize vertically-laid mineral-wool slab or geotextile-fabric felt spun into a nonwoven matrix to facilitate plant growth (Ogut et al., 2022). In this method, the soil is eliminated from around the plant roots, and the plant species are placed between two layers of felted substrate either by cutting the felt on-site or by utilizing modules with pre-prepared pockets (Fernández-Cañero et al., 2018), as depicted in Figure 2.5. This setup allows the roots of the plants to grow freely throughout the entire LWS, removing any space limitations typically encountered with modular box systems. Consequently, plants can thrive and achieve their maximum growth potential within this setup.

(a) Construction Phase
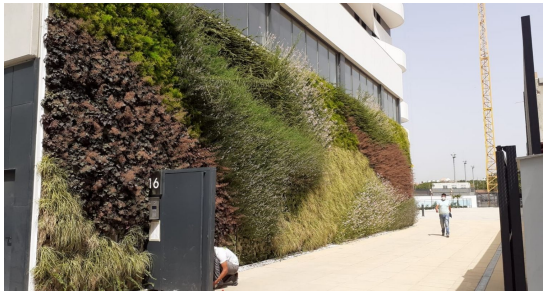
(b) Planting Phase

(c) Utilization Phase

Figure 2.5: Geotextile felt system (prod.*F+P System*) by SingularGreen in Valencia, Spain
Note. Adapted from SingularGreen (2021) (`https://www.singulargreen.com/sistema-fp-cold/`).
Copyright 2024 by SingularGreen.

(a) Module
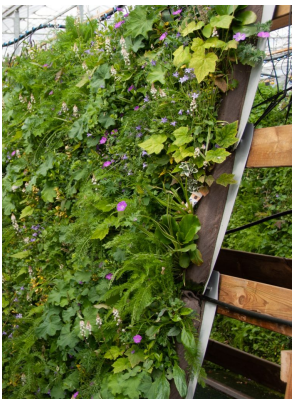
(b) Planting Phase

(c) Utilization Phase

Figure 2.6: Panel system (prod.*Flexipanel*) by SemperGreen in the Netherlands
Note. Adapted from SemperGreenwall (2024a) (`https://sempergreenwall.com/nl/flexipanel/`).
Copyright 2024 by SemperGreenwall.

(a) Construction Phase　　　　**(b)** Planting Phase　　　　**(c)** Utilization Phase

Figure 2.7: Pocket system (prod.*Vertipockets*) by Living Green Walls in Cape Town, South Africa
Note. Adapted from Living Green Walls (2020) (`https://livinggreenwalls.co.za/2017/08/09/`
`living-green-walls-vertipockets-going-green-just-became-even-easier/`). Copyright 2024 by
Living Green Walls.

Modular systems

The **panel system** in VGSs serves as the modular counterpart to geotextile felt systems. Rather than a vertically laid continuous layer, this system involves interlocking pre-fabricated panels, as depicted in Figure 2.6. These panels commonly feature a water absorption fleece atop a mineral fibre carrier substrate block (e.g. Rockwool), affixed to a waterproof membrane. The mineral fibre substrate with a capillary fleece optimizes water absorption, ensuring plant survival even without active irrigation, while also offering lightweight characteristics compared to soil-based systems. The modular design allows for easy removal and re-installation of panels, enhancing flexibility in system configuration and maintenance.

Vegetated mat systems offer a straightforward approach to creating modular LWSs, with smaller mats installed individually or in groups. This method involves attaching a fabric layer to a steel frame, which is then mounted onto the facade (Susorova, 2015). Plants cultivated in nurseries are inserted into holes cut into the fabric layer, serving as the growing medium. These systems operate hydroponically, delivering water and nutrients to the plant roots through irrigation pipes positioned behind the fabric layers. The most common implementation of vegetated mat systems is through **pocket systems**. Typically, each mat in this system comprises three synthetic layers: an external hydrophobic layer crafted from polyamide, an internal layer consisting of recycled hydrophobic fibres (geotextile), which are non-woven and micro-perforated to enhance water permeability, and a waterproof backing layer crafted from flexible PVC (Salah & Romanova, 2021). The initial two layers are stitched together using durable synthetic yarn, forming a network of pockets. These pockets accommodate multiple plants with their root balls, as shown in Figure 2.7.

Framed box systems are among the most adaptable design choices in modular VGSs. A pioneering concept within this modular approach is the **true box system**, utilizing empty square boxes typically made of plastics (Weinmaster, 2009). Additional front covers made of plastic, fabric, mesh, or metal bars can be added to further secure plants. An innovative variation arising from this system is the **cassette system** (Figure 2.8), consisting of rigid materials capable of supporting plant weight. These lightweight cassettes feature interlocking snap-on clips for easy assembly and contain a geotextile liner for growing media. Pre-planting in a controlled environment ensures proper establishment before on-site installation. Another variation is the **perforated system** (Figure 2.9), which operates on a similar principle to the cassette system but requires the pre-planting of seeds or partially grown seedlings. It features framed boxes composed of layers such as a waterproof membrane, growing media, and a 3D-shaped perforated sheet. Furthermore, it should be highlighted that beyond these mentioned systems, the market offers a plethora of additional designs for framed box systems.

(a) Module Preparation Phase

(b) Planting Phase

(c) Construction Phase

Figure 2.8: Cassette system (prod.*VersiWall GM*) by Elmich in Singapore
Note. Adapted from Elmich (2016)
(`https://elmich.com/asia/?portfolio=national-gallery-singapore`). Copyright 2023 by Elmich.

Tray systems are comprised of a series of vertically stacked troughs or horizontal mini-planters, allowing for the installation of several plants in each element along the same row (Figure 2.10). Tray systems are commonly made from materials like plastic or metal and are available in various sizes and configurations. They may consist of individual trays that are mounted one above the other or connected together to form a continuous planting surface. One of the key advantages of tray systems is their versatility and ease of installation. They allow for quick and straightforward setup, making them suitable for both temporary and permanent installations (Weinmaster, 2009). Tray systems offer flexibility in plant selection and arrangement, allowing various types of plants to be grown directly in trays filled with soil, inorganic planting media, or natural fibre (Susorova, 2015).

The **plug-in system** is a versatile modular setup designed specifically for potted plants, offering quick replacement without the need for pre-planting or re-planting. This system allows plants to be easily 'plugged-in' into racks, trays, or holes, facilitating effortless inspection and replacement without disrupting neighbouring plants or the irrigation system. Additionally, the supporting structure of the plug-in system delivers water and fertilizer directly to plant roots for optimal nourishment, featuring controlled water distribution and gravity-driven excess water flow. Depending on the manufacturer, the supporting structure of the plug-in system can be constructed from various durable materials such as plastics, metals, and ceramics (Figure 2.11). The pots for plants can either be plastic or organic, such as biodegradable containers made from organic fibres.

(a) Construction Phase   **(b)** Flourishing Phase   **(c)** Utilization Phase

Figure 2.9: Perforated system (prod.*Levande Fasader*) by Butong in Gothenburg, Sweden
Note. Adapted from Butong AB (2020) (`https://butong.eu/project/peruken/`). Copyright 2016 by
Butong AB.

(a) Construction Phase   **(b)** Planting/Utilization Phase
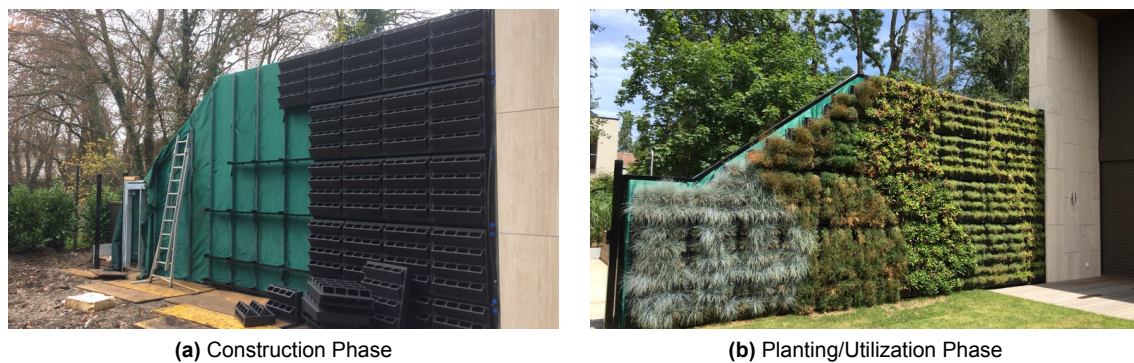
Figure 2.10: Trays system (prod.*Vertiss*) by Novintiss in France
Note. Adapted from Novintiss Society (2019)
(`https://www.vertiss.net/mur-vegetal-entretien-mise-en-oeuvr?lang=en`). Copyright 2019 by
NOVINTISS SAS.

(a) Construction Phase   **(b)** Planting Phase
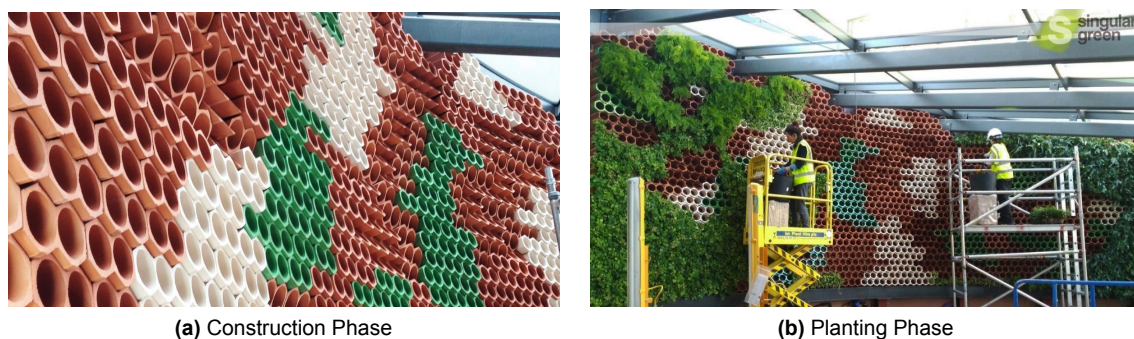
Figure 2.11: Plug-in system (prod.*EcoBin*) by SingularGreen in London, UK
Note. Adapted from SingularGreen (2015) (`https://www.singulargreen.com/en/ecobin-system/`).
Copyright 2024 by SingularGreen.

2.4. Components Overview

The main components of VGSs typically include plants (vegetation), substrates, and supporting elements that facilitate plant growth or provide structural support. Additionally, VGSs often incorporate an irrigation system comprising pipes and pumps for water and fertilizer delivery. However, for the purposes of the current review, irrigation system principles are excluded as they are deemed non-essential to the study's objectives. Furthermore, considerations regarding supporting systems receive less emphasis, as they are also considered less pertinent to the study's objectives.

2.4.1. Vegetation

Green Facades

The selection of vegetation for GFs requires careful consideration due to the relatively long time it takes for the facade to be fully covered, which can span several years depending on the planted species and the size of the facade. When designing a green facade without planter boxes, this selection becomes critical. It is essential to consider both the size and growth rate of the plants, as climbing plants can reach considerable heights, ranging from 5 to 6 meters to as high as 10 or even 25–30 meters, as seen in species like *Hedera helix* or *Wisteria* (Fernández-Cañero et al., 2018).

To ensure a conspicuous and sustainable landscape impact while minimizing horticultural maintenance (Jim, 2015), certain criteria must be met. It is preferable for the chosen plant species to be evergreen and perennial, providing continuous coverage throughout the year. Additionally, woody climber species are favoured for their robust growth and ability to effectively cover vertical surfaces. Deciduous species with vibrant fall foliage colours are also welcomed, adding seasonal interest to the facade's appearance.

The most popular species for GFs are typically climbing and self-clinging varieties (Ogut et al., 2022). For **direct GFs**, popular plant choices include *Hedera helix* (English ivy), *Parthenocissus tricuspidata* (Boston ivy), cascading ground-cover plants, and hedging plants. Additionally, species like honeysuckle, jasmine, and black-eyed Susan are common selections, known as main-stem twiners, which twine with their leaf structures. On the other hand, for **indirect GFs**, species such as Jasminum, Clematis, Lonicera, and passionflower (categorized as vine types), are well-suited due to their climbing habits and adaptability to such environments (Weinmaster, 2009). These species utilize thin, wiry tendril structures along the stem to twine or curl around another plant or a component of a facade trellis. Furthermore, other species, known as runners and scramblers, employ plant attachment mechanisms like leaf hooking, thorns, and plant strength to partially hook around trellises, netting, or wires structures until their growth advances to the surrounding support elements (Ogut et al., 2022; Susorova, 2015).

Direct GFs, the most basic type of VGSs, are simpler to integrate into existing as there is no need for any supporting structures. Consequently, one notable advantage of direct GFs is their capacity to effortlessly introduce biodiversity into urban environments. However, the choice of plants significantly affects their potential, particularly concerning the enhancement of invertebrate abundance on the building facades. Salisbury, Blanusa, Bostock, and Perry (2023) discovered that invertebrate abundance increased in correlation with both wall vegetation depth and coverage. Among the three plant species examined— *Hedera helix* (common ivy), *Parthenocissus tricuspidata* (Virginia creeper), and *Pileostegia viburnoides* (climbing hydrangea)— *Hedera helix* exhibited superior results in promoting biodiversity. The superior performance of *Hedera helix* may be attributed, despite its deeper and denser foliage, to its evergreen nature, which ensures continuous cover throughout the year. Nevertheless, incorporating mixes of *Hedera helix* with other plants may provide even greater resources.

However, employing *Hedera helix* necessitates practical considerations. *Hedera helix* faces a stigma due to its potential to damage wall surfaces by clinging to them using aerial roots (Weinmaster, 2009). These roots can pose a risk to the structural integrity of the building by penetrating cracks or joints. To effectively manage the growth of *Hedera helix*, applying colourless deterrent paints to wall surfaces can weaken its attachment. Additionally, planting *Hedera helix* around buildings made of materials resistant to aerial root damage or opting for ivy species with weaker attachment, such as *Hedera hibernica*, can help control its spread (Salisbury et al., 2023). Alternatively, considering other climbing plants like *Parthenocissus* species, such as *Parthenocissus tricuspidata* (Boston Ivy) and *Parthenocissus quinquefolia* (Virginia Creeper), which utilize tendrils with adhesive tips, presents a safer option for green facades, minimizing potential damage to building masonry (Weinmaster, 2009).

Living Wall Systems

One notable advantage of LWS over GF is the ease of achieving extensive vegetation coverage, often reaching 100%, and the ability to implement intricate planting patterns. LWSs accommodate a wider variety of vegetation species compared to GFs, largely due to their structural design and supporting mechanisms. LWSs provide a vertical or near-vertical growing environment with growing media, offering a more controlled and adaptable setting for plant growth. Nevertheless, the growing conditions in LWSs are different from those in intercropping or natural mixed plant communities, due to the vertical positioning and by having plants both above and below (Jørgensen, Thorup-Kristensen, & Dresbøll, 2018).

In practice, LWSs adhere to specific planting patterns, which may involve single-species (monospecific) or multi-species (polyspecific) arrangements (Jim, 2015). However, plants should not only be chosen for their aesthetic appeal, but also for their ability to thrive in a mixed plant community under unnatural growing conditions (Jørgensen et al., 2018). Therefore, plant selection is influenced by various factors, including microclimatic conditions, orientation (sun exposure), cultivation system, and the availability of stock in local nurseries (Fernández-Cañero et al., 2018). In the selection process, Stollberg and von Birgelen (2023) highlights several key factors impacting plant vitality:

- environmental conditions and climate,
- root space availability and accessibility to water and nutrients,
- the interplay among different plant species within the LWS (potential competition).

In terms of environmental conditions and climate adaptation, hardy plant species native to the climate zone, in which the building is located (Susorova, 2015). However, the benefits of native plants over non-native species in LWSs are uncertain, as many native plants may not thrive in the artificial environment created by such systems (Fernández-Cañero et al., 2018). Despite this uncertainty, LWSs can accommodate a diverse range of plant species, including shallow-rooted, deep-rooted, and those with specific soil and moisture requirements. The vegetation in LWSs encompasses various plant types, ranging from epiphytic (which grow on other plants) to lithophytic (which grow on rocks) and bromeliads (which store water in their leaves), as well as climbing plants (Fernández-Cañero et al., 2018). Various plant families commonly employed in landscaping and gardening are frequently utilized (Ogut et al., 2022):

- Perennial plants: Plants that live for more than two years, often returning year after year from their roots.
- Grasses (*Poaceae*): Plants with narrow leaves and jointed stems that typically grow in dense tufts or clumps.
- Sedges (*Cyperaceae*): Grass-like plants with triangular stems and solid, often sharply angled leaves, commonly found in wetland habitats.
- Ferns (*Polypodiopsida*): Non-flowering vascular plants characterized by feathery leaves and reproductive structures called spores.
- Shrubs (*Suffrutex*): Small woody plants with multiple stems, often used for landscaping or as ornamental plants.
- Succulents (*Succulentae*): Plants with thick, fleshy leaves or stems adapted to store water, such as cacti and agaves.
- Herbaceous (*Herbacea*): Plants with soft, green stems that die back to the ground at the end of the growing season, including many flowers.
- Vegetables (*Vegetabilia*): Edible plants cultivated for their nutritious fruits, leaves, roots, or stems.

In selecting suitable vegetation for LWSs, Stollberg and von Birgelen (2023) offers several recommendations to navigate the variety of plant families available:

- Take into account bio-physiological characteristics such as: growth patterns (vertical growth form and spreading behaviour), competition, dimensions (potential height), volume (foliage density), developmental stages, water requirements, substrate composition, light preferences of the plants;
- Utilize both solitary plants and spreading species, ensuring proper spacing and avoiding overcrowding;
- Opt for resilient species resilient to pests, pathogens, and winter conditions while accounting for potential failures due to frost and budgetary considerations;

- Consider incorporating wild species into the planting scheme;
- Choose plants with appealing ornamental features year-round, including during the winter months.

The selection of species for VGSs is primarily influenced by the chosen cultivation system and their orientation to cardinal directions, which directly affects light conditions (Cechová, Kunt, Jebavy, & Kozáková, 2023). Succulents, for example, are highly regarded as ideal choices for VGSs, as they can adapt to both substrate and hydroponic setups. Their compact habits and shallow root systems make them well-suited for such environments, although they are sensitive to climate variations and particularly prone to frost damage in winter, especially within hydroponic systems.

Moreover, the dimension factor plays a crucial role in plant selection for LWSs. Tall plants present significant challenges due to vertical constraints, limited rooting volume, insecure anchorage, and the risk of dislodgement (Jim, 2015). Larger plants, such as shrubs, are particularly at risk, as strong winds can easily uproot them, especially when grown in lighter substrates (Cechová et al., 2023). The use of such substrates also increases the risk of wind erosion, posing a threat to the plant root systems. Despite these challenges, leveraging construction advantages like trays or pocket systems facilitates vertical plant placement in LWSs. Unlike other types of LWSs that may only permit horizontal growth paths, these systems provide better support or anchorage possibilities for the plants.

In addition to ornamental species, several experiments have involved planting vegetables to create LWSs (Fernández-Cañero et al., 2018). Incorporating edible and evergreen plants is particularly intriguing in living wall systems, as edible plants contribute to urban ecosystem services through flowering and the potential to harvest fruits or leaves, while evergreen plants offer year-round aesthetics (Martensson, Fransson, & Emilsson, 2016). The use of edible perennials in LWSs enhances their visual and social function, providing not only an attractive appearance but also the opportunity to harvest berries, fruits, and aromatic leaves from walls at street level.

2.4.2. Substrates

The type of substrate used in a VGS gives a good idea of how "green" the product is (Weinmaster, 2009). The term 'growing media' refers to the substrate where roots and plants thrive (Ogut et al., 2022).

From the perspective of GFs, the consideration of growing media remains important, although it may be less critical compared to LWSs. GFs typically feature simpler structures and planting arrangements, with less emphasis on irrigation and nutrient delivery infrastructure. In GFs, the primary focus is on selecting plants that can endure environmental conditions such as wind and sun exposure, as well as addressing potential issues like soil loss due to wind or water-driven erosion (Ogut et al., 2022). To address these concerns, GFs often utilize alternative growing media solutions, such as biodegradable containers made of materials like coco fibres spread with latex, filled with topsoil, or arrangements on kenaf mattresses, rather than direct earth planting.

However, despite the importance of selecting optimal growing media, the variations in growing media types and compositions may not be as critical for GFs as they are for LWSs. When considering LWSs, it is essential to distinguish between modular and continuous systems concerning substrates. Continuous systems typically rely on hydroponic setups, necessitating the use of absorption screens. Conversely, only modular systems require the selection of a growing media (Manso & Castro-Gomes, 2015). Various growing media are commonly employed for modular LWSs, all of which must possess specific characteristics: lightweight, high porosity, good drainage, adequate water and nutrient-holding capacity, and local availability of materials (Pérez-Urrestarazu, Fernández-Cañero, Campos-Navarro, Sousa-Ortega, & Egea, 2019).

Continuous LWSs

Continuous LWSs rely on lightweight absorbent screens, where plants are inserted into pockets for growth (Manso & Castro-Gomes, 2015). Most commonly absorbent materials are used, such as mineral wool (e.g., rockwool), non-woven mats (e.g., geotextile-fabric felt), and foams (Jim, 2015). In addition, many companies design their own materials to develop an optimal growth medium (Fernández-Cañero et al., 2018). These materials provide a suitable medium for plant growth only if essential nutrients necessary for plant development are delivered via irrigation water to compensate for the lack of soil. These materials, being inorganic, offer the advantage of avoiding structural decay in the growing medium and preventing salt build-up when nutrients are supplied in a controlled manner (Pérez-Urrestarazu et al., 2019).

Mineral wool is a fibrous material crafted from basalt rock and chalk that undergoes heating and spinning to form thin strands. Its notable water retention capabilities make it a favoured choice for providing a consistent moisture supply to plant roots in hydroponic systems. Additionally, rock wool boasts good air porosity, ensuring sufficient oxygenation of the root zone, which is vital for plant growth. Its inert properties render it resistant to decay and decomposition, thus offering enduring support for plants in VGSs. Moreover, its lightweight nature and ease of handling facilitate installation and maintenance procedures in continuous green wall systems.

Geo-textile layers serve as common substrates for hydroponic VGSs. Synthetic fibres such as polyester, polyamide, polyethylene, and polypropylene are prevalent in the VGS market (Ogut et al., 2022). These geo-textile layers are utilized in various configurations, with one common setup involving planting bags cut at intervals and affixed to a wooden or plastic board. These bags are often comprised of double layers of stapled polyamide felt, providing support for synthetic fabric pockets where roots can thrive. Geo-textile substrates, while commonly used in hydroponic VGSs, come with several drawbacks (Ogut et al., 2022). In frosty weather conditions, there is a risk of the root zone freezing, impacting plant health. Additionally, they pose a high environmental burden according to Life Cycle Assessments, with the material often unable to be recycled. Maintenance can be challenging, as replacing dead plants requires attaching new layers of geotextile and planting in between them. Furthermore, limitations in plant species options exist due to the risk of heavy plants tearing the felt layer, and fungal and lichen growth can lead to unpleasant odours due to optimal temperature and moisture conditions.

Another frequently used substrate for continuous systems is **foam**. Foam-based VGSs are commonly supplied as pre-cultivated panels in nurseries before installation (Ogut et al., 2022). Foam substrates, while convenient, come with certain drawbacks. One major concern is the risk of root breakage, as foam-based media can be susceptible to damage from growing roots, leading to a relatively short lifespan compared to other substrates. Despite this limitation, foam substrates offer a unique advantage as vegetal and natural substratum, with some variations even consisting of aquatic foam, providing a specialized environment for certain types of cultivation.

Modular LWSs

The development of roots in modular LWSs is often influenced by the container size and the characteristics of the growing media (Ogut et al., 2022). Typically, modular LWSs are filled with a growing media that allows for root proliferation, composed of both organic and inorganic compounds, or may incorporate a layer of lightweight inorganic substrate, such as foam, to minimize weight (Manso & Castro-Gomes, 2015). Therefore, the growing media in modular LWSs can be classified into two main categories: inorganic and organic systems.

Typical **inorganic materials** in modular LWSs, **despite mineral wool** and **foam**, are **perlite**, **vermiculite**, and **expanded clay pellets** (Ogut et al., 2022). Additionally, natural unmodified materials like **pumice** have emerged, particularly for green roof applications in combination with other substrates. Perlite, a lightweight air-puffed volcanic glass (*Perlite*, 2024), and vermiculite, a lightweight heated volcanic mineral (*Vermiculite*, 2024), are both prized for their porosity, which allows them to retain moisture and hold nutrients. Expanded clay, a lightweight ceramic material formed through a high-temperature heating process, contrasts with perlite and vermiculite it has low water retention capacity and facilitates the creation of a well-draining substrate. Pumice, a porous volcanic rock (*Pumice*, 2024), also contributes to soil drainage and aeration, preventing waterlogging.

Typical **organic materials** used in modular LWSs include **stabilized peat**, **organic fibres** like coco peat and coir, and **sphagnum moss** (Fernández-Cañero et al., 2018; Pérez-Urrestarazu et al., 2019). Stabilized peat, often combined with sand, is commonly found in potting soil mixtures (Weinmaster, 2009). Peat forms from decomposed fossilized organic matter of mosses, sedges, and other semiaquatic plants over centuries. Coco peat and coco coir are by-products of coconut husk processing. Sphagnum moss is a type of moss that belongs to the genus Sphagnum. It is commonly found in wetland habitats such as bogs, swamps, and marshes. Sphagnum mosses are the most important peat-forming plants in peatlands (Joosten & Couwenberg, 2008).

Organic growing media are known for their ability to retain moisture, promote good aeration, maintain low salinity levels, and facilitate high cation exchange capacity of nutrients (Ogut et al., 2022). However, a major drawback of organic media is their decomposition over time. Nevertheless, the superior water

distribution within organic media, like coir, leads to stronger plant growth compared to inorganic media, like mineral wool (Jørgensen, Dresbøll, & Thorup-Kristensen, 2014; Jørgensen et al., 2018). This difference is attributed to mineral wool media's tendency to retain significantly higher water content in the lower part, whereas coir media distributes water more evenly throughout.

Due to the weight constraints of modular LWSs, substrate materials with relatively low specific gravity are preferred (Jim, 2015). Lightweight inorganic materials like perlite and vermiculite, as well as organic materials such as peat moss and coconut coir fibre, are commonly chosen over heavier natural soil minerals. Using soil in VGSs can strain building structures due to its added weight, especially when saturated with moisture (Riley, 2016). Therefore, nowadays, it is increasingly common to utilize mixtures of organic and inorganic substrates in LWS applications, leveraging the benefits of both types of substrates.

In many instances, the growing media in modular LWS comprises a blend of lightweight substrates and granular materials aimed at achieving optimal water retention capacity for plant growth (Pérez-Urrestarazu et al., 2019). Combining organic and inorganic materials substrates can also mitigate the need for artificial fertilizers. In addition, the research conducted by López-Rodríguez, Pérez-Esteban, Ruiz-Fernández, and Masaguer (2016) revealed more advantages of mixing mainly different organic substrates. The study included various substrate mixtures from waste materials, such as composted pine bark, coconut fibre and expanded polystyrene. Substrates containing coconut fibre exhibited low densities, indicating potential improvements in operational capacity and reduced transportation costs. Additionally, substrates combining composted pine bark with coconut fibre showed high porosities, suggesting favourable water retention and aeration properties.

2.4.3. Structural Support Systems

The Structural Support System offers resilience to the VGS, ensuring the secure transfer of all loads generated by each component (Ogut et al., 2022). Direct green facades typically do not have support structures and instead rely on climbing plants to attach themselves to vertical surfaces naturally. In contrast, indirect green facades employ support structures to prevent vegetation from falling, thus increasing resistance to environmental factors like wind and rain. These structures, whether modular or continuous, bear the weight of the vegetation, enhancing system stability. Several design factors, including climbing habit, air gap, substrate, and vegetation growth, influence the choice of structural support for green facades (Jim, 2015). Structural supports in GFs are commonly made from materials such as coated stainless steel, galvanized steel, powder/coated steel, aluminium, and plastic-wrapped steel. However, durable treated timber or synthetic materials could be used as well. Each material choice impacts both the appearance and functionality of the support system, considering factors like weight, thickness, durability, and cost (Ogut et al., 2022). Additionally, the selection of materials may be influenced by the type of facade cladding to ensure compatibility and aesthetic coherence.

Support systems for LWSs are more intricate due to the weight of the system, requiring a diverse range of materials such as metal (galvanized steel, stainless steel, aluminium), wood (plywood), and plastic. The supports for LWSs can be directly attached to the wall using uprights and brackets, or indirectly via auxiliary substructures. Among these, galvanized steel grids are commonly used for anchoring structures (Ogut et al., 2022). Continuous LWSs are typically installed with a frame fixed to the wall, creating a void space between the system and the surface. This frame supports the base panel, which acts as a protective layer against humidity and serves as the foundation for subsequent layers. The base panel, typically plywood, is covered with permeable, flexible, and root-proof screens, which are stapled to the base to secure them in place (Manso & Castro-Gomes, 2015). On the other hand, modular LWS designs offer versatility in terms of form and function, consequently allowing for the utilization of a wide range of materials. Modular systems are often composed of interlocking parts made from lightweight materials like plastic (polypropylene or polyethylene) or metal sheets (aluminium, galvanized steel, or stainless steel) (Manso & Castro-Gomes, 2015). With numerous product combinations on the market, there is no one-size-fits-all solution for structural support in various types of LWSs. **Custom solutions can be tailored to accommodate the specific needs and requirements of each typology.**

<div align="right">

3

</div>

Economic and Environmental Performance

3.1. Economic Factors

The primary obstacle impeding the widespread adoption of VGSs is their perception as costly architectural options (Riley, 2016). One of the main challenges stems from the lack of a standardized solution applicable across all projects. Consequently, costs must be tailored to each specific project, leading to significant variations. This variability complicates decision-making processes for different projects, rendering them ambiguous. Furthermore, there is often a hidden shock when considering ongoing life-cycle costs.

3.1.1. Life-cycle costs

Life-cycle costs encompass the **initial investment**, **ongoing operation and maintenance**, and **eventual replacement or demolition expenses** at the end of a product's life (Teotónio et al., 2021). It is evident that LWSs tend to be more costly than both direct and indirect GFs. This higher expense is attributed to factors such as the required maintenance (including nutrient and watering systems), the materials used, and the intricate design involved (Perini & Ottelé, 2014). Consequently, the initial capital investment for exterior LWSs is considerably greater when compared to alternative exterior cladding and greening systems (Riley, 2016).

Initial costs

The intricate nature of VGSs, coupled with the absence of a standardized solution, results in various initial costs. The foremost expense encountered is the design cost, which is contingent upon the complexity of the chosen VGS design. This cost typically ranges from a minimum of 6% to a maximum of 10% of the total project cost (Rosasco, 2018).

From the investment standpoint, the type of VGS and the components employed exert the most significant influence. For example, an indirect GF using HDPE for supporting mesh is approximately twice as economical as one utilizing steel mesh (Rosasco, 2018). The inclusion of planter boxes, especially when implemented on various levels for improved uniformity, can notably escalate costs. HDPE planter box versions are roughly half the cost of steel alternatives (Rosasco, 2018). In terms of different VGS types, both indirect GFs and LWSs require an irrigation system, with the former being approximately three times less expensive than the latter (Rosasco, 2018).

Different types of VGSs entail varying installation costs. GFs generally have lower installation expenses as they require fewer components (Manso, Teotónio, Silva, & Cruz, 2021). On the other hand, LWSs exhibit more significant cost discrepancies due to the diverse range of systems available. The installation costs associated with LWSs can vary widely, with expenses ranging from one-third to twice as high as GFs, depending on factors such as panels, plant species, and irrigation systems (Rosasco, 2018). According to Manso et al. (2021), the average installation cost for LWSs is estimated to be even higher, approximately three times that of GFs.

Operation and maintenance costs

Nevertheless, even if a VGS is well-designed, with carefully chosen plants and proper construction, its success heavily depends on maintenance. However, there is still a lack of comprehensive data on the costs associated with maintaining VGSs (Teotónio et al., 2021). As a result, clients often overlook these costs, as traditional perceptions of a building envelope's operating costs lead to a misunderstanding of the necessity of these systems.

In terms of direct GFs, the primary maintenance cost involves pruning the foliage layer, with annual adjustments to the irrigation system and occasional pipe replacements constituting minor expenses (Rosasco, 2018). Indirect GFs follow a similar trend, although additional significant costs may arise from replacing plants, particularly when planter boxes are integrated along the facade. For LWSs, the most costly maintenance activities include annual pruning and panel adjustments. Subsequently, 5% of panels and 10% of plant species must be replaced annually. The maintenance of the irrigation system, particularly the annual replacement of pipes, is contingent on factors such as length, diameter, and materials, potentially amounting to 15% of the total length of pipes annually.

Accordingly, Manso et al. (2021) distinguishes that the average maintenance cost for GFs is approximately one-third of that for LWSs. Moreover, Riley (2016) highlights that maintenance expenses per year can be as high as 15%, or even more conservatively, equivalent to one-third of a LWSs' initial costs.

Disposal costs

There are fewer successful attempts to assess replacement/demolition costs (Teotónio et al., 2021). This scarcity of information might be because many projects worldwide are relatively new and have not yet reached the end of their service life, thus resulting in a lack of readily available details. Regarding VGSs, the disposal costs at the end of the lifespan encompass factors such as plant and support removal, transportation to the landfill, dump taxes, and plaster recladding of the existing facade (Rosasco, 2018; Teotónio et al., 2021). An average disposal cost for direct GFs is estimated to be relatively lower, averaging around one-tenth of the disposal cost for LWSs (Rosasco, 2018). Meanwhile, disposal costs for indirect GFs average about one-sixth of that of LWSs. LWSs incur much higher disposal costs due to the diversity of components involved.

3.1.2. Cost Benefit Analysis

The primary barrier hindering the widespread adoption of VGSs, especially LWSs, is their associated costs, which explains the relatively low rates of implementation (Teotónio et al., 2021). To address this challenge, it is imperative to evaluate the long-term economic value of VGSs. One effective method for such assessment is through a cost-benefit analysis (CBA), which involves considering total VGS replacement costs alongside long-term maintenance expenses (Riley, 2016). A CBA essentially compares the overall lifecycle costs and benefits of a system to ascertain its viability (Teotónio et al., 2021). Throughout the CBA process, all costs and benefits are quantified in monetary terms to facilitate comparison and decision-making. Typically, the outcomes of a CBA are expressed as net present value (NPV), offering insight into the total economic impact over the system's lifespan.

As mentioned, conducting a CBA to choose the most suitable VGS for a specific purpose involves evaluating the monetary performance and effects of the solution. An example provided by Rosasco (2018) compares two variations of indirect GFs: one where ivy is supported by a steel mesh and another where it is supported by steel planter boxes also using a steel mesh. The results indicate that in both systems contribute to the longevity of the facade, and that has a positive impact on the NPV. Specifically, extending the lifespan of the facade by 5 years, which represents around 15% of its total lifespan, results in approximately a 15% increase in NPV due to the delay in restoration costs. Some studies, as noted by Teotónio et al. (2021), focus on specific goals like energy savings, while others adopt a broader perspective, assessing global sustainability and considering VGSs costs and benefits comprehensively. For instance, thermal insulation is often translated into energy savings, and improvements in air quality can be assessed using the social cost of carbon. However, the social and environmental impacts of VGS vary depending on the scale of the project. Most benefits have a significant impact on district or urban-scale projects. However, when the analysis is scaled down to a single building, some benefits lose their significance as they contribute less towards city-scale goals.

Projects yielding higher NPV are deemed more profitable (Teotónio et al., 2021). In comparison to GFs, LWSs typically demonstrate lower NPV due to their substantial initial investment and maintenance costs. GFs impose fewer financial burdens on investors, although they contribute less to social and environmental aspects. Conversely, LWSs may appear less attractive to investors due to potential losses, yet they may offer significant societal and environmental benefits. To make LWSs viable investments, incentives must be considered, with positive outcomes linked to improved building aesthetics and recreational value, resulting in enhanced property values. This highlights the current necessity for political incentives to ensure the economic sustainability of LWSs. These incentives can be categorized as tax breaks on properties, reductions in stormwater fees and other taxes, subsidies, lowered interest rates, easier construction permits, sustainability certifications, legal obligations, and streamlined administrative processes (Manso et al., 2021). Additionally, accurately estimating the benefits of LWSs is essential for their inclusion in CBA to ascertain their true potential.

3.2. Environmental Factors

Criticism frequently questions the extensive adoption of VGSs, voicing concerns regarding their superficiality, especially concerning environmental sustainability (Riley, 2016). More precisely, uncertainties persist regarding the full extent of the advantages VGSs offer throughout their lifespan. These uncertainties often lead to scepticism about environmental claims, often termed as 'greenwashing' (Rowe et al., 2022). To address this, it is crucial to accurately quantify the environmental impacts across all stages of VGS's lifecycle using a standardized, repeatable, and verifiable methodology.

3.2.1. Life Cycle Assessment
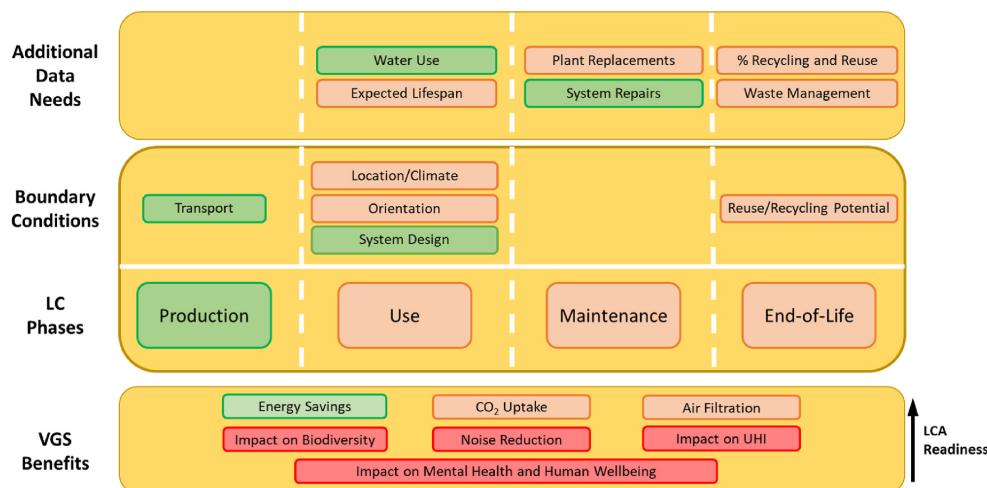
Figure 3.1: Framework for LCA of VGSs developed by Rowe et al. (2022)
Note. From "Is the sustainability potential of vertical greening systems deeply rooted? Establishing uniform outlines for environmental impact assessment of VGS," by Rowe et al. (2022), *Renewable and Sustainable Energy Reviews*, p. 3. Copyright 2022 by Elsevier Ltd.

According to Rowe et al. (2022), a Life Cycle Assessment (LCA) is recommended for evaluating the environmental practicality of implementing VGSs. LCA is a method that systematically measures all relevant emissions, resource consumption, and associated environmental and health impacts across various stages of a product or service's life cycle, following international standards (Centre, for Environment, & Sustainability, 2010). As a result, Rowe et al. (2022) propose a framework built upon the strengths and weaknesses identified in LCA approaches found in reviewed empirical studies from 2011 to 2021. This framework, illustrated in Figure 3.1, outlines lifecycle phases and boundary conditions, supplemented by sections detailing **additional data requirements** and the **benefits** associated with VGS. In the case of VGSs, the main phases to examine are **production**, **usage**, **maintenance**, and **end-of-life**. Using a traffic light system, the framework visually represents the readiness for including each parameter in LCA studies, indicating the level of available data or information for each parameter. Red signifies a severe lack of information, orange indicates data availability but inconsistency, and green denotes well-established

knowledge.

As noted from Figure 3.1, accurately defining the environmental performance of VGSs is challenging due to a lack of data for most of the parameters. Typically, VGS systems are developed by commercial entities where experts, often entrepreneurs, are understandably hesitant to openly share their hard-earned knowledge gained through trial and error during the development of their proprietary systems. Consequently, empirical research studies often rely on a combination of empirical data and assumptions regarding factors such as **expected lifespan**, **water usage**, **required maintenance**, and **end-of-life considerations** (Rowe et al., 2022).

Expected lifespan

The longevity of most competing VGSs remains uncertain, primarily due to the novelty of modern systems, particularly LWSs, which are considered cutting-edge technologies (Riley, 2016). Consequently, there is limited established knowledge concerning their lifespan. VGSs operational lifespan depends on the estimated durability of their materials before significant repairs or replacements are necessary (Manso et al., 2021). Therefore, it can be speculated that the lifespan of the entire system can be estimated based on the lifetime of its major components.

It is suggested that felt-based systems typically have the shortest lifespan, typically around 10 years (Rowe et al., 2022). According to Ottelé, Perini, and Haas (2014), this may be attributed to the 10-year service life of PVC layers, which serve as structural support for the felt layers, leading to a similar life expectancy for the entire module. On the other hand, other LWSs utilizing plastic planters or modules, such as those made from HDPE, are generally assumed to have a lifespan of around 50 years. Although Rowe et al. (2022) suggested being more sceptical about the lifespan of polyethylene parts, which are estimated to last approximately 20–25 years. Moreover, GFs with metal growing supports, like stainless steel, are expected to have a longer lifespan due to the high-quality material used.

Regarding the irrigation system, it is generally assumed to have an average lifespan of 7.5 years, with a maximum of 10 years (Rowe et al., 2022). This estimation is primarily due to the tendency for pipes used in irrigation to become clogged over time due to salt crystallization and sediment accumulation. This issue is particularly significant for hydroponic structures, where nutrients are delivered to plants via irrigation without using soil as a substrate. Concerning substrates, while specific information regarding the lifespan of inorganic substrates in such cases is lacking, organic substrates are expected to last no more than 10 years (Reyhani, Santolini, Torreggiani, & Tassinari, 2022).

Water usage

It has been established that the primary factors influencing water usage in VGSs include the type of VGS, local climate conditions, and the orientation of the wall (Riley, 2016). However, despite this understanding, there remains a lack of consensus among studies regarding which type of VGS utilizes the most water (Rowe et al., 2022), and more broadly, the average water requirements for specific systems are not universally agreed upon.

It is clear that GFs typically require minimal irrigation since the plants are directly rooted in the soil. In regions where rainfall adequately fulfils the water requirements of climbers, irrigation may not be needed at all (Jim, 2015). In the case of small GFs, manual irrigation might be sufficient. However, discrepancies in water consumption exist among different LWSs (Rowe et al., 2022). These differences are expected because environmental conditions, such as dry or wet climates, significantly influence the water requirements of plants. Additionally, variations can be observed between continuous and modular systems, primarily due to differences in water distribution and the water retention capabilities of substrates. For instance, Rowe et al. (2022) provided examples where water usage ranged from 730 to 2190 L/m^2/year for felt-based systems and from 146 to 2920 L/m^2/year for LWSs based on plastic planters. However, these figures may not be highly indicative due to the wide range of values and the specific design characteristics of each individual system.

According to Riley (2016), LWSs can be devised to alleviate the overconsumption of potable water by either harvesting rainwater or recycling water, which can offer simultaneous benefits for stormwater management. For instance, to reduce the burden of water usage, examples such as The Rubens at the Palace in London are cited (Riley, 2016). It is reported that it is possible to achieve rainwater-only

irrigation by harvesting rainwater in rooftop storage tanks instead of relying on tap water. On the other hand, recycling—the process of collecting and filtering recycled irrigation water in a reservoir—can be costly. Additionally, many system providers express concerns about using recycled water, as it could potentially expose plants to their own waste and non-nutrient salts.

Required maintenance

The uncertainty regarding the lifespan estimation of VGSs arises because while the entire system's longevity can be predicted based on its major components, the primary uncertainty lies in the vegetation. The replacement rate of plants (%/year) further contributes to this uncertainty, as it varies depending on various factors such as system design, plant species, local climate, irrigation scheme, and orientation of the VGS (Rowe et al., 2022). Empirical studies typically report replacement values ranging from 10 to around 30% for modular systems, with higher rates observed for geotextile felt systems. Interestingly, the replacement percentage tends to decrease with each passing year, as plants are more likely to survive beyond the first year. This phenomenon could be attributed to a grow-in period during which plants adapt better to the specific conditions of the VGS.

Furthermore, there is the possibility of systems, such as structural elements and irrigation systems, breaking before their expected lifetime, necessitating maintenance. In the case of VGSs, the most costly maintenance activities include annual pruning, while for LWSs, panel adjustments are also required (Rowe et al., 2022). As mentioned previously, approximately 5% of the panels may require annual replacement. Moreover, considering the potential annual replacement of 15% of the total length of the irrigation system may be necessary for more realistic estimations of VGS performance.

End of life considerations

The primary question that requires addressing is determining which components, if any, are suitable for direct reuse or recycling, and which ones need to be incinerated or landfilled at the end of the system's lifespan (Rowe et al., 2022). Ideally, the system should be modular, allowing for the replacement of all functional pieces without necessitating the destruction of the entire system. Continuous systems may present a significant risk of functional impairment if some components are still operational but cannot be removed due to the system's characteristics. Moreover, continuous systems, as mentioned previously, typically utilize felt and mineral wool as substrates, leading to a high impact in the end-of-life stage as these materials cannot be recycled. However, many researchers have concluded that, for all considered scenarios, the end-of-life phase has a negligible contribution to the overall environmental impact of the VGS.

3.2.2. Review of empirical studies

While numerous authors contribute to developing methodologies for analysing the environmental performance of VGSs by addressing challenges in data equations and quantifying benefits for LCA, there remains a lack of standardized methodology. Each author tends to have different initial assumptions and approaches in considering life cycle phases and the corresponding necessities of VGSs. This variability complicates the comparison of results across studies. Nonetheless, the current focus is to highlight the primary findings of recent empirical studies, dating up to five years ago, to elucidate the performance of VGSs and its components across key life cycle phases such as **production, usage, maintenance, and end-of-life**.

Chàfer, Pérez, Coma, and Cabeza (2021) compared the environmental impact of buildings with LWS, GF, and a reference building in a Mediterranean climate. They found that during the **production phase**, structural construction systems had the most significant environmental impact. GF had a lower impact than LWS in manufacturing because they required minimal additional materials, mainly mesh for vegetation support. The higher environmental impact of LWS, however, was notably influenced by the presence of stainless steel supports and recycled polyethylene modules. Interestingly, the substrate in LWS had the least impact due to the use of recycled organic components and coco fibre. During the **use phase**, the high impact of LWS was attributed to fertilizer and nutrient supply, comprising up to 71% of the total impact. Overall, the study highlighted the dominance of the **use phase** in environmental impact, comprising around 85%, overshadowing maintenance and disposal stages. It emphasized the importance of material selection and maintenance for mitigating environmental impact, particularly advocating for the use of fewer or organic fertilizers in maintaining VGSs.

Blanco, Vox, Schettini, and Russo (2021) aimed to assess the environmental performance of an indirect GF system compared to conventional non-vegetated building solutions. The study utilized a prototype GF system with vegetation climbing on a steel frame. Environmental comparisons were made between the green facade system and non-vegetated solutions with similar thermal effects. Results revealed that the GF system posed significant environmental challenges compared to conventional solutions. Interestingly, substituting the steel frame with a wooden one reduced the carbon footprint of the GF by 58%, indicating potential mitigation strategies for environmental impact. Furthermore, the study found that the shading effect by green facades exhibited superior environmental performance compared to non-vegetated systems.

Cortês, Almeida, et al. (2021) conducted an LCA analysis using a novel modular LWS constructed with expanded cork agglomerate (ICB) filled with lightweight substrate and enriched fertilizer, and tested with two plant species for carbon acquisition. The results underscored the substantial impact of ICB modules on overall performance, primarily due to their abundance. Moreover, their organic origin, which involves carbon sequestration during the growth of cork oak, contributes significantly to reducing global warming potential. The **production phase** had the highest contribution to the majority of the impact categories, while the **use phase** notably contributed to abiotic depletion potential (which involves the depletion of non-living resources) and fossil impacts (related to fossil fuel consumption), primarily because of high water consumption and plant fertilization. Comparison with conventional building walls revealed the superior environmental performance of the new modular LWS solution across all assessed impact categories. Installation benefits over time compensated for environmental burdens associated with adding LWS components.

Reyhani et al. (2022) aimed to evaluate the environmental performance of two types of LWSs throughout their life cycle, focusing on embodied energy, greenhouse gas emissions, material and energy consumption, and embodied carbon. The study compared a felt-based system without an organic growth medium (pocket system) to a system utilizing plastic (Expanded Polypropylene) modules with an organic growth medium (tray system). Findings revealed that the **production phase** accounted for the most significant environmental impacts, while the **installation phase** had the lowest impact due to manual assembly without specialized machinery. The felt-based system exhibited greater environmental impact across most categories, attributed to aluminium components in the supporting system and the need for inorganic chemical fertilizers due to the absence of a growing medium for plants. Conversely, the plastic-based system's environmental impact was primarily driven by the high volume of polypropylene used in panel production, water usage for plant irrigation, and potting soil composition. Additionally, plants could offset the carbon released during production within 12 to 14 years, contributing to air purification over the building's estimated 50-year lifespan.

Reyhani, Santolini, Tassinari, and et al. (2023) conducted a study to dissect different types of LWSs, analysing the contribution of materials and components to their environmental performance. Two systems were studied: System A, a modular system using soil mix as a growth medium, and System B, a felt modular system allowing plants to grow in embedded pockets without soil. Eight scenarios of component composition were evaluated for each system over a 10-year period. Results indicated that System A generally outperformed System B in most impact categories, attributed to the significant impact of aluminium parts in System B's supporting system and the use of fertilizer for plant growth. For System A, the optimal combination included HDPE or Polypropylene modules, Perlite, compost, sand substrate, and *Pteropsida* plants. In contrast, for System B, the best combination comprised organic fertilizer, HDPE panels, and a steel supporting system. Additionally, due to plants' ability to absorb carbon, it was determined that all carbon produced during the **production phase** was compensated by the fourth year of **use phase**, making the system a carbon-capturing technology from the fifth year onwards.

3.3. Ecosystem Services

Including all the ecosystem services that VGSs provide is crucial not only for accurately assessing their environmental impact in LCA, but also for conducting a comprehensive CBA. Nevertheless, there are challenges associated with determining the measurable and monetary values of these benefits. These obstacles arise from a lack of sufficient data and suitable models, as well as the complex nature of certain benefits. As a result, most benefits of VGSs are often only partially acknowledged or entirely overlooked due to the difficulties in evaluating and incorporating them into environmental impact and

economic assessments.

Most benefits have a significant impact on district or urban-scale projects. However, when the analysis is scaled down to a single building, some benefits lose their significance as they contribute less towards city-scale goals. As a result, the advantages of VGSs can be divided into two main categories: private and social. Private benefits are those that directly affect individual residences, while social benefits extend to the broader urban environment.

3.3.1. Private benefits

Private benefits associated with VGSs primarily revolve around passive energy savings, particularly in the context of building operations. Acting as an additional layer on building walls, VGS can significantly enhance the thermal performance of building envelopes, consequently impacting the operational costs required to maintain optimal indoor quality (Riley, 2016). This influence is especially pronounced in reducing cooling and heating loads, thus enhancing energy efficiency.

Reducing cooling demands

Plants have the ability to absorb solar radiation as part of their biological processes, including photosynthesis, transpiration, evaporation, and respiration (Manso et al., 2021). This intrinsic characteristic allows them to create a cooler microclimate by effectively cooling both their foliage and the surrounding air through evapotranspiration. Additionally, VGSs provide shading for buildings, reducing overheating by reflecting, absorbing, or transmitting solar radiation through foliage (Raji, Tenpierik, & van den Dobbelsteen, 2015). This lowers external surface temperatures and minimizes heat flux into the building envelope. Overall, VGSs have the potential to significantly decrease cooling loads by facilitating evaporative cooling, providing shading, increasing surface albedo, improving emissivity, and complementing building insulation performance (Manso et al., 2021), thereby reducing the overall demand for cooling during warmer periods.

Reducing heating demands

During cooler periods, simple GF can lead to a reduction in energy costs due to the warmer temperatures maintained between the plants and the wall surface. The phenomenon, known as the "thermal buffering effect", is attributed to increased thermal resistance resulting from additional building layers, such as air cavities and plant tissue (Raji et al., 2015). Consequently, by utilizing a "thermal greenery" approach, existing under-insulated facades can be upgraded or retrofitted without the expense of traditional interior or exterior insulation systems (Perini & Ottelé, 2014). However, heating loads in winter can be reduced only if insulation by VGS outweighs the shading effect (latter useful for reduction of cooling loads) (Raji et al., 2015). Moreover, the thermal insulation provided by vegetation, substrates, and configurations of both, particularly in LWSs, further enhances thermal resistance. Additionally, vegetation acts as a buffer against wind, trapping an air layer within the plant foliage. This feature is significant as the wind can decrease a building's energy efficiency by up to 50%, making the plant layer an effective barrier that prevents wind from moving along the building surface (Perini & Ottelé, 2014).

3.3.2. Social benefits

Combating urban heat island effect

As mentioned, plant evapotranspiration and shading significantly reduce heat re-radiation from façades and hard surfaces. This shields against heat accumulation in the outer facade layer, mitigating the Urban Heat Island (UHI) effect. UHI, caused by excessive heat uptake and storage in man-made materials like concrete and asphalt, elevates city air temperatures by a couple of degrees compared to surrounding rural areas (Rosasco, 2018). The UHI phenomenon results mainly from artificial surfaces' high albedo and anthropogenic activities. Assessing the exact mitigation impact of VGSs on UHI is difficult because the effect of a single VGS on UHI mitigation cannot be accurately measured, as the potential of an individual VGS to mitigate UHI is minimal at the urban scale. Substantial urban greening is required to achieve noticeable UHI mitigation. Consequently, incorporating the UHI reduction benefit of a single building's VGS into LCA and CBA is expected to have minimal significance.

CO$_2$ uptake and air pollution reduction

Urban areas usually have higher concentrations of air pollutants, which are harmful to human health, mainly due to intense road and air traffic, and the concentration of industries (Manso et al., 2021). Plant species, depending on their form and dimension, are able to sequester air pollutants and consume carbon dioxide to develop their vital functions. For instance, gaseous pollutants can be dissolved or sequestered through stomata on plants and leaves (Rosasco, 2018). Plants growing take up CO$_2$ and use it to form biomass via a process called photosynthesis. Moreover, each year a percentage of plants on a VGS will need to be replaced (Rowe et al., 2022). The removed plants are sent to a composting facility, where part of the carbon is released again as CO$_2$. The compost is then applied to agricultural soils, where some of the remaining carbon is taken up by soil bacteria and finally sequestered in the soil. As a result, this contributes to a circular life cycle, having a positive influence on LCA and CBA.

Noise reduction

VGSs offer a potential solution for reducing noise pollution in urban areas. These systems absorb, scatter, and alter the reflection of airborne sound, thereby enhancing the acoustic properties of the surrounding environment (Manso et al., 2021). Moreover, they not only decrease noise levels in the urban vicinity, but also mitigate sound transmission into building interiors where they are installed. The amount of plant biomass plays a crucial role in determining the sound attenuation capacity of a VGS (Rowe et al., 2022). Additionally, for LWSs, factors such as substrate characteristics (material, porosity, thickness, etc.) and other components are also important considerations. However, despite the potential benefits, further research is needed to precisely quantify the impact of VGSs on noise levels. Additionally, there is a methodological challenge in integrating noise pollution reduction into LCA and CBA, particularly because the effect of individual VGS on a broader urban scale is not well-established.

Unquantified benefits

While certain benefits of VGSs, such as improved well-being (mental health) and aesthetic appeal, are subjective and challenging to quantify, others, like biodiversity, can be assessed qualitatively (Rosasco, 2018). VGSs directly impact biodiversity by providing habitats for flora and fauna (Rowe et al., 2022). These systems have been observed to support various invertebrate species, including insects and spiders. The effect on flora largely depends on the selection of plant species within the VGS. A more diverse array of plants tends to attract a greater variety of animal species, particularly when local plant species are chosen, benefiting native wildlife. Hence, these systems should be incorporated alongside other green infrastructures in urban environments to help establish wildlife corridors, especially in densely populated areas (Manso et al., 2021). Despite some studies exploring the biodiversity increase facilitated by VGSs, integrating such a complex benefit into LCA and CBA remains methodologically challenging.

3.4. Discussion

Revisiting the criticisms regarding VGSs established at the beginning, to achieve genuine sustainability in the industry, there is a pressing need for a fundamental shift in perspective. Rather than solely marketing the concept of a VGS as a "wall," the emphasis should transition towards promoting comprehensive systems that provide a multitude of benefits in contrast to the conventional cladding materials (Riley, 2016). Consequently, it has been determined that methodologies like LCA and CBA can play a crucial role in either dispelling or validating the accusations of greenwashing associated with VGSs.

It has been observed that the financial performance of VGSs tends to be generally poor, frequently resulting in negative outcomes. This is primarily due to the fact that VGS installations typically incur higher costs for materials, operation, and maintenance compared to traditional alternatives. Consequently, enhancing the economic assessment of VGSs requires incorporating their environmental and social benefits to ensure a comprehensive evaluation of both costs and advantages. By accounting for all the tangible benefits they offer to buildings and urban environments, VGSs may demonstrate the greatest long-term cost savings, thereby justifying their added expense.

VGSs should ideally offset high investment costs over their lifespan for private investors through economic advantages like passive energy saving, and as a consequence, increased real estate value. Additionally, VGSs contribute to various social benefits such as reducing UHI effect, carbon uptake and air pollution reduction, attenuating urban noise pollution, and fostering biodiversity and habitat creation. While

economic benefits like energy savings, carbon sequestration, and air pollution reduction can be readily incorporated into LCA and CBA studies due to the availability of basic models and data, other benefits such as impacts on biodiversity, noise reduction, and well-being effects lack quantitative data (Rowe et al., 2022).

Increasing return on investments for VGS relies on quantifying their tangible benefits. However, VGSs, particularly LWSs, are relatively new in the built environment, considered cutting-edge technologies. Consequently, there is limited research quantifying all their benefits. Additionally, as LWSs are mainly developed by businesses, open-source data is scarce. This lack of empirical data, especially for intangible benefits, makes valuation challenging. Furthermore, there is insufficient awareness about the multiple benefits and co-benefits of VGSs, as empirical studies often focus on only a few aspects in depth. As a result, the full potential of VGSs remains untapped.

In addition, empirical studies evaluating the feasibility of different types of VGSs encounter challenges in comparing results due to variations in initial assumptions made by different authors (Rowe et al., 2022). Inconsistencies in the methodologies used for LCA and CBA pose another obstacle. Authors often employ different definitions for the scope of their studies, which can lead to misunderstandings when comparing findings across different research endeavours. To mitigate these issues and ensure accurate comparisons, there is a need to standardize the metrics used to quantify the performance of VGSs. By establishing uniform criteria, researchers can effectively compare data between different systems, thereby facilitating the optimization of VGSs.

In conclusion, VGSs have yet to achieve widespread acceptance as a building component for improving environmental quality and enhancing property value. This hesitation primarily stems from insufficient data to accurately quantify their effects and assess their overall sustainability, encompassing both environmental and economic considerations. Further research is crucial to integrate VGSs into comprehensive evaluations effectively. Additionally, clear metric targets within the criteria guiding VGS design and implementation are essential for stakeholders to analyse designs, select appropriate materials, and choose suitable plant species (Riley, 2016).

<div align="right">4</div>

Acoustic Performance

4.1. Review of Empirical Studies

Before exploring the specific mechanisms that define the acoustic performance of VGS components, conducting a comprehensive review of existing scientific research on measurement techniques, experimental setups and assessment of acoustic properties was considered essential. This step ensures that the current study maintains high standards of methodology and research integrity.

Consequently, the following section presents an exploration of 18 empirical research articles. The review of the articles is organized based on the measurement setup used in the research. Table 4.1 provides a summary of the articles, outlining the corresponding measurement methods and the derived acoustical properties associated with the chosen measurement setup.

Furthermore, the discussion aims to critically analyse and organize the findings and results uncovered during the review of these articles. Insights gained will help identify specific VGS components that exhibit good acoustic performance and guide the exploration of mechanisms that govern the acoustic behaviour of VGS components. Moreover, the discussion elaborates on how different measurement setups influence the assessment of VGSs acoustic performance. Comparing and contrasting the measurement methods used across the reviewed studies is crucial for understanding the robustness and reliability of acoustic performance assessments in various experimental contexts.

4.1.1. Impedance tube measurements

Horoshenkov et al. (2011) examined the influence of moisture on acoustic absorption using standard impedance tube measurements in two types of soils: ordinary clay-based soil and lightweight substratum soil. Moisture in soil affects acoustic absorption through three major mechanisms: reduction in apparent soil porosity, reduction in soil permeability, and stimulation of soil aggregation by clay particles coated in water menisci. The study found that the lightweight soil substratum, comprising perlite, coconut fibres, and polymer gel, exhibits minimal aggregation compared to clay-based soil and could retain water up to three times its weight due to the hydrophilic polymer gel. Consequently, the ability of hydrophilic granules to retain water keeps the soil pores relatively dry, thereby significantly enhancing its acoustic absorption coefficient.

Horoshenkov et al. (2013) systematically investigated the influence of leaf morphology and area on the acoustic absorption coefficient of low-growing plants with relatively high leaf area density, both with and without soil substratum. Laboratory experiments were conducted using a large impedance tube with a diameter of 100 mm. Five plant species were examined, alongside two types of soil: a light-density mixture comprising perlite, coconut fibres, and hydrophilic polymer gel, and a heavy-density natural clay base soil. Results showed that plants with higher leaf area density and larger dominant leaf orientation angles tended to exhibit higher acoustic absorption coefficients, particularly those with leaves oriented largely perpendicular to the direction of the incident sound wave. For instance, Winter Primula vulgaris with a height of 100 mm absorbed up to 60% of incident sound energy in the frequency range of 50 – 1600 Hz. Furthermore, the study revealed that low-permeability, high-density clay base soil had lower absorption coefficients compared to light-density, high-permeability soils, which displayed absorption coefficients comparable to fibreglass of similar thickness. Notably, the presence of plants on light-density soil significantly influenced absorption coefficient spectra in the low-frequency range.

Table 4.1: Measurement methods and associated acoustic properties considered in reviewed studies

Measurement Setup	Author	Acoustical Property	Method / Standard
Impedance tube	Horoshenkov, Khan, Benkreira, Mandon, and Rohr (2011)	Absorption Coefficient	ISO 10534-2
	Horoshenkov, Khan, and Benkreira (2013)	Absorption Coefficient	ISO 10534-2
	D'Alessandro, Asdrubali, and Mencarelli (2015)	Absorption Coefficient	ISO 10534-2
	Attal, Buot de l'Epine, Dauchez, and Dubus (2021)	Absorption Coefficient	Three-microphone two-load method
Reveberation chamber	Wong, Kwang Tan, Tan, Chiang, and Wong (2010)*	Absorption Coefficient	ISO 354
	Yang, Kang, and Cheal (2013)	Absorption Coefficient	ISO 354
		Scattering Coefficient	ISO 17497-1
	Azkorra et al. (2015)	Absorption Coefficient	ISO 354
	Davis, Tenpierik, Ramírez, and Pérez (2017)	Absorption Coefficient	ISO 354
	Thomazelli, Caetano, and Bertoli (2017)*	Absorption Coefficient	ISO 354
	Manso et al. (2017)	Absorption Coefficient	ISO 354
	Chang and Chang (2022)	Absorption Coefficient	ISO 354
	Scamoni, Scrosati, Depalma, and Barozzi (2022)	Absorption Coefficient	ISO 354
In situ	Wong et al. (2010)*	Insertion Loss	SPL measurements before-and-after
	Lacasta et al. (2016)*	Absorption Coefficient	ISO 13472-1
	Lunain, Ecotiere, and Gauvreau (2016)	Sound Level Reduction	SPL measurements before-and-after
	Pérez et al. (2016)	Sound Insulation	ISO 140-5
	Thomazelli et al. (2017)*	Sound Insulation	ISO 140-5
	Romanova, Horoshenkov, and Hurrell (2019)	Absorption Coefficient	Parametric transducer method
Computational	Van Renterghem, Hornikx, Forssen, and Botteldooren (2013)	Insertion Loss	Finite-difference time-domain (FDTD) method & Pseudospectral time-domain (PSTD) method
	Guillaume, Gauvreau, and L'Hermite (2015)	Equivalent SPL (L_{eq}) Early decay times (EDT)	Transmission Line Matrix (TLM) method
	Lacasta et al. (2016)*	Sound Level Reduction	Software CadnaA

∗ Indicates multiple measurement setups per study. In subsequent reviews, the repetition of the study with another measurement setup is emphasized by in-text notation "also".

D'Alessandro et al. (2015) investigated indoor green walls to determine suitable plant species for indoor use. They measured the normal incidence sound absorption coefficients of two plant types, Nephrolepis Exaltata (Boston Fern) and Helxine soleirolii (Baby Tears), in an impedance tube with and without a porous soil substrate. The tube, with a 100 mm diameter, allowed measurement in the 50-1600 Hz range. The substrate, comprising 70% coconut fibres and 30% expanded perlite, was chosen for its high porosity. Results showed soil's significant role in sound absorption, absorbing up to 80% of incident acoustic energy. Additionally, the presence of tested plants enhanced absorption across the whole frequency range. Moreover, D'Alessandro et al. (2015) utilized Miki's equivalent fluid model for sound propagation to deduce non-acoustical properties such as tortuosity and flow resistivity of the samples. Their findings revealed a close relationship between leaf area density and flow resistivity.

Attal, Buot de l'Epine, et al. (2021) investigated the impact of moisture on acoustic absorption in lightweight substrates—coir dust and perlite—using large impedance tube measurements. They assessed properties like speed of sound, attenuation, characteristic impedance, compressibility, and density between 100 Hz and 1000 Hz. Dry substrates showed a lower speed of sound and higher attenuation compared to air. Moisture induced significant changes, notably decreasing the speed of sound and increasing attenuation for coir dust. Consequently, coir dust exhibited an increase in characteristic impedance, while perlite demonstrated a decrease with added moisture. The distinction in properties stems from the differing characteristics of the particles and their ability to retain water. While perlite particles are rigid and can solely retain water in their tiny pores, the majority of coir dust consists of soft, spongy tissue particles capable of storing water within their cells. As a result, coir dust particles form a soft frame that expands in volume as moisture content increases, which allows for keeping pores between the particles open.

4.1.2. Reverberation chamber measurements

Wong et al. (2010) conducted practical measurements, including one in a reverberation chamber, where *Nephrolepis exaltata* (Boston fern) was utilized for measurements due to its high leaf area density. The researchers defined the equivalent sound absorption area of the test specimen. The results confirmed that the substrate, composed of soil, exhibited effective performance in absorbing acoustics energy in low frequencies (200 Hz to 1 kHz), leading to a substantial decrease in reverberation time. Conversely, plants were found to be more effective in high frequencies (1 kHz to 5 kHz), where it was observed that the larger

greenery coverage resulted in decreased reverberation time. Eventually, it was found that as frequency increases, discrepancies in sound absorption coefficients among different greenery coverage percentages (100%, 71%, and 43%) become more pronounced, with minimal differences at lower frequencies (100 Hz to 250 Hz) but progressively widening with higher frequencies, and stabilizing beyond 1 kHz.

Yang et al. (2013) conducted a series of measurements in a reverberation chamber to assess the random incidence absorption and scattering coefficients of various vegetation types, including Buxus, Holly, and Ivy. They considered factors such as soil depth, moisture content, and vegetation coverage. Additionally, they examined an unplanted VGS modular system composed of galvanized steel frames filled with coconut fibres, perlite, and a water-retaining polymer. The results indicated that even a thin soil layer of 50 mm depth provided significant absorption coefficients, particularly around 1000 Hz. Soil depth variations showed minimal changes in absorption coefficients. However, increased soil moisture content led to a notable decrease in absorption coefficients. Moreover, higher vegetation coverage resulted in increased absorption coefficients at low and mid-frequencies but slight decreases at frequencies above 2000 Hz. The study also highlighted the significant effect of aboveground vegetation components on sound absorption and scattering, particularly at higher frequencies and with increased vegetation coverage. Additionally, the VGS with a highly porous substrate maintained a relatively high absorption coefficient, even under nearly saturated conditions, due to the use of a water-retaining polymer.

Azkorra et al. (2015) aimed to evaluate the acoustic characteristics of a module-based LWS utilizing recycled polyethylene modules (containers) filled with coconut fiber substrate, with the inclusion of Helichrysum thianschanicum species. They found that introducing the LWS into the reverberation chamber notably reduced reverberation time, particularly in the frequency range from 0.200 kHz to 1 kHz. The tested green wall exhibited consistent sound absorption coefficients between 0.35 and 0.51, indicating effective performance across both low and high frequencies. Overall, the study concluded that LWSs offer good sound absorption capabilities, though the extent of their contribution depends on the specific design and materials employed in each system. The VGS configuration utilized in this study demonstrated comparable or superior acoustic absorption coefficients compared to other conventional building materials.

Davis et al. (2017) constructed an LWS to investigate how different setups affected the sound absorption of LWS modules. They examined two scenarios: modules filled only with substrate (case 1) and modules densely planted with ferns (case 2). Boston ferns (Nephrolepsis) per module were planted in the LWS alongside the substrate mixture of potting soil (50%), coco chips (33%), and sphagnum moss (17%). Variations of module configurations were tested, including different arrangements (connected or dispersed) and placements (directly on the floor or with an air gap of 5 or 10 cm). Results showed that variations in configuration had minimal impact on sound absorption; neither air gaps nor module dispersion significantly affected the outcome. However, raising modules from the floor to create an air gap slightly shifted absorption towards lower frequencies. Moreover, densely planting modules with ferns slightly improved sound absorption. Nonetheless, the substrate remained the primary contributor to sound absorption. Comparing the findings with a theoretical model by Delany-Bazley revealed that thicker substrates led to higher absorption coefficients, especially at lower frequencies. Thus, for better absorption at lower frequencies, opting for a thicker substrate could be advantageous.

Thomazelli et al. (2017) used a reverberation chamber to measure the absorption coefficient of a modular LWS. The system consisted of plywood boards with attached geotextile bags holding substrate and plants (Callisia repens). Three configurations were tested: baseplate with geotextile bags, baseplate with geotextile bags and substrate, and baseplate with geotextile bags, substrate, and vegetation. The study found that geotextile bags were the main factor contributing to enhanced absorption due to their non-rigid and non-reflective nature compared to plastic trays. Additionally, the wooden laths substructure beneath the LWS panels created an air gap between the specimen and the floor, which contributed to enhanced absorption, particularly at lower frequencies, by allowing the materials to function as vibrant panels.

Manso et al. (2017) analyzed random incidence absorption coefficients for four configurations: the GEOGREEN support system, substrate soil added to the system, plants introduced, and a variation with taller plants replacing 10% of the original ones. The GEOGREEN modules were constructed using a geopolymeric lightweight binder derived from mining waste, which includes granulated expanded cork as a key component. The GEOGREEN modules exhibited considerable sound absorption, particularly in the 630-800 Hz range, albeit the lowest among the configurations. Addition of soil increased absorption,

reaching absorption class D with a 15% increase in weighted sound absorption. Further enhancement occurred with the introduction of plants, improving absorption by an additional 20% and classifying the sample as absorption class C. Introducing taller plants resulted in a further 5% improvement, classifying the configuration as absorption class B.

Chang and Chang (2022) constructed the LWS using a support system made from wood plastic composites. They investigated two structural types of support systems, including panel absorbers and perforation boards with various acoustic designs. Jacobaea maritima was chosen for the greenery system due to its potential for noise reduction, exhibiting comparable performance to Boston ferns while requiring less space and substrate depth. The study found that as the coverage of Jacobaea maritima increased, sound absorption across all octave bands improved, particularly in mid-high frequencies. Additionally, the introduction of the support system enhanced sound absorption performance, especially for low to mid-range frequencies. Weight was identified as a key factor influencing sound absorption, given the LWS's form as a panel absorber. Implementing acoustic methods with panel absorbers and perforation structures improved sound absorption at frequencies below 1000 Hz, highlighting the significance of support system design in conjunction with urban greenery.

Scamoni et al. (2022) investigated the acoustic absorption performance of an innovative indoor LWS where plants are rooted in felt layers and grown hydroponically without a growing medium. Panels without plants, with dry felts, and with wet felts were tested to assess the impact of irrigation. The plants utilized in the study were categorized into two groups: those with large leaves, including Philodendron Imperial Green, Monstera Deliciosa, and Ficus Benjamin Danielle, and those with small leaves, represented by Ficus Pumila. Results indicated that the presence of water does not influence the absorption of the felt, except for a small increase at the highest frequencies starting from 2000 Hz. In addition, the presence of vegetation significantly contributed to the system's performance, while the felt material did not offer significant absorption, except at higher frequencies. Additionally, the type of plant species influenced the sound absorption, with large-leaved plants demonstrating higher absorption at medium-high frequencies (315–2000 Hz) and small-leaved plants performing better at high frequencies (2500–5000 Hz).

4.1.3. In situ measurements

Wong et al. (2010) <u>also</u> conducted in situ measurements to assess eight different VGSs installed on concrete walls in HortPark, Singapore. Their research, which included in situ measurements, focused on assessing insertion loss—a measure of sound attenuation. The results highlighted the impact of VGS configurations on middle frequencies (125 Hz to 1250 Hz), with a general insertion loss peak around 800 Hz. Systems featuring densely packed foliage demonstrated moderate to high insertion losses, ranging from 5.4 dB to 8.4 dB. Counterintuitively, systems with sparse plant coverage or gaps between modules also exhibited relatively moderate losses, ranging from 5.6 dB to 7.0 dB. Additionally, VGS incorporating specific design elements, such as thick soil pots positioned at the noise source height, achieved notable insertion losses, reaching up to 9.9 dB. Similarly, VGS utilizing an air cavity achieved insertion losses of up to 7.0 dB. These findings underscore the significant influence of various VGS features on sound attenuation properties, emphasizing the necessity for a thorough investigation to address potential anomalies.

Lacasta et al. (2016) evaluated a modular LWS noise barrier using an experimental prototype for in situ measurements of noise reflection. The barrier, constructed from concrete, incorporated a LWS based on recycled polyethylene modules, each functioning as an independent hydroponic crop unit (MCU). These MCU-s contained a recyclable and environmentally friendly substrate, composed of a 50/50 volume mix of compost and coconut fibres. The study utilized the Helichrysum thianschanicum species. Their in situ measurements of the barrier's performance revealed that, overall, the values for all frequency bands were higher than those previously obtained in laboratory settings. This discrepancy could be attributed to the development of plant morphology over time. These findings underscored the importance of in situ measurements for realistically evaluating greenery walls, which undergo significant changes throughout the year that cannot be adequately assessed in laboratory conditions.

Lunain et al. (2016) examined a U-shaped street and installed metal modules or cages filled with polypropylene rot-proof fabric surrounding the planting substrate, comprising a mix of organic and plant materials. The foliage consisted of 39 local species. The green wall installation led to a reduction in overall sound pressure levels from road traffic noise. Moderate noise reduction, ranging from 0 to 6 dB gain, was observed at medium frequencies (400-2500 Hz), attributed to the acoustic absorption provided by

the substrate. The green wall exhibited maximum efficiency at high frequencies, with gains of 0 to 10 dB observed above 3150 Hz, where a scattering phenomenon induced by the foliage contributed significantly.

Pérez et al. (2016) investigated the sound insulation effects of a LWS and a GF in situ. The LWS comprised recycled polyethylene modules filled with coconut fiber substrate, hosting Rosmarinus officinalis and Helichrysum thianschanicum plants, while the double-skin GF featured Boston Ivy (Parthenocissus Tricuspidata). Results showed increased insulation at intermediate frequencies (peaking at 800 Hz) due to substrate absorption, but a reduction at 2000 Hz due to the focusing effect caused by the periodic arrangement of greenery. High-frequency insulation improved due to scattering by greenery. The study emphasized the importance of substrate in LWS for acoustic performance and noted that an additional 20–30 cm vegetation layer could increase insulation by 1 dB for traffic noise and 2–3 dB for pink noise.

Thomazelli et al. (2017) also conducted field measurements on a modular geotextile felt pocket LWS to evaluate its sound insulation capabilities. They tested three conditions: (a) facade without panels; (b) panels with a baseplate and geotextile bags; and (c) panels with a baseplate, geotextile bags, substrate, and vegetation. The complete modular panel improved sound insulation by 2 dB, suggesting that vegetation in green walls contributes minimally to soundproofing. This indicates that optimizing a LWS to enhance the insertion loss should prioritize factors like panel thickness, substrate composition, sealing between system components, and panel-facade coupling, rather than vegetation alone.

Romanova et al. (2019) aimed to devise a new method for measuring the absorption coefficient of LWSs in-situ. They utilized specialized equipment with directional sensitivities to test this method, focusing on a specific LWS module system known as the tray system, which featured compartments for plants. Their investigation involved testing these compartments filled with soil, and with Hedera helix and Bergenia cassifolia plants. Their results demonstrated that plants with higher leaf area density enhanced the absorption properties of the LWS, particularly in the medium and high-frequency ranges (above 1000 Hz) by 1-2 %. Additionally, they noted that the compartmentalized design of the LWS could generate acoustic resonances at frequencies determined by compartment dimensions and wall thickness. Specifically, resonances at 1280 Hz (due to a half-wavelength resonance at a compartment width of 250 mm) and 2200 Hz (due to a half-wavelength resonance at a compartment height of 72 mm) caused drops in absorption. However, these resonances were attenuated when the wall was planted with species possessing higher leaf area density, such as Bergenia cassifolia.

4.1.4. Computational models

Van Renterghem et al. (2013) employed the finite-difference time-domain (FDTD) and pseudospectral time-domain (PSTD) methods to analyse VGS strategies, with a focus on traffic noise propagation from canyon street to the courtyard. Their study revealed that the effectiveness of VGS depends on material assumptions, with street VGS most effective when street canyon materials are rigid. Conversely, with softer masonry, green wall effectiveness is less pronounced, and greening entire facades offers no additional benefits compared to treating only the upper half. VGS in the lower part only provides limited noise reduction in the receiver courtyard due to direct sound propagation from the street to the building's roof edge.

Guillaume et al. (2015) investigated the benefits of integrating greenery onto building facades and rooftops to enhance acoustic conditions within a canyon street setup. Employing numerical simulations with the Transmission Line Matrix (TLM) method, they analysed 14 different arrangements of rooftop and facade greenery in a canyon street bordered by two 4-storey buildings. Prior to the simulations, they conducted on-site measurements of the acoustic impedance of various plant species and utilized Miki's model to estimate the specific airflow resistivity. Their results highlighted notable enhancements in acoustic levels, especially on the upper floors of treated buildings and in adjacent streets. These enhancements were influenced by factors such as the layout of vegetation surfaces, frequency ranges, and the number of reflections encountered along the sound propagation path.

Lacasta et al. (2016) also evaluated the performance of a modular LWS noise barrier using numerical predictions conducted in the CadnaA (environmental noise prediction software). When evaluating the effectiveness of noise barriers, especially when placed in pairs to shield areas near roadways, the multiple reflections between barriers can significantly degrade attenuation performance compared to a single barrier setup. The study aimed to minimize this issue by utilizing greenery on the barriers. Three configurations

were tested: a single reflective barrier, a pair of parallel reflective barriers, and a pair of parallel greenery (absorbing) barriers. As anticipated, comparing the results of the three configurations revealed that the use of greenery on the barriers notably mitigated the reflection and amplification effect.

4.1.5. Discussion

The main aim of reviewing empirical studies was to uncover the acoustic properties and performance of various types of VGSs and their components. As a result, conclusions can be drawn:

1. **Vegetation performance:**

   - Plants with higher leaf area density and those oriented perpendicular to the incident sound wave direction exhibit enhanced absorption capabilities.
   - Vegetation provides higher sound absorption at higher frequencies, particularly above 1000 Hz.
   - At high frequencies, beginning at 2500 Hz, the scattering effect on vegetation becomes more pronounced, with the scattering coefficient rising as frequency increases.

2. **Substrate performance:**

   - Adequate soil depth is vital for sound absorption, yet beyond a certain threshold, further increases show minimal impact on the absorption coefficient.
   - The substrate is the primary contributor to sound absorption of the VGS (accounts for ca 80% of sound absorption of the VGS).
   - The more porous the substrate, the greater its sound absorption capacity.
   - Moisture in the soil affects acoustic absorption through a reduction in apparent soil porosity, soil permeability.
   - The microstructure of the particles plays a role in how they respond to moisture and subsequently affect acoustic performance.
   - Incorporating hydrophilic polymer gel into the substrate aids in water retention for plants while keeping soil pores dry, consequently enhancing acoustic absorption.
   - The substrate predominantly governs sound absorption within the lower-frequency range (250 Hz up to 1000 Hz).

3. **VGS design considerations:**

   - Introducing an air cavity between the wall and the VGS can slightly shift absorption towards lower frequencies.
   - VGSs utilizing felt allow for better absorption due to their non-rigid and non-reflective nature, particularly at higher frequencies.
   - Implementing acoustic methods such as panel absorbers and perforation structures improves sound absorption, especially at lower frequencies.
   - Plastic trays in VGSs may induce local resonance of incident waves, potentially reducing absorption capabilities.

4. **Sustainability considerations:**

   - Full facade planting may not be necessary to effectively reduce street/courtyard noise; instead, prioritizing the treatment of higher stories is preferable from a sustainability perspective.

Table 4.1 illustrates that the primary acoustic property examined in the reviewed articles was the absorption coefficient derived in laboratory settings. In situ measurements mainly focused on assessing the sound insulation performance offered by the VGSs, while also considering other parameters related to sound attenuation. The measurement of absorption coefficients in laboratory settings involved using impedance tube measurement setup as specified in NEN-EN-ISO 10534-2:2023 (2023), or reverberation chamber measurement setup as outlined in NEN-EN-ISO 354:2003 (2003). The primary distinction between these standardized measurement methods lies in the angle of incidence and the size of the required test samples. According to ISO 354, the reverberation room method determines the sound absorption coefficient of the test sample under conditions of random sound incidence, typically using large test samples

with an area between 10 and 12 m^2. In contrast, the impedance tube method involves using relatively small-size test samples of a few square centimetres and considers only normal incidence.

In the reviewed empirical studies, numerous VGS designs as well as individual VGS components were investigated numerically, focusing on frequency-dependent absorption coefficients. Numerical data facilitates cross-study comparisons to identify promising components, yet directly comparing the VGSs and their respective components analyzed in the studies presents challenges. Those challenges were highlighted by Bakker et al. (2023), who synthesized absorption coefficient data from various sources, including those currently examined, such as *Romanova et al. (2019), Horoshenkov et al. (2011), Van Renterghem et al. (2013), D'Alessandro et al. (2015), Davis et al. (2017), Thomazelli et al. (2017), Lacasta et al. (2016), Wong et al. (2010), and Horoshenkov et al. (2013).* Their analysis, depicted in Figure 4.1, revealed that absorption coefficients obtained according to ISO 354 tend to be higher compared to ISO10534-2 and in-situ measurements.
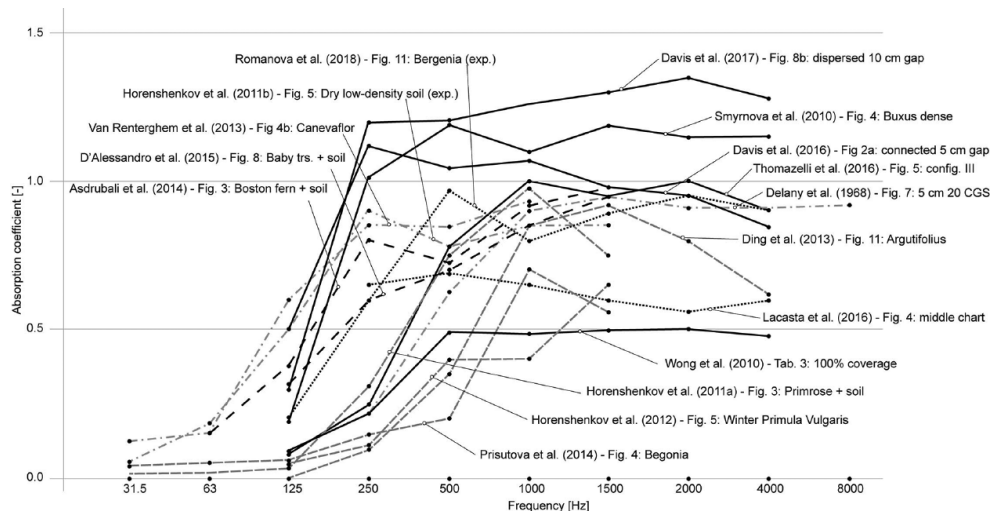
Figure 4.1: A compilation of absorption coefficients of various VGSs collected by Bakker et al. (2023)
Note. From "Applying vertical greening systems to reduce traffic noise in outdoor environments: Overview of key design parameters and research methods," by Bakker et al. (2023), *Building Acoustics*, p. 3.
Licensed under CC BY 4.0.

——————   Reverberation chamber (plant-substrate systems)
- - - - -   Impedance tube (plant-substrate systems)
·—·—·—·   Impedance tube (substrates only)
- - - - -   In-situ measurements

The higher absorption coefficients obtained according to ISO 354 are mainly due to ((Cox & D'Antonio, 2017)):

- **Absence of Diffuse Sound Field:** Errors in reverberation chamber measurements often result from the difficulty in achieving a uniform diffuse sound field due to chamber construction inaccuracies or improper diffuser setup.

- **Large Sample Size Impact:** The requirement for large sample areas in reverberation chambers can lead to inaccuracies. Slow horizontal sound decay and edge effects from large samples lead to increased variation in reflected sound throughout the room and restrict energy propagation evenly in all directions, hindering the creation of a diffuse field.

These factors contribute to higher absorption coefficients, sometimes exceeding theoretical limits of 1, as observed in Figure 4.1, highlighting significant weaknesses in the reverberation chamber method. Therefore, the impedance tube method offers advantages, particularly due to the convenience of calibrating the apparatus in laboratory settings, which helps minimize inaccuracies in measurement results. Moreover, the apparatus' compact size allows for small sample usage, minimizing wastage, and shortening measurement times to just a few minutes (Koruk, 2021).

On the other hand, the impedance tube method has its limiting factors, notably in its ability to measure

only the normal-incidence sound absorption coefficient within a restricted frequency range determined by the tube's dimensions. Additionally, reflections and scattering within the tube can cause fluctuations in the acoustic absorption coefficient, especially when testing highly scattering test samples, such as plants without soil. Moreover, the mounting conditions of the test sample within the tubes can exert a considerable influence on the measured sound performance, potentially introducing variabilities and uncertainties into the measurement results (Koruk, 2021).

Consequently, recognizing the limitations of both commonly used laboratory measurement setups, it was concluded that solely focusing on numerical comparisons of frequency-dependent absorption coefficients may not provide a complete representation. Therefore, instead of emphasizing detailed numerical comparisons, it is more effective to highlight the VGS components identified as performing best in the reviewed studies. Authors often indicated the superior performance of specific components either from the outset of their research, referencing previous studies or literature reviews, or based on experimental results showing certain components outperforming others. As a result, the table 4.2 presents the VGS components identified as the most acoustically efficient across the reviewed studies.

Table 4.2: Best performing VGS components per study

Measurement Setup	Author	Vegetation	Substrate
Impedance tube	Horoshenkov et al. (2011)	-	Canevaflor: perlite + coconut fibres + polymer gel
	Horoshenkov et al. (2013)	Winter Primula vulgaris (Winter primrose)	Canevaflor: perlite + coconut fibres + polymer gel
	D'Alessandro et al. (2015)	Nephrolepis Exaltata (Boston Fern)	Coconut fibres (70%) + expanded perlite (30%)
	Attal, Buot de l'Epine, et al. (2021)	-	Coir dust
Reveberation Chamber	Wong et al. (2010)	Nephrolepis exaltata (Boston fern)	Planting soil
	Yang et al. (2013)	Ivy (Hedera helix)	Canevaflor: perlite + coconut fibres + polymer gel
	Azkorra et al. (2015)	Helichrysum thianschanicum (Silver spike)	Coconut fibres
	Davis et al. (2017)	Nephrolepis exaltata (Boston fern)	Potting soil (50%) + coco chips (33%) + sphagnum moss (17%)
	Thomazelli et al. (2017)	Callisia repens (Creeping inchplant)	Coconut fibres + perlite
	Manso et al. (2017)	Sedum spectabile (Stardust)	Planting soil
	Chang and Chang (2022)	Jacobaea maritima (Silver Ragwort)	Planting soil
	Scamoni et al. (2022)	Indoor large leaves plants	Felt
In situ	Lacasta et al. (2016)	Helichrysum thianschanicum (Silver spike)	Compost (50%) + coconut fibres (50%)
	Lunain et al. (2016)	Mix of species	Compost
	Pérez et al. (2016)	Parthenocissus Tricuspidata (Boston Ivy)	Coconut fibres
	Romanova et al. (2019)	Bergenia cassifolia (Badan)	Planting soil

4.2. Mechanisms Defining Acoustic Performance

In the studies reviewed, VGSs have shown promise in managing outdoor noise through two main mechanisms: Firstly, by utilizing the absorption properties of plants and substrates to reduce the reflected sound field. Secondly, by adding an extra layer to the building surface layers, thereby enhancing acoustic insulation.

However, to enhance the effectiveness of VGSs, it is crucial to develop a thorough understanding of the mechanisms governing all system components. The characteristics of vegetation morphology and substrate properties are identified as the two key factors that determine the acoustic properties of VGSs (Yan, Shen, Zhang, Ye, & Lin, 2022). **Therefore, the primary focus will be on delineating the performance of LWSs.** Additionally, the inclusion of a cavity is acknowledged to enhance the attenuation properties of VGSs.

As a result, the current review predominantly focuses on mechanisms that influence improving sound attenuation qualities of VGSs, particularly LWSs, to reduce the impact of reflected sound waves and mitigate urban noise pollution. This emphasis takes priority over exploring methods to achieve superior insulation properties for building infrastructures.

4.2.1. Foliage mechanisms

The term "vegetation" encompasses the collective plant life in the VGSs, including shrubs, grasses, and other vegetation types. On the other hand, "foliage" specifically refers to the leaves of plants. Foliage constitutes the green, leafy part of a plant responsible for photosynthesis and other vital functions. While foliage is a component of vegetation, not all vegetation consists solely of foliage. Vegetation includes other plant parts such as stems, branches, flowers, and fruits. Nevertheless, for a more focused analysis,

the acoustical performance of vegetation will be examined specifically from the perspective of foliage membranes and the air volumes surrounding them within the vegetation layer of VGS.

Martens, Severens, Van Wissen, and Van Der Heijden (1985) conducted a seminal pilot study on the reflection of sound waves from individual plant leaf. Their interest stemmed from prior experiments revealing vibration patterns across leaf surfaces in the presence of a sound field. Despite these observations, the precise mechanisms governing sound wave reflection, diffraction, and absorption around deciduous plant leaves remained poorly understood. Employing the Theory of Reflections Caused by Discs, they experimented with aluminium discs and leaf cuttings from *Sparmannia africana*. Their findings underscored two key points: firstly, the reflection characteristics of plant leaves, particularly at higher sound frequencies, bear resemblance to reflections from thin plates. Secondly, the mass of leaf tissue plays a significant role in sound wave reflection, especially evident at higher frequencies where the wavelength approaches the leaf radius. Hence, to enhance transmission loss, it is imperative to utilize a heavier leaf mass.

Consequently, the initial premise of regarding a single leaf as akin to a thin plate suggests that when subjected to a sound wave, individual leaves may oscillate, functioning as vibrating panels that absorb sound locally. This phenomenon occurs across a broad range of frequencies, dependent on the wavelength and dimensions of the leaves (i.e., width, length), rather than their shape (Bakker et al., 2023). For example, resonance in vibration typically arises when the sound wavelength matches the size of a leaf (e.g. 15–250 mm for typical plants). In practical terms, a single leaf may resonate more effectively with higher frequency sounds (above 2000 Hz), where the wavelengths are shorter and closer to the size of the leaf. Consequently, the mechanical vibration of individual leaves, triggered by sound waves, results in energy dissipation due to friction with air molecules, converting sound energy into heat (Pérez, Coma, & Cabeza, 2018). Nevertheless, the resulting sound attenuation induced by a single leaf is very small, as mentioned by Bakker et al. (2023), referring to a study they reviewed, which stated that the resonance velocity of a single leaf is 1–3 orders of magnitude slower than the velocity of air particles.

Nevertheless, the VGSs consist of multiple leaves, and if we consider them as an integral foliage element, then the vegetation layer can be considered a (uniform) porous medium (Bakker et al., 2023). This means that when a sound wave hits the foliage layer, the visco-thermal loss mechanism occurs. The visco-thermal mechanism represents the loss of energy due to the transformation from mechanical into thermal energy, the same mechanism as described for individual leaf vibration. However, viscous attenuation occurs due to the interaction between the sound wave and the air molecules within the vegetation layer. Viscosity is a measure of a medium's resistance to deformation. As the sound wave travels through the foliage medium, it displaces the air molecules, causing them to move and exert viscous forces on each other. This interaction results in the dissipation of sound energy, further reducing the intensity of the sound wave. The visco-thermal dissipation mechanism happens mainly in the medium frequency (e.g. 400–2000 Hz) where the acoustic wavelength is larger than the individual leaf dimension (Romanova et al., 2019).

The visco-thermal model of porous layers involves determining various material parameters such as flow resistivity, porosity, tortuosity, and thickness (Bakker et al., 2023; Horoshenkov et al., 2013). However, when it comes to the foliage layer, the visco-thermal properties are primarily influenced by non-acoustic parameters, with leaf area density and dominant directional angle of leaves (Figure 4.2) being key factors. Leaf area density is defined as the ratio between the total leaf area of a plant and an imaginary cylindrical volume drawn around the plant. Research by Horoshenkov et al. (2013) demonstrated that as leaf area density increases, air flow resistivity also rises exponentially. On the other hand, a greater leaf angle extends the propagation path (Bakker et al., 2023), resulting in increased tortuosity. Maximum tortuosity occurs when leaves protrude perpendicularly to the direction of the sound wave's front (Horoshenkov et al., 2013). Consequently, higher leaf area density and larger dominant leaf orientation angles lead to higher values of the acoustic absorption coefficient achievable.

Furthermore, despite being labelled as a porous medium, the foliage layer also possesses unique geometric features. It can be considered as an array of reflectors with randomly sized and oriented leaves (Bakker et al., 2023). Consequently, plant leaves cause diffraction, where sound waves interact by being reflected and scattered by various foliage elements such as trunks, branches, twigs, and leaves (Pérez et al., 2018). Diffraction refers to the bending or spreading out of waves when encountering obstacles. Meanwhile, scattering involves waves being redirected or dispersed in different directions upon encountering rough surfaces or irregularities within a medium. The diffraction, including the scattering effect, can modify the direction and distribution of energy within the nearby sound field near the VGSs,
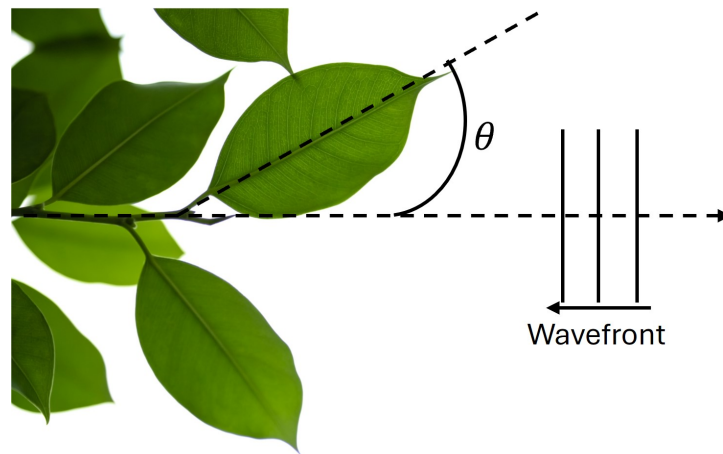
Figure 4.2: Directional angle of leaves relative to incoming wavefront
Note. Adapted from "Vecteezy," by Thipsorn (2022) (`https://www.vecteezy.com/photo/`
`7360323-close-up-of-nature-view-green-leaf-on-white-isolated-background-under-sunlight`
`-with-copy-space-using-as-background-natural-plants-landscape-ecology-cover-concept`).
Licensed under CC BY 4.0.

potentially leading to localized reductions in sound levels, for instance around observers (Bakker et al., 2023).

In these instances, localized reductions in sound levels occur due to a phenomenon called destructive interference, as noted by (Bakker et al., 2023). This occurs when direct and reflected sound waves cancel each other out. The variations in path lengths between these waves contribute to this effect. Moreover, interactions between a porous medium and waves may induce a phase delay, leading to similar cancellations. The frequency at which local destructive interferences become significant for a foliage layer's sound attenuation abilities depends on leaf size. Typically, in higher frequency ranges (above 2000 Hz), where the acoustic wavelength is comparable or smaller than the characteristic leaf dimension, leaf vibration and multiple scattering play a primary role in dissipating energy in the incident sound wave (Romanova et al., 2019). Forecasting the onset of interference in vertical greenery presents a challenge due to the diverse array of factors influencing it. These include wavelengths, leaf size, surface texture, and propagation path length. The irregularity of the foliage layer, coupled with the unpredictability of urban environments, further complicates prediction efforts.

4.2.2. Substrate mechanisms

LWSs are divided into two primary categories: continuous and modular systems. Continuous systems typically incorporate absorption screens made from materials like mineral wool, non-woven mats, and foams, while modular systems utilize a growing medium such as planting soil, organic fibres, or inorganic materials like perlite and expanded clay. Consequently, in both VGSs, the materials used typically possess porous properties, which allow them to absorb sound waves and contribute to the damping of acoustic energy through mechanisms like viscous and thermal losses. This happens due to air behaving like a viscous fluid, experiencing boundary layer effects along the pore walls, where frictional forces convert sound energy into heat (Cox & D'Antonio, 2017). The most basic parameters used to characterise a VGSs are open porosity, tortuosity, pore size, flow resistivity, substrate thickness and moisture content (Bakker et al., 2023).

Open porosity refers to the volume of empty space within a material that can be filled with fluids or gases. It is calculated by comparing the volume of interconnected air spaces in a material to its total volume. In terms of sound absorption, higher open porosity means there are more paths for sound waves to travel through the material and be absorbed. This is because when a sound wave hits a surface, the pores allow it to enter and propagate inside. **Tortuosity**, on the other hand, describes how complex the network of interconnected pores is within a material. It refers to the indirect and irregular path that sound waves must take due to the material's internal structure. Materials with higher tortuosity force sound waves to travel a longer path, resulting in better sound absorption as the waves have more chances to be

absorbed or dissipated within the material. Therefore, both high open porosity and tortuosity are beneficial for sound absorption.

Acoustic sound waves are frequency-dependent, meaning that each frequency has a specific wavelength. Therefore, the **size of pores** in a material plays a crucial role in determining which frequencies can affect the medium. Larger pores offer several advantages for sound absorption. They provide more surface area for sound waves to interact with the material, allowing for deeper propagation and increased absorption through frictional losses and conversion of acoustic energy into heat. Additionally, larger pores reduce the likelihood of sound waves being reflected back into the environment, resulting in improved absorption. Larger pores are also more effective at absorbing lower frequencies of sound because they allow for larger wavelengths to reflect and refract when colliding with pore walls, thereby losing energy (Liu & Chen, 2014). The size of pores in typical planting soil is primarily determined by the texture and roughness of the soil particles. However, these pore sizes can be enlarged through both natural processes, such as bioturbation (Ruiz, Hallett, & Or, 2023), and by human intervention. One method involves incorporating larger inorganic particles, such as perlite and polymer gel, into the soil, or alternatively, incorporating sphagnum moss.

In acoustics, the effectiveness of sound-absorbing materials depends significantly on characteristics such as porosity, pore size, and tortuosity—the extent to which flow paths within the material wind or twist. However, quantifying these metrics consistently across a given fibrous or porous material can be challenging due to inherent variability and complexity. Therefore, a more comprehensive and representative metric for assessing the acoustic performance of such materials is air **flow resistivity**. Flow resistivity, σ refers to the resistance encountered by airflow within a given thickness of material, and serves as an indicator of the air permeability through porous substances (Liu & Chen, 2014). A higher flow resistivity indicates lower air permeability, causing the impedance mismatch between the air and the absorbent (Cox & D'Antonio, 2017). As a consequence, sound reflects from the front face, resulting in reduced absorption due to insufficient propagation of the acoustic wave into the material. However, excessively low flow resistivity diminishes the efficiency of converting sound energy into thermal energy via inner friction and viscosity. Consequently, there exists an optimal value of flow resistivity to achieve optimal sound absorption. Typical average flow resistivity for granular and fibrous materials ranges between 5 and 100 $kPa{\cdot}s/m^2$ (Bakker et al., 2023).

The **thickness** of the porous body significantly influences its ability to attenuate sound. As the material becomes thicker, the pore channels within it extend, allowing for a longer path for the occurrence of energy loss. Additionally, thicker porous bodies tend to shift the peak of their sound absorption coefficient towards lower frequencies (Bakker et al., 2023). However, it is essential to note that while thicker layers may enhance low-frequency attenuation, they may also elevate the material's surface impedance, which can potentially hinder overall sound absorption effectiveness. Therefore, enhancing low-frequency attenuation can also be achieved by incorporating a back cavity behind porous materials, effectively forming a Helmholtz resonance cavity (Liu & Chen, 2014). This principle aligns with the general guideline that porous absorbers perform optimally when positioned at a quarter wavelength distance from a rigid wall relative to the sound frequency they aim to absorb (preferably for the lowest frequency one wishes to treat). This positioning induces a phase shift in the reflected sound wave, aligning it with the absorbed wave, thereby maximizing their cancellation.

Moisture can detrimentally affect the absorption properties of materials, primarily due to its impact on the pore structure and surface properties Bakker et al. (2023). When materials absorb moisture, the water molecules occupy the pore spaces, reducing the volume available for air to flow. This reduction in pore volume diminishes the material's ability to trap and dissipate sound energy effectively. Furthermore, moisture can alter the surface properties of materials, leading to changes in surface impedance. This alteration can affect how sound waves interact with the material's surface, potentially reducing the material's initial absorption efficiency. Research conducted by Horoshenkov et al. (2011) highlighted the significant impact of moisture in the substrate, primarily attributed to capillary forces, which are notably pronounced in the small pores of low-permeable clay-based soil, leading to a drastic decrease in the material's absorption capacity. Furthermore, the presence of polymer gel particles within the low-density substrate resulted in the absorption of a substantial portion of moisture, thereby maintaining the clarity of deeper pores within the material.

As a result, density, depth, and moisture content are identified as the three main factors that influence

the absorption properties of substrates (Yan et al., 2022). Consequently, lightweight substrates are the preferred option for VGSs (Figure 4.3). The substrate's density is intricately linked to its porosity. With increasing porosity, the material's density decreases as the empty voids occupy volume without significantly adding mass. Consequently, lightweight substrates excel in acoustical absorption as described previously, compared to heavy-weighted soils. Moreover, lightweight substrates streamline the construction of VGSs. In contrast, heavy systems pose challenges in their integration into facade structures due to additional structural considerations and potential load-bearing requirements.
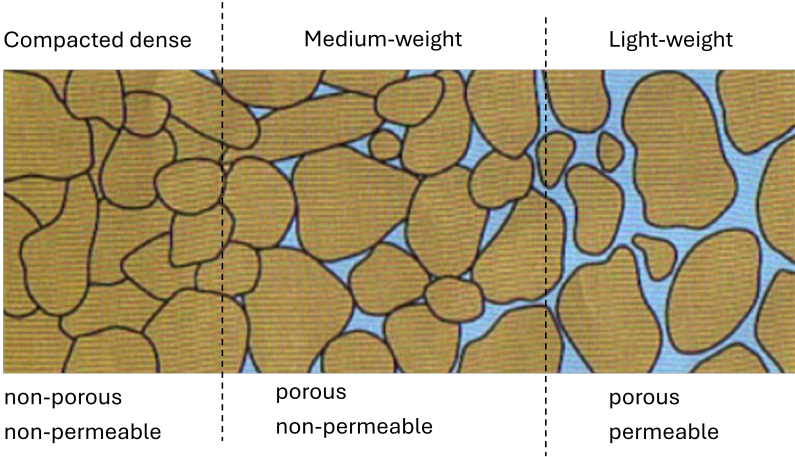
Figure 4.3: Substrate density spectrum
Note. Adapted from "Soil Ecology Wiki," by Cilaird (2023)
(https://soil.evs.buffalo.edu/index.php/File:9FDE2B38-94FC-495B-A12B-F57898660EFC.png).
Licensed under CC BY 4.0.

Additionally, it must be mentioned that temperature changes can also affect sound absorption in typical absorber materials, causing the absorption peak to shift towards higher frequencies with increasing temperature, and vice versa (Liu & Chen, 2014). This phenomenon occurs due to changes in sound speed, wavelength, and airflow resistance as temperatures fluctuate. However, quantifying these mechanisms for VGSs is challenging due to their complex nature, which includes living organisms that respond differently to temperature changes. Moreover, seasonal variations add further complexity to the urban environment, making it difficult to ascertain the precise mechanisms that will affect the absorption capabilities of the substrate.

4.2.3. Cavity Mechanisms

Drawing from the theoretical foundation of foliage and substrate acoustical principles, it is evident that VGSs function as porous absorbers. When strategically positioned in front of rigid facades, VGSs facilitate a complex interaction with impinging sound waves. When VGSs are positioned directly in front of a rigid facade, a portion of the incoming wave is promptly reflected from the VGS surface, while another segment propagates to the VGS and undergoes multiple reflections between the VGS surface and the rear boundary, gradually decreasing in amplitude (Kuttruff, 2007). The reflected sound wave, emerging from the VGS surface, is composed of multiple components that have followed different paths through the porous medium, leading to constructive or destructive interference upon their recombination.

Based on an examination of both researched studies and theoretical principles guiding component performance, it is clear that VGSs exhibit efficient absorption of sound waves within mid- and high-frequency ranges. Consequently, they do not offer significant benefits for attenuating low-frequency noise (below 250 Hz). This limitation in low-frequency absorption can be attributed to the impedance mismatch between the air and the VGS. At a microscale, lower frequencies with longer wavelengths struggle to fit into the pores of the VGS, resulting in high flow resistivity of the layer (Cox & D'Antonio, 2017). Consequently, insufficient acoustic wave propagation diminishes visco-thermal absorption mechanisms.

At a macro-scale, the thinness of the VGS layer compared to the wavelengths of interest, along with its relatively lightweight nature, allows low-frequency sound waves to directly interact with the rigid boundary

behind the VGS, such as building facades. These facades, being acoustically rigid ($z_c \rightarrow \infty$), perfectly reflect incoming waves.

At the interface between the facade and the surrounding air, the sound wave experiences a velocity of zero due to its inability to displace the rigid wall (Howard & Angus, 2017). Consequently, the energy within the sound wave becomes entirely concentrated in the compression of the air, resulting in increased pressure. As this pressure energy cannot propagate in the direction of the advancing wave, it reflects in the reverse direction, inducing a phase shift of 180°in the velocity component of the wave. Therefore, the velocity component of the reflected wave starts to move in the opposite direction (negative x-direction) to that of the incoming wave. This implies that the peak amplitude of velocity starts to align with the lowest amplitude of pressure, and conversely, the peak amplitude of pressure coincides with the lowest velocity amplitude (Kuttruff, 2007).

At points where the sound pressures of both, incident and reflected waves have equal phases, they combine to form pressure maxima (constructive interference), while at points where they have opposite phases, they partially cancel each other (destructive interference) (Kuttruff, 2007). The same holds for the particle velocity. According to the quarter wavelength theory (Field & Fricke, 1998), the reflected sound waves from the rigid facade interfere with the incident waves, forming particle pressure maxima (particle velocity minima) at $n\lambda/4$ distances from the facade, where $n = 0, 2, 4, 6...$ and λ is the wavelength. Conversely, particle pressure minima (particle velocity maxima) are formed at $m\lambda/4$ distances from the facade, where $m = 1, 3, 5, 7....$ According to this theory, in an ideal scenario, the particle velocity at the facade is zero, reaching minima at intervals of $n\lambda/4$, and peaking at intervals of $m\lambda/4$.

Particle velocity rather than pressure is prioritized when positioning absorbers because they efficiently attenuate particle velocity, dissipating sound energy by converting it into other forms like heat. Therefore, to mitigate the mechanism of low-frequency reflection from rigid facades, measures must be taken to prevent the formation of particle velocity maxima. At the first particle velocity maxima, the particles are moving with the highest velocity. In the case of low frequencies, characterized by large wavelengths, it is essential for a reflected wave to travel a considerable distance from the wall to a point where interference can occur and particle velocity maxima occurs. Hence, the typical thickness of VGSs is insufficient to reach this point. Alternatively, one potential solution is to introduce a cavity between the VGS and the rigid facade. The first particle velocity maxima occurs exactly at a quarter of a wavelength distance from the rear facade (Figure 4.4). Placing an absorber at this point allows it to intercept these high-velocity particles effectively, thereby efficiently absorbing sound energy. This, in turn, would decrease the likelihood of the reflected field in the urban environment.
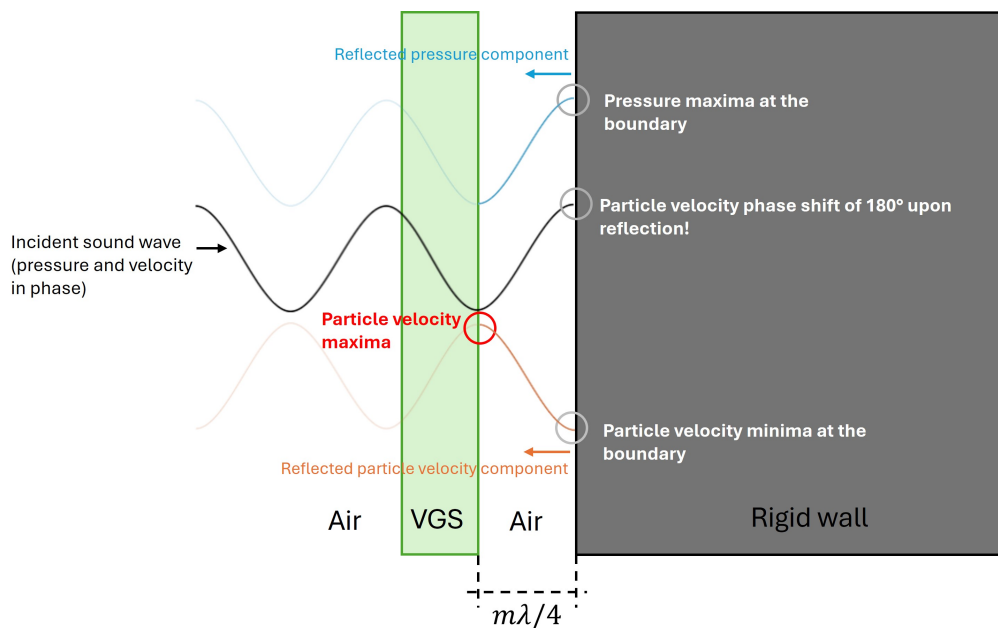
Figure 4.4: Interaction of a reflected wave from a rigid facade with VGS

Part II

Empirical Study: Transfer Matrix Method

<div align="right">

5

</div>

Fundamentals

5.1. Acoustic Theory

5.1.1. Longitudinal plane waves

A sound wave, an acoustic form of a mechanical wave, carries energy by causing the atoms and molecules (particles) in its medium to move. It travels through fluids (liquids or gases) in a manner where the particles move parallel to the wave's direction, known as longitudinal transmission. Consequently, displacement of the medium aligns with, or opposes, the direction of the wave's propagation.

Rarefaction   Compression
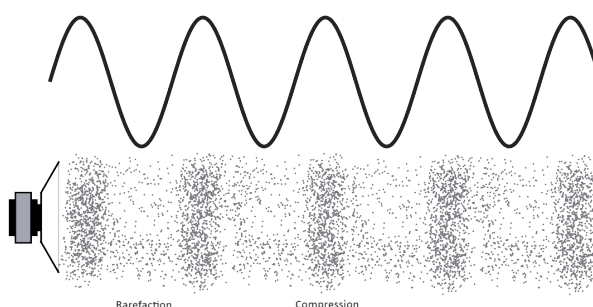
Figure 5.1: Propagation of a longitudinal wave in the right direction; and a sinusoidal pattern projection
Note. From "Wikimedia Commons," by Pluke (2012)
(`https://commons.wikimedia.org/w/index.php?title=File:Plane_Wave_Oblique_View.jpg`).
Licensed under CC BY 4.0.

Longitudinal waves travel with a characteristic acoustic velocity that depends on the medium they pass through (Howard & Angus, 2017). As depicted in Figure 5.1, while propagating, a longitudinal wave creates both compressions and rarefactions within the medium, leading to fluctuations in pressure. These fluctuations in pressure vary according to a harmonic time law (Kuttruff, 2007). In other words, they follow a sinusoidal pattern with a constant frequency and phase across a plane perpendicular to its propagation direction. Consequently, the displacement of the particles along the positive x-direction, y for any position, x and any time, t is represented by Eq.5.1 (Allard, 1993).

$$y(x,t) = A\sin(kx - \omega t + \phi) = Ae^{j(kx - \omega t + \phi)} \tag{5.1}$$

Where: A = Maximum amplitude of the wave

        k = Wavenumber

        ω = Angular frequency

        ϕ = Phase

The force required to displace and accelerate particles forms the pressure component of a wave (Howard & Angus, 2017). For compressions and rarefactions to happen, particles need to either come

closer together or move farther apart. Since motion involves velocity, there's also a velocity component present. Consequently, in a longitudinal wave, pressure and particle velocity synchronize, indicating they travel at the same speed through the medium. When particles move closer for compression, they possess a velocity directed towards each other. This velocity diminishes to zero when compression peaks, as particles momentarily become stationary. Subsequently, as particles move apart during rarefaction, their velocity shifts in the opposite direction until it reaches zero at the trough. Therefore, as illustrated in Figure 5.2, there exists a 90° phase difference between displacement and pressure, and particle velocity components, resulting in the sine-to-cosine relationship. Hence, the harmonic motion of pressure, p and particle velocity, u can be mathematically described for any position, x and time, t as in Eq. 5.2 and 5.3 (Cox & D'Antonio, 2017).
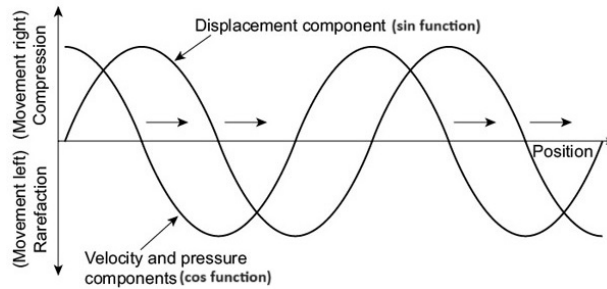
Figure 5.2: Components of a longitudinal wave propagating in a material
Note. From *Acoustics and psychoacoustics* (5th ed.) by Howard and Angus (2017), *Routledge*, Copyright 2017 by Routledge.

$$p(x,t) = A\cos(kx - \omega t + \phi) = Ae^{j(\omega t - kx + \phi)} \tag{5.2}$$

$$u(x,t) = \frac{A}{\rho c}\cos(kx - \omega t + \phi) = \frac{A}{\rho c}e^{j(\omega t - kx + \phi)} \tag{5.3}$$

Where: ρ = Density of the acoustic medium
c = Speed of sound in the acoustic medium
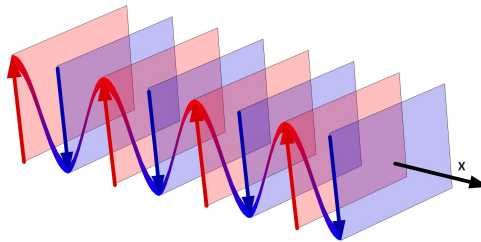
Figure 5.3: Plane wave propagation in x-direction at a constant pressure where velocity and pressure are in phase
Note. From "Wikimedia Commons," by Constant314 (2010)
(https://commons.wikimedia.org/w/index.php?title=File:Plane_Wave_Oblique_View.jpg).
Licensed under CC BY 4.0.

For a longitudinal wave, the plane wave represents an idealized mathematical abstraction. It posits that at any given instant, all variables remain constant on any plane perpendicular to this coordinate (Kuttruff, 2007). Moreover, the plane wave is fundamental in that it serves as a building block, as more complex waveforms can be broken down into combinations of plane waves. Figure 5.3 schematically displays a plane wave propagation pattern, illustrating the transmission of wavefronts that are flat and perpendicular to the direction of propagation.

The propagation of the plane wave in a medium can be described with an analogue to the simple one-dimensional model called the mass-spring model. This model comprises a sequence of masses linked by springs, with the masses symbolizing the point masses of particles in a medium, and the springs depicting the intermolecular forces between them. The mechanism of the plane wave affecting the particles is depicted in Figure 5.4. When one particle is pushed, the connected spring compresses, transferring the push to the next particle, and so forth. Similarly, when one particle is pulled, the spring expands, causing a rarefaction. This periodic alternation between compression and rarefaction allows the medium to return to its normal state, with compressions followed by rarefactions or vice versa.
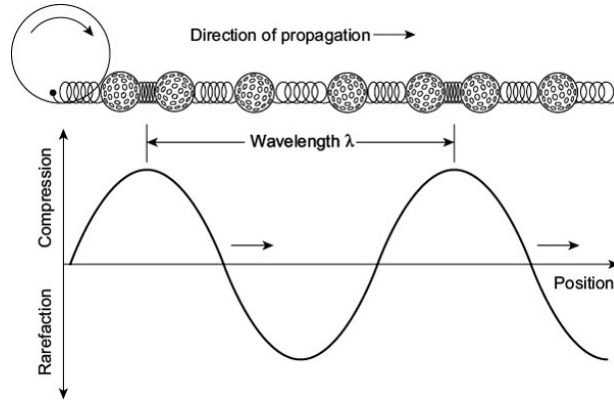
Figure 5.4: Mass-spring model of a plane wave propagating in a medium
Note. From *Acoustics and psychoacoustics* (5th ed.) by Howard and Angus (2017), *Routledge*, Copyright 2017 by Routledge.

5.1.2. Impedance and reactance

The relationship between Eq. 5.2 and 5.3 can be described by their ratio. The ratio of pressure to particle velocity yields the **characteristic specific acoustic impedance** of the medium, z_c (Eq.5.4). The term "characteristic" indicates that the impedance for a wave depends on the characteristics of the propagating medium. Conversely, the term "specific" refers to impedance, representing the pressure–velocity relationship at a particular point in unbound space. As a result, it is also known as "point impedance". The unit of the characteristic specific acoustic impedance in SI system is $Pa{\cdot}s/m$ or $rayl$. Consequently, 1 $rayl$ results from applying 1 pascal of sound pressure, producing a particle velocity of magnitude 1 meter per second.

$$z_c = \frac{p(x,t)}{u(x,t)}$$

(5.4)

If the pressure and particle velocity are in phase, thus have the same time-dependant term $e^{j(\omega t - kx + \phi)}$, then the resulting ratio is equal to a product of the ambient density of the acoustic medium, ρ_0 and speed of sound, c (the speed at which a wavefront advances in a medium). In this case, the characteristic specific acoustic impedance can be referred to as **intrinsic impedance or characteristic impedance**, z_0 (Beranek, 1972), and it describes the lossless (without dissipation) propagation conditions for sound waves moving through a medium, without any reactive (imaginary) component. It represents a bulk property of the medium, assuming the medium's dimensions are infinite (infinite transmission line). Its numerical value in air at 20 °C and at normal pressure is 413 $rayl$.

However, when pressure and particle velocity are not in phase, then characteristic specific acoustic impedance, z_c at a point, x in the medium, by definition, is the complex ratio of a sound pressure amplitude to a vector component of the associated particle velocity (in the direction of the wave propagation) (Acoustical Society of America, 2016; Beranek, 1972; Fahy, 2001). Velocities in the direction along which the complex impedance is typically specified are considered positive (Beranek, 1972). Complex value means that it encompasses both real and imaginary components (Equation 5.5). Consequently, impedance has a magnitude and phase that fluctuate as a function of frequency. In Figure 5.5, the horizontal axis represents the real component, R, while the vertical axis represents the imaginary component X. The subscripts M

and S denote mass and stiffness, respectively. On the plot for a specific frequency, the impedance z is depicted as a vector with magnitude $|Z|$, while its direction indicates the phase angle ϕ.

$$z(f) = R + j(X_M - X_S) \tag{5.5}$$

Where: R = Resistance (real component)

X = Reactance (imaginary component)
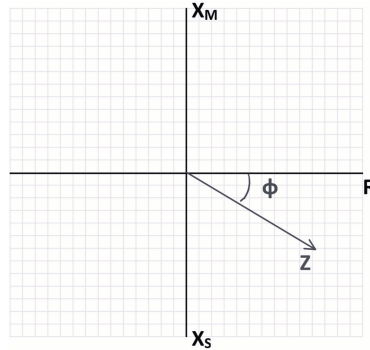
Figure 5.5: Phasor plot representation of the complex impedance
Note. From "Fundamental Concepts for Assessment and Interpretation of Wideband Acoustic Immittance Measurements," by AlMakadma, Kei, Yeager, and Feeney (2023), *Thieme Medical Publishers*, p. 19. Licensed under CC BY-NC-ND 4.0.

The real component of the complex impedance is resistance. Resistance is an aspect of acoustic impedance caused by the internal friction of the transmitting medium. In other words, resistance represents aspects of a vibrating object that loses or dissipates vibratory energy into other forms (AlMakadma et al., 2023). Similar to electrical resistance, which causes the dissipation of power within a circuit and induces a voltage drop in phase with the electrical current, acoustic resistance causes thermoviscous energy losses, characterized by pressure and flow being in phase (Wolfe & Hatsidimitris, 1991).

The imaginary part of the complex impedance is reactance. Reactance is an aspect of acoustic impedance caused by the mass/density and elasticity/stiffness of the transmitting medium (AlMakadma et al., 2023). The principle of mass-reactance, X_M is explained by the behaviour of vibrating particles within the medium, which retain momentum when displaced from a neutral position. Conversely, the principle of stiffness-reactance, X_S entails elastic forces connecting the particles that store and release energy during compression or rarefaction. Even though both mass and stiffness reactance hinder sound vibrations by necessitating energy either for accelerating the mass elements or overcoming the elastic restorative forces, these two types of reactance counteract each other in impeding sound vibrations.

In Equation 5.5, when the $X_S \to 0$, the dominant component becomes the **mass-reactance**, indicating that the medium behaves similarly to a mass-dominated system. In physics, inertia, directly proportional to mass, influences the resistance to changes in velocity over time, while in fluid mechanics, inertance denotes the resistance of a fluid system to changes in flow rate over time. Mass-reactance is, therefore, often referred to as **inertive reactance**.

In a mass-dominated system, higher inertance leads to greater resistance of the medium's response to vibrations. In a mass-spring system analogue, greater inertia implies that the spring will require a larger restorative force to initiate the change in motion of the mass, thereby altering its direction of motion swiftly. This increased resistance to change in motion translates to slower rates of oscillations, as more time is necessary to decelerate the mass in one direction and then accelerate it in the opposite direction. Consequently, mass-dominated systems exhibit vibrations with greater amplitude at low frequencies. At higher frequencies, the rapid oscillations leave less time for the system to overcome its inertia and achieve significant displacement, and, as a result, vibrations are impeded. Moreover, the inertance of the medium introduces a delay between the application of pressure application and the subsequent flow increase, because pressure must be sustained to initiate mass acceleration, thereby inducing flow and enabling the

propagation of a wavefront (Wolfe & Hatsidimitris, 1991). This delay causes the pressure to lead the flow by a phase difference of 90°.

In Equation 5.5, when the $X_M \to 0$, the dominant component shifts to **stiffness-reactance**, indicating the medium's behaviour akin to a stiffness-dominated system. Stiffness, in physics, measures a material's resistance to deformation under applied force, where higher stiffness means minimal displacement for a given force. Compliance, the inverse of stiffness, refers to a material's tendency to deform significantly under load. In acoustics, compliance is analogous to a capacitor's behaviour in AC circuits (Wolfe & Hatsidimitris, 1991). When a wavefront impacts the medium, it deforms slightly, storing energy, which is then released as the material returns to its original state, akin to a capacitor discharging. This phenomenon is why stiffness-reactance is often referred to as **compliant reactance**.

In a stiffness-dominated system, the stiffness overcomes the inertia associated with mass, enabling a rapid restoration of vibratory motion. In a mass-spring system analogue, this rapid restoration is facilitated by the strong restorative force provided by the stiffness of the spring, which counteracts any displacement caused by the applied pressure. As a result, particles quickly return to their original positions. This allows particles to oscillate at faster rates, and consequently, the material vibrates with greater amplitudes. This characteristic of stiffness-dominated systems explains why they impede low-frequency vibrations while facilitating self-sustained vibrations at higher frequencies. Moreover, the stiffness of the medium introduces a delay between the applied pressure and the flow, because there is a need for the flow for a while before the pressure increases much to overcome the elastic restorative forces, and for a wavefront to propagate further (Wolfe & Hatsidimitris, 1991). This delay causes the pressure to lag behind the flow by 90° in terms of phase difference.

5.1.3. Resonance

Acoustic resonance is observed when an object oscillates in phase with incoming sound waves, exhibiting increased vibrational amplitude compared to non-resonant states. Consequently, in the context of a mass-spring system analogy, resonance manifests as significant displacements of the particles (mass) from the equilibrium position at specific driving frequencies. Resonance occurs when the frequency of an external driving force aligns with or is close to the natural frequency, ω_0 of the system. The natural frequency is unique to each system and is determined by its effective mass, m and stiffness, k (Eq.5.6).

$$\omega_0 = \frac{1}{2\pi}\sqrt{\frac{k}{m}} \tag{5.6}$$

However, systems classified as lossy experience a quicker attenuation of vibrations due to energy dissipation, such as thermoviscous losses. The damping ratio, ζ of the system can be calculated using Equation 5.7.

$$\zeta = \frac{c}{1\sqrt{mk}} \tag{5.7}$$

Where: $c =$ Speed of sound of the system

Consequently, the resonant frequency, where the maximum oscillation amplitude is attained, is determined by the interplay of mass, stiffness, and damping within the system. The resonant frequency, denoted as ω_r, can be calculated using Equation 5.8.

$$\omega_r = \omega_0\sqrt{1 - 2\zeta^2} \tag{5.8}$$

Impedance, as the measure of resistance to the propagation of sound waves within a system, determines the acoustic response of the system. Referring to Equation 5.5, the reactance is responsible for the dissipation of the sound energy along the transmission line. When the reactances from mass and stiffness are equal in magnitude but opposite in direction, they cancel each other out, resulting in no net contribution (AlMakadma et al., 2023). This implies that impedance, z equals resistance, R with a phase angle, ϕ of

zero. In other words, when there are no losses, meaning no dissipation of vibrating energy, the opposition to the flow of sound waves is solely due to resistance. Therefore, the resonant behaviour of the system amplifies as the sound waves propagate consistently through the transmission line. As a result, the precisely timed arrival of wavefronts on the system during each cycle results in a gradual amplification of vibrational amplitude.

5.1.4. Wavenumber

The wavelength of a sinusoidal wave is measured as the length of a single wave in meters. Alternatively, the number of radians the wave changes in one meter can be measured to quantify the relationship between frequency and space. This quantity, representing the amount of phase change of the wave per meter, is referred to as the acoustic wavenumber. The wavenumber of a sound wave is given by Eq.5.9, and it has a unit of radians per meter (rad/m). The wavenumber is proportional to frequency.

$$k = \frac{\omega}{c} = \frac{2\pi f}{c} = \frac{2\pi}{\lambda} \tag{5.9}$$

When a material is lossy, meaning that waves dissipate as they propagate, the wavenumber becomes complex. This complex wavenumber determines both the wavelength in the material and the rate of decay of the wave's amplitude (Colton, 2010). When taking the formula for plane wave propagation in the x-direction, if the wavenumber is complex, the wave equation takes on a specific form as described in Eq.5.10.

$$y(x,t) = Ae^{j(kx-\omega t)} = Ae^{j((k_{real}+jk_{imag})x-\omega t)} = Ae^{-k_{imag}x}\cos(k_{real}x-\omega t) \tag{5.10}$$

Consequently, the real part of the wavenumber, referred to as the phase constant, relates to oscillations in space following the typical definition of wavenumber, expressed through the $\cos(k_{real}x-\omega t)$ term. Meanwhile, the imaginary part, also termed the attenuation constant, governs how the wave's amplitude decays as it traverses the material, indicated by the $e^{-k_{imag}x}$ term. Thus, the complex wavenumber is represented by Eq.5.11. The chosen sign convention ensures consistency with propagation in lossy media. When the attenuation constant, $k\prime\prime$, is positive, the wave amplitude diminishes as it propagates in the x-direction.

$$k = k\prime - jk\prime\prime \tag{5.11}$$

Where: $k\prime$ = Phase constant (real component) [rad/m]

  $k\prime\prime$ = Attenuation constant (imaginary component) [Np/m]

The speed of sound in a lossy medium is given by the angular frequency divided by the real part of the complex wavenumber:

$$c = \frac{\omega}{k\prime} \tag{5.12}$$

5.2. Transfer Matrix Method

If the characteristic specific acoustic impedance and wavenumber are known, sound propagation behaviour through the medium can be predicted. That can be accomplished by the TMM, which is a simple and powerful method to model acoustical systems (Dell, Krynkin, & Horoshenkov, 2021). In consideration of the situation depicted in Figure 5.6, TMM establishes a relationship between pressure, p and particle velocity, u across a system, which extends from $x = 0$ to $x = h$. This relationship is described by the 2x2 transfer matrix **T**, which links the acoustic properties on either side of a one-dimensional fluid layer (Eq. 5.13). The transfer matrix **T** is derived under the assumption that only plane waves propagate through the system in the x-direction, meaning it provides the solution for a 1D wave propagation problem (Dell et al., 2021).
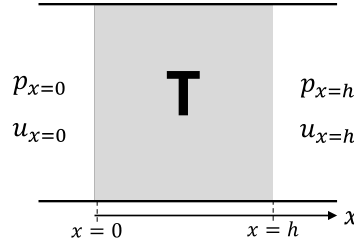
Figure 5.6: 1-D scheme of the TMM applied to a single fluid layer

$$\begin{bmatrix} p \\ u \end{bmatrix}_{x=0} = \mathbf{T} \begin{bmatrix} p \\ u \end{bmatrix}_{x=h} = \begin{bmatrix} T_{11} & T_{12} \\ T_{21} & T_{22} \end{bmatrix} \begin{bmatrix} p \\ u \end{bmatrix}_{x=h} \tag{5.13}$$

Figure 5.7 illustrates a schematic representation of three equivalent fluid layers, each characterized by their own parameters of complex characteristic impedance, z_c and wavenumber, k. By ensuring the continuity of pressure, p and particle velocity, u at the boundaries between these layers, it is possible to establish a relationship between the surface pressure of one layer and that of the next (Eq.5.14). Consequently, the established 2×2 matrix $\mathbf{T}^{Layer2}$ relates the p and the x-component of the u at each face of Layer 2. For a Layer 2, the transfer matrix elements are given by Eq.5.15. The detailed derivation of elements can be found in the work of Allard (1993).
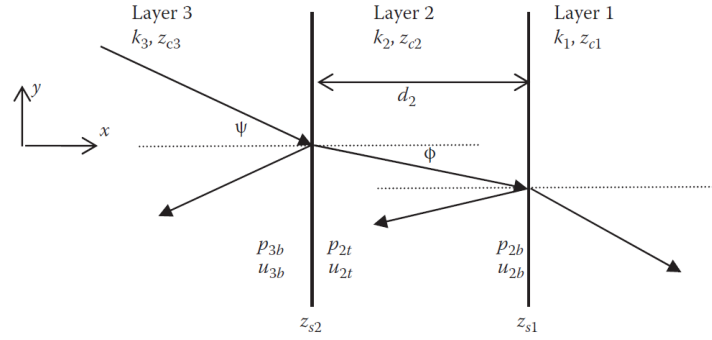
Figure 5.7: Multilayer equivalent fluid system
Note. From *Acoustic absorbers and diffusers : Theory, Design and Application* (3rd ed. p. 30) by Cox and D'Antonio (2017), *Taylor & Francis*, Copyright 2017 by Taylor & Francis.

$$\begin{bmatrix} p_{3b} \\ u_{3b} \end{bmatrix} = \begin{bmatrix} p_{2t} \\ u_{2t} \end{bmatrix} = \mathbf{T}^{Layer2} \begin{bmatrix} p_{2b} \\ u_{2b} \end{bmatrix} \tag{5.14}$$

$$\mathbf{T}^{Layer2} = \begin{bmatrix} \cos(k_{x2}d_2) & j\frac{\omega\rho_2}{k_{x2}}\sin(k_{x2}d_2) \\ j\frac{k_{x2}}{\omega\rho_2}\sin(k_{x2}d_2) & \cos(k_{x2}d_2) \end{bmatrix} \tag{5.15}$$

Where: $k_x = $ x-component of the complex wavenumber
d = Thickness of the fluid layer

Consequently, for a generalization, considering Layer 2 as representative, it is considered that $k_{x2} = k$, $d_2 = d$, and $\rho_2 = \rho$. Additionally, $\omega = 2\pi f$; $k = \frac{2\pi f}{c}$, and $\frac{2\pi f\rho}{2\pi f} = \rho c = z_c$. This leads to the general formulation of the transfer matrix for an arbitrary fluid layer. Eq. 5.16 represents the fundamental formulation

of a transfer matrix for an acoustic fluid layer. A detailed explanation of the parameters can be found in the work of Jiménez et al. (2021).

$$\mathbf{T} = \begin{bmatrix} \cos(kd) & jz_c\sin(kd) \\ j\frac{1}{z_c}\sin(kd) & \cos(kd) \end{bmatrix} \tag{5.16}$$

When a fluid medium is bordered by layers with varying impedances, an impedance mismatch occurs. This mismatch confines the system geometrically, allowing for the assessment of its scattering properties (Jiménez et al., 2021). In acoustics, the scattering behaviour of the material influences both transmitted and reflected waves. Additionally, when losses are considered, the absorption characteristics of the system are affected. A notable characteristic of the fluid transfer matrix, owing to the homogeneous geometric considerations of the model, is that the scattering is reciprocal and symmetric (Herrero Durá, Cebrecos Ruiz, García Raffi, & Romero-García, 2019; Jiménez et al., 2021). Within the linear regime, if the scattering process is reciprocal, transmission through the system is identical in both directions. In other words, the transmission does not depend on the direction of the incident wave. These conditions are satisfied by most of the acoustic materials (Jiménez et al., 2021). Consequently, the determinant of the transfer matrix (Eq.5.16) is unity, expressed as $T_{11}T_{22} - T_{12}T_{21} = 1$. Moreover, the (mirror) symmetry implies that the reflection coefficients, r, obtained from both sides of the system are identical. This condition is met, since in Eq.5.16 $T_{11} = T_{22}$. This implies that the absorption of the fluid layer does not depend on the direction of the wave propagation.

The transfer matrices of individual materials enable the prediction of propagation properties within a multilayered system—a complex acoustic structure composed of several layers. This arrangement can be modelled by repeated application of the transfer matrix equations, as depicted in Figure 5.8. This approach is rooted in the fundamental principle that the transfer matrix characterizing the entire system results from the product of the transfer matrices of the M layers (Eq. 5.17). The multiplication of transfer matrices associated with each constituent layer must be arranged in the order in which they are encountered by the sound wave (Dell et al., 2021). As a result, $\mathbf{T}_{\text{total}}$ offers abundant information about the system as a whole.
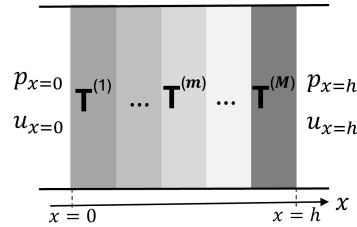
$$\mathbf{T}_{\text{total}} = \prod_{m=1}^{M} \mathbf{T}^m \tag{5.17}$$

Figure 5.8: 1-D scheme of the multilayered system

5.2.1. Equivalent Fluid Model

Porous materials, such as foams or fibrous materials, are composed of a solid skeleton housing pores filled with a fluid, typically air (Figure 5.9)(Jiménez et al., 2021). Understanding sound propagation in porous rigid structures at a microscopic level presents challenges as sound travels both through the pores and within the material's skeleton (Allard, 1993). However, certain simplified assumptions can be made (Jiménez et al., 2021): 1) Given that the pores are much smaller than the characteristic wavelength of sound waves, it becomes feasible to model microscale processes on a macro-scale using an effective medium with effective properties; 2) In practical acoustics, despite elastic waves being able to propagate within the solid framework, the solid skeleton is often considered motionless due to its substantial impedance contrast with the surrounding fluid; 3) In many absorbent materials, the speed of sound is significantly lower than in air, allowing for the assumption, according to Snell's law, that the angle of propagation can be taken as normal to the surface, i.e., $\phi \to 0$ (Cox & D'Antonio, 2017).

Those assumptions align with the understanding that waves travelling through the bulk of a fluid primarily exhibit longitudinal wave characteristics. The absence of rigidity in fluids inhibits particles from exerting forces perpendicular to their neighbours, thereby impeding the propagation of transverse waves. Consequently, longitudinal waves are the predominant mode of wave propagation observed within the bulk of fluids. Therefore, employing the equivalent fluid model is beneficial for modelling porous materials. This model incorporates dissipative processes and is characterized by effective density and bulk modulus (compressibility). Compressibility facilitates the transmission of energy across space within a fluid medium. These parameters depend on the bulk properties of the fluid and the geometry of the fluid domain. That implies that wave propagation through the equivalent fluid medium can be analyzed using frequency-dependant complex characteristic effective impedance and the complex wavenumber (Cox & D'Antonio, 2017; Jiménez et al., 2021).

(a) Original structure **(b)** Equivalent porous structure
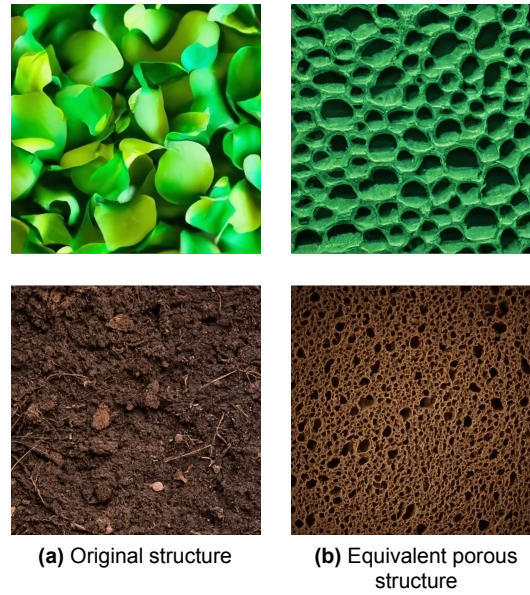
Figure 5.9: Representation of VGS components as porous structures
Note. Adapted from Craiyon (2024) (`https://www.craiyon.com/`). Licensed under CC BY 4.0.

5.2.2. Reflection, Return Loss and absorption

VGSs, whether single-layer or multi-layer structures, are typically enclosed in air. This implies that air impedance, denoted as z_0, remains consistent from both sides. Consequently, the impedance discontinuity between the air and VGS leads to reflections, for which the pressure reflection coefficient can be derived using Eq.5.18. Work by Herrero Durá et al. (2019) offers a derivation of the pressure reflection coefficient, r from a 2×2 transfer matrix. The pressure reflection coefficient provides information about both the relative amplitude (real part) and phase (imaginary part) of the reflected wave with respect to the incident pressure (Kuttruff, 2007).

$$r = \frac{T_{11} + \frac{T_{12}}{z_0} - T_{21}z_0 - T_{22}}{T_{11} + \frac{T_{12}}{z_0} + T_{21}z_0 + T_{22}} \tag{5.18}$$

Where: $z_0 =$ Characteristic impedance of the medium surrounding the system (e.g. air)

However, VGSs can also be rigidly backed with concrete or masonry wall, having boundary condition $v = 0$ at $x = L$ (see Figure 5.6), thus no waves are transmitted through the VGS-wall system. For such conditions, the reflection coefficient can be obtained using Eq.5.19 (Jiménez et al., 2021).

$$r = \frac{T_{11} + \frac{T_{12}}{z_0}}{T_{11} + \frac{T_{12}}{z_0} + T_{21}z_0} \tag{5.19}$$

The portion of incident power reflected from the surface is represented by the reflection power, denoted as $\mathcal{R}$. This coefficient is proportional to the square of the wave's pressure amplitude (Eq.5.20) (Attal, Dubus, et al., 2021).

$$\mathcal{R} = |r|^2 \tag{5.20}$$

If there is no transmission through the rigidly-backed system and only reflection occurs, as described by Eq.5.19, then the absorption coefficient can be derived using Eq.5.21.

$$\alpha = 1 - \mathcal{R} \tag{5.21}$$

Return loss, RL is the ratio, expressed in decibels (dB), which shows what portion of the incident power is reflected from the surface. It focuses solely on the magnitude of the reflected wave compared to the incident wave. RL can be calculated directly from the power reflection coefficient, as expressed in Eq.5.22. In practical terms, a large positive RL value indicates that the reflected power, P_r is small compared to the incident power, P_i. This suggests an efficient transmission or absorption of energy across the system's boundary.

$$RL = 10\log_{10}(\mathcal{R}) = 10\log_{10}\left(\frac{P_r}{P_i}\right) \tag{5.22}$$

6

Experimental Method

6.1. Impedance Tube Working Principle

One common method for characterizing porous materials is through impedance tube measurements using plane wave excitation. The properties of materials can be identified using a quick measurement method known as the "Two-microphone technique for normal sound absorption coefficient and normal surface impedance," which is standardized according to NEN-EN-ISO 10534-2:2023 (2023). The measurements are conducted in a standing wave tube, also referred to as an impedance tube or Kundt tube. As depicted in Figure 6.1, in this measurement setup, a sound source is connected to one end of a tube and the sample to be tested is mounted at the opposite end, with microphones positioned transversely within the tube.
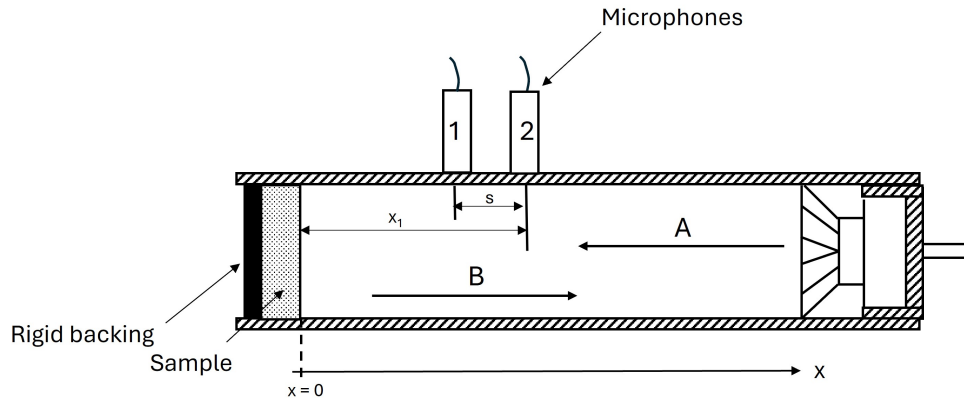
Figure 6.1: Schematic representation of the impedance tube

The sound source emits a wave that, upon reaching the test sample, reflects, causing forward (A) and backward (B) waves to form inside the tube. As denoted in Figure 6.1, the pressure component of the backward travelling wave, occurs along the x-axis, and thus is represented by Eq.5.2. This backward travelling wave experiences a decrease in amplitude due to reflection, resulting in the pressure component described by Eq.6.1.

$$p_B(x,t) = A \cdot r \cdot e^{j(\omega t - kx)} \tag{6.1}$$

Where: r = Pressure reflection coefficient

Hence, the pressure component of the forward travelling wave is described by Eq.6.2.

$$p_A(x,t) = A \cdot e^{j(kx + \omega t)} \tag{6.2}$$

66

Inside the impedance tube, a standing wave pattern is formed due to the combination of a forward travelling sound wave and a backward wave. This standing wave is described by Eq.6.3.

$$p_{tot}(x,t) = p_A + p_B = A\left(e^{j(kx+\omega t)} + r \cdot e^{j(\omega t - kx)}\right) \tag{6.3}$$

The two microphones, as depicted in Figure 6.1, simultaneously measure the sound pressures, p_1 and p_2, respectively, at two locations near the sample, identified along the x-axis as x_1 and x_2, at the same arbitrary time ($t = 0$ for simplicity).

$$p_{tot}(x = x_1, t = 0) = p_1 = A(e^{j(kx_1)} + r \cdot e^{-j(kx_1)}) \tag{6.4}$$

$$p_{tot}(x = x_2, t = 0) = p_2 = A(e^{j(kx_2)} + r \cdot e^{-j(kx_2)}) \tag{6.5}$$

Consequently, the complex acoustic transfer function H_{12} of the two microphone signals is subsequently determined. This transfer function is merely the ratio of pressures measured by the microphones. The transfer function between microphone positions 1 and 2 is defined in Eq.6.6.

$$H_{12} = \frac{p_2}{p_1} = \frac{e^{j(kx_2)} + r \cdot e^{-j(kx_2)}}{e^{j(kx_1)} + r \cdot e^{-j(kx_1)}} \tag{6.6}$$

Rearranging Eq.6.6 directly yields the normal-incidence complex pressure reflection coefficient, r at the reference plane (x = 0) (Eq.6.7).

$$r = \frac{-H_{12} \cdot e^{j(kx_1)} + e^{j(kx_2)}}{H_{12} \cdot e^{-j(kx_1)} - e^{-j(kx_2)}} \tag{6.7}$$

With the reflection coefficient, it is possible to obtain the normal-incidence absorption coefficient, α_n (Eq.6.8).

$$\alpha_n = 1 - |r|^2 \tag{6.8}$$

Impedance, being the ratio of pressure to particle velocity, necessitates consideration of the particle velocity component. Similar to the pressure component, the particle velocity component of the forward travelling wave is described by Eq.6.9, while that of the backward travelling wave is given by Eq.6.10. Upon reflection, the particle velocity component of the backward travelling wave changes its direction by 180 degrees, resulting in a negative sign. Consequently, by accounting for both the forward and backward travelling waves, the particle velocity in the tube can be determined by Eq.6.11.

$$u_A(x,t) = \frac{A}{\rho c} e^{j(kx+\omega t)} \tag{6.9}$$

$$u_B(x,t) = -\frac{A \cdot r}{\rho c} e^{j(\omega t - kx)} \tag{6.10}$$

$$u_{tot}(x,t) = u_A + u_B = \rho c \left(e^{j(kx+\omega t)} - r \cdot e^{j(\omega t - kx)}\right) \tag{6.11}$$

After that, the impedance of the air inside the tube is determined in accordance with Eq.6.12.

$$z(x) = \frac{p_{tot}}{u_{tot}} = \rho c \frac{e^{j(kx+\omega t)} + r \cdot e^{j(\omega t - kx)}}{e^{j(kx+\omega t)} - r \cdot e^{j(\omega t - kx)}} \tag{6.12}$$

As a result, it is possible to derive the impedance, z at the reference plane (x=0) as described in Eq.6.13. This impedance z_s is known as the normal-incidence surface impedance.

$$z(x=0) = z_s = \rho c \frac{e^{j0} + r \cdot e^{j0}}{e^{j0} - r \cdot e^{0j}} = \rho c \frac{1+r}{1-r} \qquad (6.13)$$

Typically, z_s is normalized by the impedance of air (Eq.6.14).

$$z_n = \frac{z_s}{\rho c} = \frac{1+r}{1-r} \qquad (6.14)$$

Normal-incidence surface specific impedance, z_s at any one point on the interface between different media, by definition, is the complex ratio of the sound pressure to the normal component of the sound particle velocity (NEN-EN-ISO 10534-2:2023, 2023; Fahy, 2001). It describes the transmission conditions for sound energy moving from one medium to another. Consequently, this quantity is useful to analyse the impedance matching of a given test sample with the surrounding media, e.g. air.

As described by Eq. 6.14, the (normalized) surface impedance serves to elucidate alterations in both the magnitude and phase of a reflected pressure at the surface of interest. This impedance encompasses both resistance (real part) and reactance (imaginary part) concerning the surface's interaction with sound waves. Broadly, the real term of surface impedance correlates with energy dissipation (resistance component), while the imaginary term relates to phase alterations (reactance component). The resistance component indicates how effectively a surface absorbs sound energy. Surfaces with high resistance absorb very little sound energy and mostly reflect it, while those with low resistance absorb more sound energy and reflect less. For example, when a wall is rigid, its surface impedance approaches infinity because air particles cannot move against it. The reactance component of surface impedance reflects the surface's reactive nature, leading to differences in phase between reflected and incoming sound waves.

All derived quantities in this section, including H_{12}, r, α_n, and z_s, are frequency-dependent.

6.1.1. Working frequency range

Within an impedance tube, the mathematical problem simplifies to one dimension: sound waves propagate solely along a single axis. However, this limitation exists only within a specific frequency range, corresponding to $f_1 < f < f_u$ (NEN-EN-ISO 10534-2:2023, 2023). The working frequency range hinges on the lateral dimensions or diameter of the tube and the spacing between microphones.

To ensure the generation of plane propagating waves in the tube, the frequency of the sound waves must be maintained below the cut-off frequency, f_u. Beyond this frequency, the specific acoustic impedance within the tube alters due to the presence of standing waves perpendicular to the direction of the sound wave (de Bree, 2009). The cut-off frequency is inversely proportional to the tube diameter (Eq.6.15).

$$f_u < \frac{0.58c}{d} \qquad (6.15)$$

Where: d = Diameter of the tube

c = Speed of sound inside the tube

Furthermore, it is essential to establish the lowest working frequency limit, f_1 in order to avoid singularities. This limit is contingent upon the spacing between the microphones. As a general guideline in NEN-EN-ISO 10534-2:2023 (2023), the spacing between microphones should exceed 1.5% of the wavelength corresponding to the lowest frequency of interest (Eq.6.16).

$$s > 0.015\lambda_1 \rightarrow f_1 > \frac{0.015c}{s} \qquad (6.16)$$

Where: s = Spacing between two microphones

Nevertheless, at low frequencies, the impedance tube method may not yield accurate results, even for frequencies above f_1, due to the requirement for an airtight fit of the sample while also allowing it to vibrate freely. Consequently, the influence of the rigid tube wall on the test sample cannot always be disregarded. Materials with high flow resistivity react to a sound field by vibrating, causing friction losses in the tube and altering the measured damping properties. Therefore, there remains a need for free-field measurements to accurately assess material performance and validate the collected data. (de Bree, 2009)

6.2. Measurement Protocol

In the impedance tube, the test sample layer between x = 0 and the rigid backing behaves in a specific manner when waves interact with it. Upon arrival, some of the incoming wave bounces off the surface of the test sample right away. Simultaneously, another portion of the wave penetrates the sample material, subsequently initiating a series of reflections between the surface and the rigid backing. Throughout these reflections, the amplitude of the wave gradually diminishes, ultimately dissipating within the material. Whenever this internal wave reaches the plane x = 0, a fraction of it will leave the layer. The reflected sound wave is formed by the superposition of all these sound wave portions, each of which has travelled varying distances within the test sample layer, resulting in either constructive or destructive interference. (Kuttruff, 2007)

As a result, the directly measured surface impedance is contingent upon the specific parameters of the measurement setup, including factors like the thickness of the test sample and the conditions of the backing material. Consequently, there arises a necessity for acoustic properties of the test sample that remain unaffected by variations in the measurement configuration. These properties, such as characteristic impedance and wavenumber, provide a more comprehensive understanding of the sample's bulk behaviour.

The relationship between surface impedance, z_s, characteristic impedance, z_c as well as wavenumber, k, for the measurement setup with rigid backing, is shown in Eq.6.17 (Kuttruff, 2007).

$$z_s = -jz_c cot(kd) \tag{6.17}$$

Where: $d = $ Thickness of the sample

Mathematically, deriving z_c and k is feasible by considering two distinct surface impedances that are dependent on the geometry of the sample as well as backing conditions. Consequently, there exist measurement methods specifically designed to facilitate this derivation. In the methods discussed below, the original publications use the propagation constant, γ instead of the wavenumber, k. However, k and γ are related by $k = -j\gamma$ or $\gamma = jk$ (Cox & D'Antonio, 2017).

6.2.1. Two-thickness method
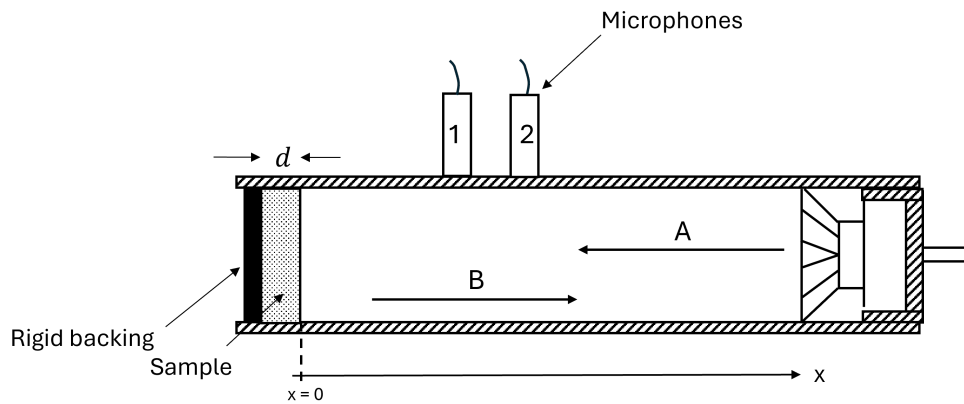
Figure 6.2: Schematic representation of the two-thickness method

Smith and Parrott (1983) had developed a method denoted as "two-thickness". The surface impedances are measured for two different thicknesses of the samples with a rigid backing (Figure 6.2). The thicknesses of the test samples should be such that $d_2 = 2d_1$. Consequently, the measured surface impedances are related to the characteristic impedance and wavenumber by:

$$z_{s1} = -jz_c \cot(kd_1) \tag{6.18}$$

$$z_{s2} = -jz_c \cot(kd_2) \tag{6.19}$$

Where: z_{s1} = Surface impedance of the sample with thickness d_1
z_{s2} = Surface impedance of the sample with thickness d_2
z_c = Characteristic impedance of the material
k = Wavenumber

The equations for z_{s1} and z_{s2} can then be rearranged using trigonometric identities and solved to give the characteristic impedance, z_c and wavenumber, k:

$$z_c = \sqrt{z_{s1}(2z_{s2} - z_{s1})} \tag{6.20}$$

$$k = \frac{-1j}{d_2} \ln\left(\frac{1+a}{1-a}\right) \tag{6.21}$$

Where: $a = \sqrt{(2z_{s2} - z_{s1})/z_{s1}}$.

As noted by Smith and Parrott (1983), two-thickness method becomes unreliable when z_{s1} approaches z_{s2}. This happens when $kd_1 = kd_2 \pm n\pi$, where n is an integer. Consequently, in order to avoid that, it is necessary to choose the thicknesses of the layers so that $z_{s1} \neq z_{s2}$. Unfortunately, there is no way to test for this before the measurements, as the wavenumber is unknown. As a result, these criteria must be checked for in analysing the results, and if necessary, another set of thicknesses measured.

6.2.2. Two-cavity method
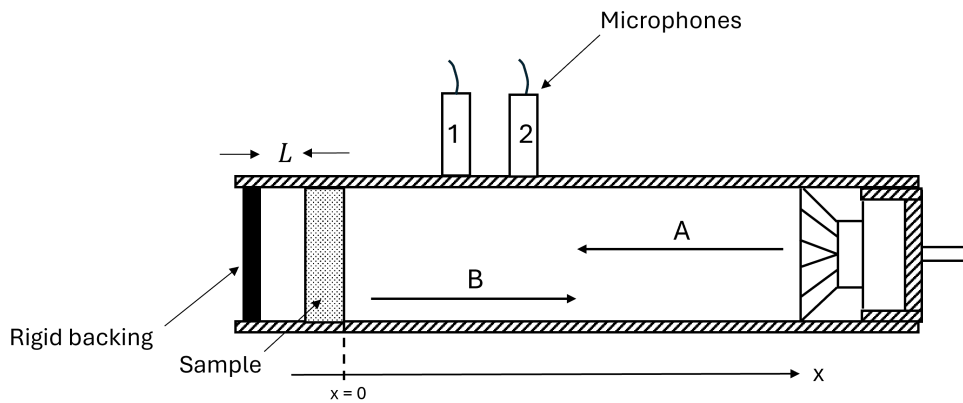
Figure 6.3: Schematic representation of the two-cavity method

Utsuno, Tanaka, Fujikawa, and Seybert (1989) had developed a method denoted as "two-cavity". The surface impedances are measured for a single test sample with two distinct rear cavity depths, indicating that the sample is backed by an arbitrary impedance (Figure 6.3). The impedances of the arbitrary cavities can be obtained by:

$$z_{l1} = -jz_{air} \cot(kL_1) \qquad (6.22)$$

$$z_{l2} = -jz_{air} \cot(kL_2) \qquad (6.23)$$

Where: z_{l1} = Surface impedance of the cavity with depth L_1
z_{l2} = Surface impedance of the cavity with depth L_2
z_{air} = Characteristic impedance of air $\rho_0 c$
k = Wavenumber of air

Parameters z_{l1} and z_{l2} can then be used to solve for the characteristic impedance z_c and wavenumber k:

$$z_c = \pm\sqrt{\frac{z_{s1}z_{s2}(z_{l1} - z_{l2}) - z_{l1}z_{l2}(z_{s1} - z_{s2})}{(z_{l1} - z_{l2}) - (z_{s1} - z_{s2})}} \qquad (6.24)$$

$$k = \frac{-1j}{2d} \ln\left(\frac{z_{s1} + z_c}{z_{s1} - z_c}\frac{z_{l1} - z_c}{z_{l1} + z_c}\right) = \frac{-1j}{2d} \ln\left(\frac{z_{s2} + z_c}{z_{s2} - z_c}\frac{z_{l2} - z_c}{z_{l2} + z_c}\right) \qquad (6.25)$$

Where: d = Thickness of the sample
z_{s1} = Surface impedance of the sample with the cavity depth L_1
z_{s2} = Surface impedance of the sample with the cavity depth L_2

The sign in Eq. 6.24 must be chosen to ensure that the real part is positive.

In this method, Utsuno et al. (1989) emphasize the importance of selecting an appropriate set of cavity depths to ensure reliable results. This selection is crucial for avoiding the condition where $f(L_1 - L_2) = nc/2$, where, n is an integer and c is the speed of sound in the cavity. Otherwise, z_{l1} approaches z_{l2}, leading to z_c approaching $\pm z_{l1}$, that is, the characteristic impedance of the test sample equals the impedance of the closed tube.

6.2.3. Modified two-cavity method
Larner and Davy (2014) had combined the two above prediction methods and called it a "modified two-cavity method". The surface impedances are measured for a single test sample with a rigid backing and an arbitrary cavity depth. Consequently, the surface impedances of the two backing boundaries are:

$$z_{l1} = \infty \qquad (6.26)$$

$$z_{l2} = -jz_{air} \cot(kL) \qquad (6.27)$$

Where: z_{l1} = Surface impedance of the rigid backing
z_{l2} = Surface impedance of the cavity with depth L

As a result, a modified version of the Eq.6.24 and 6.25 yields the characteristic impedance z_c and wavenumber k as follows:

$$z_c = \pm\sqrt{z_{l2}(z_{s2} - z_{s1}) + z_{s1}z_{s2}} \qquad (6.28)$$

$$k = \frac{-j}{2d} \ln \left(\frac{z_{s1} + z_c}{z_{s1} - z_c} \right) \tag{6.29}$$

Where: z_{s1} = Surface impedance of the material with the rigid backing

z_{s2} = Surface impedance of the material with the cavity depth L

As a result, this method eliminates two uncertainties: first, only one test sample is used, removing the need to alter the measurement setup by changing the test samples as it is in the two-thickness method. Second, it eliminates the imprecision associated with measurement condition checks. For Smith and Parrott (1983), this involved ensuring appropriate test sample thicknesses, while for Utsuno et al. (1989), it entailed ensuring appropriate cavity depths.

7

Experimental Procedure

7.1. Test Samples

7.1.1. Selection procedure

To identify the optimized design solution for VGS addressing urban noise mitigation, it is essential to consider VGS types that offer flexibility in design. From the literature study on VGSs taxonomy (Section 2.3), **it was determined that LWSs show the greatest potential for design adjustability in terms of thickness and components.** Specifically, systems such as the Geotextile Felt System, Panel System, and Framed Box System — details of which are highlighted in Figure 7.1 — are noted for their flexibility and potential application in noise mitigation strategies. Notably, LWSs have also been found to outperform GFs in terms of acoustic performance (Chapter 4). Therefore, particular emphasis should be placed on the components comprising the highlighted LWSs.

(a) prod. *F+P System*
Note. Adapted from SingularGreen (2021) (`https://www .singulargreen.com/ sistema-fp-cold/`). Copyright 2024 by SingularGreen.

(b) prod. *VersiWall GM*
Note. Adapted from Elmich (2016) (`https://elmich.com/asia/ ?portfolio=national-gallery -singapore`). Copyright 2023 by Elmich.

(c) prod. *Flexipanel*
Note. Adapted from SemperGreenwall (2023) (`https:// sempergreenwall.com/news/ on-what-kind-of-rear-walls-can -you-mount-a-living-wall/`). Copyright 2024 by SemperGreenwall.

Figure 7.1: Flexible LWS types for design modifications

Selecting plant test samples

LWSs have the potential to thrive in various climates, provided that the appropriate plant selection is made (Ogut et al., 2022). Prioritizing environmental conditions (temperature, humidity, wind, drought, frost,
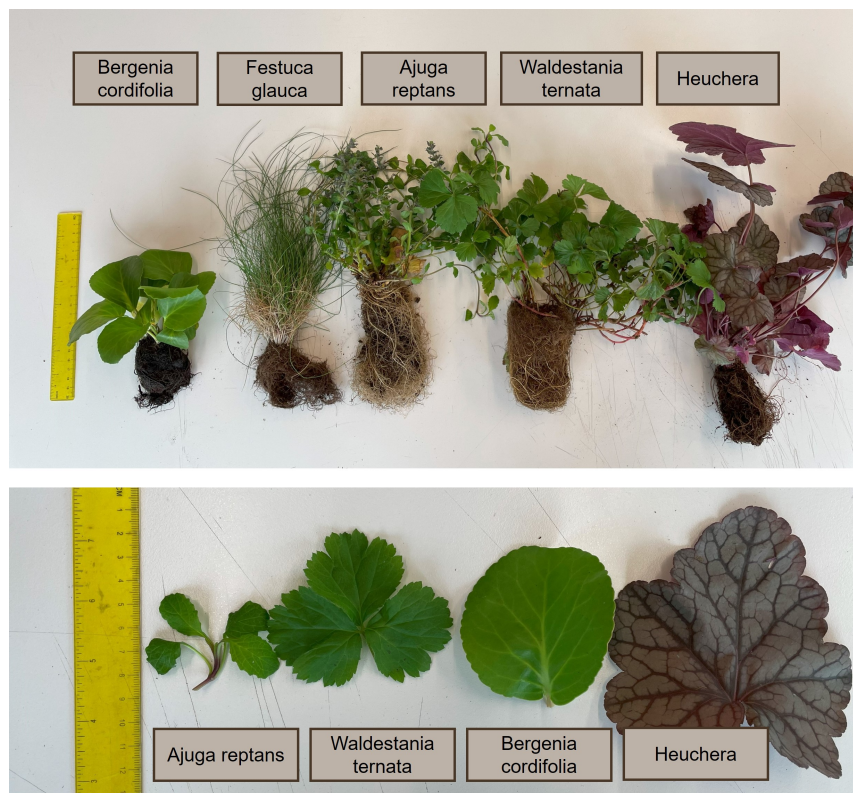
Figure 7.2: Selected plant species with corresponding leaf morphologies

rainfall) and light availability (orientation, sun, shade, semi-shade) over aesthetics during plant selection enhances durability, regardless of the location or climate (Manso & Castro-Gomes, 2015; Riley, 2016). However, the current research does not focus extensively on these factors due to its primary emphasis on the research objectives. Yet, to effectively achieve sustainability goals, it is crucial to prioritize vegetation that requires minimal maintenance, with a focus on native perennial plants, ideally evergreens. In the current study, native plants must be compatible with the temperate (maritime) climate.

During the literature review concerning suitable vegetation for LWSs as discussed in Section 2.4.1, various authors have presented plants suitable for specific climates. For instance, Stollberg and von Birgelen (2023) conducted experiments under a temperate climate in Germany, observing that Tellima grandiflora 'Rubra', **Waldsteinia ternata**, Pachysandra terminalis, and **Heuchera Hybride 'Purple Petticoats'** were among the most attractive perennial plants throughout the year. Similarly, Martensson et al. (2016) explored a temperate maritime climate in Sweden, suggesting evergreen perennial species such as Chamaecyparis pisifera, Euonymus fortuneii, Euphorbia polychroma, Vinca minor, and **Waldsteinia ternata** as suitable for LWSs. However, some studies focused on more continental European climates. For example, Cojocariu, Chelariu, and Chirută (2022) investigated flowering species in a continental climate in Romania, identifying **Heuchera x hybrida 'Fire Alarm'**, **Heuchera x hybrida 'Marmalade'**, and **Festuca galuca** as promising options for LWSs. Similarly, Cechová et al. (2023) provided insights into a humid continental climate in the Czech Republic, suggesting species like Deschampsia caespitosa 'Goldtau', **Festuca glauca**, and Festuca ovina as suitable choices for LWSs, particularly due to their adaptability across different cardinal directions and substrates. In addition to research publications, industry representatives and their guidelines and proposals can provide valuable insights into which plant species are suitable for specific locations. For instance, Sempergreen company's assortment (SemperGreenwall, 2024b) of suitable outdoor plants in temperate maritime climate for the system depicted in Figure 2.6, confirms the suitability of plants like **Waldsteinia ternata**.

However, in line with the research objective, the primary focus regarding the performance of LWSs plants, besides their suitability for climatic conditions, is their acoustic performance. Generally, it has been observed that plants with higher leaf area density and those oriented perpendicular to the incident sound

wave direction demonstrate enhanced absorption capabilities. The most promising plant species in terms of sound attenuation, as gathered from various empirical studies analyzed, are compiled in Table 4.2. For example, **Bergenia cordifolia** serves as a suitable representative due to its adaptation to the local climate, as outlined in Sempergreen's guidelines, and it demonstrated significant acoustical attenuation capabilities, as evidenced by Romanova et al. (2019).

As a result, the suitable plant species were selected for the current study as depicted in Table 7.1 and Figure 7.2. It is evident that for LWSs evergreen grasses like **Festuca glauca**, along with perennial plants such as **Heuchera** and **Waldsteinia ternata**, are considered versatile, thriving across various climatic conditions. **Bergenia cordifolia** stands out as a notable example, excelling not only in specific climatic conditions but also in acoustic performance. Additionally, **Ajuga reptans** was chosen from Sempergreen's guideline list. Its suitability for the local climate, combined with its relatively small leaves, makes it a valuable candidate for investigating and validating the mentioned design considerations related to acoustic performance.

Selecting substrate test samples

In the literature review addressing suitable substrates for both continuous and modular LWSs, discussed in Section 2.4.2, specific substrates emerged as the most suitable options for both system types. For continuous LWSs, the typical substrates used are mineral wool, geotextile, and foam. Regarding the main research aim of enhancing LWSs in terms of their acoustical performance, it was found that adequate soil depth is vital for sound absorption. Geotextile layers, due to their relatively thin layer thickness, are challenging to modify to meet enhanced performance requirements. Foam, though considered a convenient substrate and modifiable in terms of layer thickness, has a relatively low lifespan. This is because foam is more susceptible to damage from growing roots compared to mineral wool. Therefore, mineral wool is found to be a more sustainable choice for modular LWSs. Mineral wool, due to its microstructure, offers great water retention capabilities and sufficient oxygenation of the root zone. The open pores in mineral wool enhance its acoustical performance.

In modular LWSs, substrates can be categorized into inorganic and organic materials. Common inorganic substrates include mineral wool, geotextile, and foam, as well as perlite, vermiculite, and expanded clay. Pumice, already popular in green roofs, also shows potential for LWSs; however, its heavy structure presents challenges in achieving lightweight systems. Typical organic materials used in modular LWSs are (stabilized) peat, coco peat, coco coir, and sphagnum moss. Peat is not considered sustainable due to its extraction from finite peatlands, which are crucial for climate change mitigation and carbon sequestration. As a result, it is not considered in the current study. Conversely, coco peat and coco coir, derived from the fibrous outer husk of coconuts, are more sustainable alternatives. Coco coir and coco peat are made from the same material: the fibrous outer husk of a coconut. Characterized by differences in texture, with coco peat having a finer, powdery texture and coco coir possessing a coarser, more fiber-like structure, they are often considered similar or even the same. Therefore, for this study, coco husk was chosen instead of coco peat to compare the acoustical properties of substrates with coarse particles to those with fine constituents. Additionally, sphagnum moss, although an aquatic plant found in peatlands, is considered renewable as it regenerates after harvesting (Pouliot, Hugron, & Rochefort, 2015). Its cellular microstructure enables it to absorb water effectively and enhance water-holding capacity (of California Museum of Paleontology, 1999). Hence, it is being examined in this study to assess its acoustical properties.

Consequently, suitable substrates were meticulously chosen for the study, detailed in Table 7.1 and visually represented in Figures 7.3 and 7.4. These test samples were selected to encompass both organic and inorganic materials, ensuring representation across modular and continuous LWSs. Figure 7.4 showcases a module from the panel system previously discussed (Figure 2.6). Despite the system being predominantly considered in the context of modular LWSs, mineral wool, its substrate, finds extensive use in continuous LWSs as well. While the panel comprises multiple layers, mineral wool primarily functions as the key acoustic attenuation layer due to its modifiability in terms of thickness. Thus, the study will focus primarily on assessing the quality of mineral wool in further detail.

Figure 7.3: Selected substrates: from left to right — top row (inorganic): expanded clay balls, perlite, vermiculite, pumice; bottom row (organic): coco coir, coco husk, sphagnum moss. Supplied by Sybotanica.
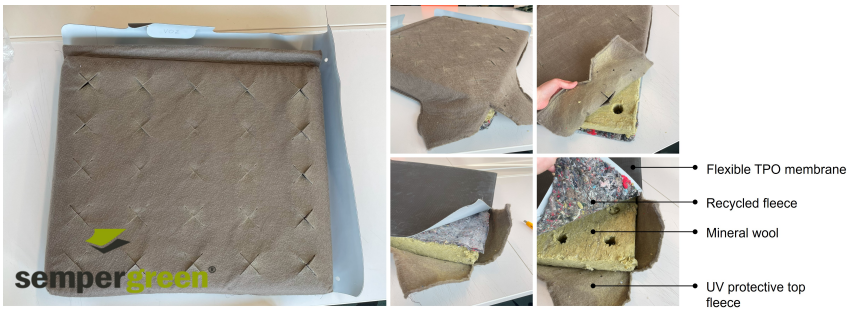
Figure 7.4: Selected test sample: mineral wool. Extracted from Sempergreen's *Flexipanel* module.

Table 7.1: Selected test samples

Layer	Component name	Label in the empirical study
Substrates	Expanded clay balls	Clay balls
	Coco coir	Coco coir
	Coco husk	Coco husk
	Mineral wool	Mineral wool
	Sphagnum moss	Moss
	Perlite	Perlite
	Pumice	Pumice
	Vermiculite	Vermiculite
Vegetation	Heuchera 'Cascade Dawn'	Heuchera
	Bergenia cordifolia	Bergenia
	Waldestania ternata	Waldestania
	Ajuga reptans	Ajuga
	Festuca glauca	Grass

7.1.2. Preparation procedure

The test samples needed to be prepared to ensure suitability for the measurement setup, as outlined in Section 7.2. To prepare the plant test samples, it was necessary to construct test sample holders made of cardboard (Figure 7.5). This served two main purposes: firstly, to ensure that the foliage is evenly distributed throughout the entire volume of the sample holder, achieving the most homogeneous distribution possible; and secondly, to incorporate textile nets on the top and bottom of the sample holder. These nets help maintain the air/plants interface perpendicular to the tube axis and serve as reference surfaces.

The procedure for preparing plant test samples is depicted in Figure 7.6. Unfortunately, conducting plant measurements in the impedance tube presents significant challenges, as the required procedure often alters the original morphology of the plant. To minimize these changes, sample holders were carefully selected to accommodate the height of the plants as closely as possible, without exerting excessive compression. The goal was to achieve a homogeneous distribution of leaves in the test sample, allowing it to replicate the porous structure and real-life conditions where foliage is fully exposed. In natural settings, this foliage forms a continuous layer without significant gaps or bald spots.

Despite efforts to achieve homogeneity, as illustrated in Figure 7.7, this proved to be challenging. For several plants, the leaf size exceeded the diameter of the sample holder, significantly altering the leaves' morphology and, in some cases, causing them to fold. Furthermore, it was essential to minimize the influence of roots on sample absorption to ensure that the performance assessment was focused solely on the foliage.

Perlite, vermiculite, expanded clay, pumice, and sphagnum mosses are considered loose substrates, necessitating the use of a sample holder. The procedure for preparing these test samples is the same as for plants and is depicted in Figure 7.8. Substrates with larger particle sizes, such as clay balls, perlite, and coco husk, required a taller sample holder — 4 cm and 8 cm — than those used for smaller particle substrates, which were 3 cm and 6 cm tall. This adjustment was necessary to achieve the optimal thickness of the test samples.

Due to their loose nature, it is essential to stretch a fabric net to hold the substrate in place. Additionally, it must be ensured that there are no gaps in the vertical orientation so that the substrate is tightly contained within the sample holder. The latter is a tricky procedure as it depends strongly on the degree of soil compaction, which is difficult to match exactly between two test samples of the same substrate.

On the other hand, the mineral wool test sample was precisely cut to the appropriate diameter from the Flexipanel module, as illustrated in Figure 7.9.
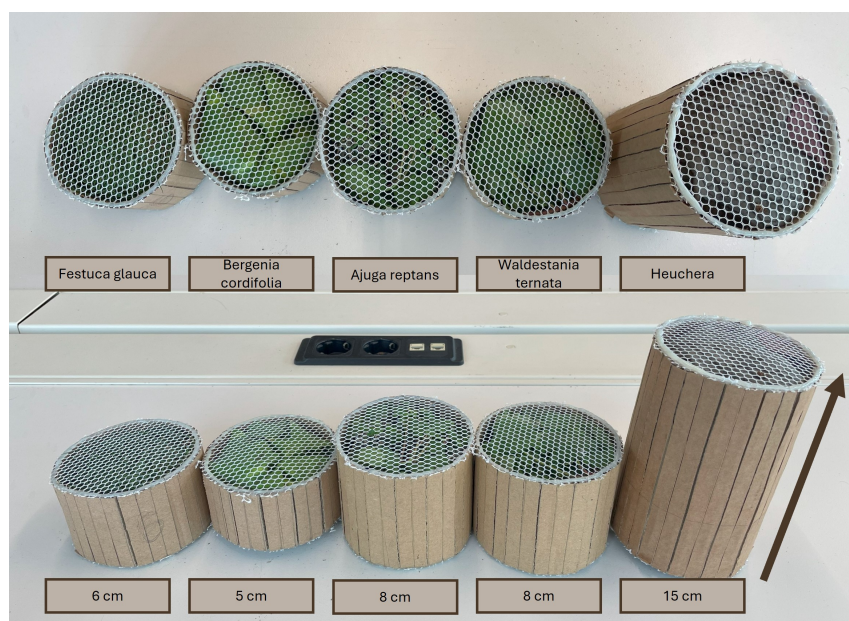
Figure 7.5: Test samples utilized in the experiment
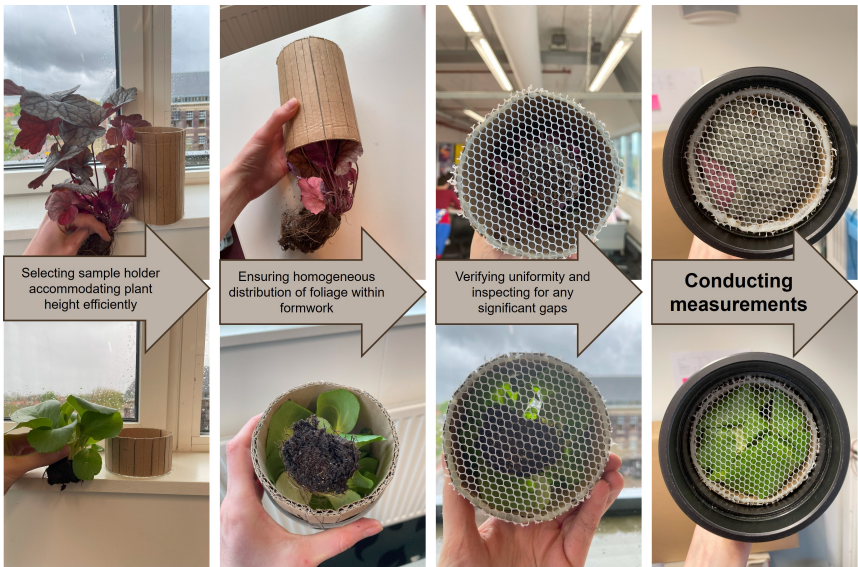
Figure 7.6: Procedure for preparing plant test samples

Figure 7.7: Main challenges in plant test samples preparation: left: altering the morphology of the plant and its leaves, right: minimizing the influence of roots on the experiment
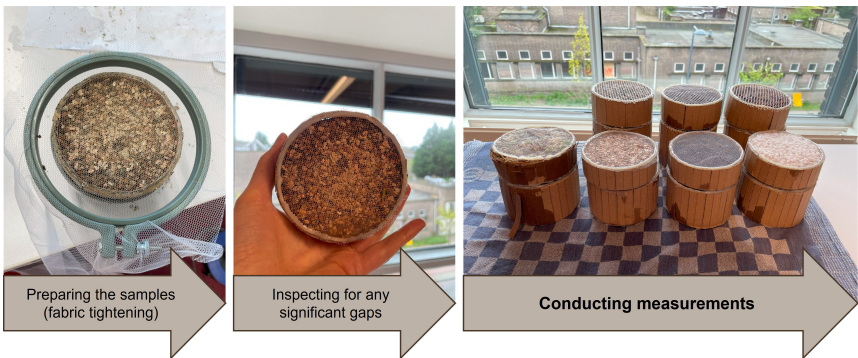
Figure 7.8: Procedure for preparing loose substrate test samples
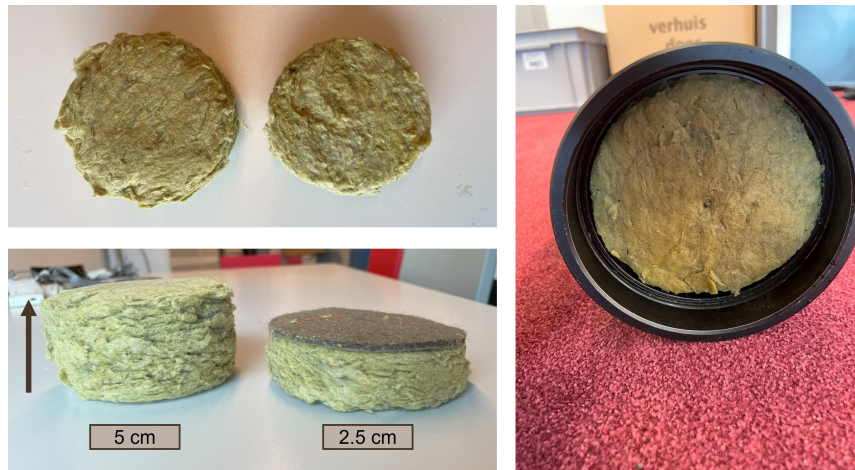
Figure 7.9: Procedure for preparing mineral wool test samples

7.1.3. Saturation procedure

As noted in the literature review on the acoustic performance of LWS components (Chapter 4), moisture in the substrate affects acoustic absorption by reducing apparent soil porosity and soil permeability. Since LWSs require regular irrigation, the substrates undergo changes in their saturation levels throughout the day. To capture the impact of different saturation levels on acoustic performance, two sets of measurements were conducted: one with dry test samples and one with saturated samples.

The saturation process is depicted in Figure 7.10. Dry substrates were left in a water column for 24 hours to achieve 100% saturation of the pores. Given that the substrates used for hydroponics typically have either good water retention capabilities or efficient water drainage, the influence of both conditions needed to be tested. Since irrigation occurs only a couple of times per day, the substrates spend most of the day in a state between fully saturated and dry. To simulate this intermediate state, the substrates were left to dry for 1–2 hours, allowing some water to evaporate before testing.
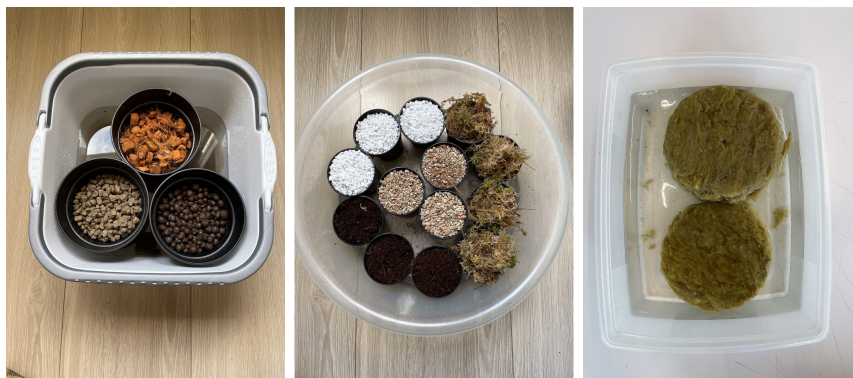
Figure 7.10: Saturation procedure for the substrate test samples

7.2. Measurement Setup

The measurements of the test samples were conducted using the Impedance Tube Kit Type 4206 by Brüel & Kjær, as illustrated in Figure 7.11 (Brüel & Kjær, 2019a). A large tube with a diameter of 100 mm was employed, with a microphone spacing of 50 mm. The usable frequency range is contingent upon the diameter of the tube and the spacing between the microphone positions. As per Eq.6.15, the cut-off frequency is estimated to be around 1600 Hz, whereas the lowest working frequency, according to Eq.6.16, is 100 Hz.

Measurements were conducted based on the two-microphone transfer function method outlined in ISO 10534-2, as detailed in Section 6.1. Utilizing the specialized software, Pulse Acoustic Material Testing (Brüel & Kjær, 2019b), the measurements were generated. The impedance tube loudspeaker was connected to the power amplifier, producing broadband, stationary random sound waves that propagated as plane waves within the tube, interacting with the sample and causing reflection. Consequently, a standing wave formed inside the tube. By measuring the sound pressure at two predetermined locations and employing a two-channel digital frequency analyzer (generator module), it became feasible to obtain the normal-incidence surface impedance of the test sample.

Pulse adhered to the procedural guidelines outlined in ISO 10534-2 (NEN-EN-ISO 10534-2:2023, 2023), which involved conducting microphone calibration, determining the signal-to-noise ratio, and calibrating the transfer function:

- Firstly, before commencing each measurement session, it was necessary to adjust the amplitude of each microphone to within a tolerance of ±0.3 dB or better. This step was conducted using a Type 4231 Sound Calibrator.

- Secondly, it was imperative to assess the sound pressure spectrum at each microphone position with both the source sound on and off. The sound spectra from the source had to exhibit at least a 10 dB higher level than the background noise across all frequencies reported, ensuring a clear distinction between the signal and noise.

- Lastly, the process of transfer function calibration was undertaken. The calibration of the transfer function aims to rectify any discrepancies in phase and amplitude between the two measurement channels. Each channel comprises a microphone, preamplifier, and analyser. To address microphone mismatches, measurements with channels interchanged were conducted. This measurement procedure utilized a specialized test sample provided by the manufacturer.
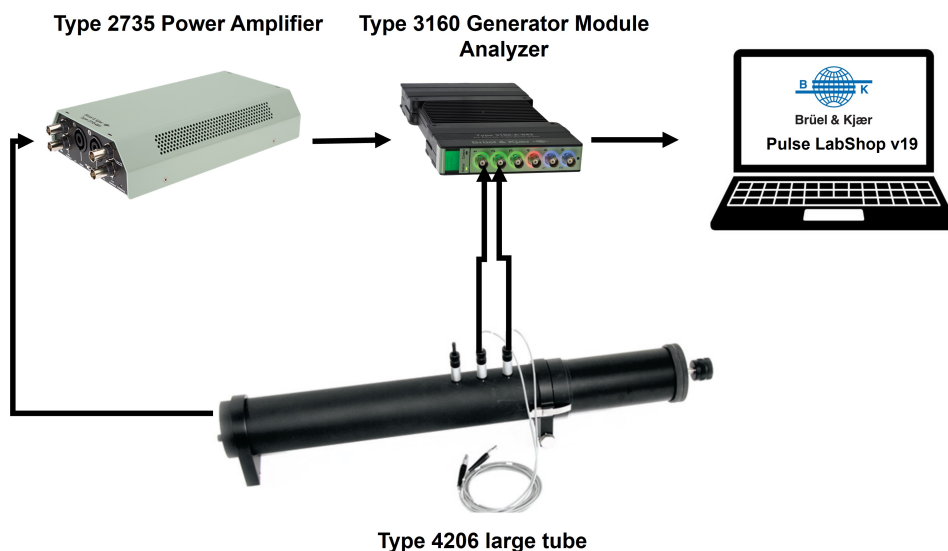
Figure 7.11: Measurement setup kit (Brüel & Kjær)

7.3. Data Processing and Outcomes

Impedance tube measurements were conducted to gather surface impedance data for each test sample across frequencies from 100 Hz to 1600 Hz, with measurements taken at 2 Hz intervals. To manage this extensive dataset effectively, the derivation of effective parameters was automated using Python. This automated process facilitated coherent analysis across three stages: preliminary, intermediate, and final data analysis. **The schematic workflow of the codes and the repository link to access the files are provided in Appendix A.**

7.3.1. Data processing procedure for plants

Effective parameters for the plants were derived using a modified two-cavity method (Section 6.2.3). This method was chosen because only one exemplar of each plant was available, allowing for the use of a single test sample with two distinct backing conditions: rigid termination and cavity. Six different backing conditions were utilized throughout the measurements, including a rigid backing and five distinct cavities with varying depths.

The preliminary data analysis assisted in visualizing the results of the surface impedance measurements for all backing conditions, provided in Appendix A.1.1. The visualizations reveal a clear influence of the introduced cavities on the measurement outcomes, with a noticeable peak in the real part of the surface impedance shifting towards lower frequencies as the cavity widens. Corresponding variations in the imaginary part accompany this peak.

The intermediate data analysis aimed to determine the effective parameters for each combination of rigid backing and cavity. Visualizations illustrating the outcomes are provided in Appendix A.2.1. From the results, it is evident that the peaks observed in the preliminary analysis significantly impact the derived effective parameters. Ideally, the characteristic impedance and wavenumber should remain consistent across all backing combinations, regardless of cavity thickness. However, this consistency is not observed in practice. To address these discrepancies, the mean characteristic impedance was derived for each plant, averaging out variations between the backing combinations. The results of this procedure are presented in Appendix A.2.2. The analysis of mean characteristic impedance reveals that for Ajuga, Heuchera, and Waldestania, the standard deviation in the discrepancies is substantial. Additionally, fluctuations in the results below 200 Hz for all plants are mainly due to measurement inaccuracies. Therefore, the valid frequency range for accurate results is determined to be above 200 Hz.

In the final data analysis, the derived mean characteristic impedance was combined with the surface impedance measured under rigidly backed conditions to derive the complex wavenumber. As seen previously and depicted in Appendix A.2.1, the derived wavenumber exhibits abrupt jumps and a loss of continuity, which were addressed using the phase unwrapping procedure described in Section 7.3.3. Since this procedure requires a starting frequency, all values that remain unwrapped before that frequency must be checked for alignment, with negative values being eliminated to ensure consistency. Consequently, the final data analysis revealed derived effective parameters that were processed, validated, and presented in the Appendix A.3.1. These parameters, stored in binary files, serve as inputs for the simulation tool.

7.3.2. Data processing procedure for substrates

Effective parameters for the substrates were obtained using a two-thickness method (Section 6.2.1). This approach was chosen due to potential inconsistencies in measured results, especially with loose substrates, as the test samples may possess inhomogeneities. Consequently, stemming from the lack of reciprocity and symmetry of the test samples, employing a two-sample method aims to mitigate these issues, resulting in more representative effective parameters.

In anticipation of the asymmetry in the test samples, each underwent two measurement rounds by "flipping" it inside the impedance tube, ensuring exposure of both sides to incoming sound waves during testing. The sides were labelled as "v1" and "v2" for clarity during analysis. Consequently, surface impedance measurements were conducted for both dry and saturated samples, as well as for both sides of each sample. The outcomes are depicted in Appendix A.1.2. The primary objective of the preliminary data analysis was to reconcile any observed discrepancies among the different sides of the same sample. The mean surface impedance was computed for each test sample and is presented in the Appendix A.1.3. Minimal divergence was observed in the measured results, indicating a small standard deviation. However, notable variations were observed in the saturated mineral wool sample of 5 cm thickness.

The intermediate data analysis aimed to directly derive the effective parameters from the analyzed surface impedances. The outcomes are presented in Appendix A.2.3. As noted earlier, with plants, two issues were observed. Firstly, the outcomes exhibit erratic data in frequencies below 200 Hz, attributed to measurement limitations. Secondly, in the real part of the wavenumber, abrupt jumps from positive to negative values were observed, resulting in a loss of continuity.

Consequently, the final data analysis addressed these issues. The procedure for handling the phase information in the real part of the wavenumber is described in Section 7.3.3. Similarly, all unwrapped values were assessed, as any negative wavenumber data is erroneous. As a result, the final data analysis revealed derived effective parameters that were processed and validated to ensure representativeness. The outcomes are presented in the Appendix A.3.2. These outcomes, stored in binary files, serve as inputs for the simulation tool.

7.3.3. Phase unwrapping

The current data processing procedure involves a crucial step: unwrapping the phase information inherent in the wavenumber solution, as explained by Palumbo, Jones, Klos, and Park (2004). The wavenumber derivation in the presented methods relies on the natural logarithm of a complex ratio. However, the logarithmic operation applied to complex numbers introduces a phase component confined within the principal value range of $-\pi$ to π. Consequently, discontinuities may arise, particularly when the phase crosses the $\pm\pi$ boundary. This wrapping phenomenon compresses the phase information, leading to abrupt jumps and loss of continuity, necessitating phase unwrapping to recover the true phase representation.

Automating phase unwrapping poses challenges and can obscure pertinent data (Palumbo et al., 2004). Primarily, the erratic nature of low-frequency wavenumber data complicates the unwrapping process. Phase unwrapping initiation from excessively low frequencies, where wavenumbers are minimal or even negative, can induce substantial shifts in wavenumber values across subsequent frequencies. Consequently, it underscores the importance of selecting an appropriate starting frequency for the phase unwrapping procedure. In the current data analysis, it was observed that data continuity and consistency generally improve beyond frequencies of 200 Hz. However, certain components still exhibit errors or significant fluctuations in data beyond this threshold. **Consequently, it was determined during the intermediate data analysis that the phase unwrapping algorithm could be reliably applied for plants from 300 Hz and substrates from 400 Hz.**

The phase unwrapping algorithm, *numpy.unwrap*, was sourced from the Python library Numpy (Oliphant & et al., 2020). The algorithm works by iteratively adjusting the phase values to remove discontinuities caused by the wrapping effect, ensuring a more continuous representation of the phase information. This involves adding or subtracting multiples of 2π to the phase values until they are properly unwrapped. However, in some cases, minor discontinuities may persist in the data (Figure 7.12), since the algorithm avoids unwrapping phases smaller than half the period to prevent introducing larger discontinuities.

(a) Before phase unwraping

(b) After phase unwrapping
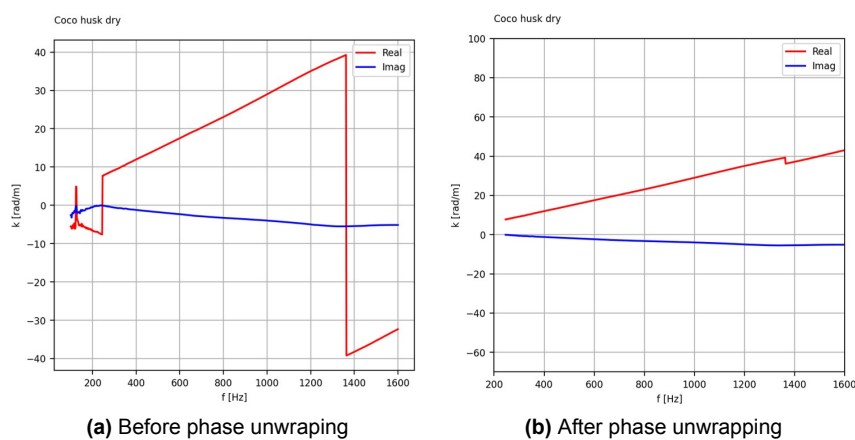
Figure 7.12: Application of the phase unwrapping

<div align="right">

8

</div>
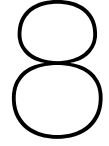
Data Interpretation

8.1. Data Analysis

To understand the performance of individual LWS components in terms of mitigating urban noise, analysing their characteristic impedance is essential. Characteristic impedance quantifies the resistance encountered by a sound wave as it traverses through the medium. Section 5.1.2 explains that complex characteristic impedance can be comprehended by considering both its real and imaginary parts. The real part corresponds to resistance, while the imaginary part represents reactance. Resistance accounts for the dissipation of sound wave energy within the medium, whereas reactance relates to the effects of mass and elasticity of the medium, hindering wave transmission. Thus, the analysis primarily focuses on two key characteristics: **resistance** and **reactance**. The impact of these characteristics on the performance of individual LWS components can be explored by analysing components as separate layers within specific boundary conditions. Consequently, theoretical boundary conditions are chosen, as depicted in Figure 8.1. The considered configuration is referred to as the air-layer-air system. For this configuration, the **RL performance** (see Section 5.2.2) across frequencies for different layer thicknesses is presented.

When sound waves encounter interfaces between mediums with different acoustic impedances, such as in the air-layer-air system, they undergo both reflection and transmission. The VGS component, with its higher acoustic impedance compared to air, ensures that the pressure component of reflected waves maintains its phase upon reflection from its surface (see Section 4.2.3 and Figure **??**). In contrast, the pressure component of the transmitted wave undergoes a phase reversal upon encountering the lower impedance of air at the opposite surface of the VGS (Howard & Angus, 2017). This reversal occurs because there is less resistance for the particles to move into the region with lower impedance. Consequently, the sound wave exhibits a pressure component close to zero and a large velocity component at the boundary. The latter denotes the rarefaction upon reflection, as opposed to compression. Reflective phenomena can be likened to the behaviour of a mass-spring model. In this analogy, the springs experience increased tension as a result of rarefaction, leading to momentum transfer to the particles at the boundary of the layer. Eventually, this momentum is redirected back to the springs due to their stiffness. This action causes the reflected wave to commence.

By exploiting the phase shift between two reflected waves, constructive or destructive interference can be achieved. For instance, adjusting the thickness of the layer to correspond to n-quarter of the incident sound wave's wavelength results in destructive interference (Figure 8.1). This occurs because the reversed sound wave reflected at the back interface travels an additional half wavelength compared to the wave reflected at the front surface. As a result, the destructive interference significantly reduces surface reflection, enhancing the system's RL and overall performance. Consequently, in each RL performance visualizations, dashed lines highlight the quarter-wavelength thickness of the layer relative to the incident wave's wavelength. Blue lines indicate layer thicknesses where the shift between the incident and reflected waves results in constructive interference (Eq. 8.2). Conversely, red lines indicate thicknesses where the incident and reflected waves experience a phase shift that leads to destructive interference (Eq. 8.1).

$$d = n \frac{c_{layer}}{4f} \tag{8.1}$$

$$d = m\frac{c_{layer}}{4f} \tag{8.2}$$

Where: d = Quarter-wavelength thickness of the layer
c = Speed of sound in the layer (Eq.5.12)
f = Frequency of the incident wave
n = Mode number for destructive interference (2, 4, 6 ...)
m = Mode number for constructive interference (1, 3, 5 ...)
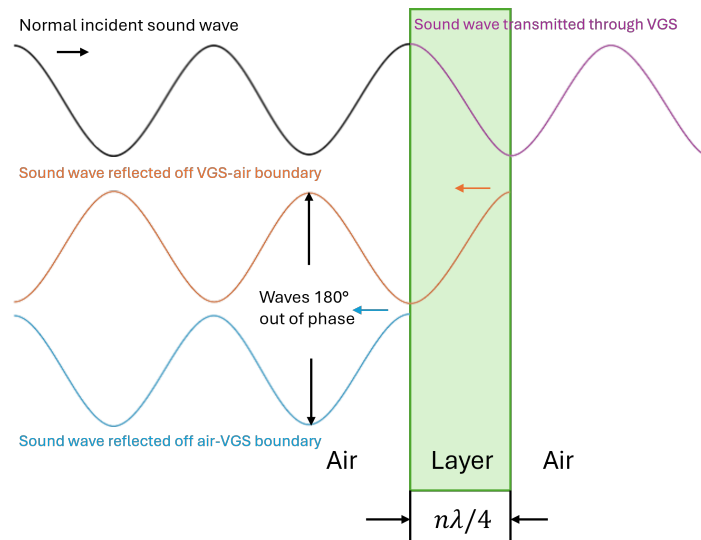
Figure 8.1: Transmission and reflection of a sound wave in air-layer-air system

8.1.1. Foliage layers

The RL performance of Ajuga, Bergenia, Heuchera, and Waldestania plants exhibits a distinctive feature: a vertical beam indicating higher RL values (Figures 8.2(b), 8.3(b), 8.5(b), and 8.6(b)). This beam spans across all layer thicknesses and happens in a specific frequency range. This frequency range corresponds to the region where the resistance component of the complex characteristic impedance approaches the impedance of air (Figures 8.2(a), 8.3(a), 8.5(a), and 8.6(a)). This results in reduced reflections as a nearly constant transmission line in an air-layer-air system is maintained.

However, the frequency at which the highest recorded RL performance happens does not perfectly align with the frequency at which the impedance match between the layer and air takes place. This discrepancy is caused by the influence of the reactance component. Particularly noteworthy is the increase in mass-reactance beyond the impedance-matching frequency for all the plants. Mass-reactance, speculated to be dependent on the leaf area density, serves as a significant barrier to sound wave propagation. The dominance of mass-reactance results in a substantial portion of waves being reflected back. In general, it can be concluded that the frequency at which the mass-dominated region starts depends on leaf size: smaller leaves (Ajuga, Waldestania, Bergenia) exhibit dominance starting around 1000-1200 Hz, while large leaves (Heuchera) start around 500 Hz. However, Heuchera displays more comprehensive behaviour, resulting in two impedance-matching regions, thereby leading to a mass-dominant governing region at higher frequencies as well.

In contrast to other plants, grass exhibits unique acoustic properties due to its relatively low reactance (Figure 8.4(a)). The low reactance component explains the resonant behaviour of the grass layer. This is anticipated to arise from the sparse arrangement of blades, which allows sound waves to induce vibrational motions and transmit further with minimal opposition. Consequently, the primary factor governing sound wave interaction with a grass layer is the resistance component. As a result, grass demonstrates consistent

RL behaviour across all frequencies (Figure 8.4(b)), without the characteristic reduction in RL at higher frequencies observed in other plants.

(a) Characteristics   **(b)** Performance
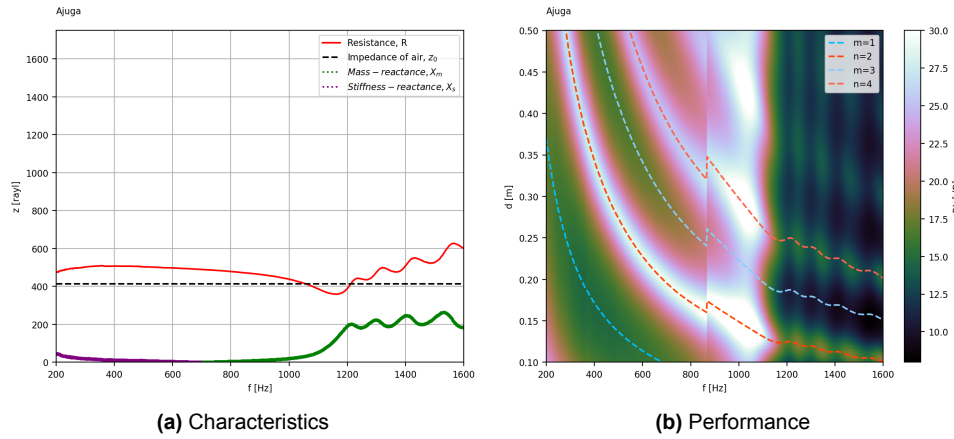
Figure 8.2: Resulting behaviour of the Ajuga reptans

(a) Characteristics   **(b)** Performance
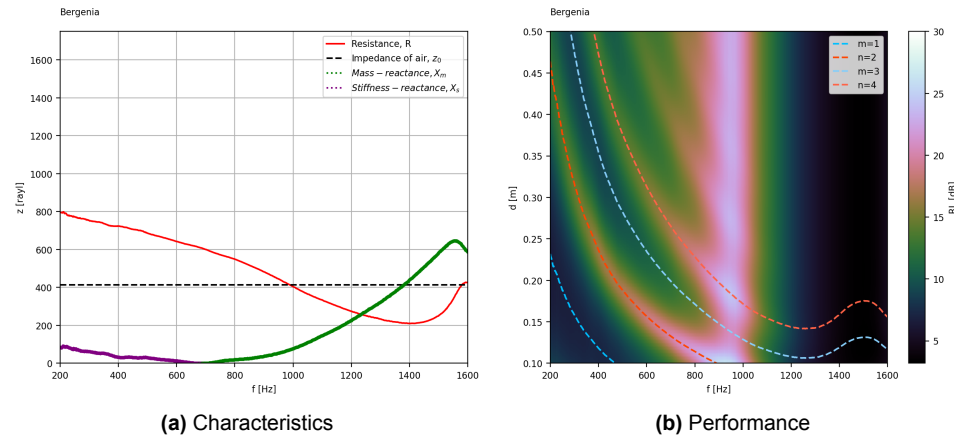
Figure 8.3: Resulting behaviour of the Bergenia cordifolia

(a) Characteristics   **(b)** Performance
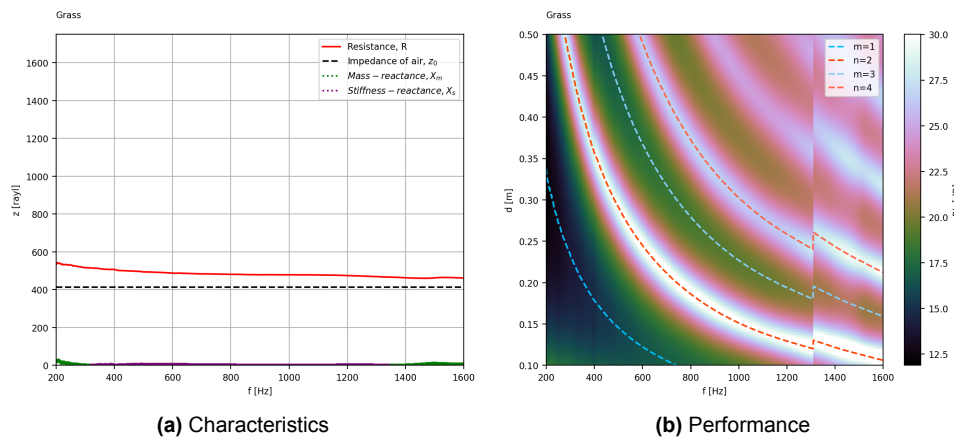
Figure 8.4: Resulting behaviour of the Festuca glauca (grass)

(a) Characteristics

(b) Performance
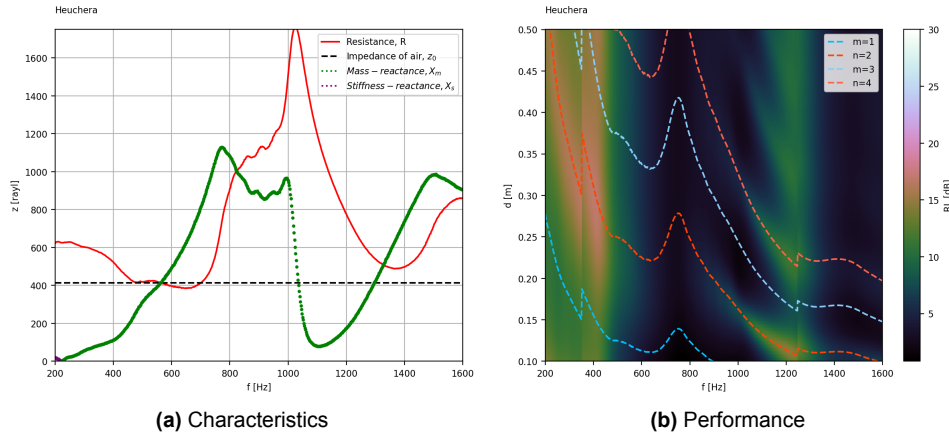
Figure 8.5: Resulting behaviour of the Heuchera 'Cascade Dawn'

(a) Characteristics
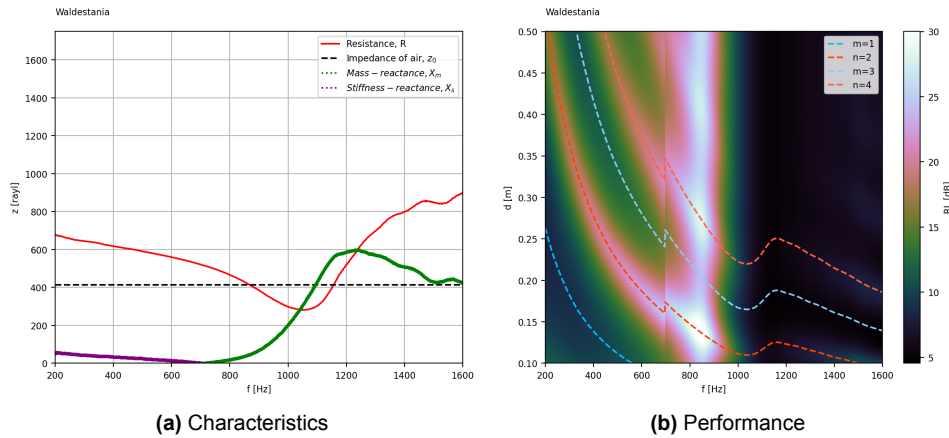
(b) Performance

Figure 8.6: Resulting behaviour of the Waldestania ternata

8.1.2. Substrate layers

Clay balls, **coco husk**, and **pumice** consistently perform well irrespective of whether they are dry or saturated, as illustrated in RL performance Figures 8.8(b), 8.9(b), and 8.10(b). The consistent performance of these substrates is thought to be due to their superior drainage and limited water retention properties, which means that moisture does not significantly affect the properties of the medium. While clay balls and pumice lack significant water absorption capacities, coco husk, despite its ability to absorb water, showed ineffective water retention due to its coarse fibres. This observation was noted during the preparation of test samples.

Based on the derived characteristics (Figures 8.8(a), 8.9(a), and 8.10(a)), it is apparent that the resistance component in the dry state is comparable across all substrates, albeit with slightly lower values observed in coco husk. This discrepancy could be attributed to the larger particle size of coco husk in the test sample, resulting in larger pores that facilitate easier wave transmission. Near frequencies around 1200 Hz, the resistance component curve for all substrates approaches the impedance of air, resulting in a slightly higher RL performance across all layer thicknesses. However, above 1200 Hz, the dominance of the mass-reactance component becomes apparent, resulting in a consistent decline in RL performance. With the addition of water, the resistance curve for all substrates shifts to lower values at higher frequencies, while the mass-reactance in the same region increases. As a result, this adjustment balances the RL performance to closely align with that observed in the dry state.

The introduction of moisture to both **coco coir** and **perlite** significantly enhanced their RL performance, as illustrated in Figures 8.11(b) and 8.12(b). During the preparation of the test samples, it was evident that

these substrates exhibited notable water retention as well as effective drainage properties. The moisture in these substrates was primarily held on the particle surfaces through adsorption, while the excess water was drained through open pores (Figure 8.7(a)).

Based on the derived characteristics (Figures 8.11(a) and 8.12(a)), when coco coir and perlite become saturated, there is a discernible decrease in the resistance component, particularly noticeable at higher frequencies. This change brings their impedance closer to that of air. While impedance matching may occur, a significant portion of RL in saturated substrates is hampered due to the prevalence of mass-reactance. In a dry state, stiffness reactance is demonstrated to be predominant in coco coir and pumice. However, as these substrates accumulate water molecules, their density rises, leading to a transition from stiffness-dominated reactance to mass-dominated reactance. This shift becomes particularly pronounced at both lower and higher frequencies. However, in mid-frequencies, the reactance tends to approach zero. This phenomenon is a major contributing factor to the improved RL performance in saturated substrates.

Mineral wool, **moss**, and **vermiculite** each displayed diminished performance when saturated compared to their dry states, as evidenced in RL performance Figures 8.13(b), 8.14(b), and 8.15(b). Despite their proficiency in retaining water, these substrates showcase relatively poor drainage properties. Saturated moss fibres gradually compact, impeding water flow through substrate pores over time. Likewise, saturated mineral wool fibres become denser and tightly packed, exacerbating drainage issues. Moreover, saturated vermiculite particles compress significantly under their weight, reducing the available pore spaces within the substrate essential for drainage (Figure 8.7(b)).

Based on the derived characteristics (Figures 8.13(a), 8.14(a) and 8.15(a)), the occurrence of waterlogging within the substrates contributes collectively to an elevation in the resistance component, leading to a pronounced impedance mismatch with the surrounding air. Additionally, the predominance of mass-reactance, observable across all saturated samples and particularly pronounced at higher frequencies, acts as a hindrance to the magnitude of RL enhancement.

(a) Perlite   (b) Vermiculite

Figure 8.7: Saturated substrate microstructure

(a) Characteristics   **(b)** Performance
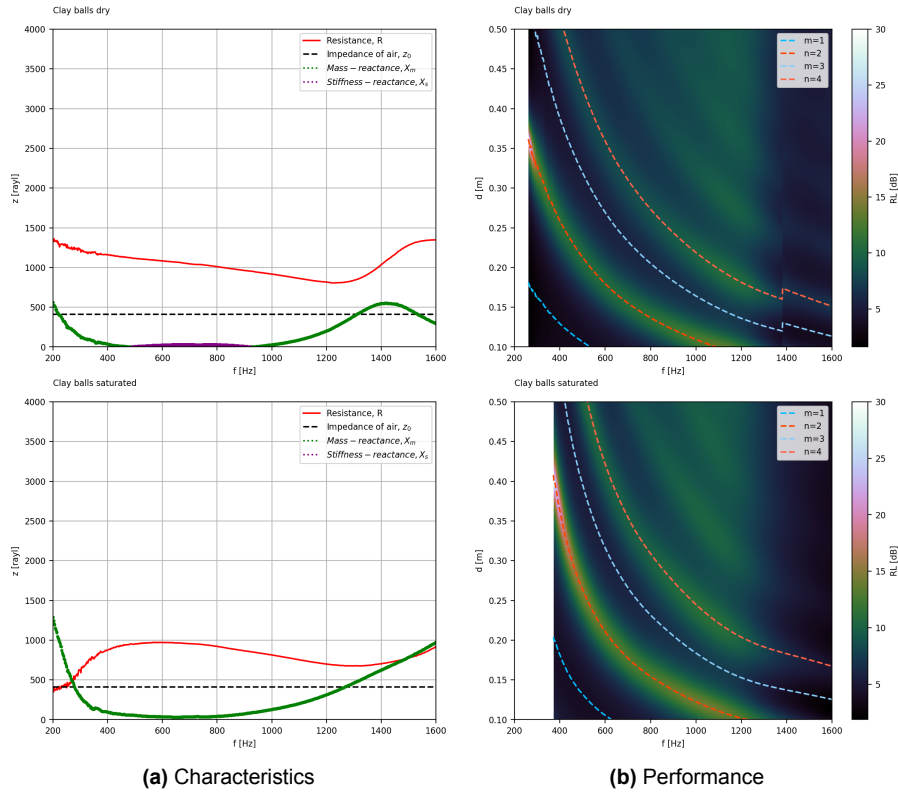
Figure 8.8: Resulting behaviour of the Clay balls

(a) Characteristics   **(b)** Performance
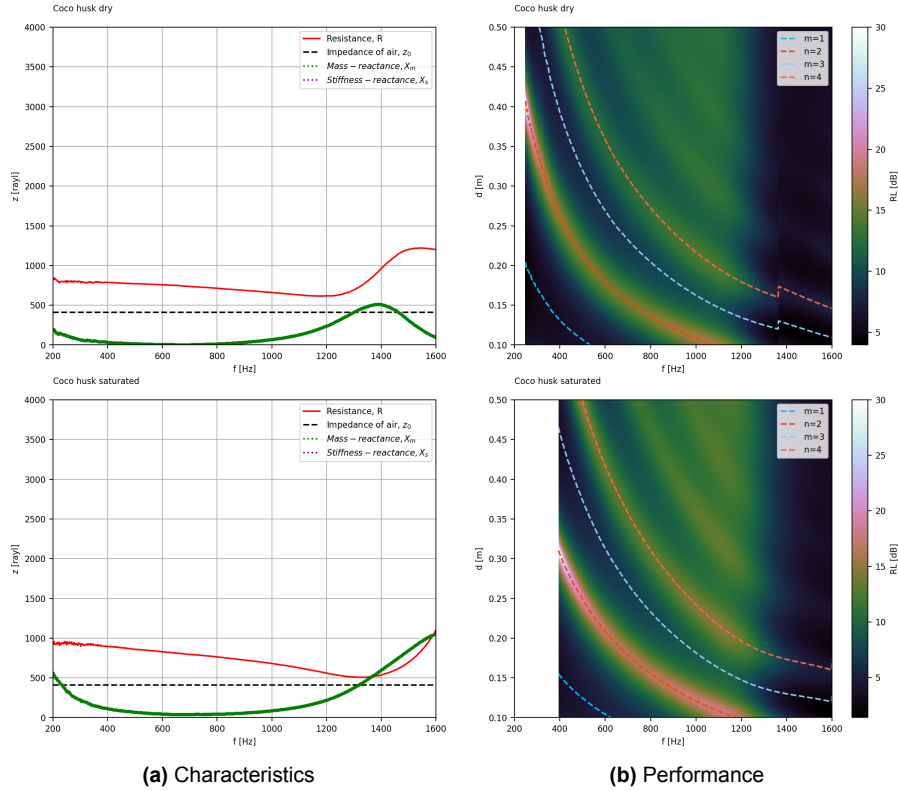
Figure 8.9: Resulting behaviour of the Coco husk

(a) Characteristics   **(b)** Performance
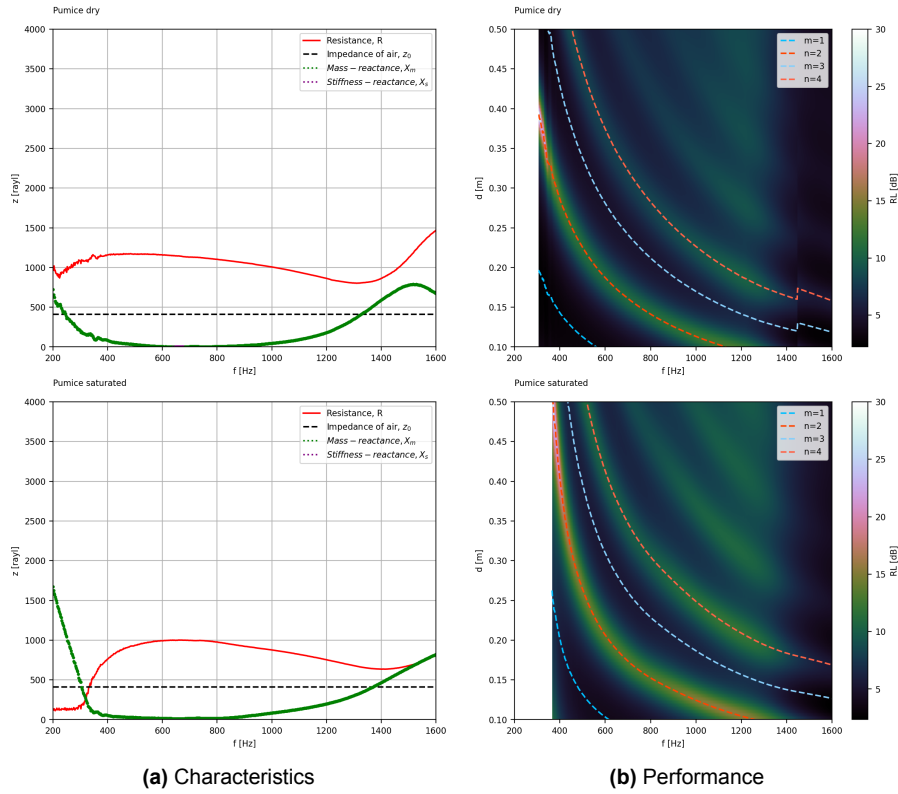
Figure 8.10: Resulting behaviour of the Pumice

(a) Characteristics   **(b)** Performance
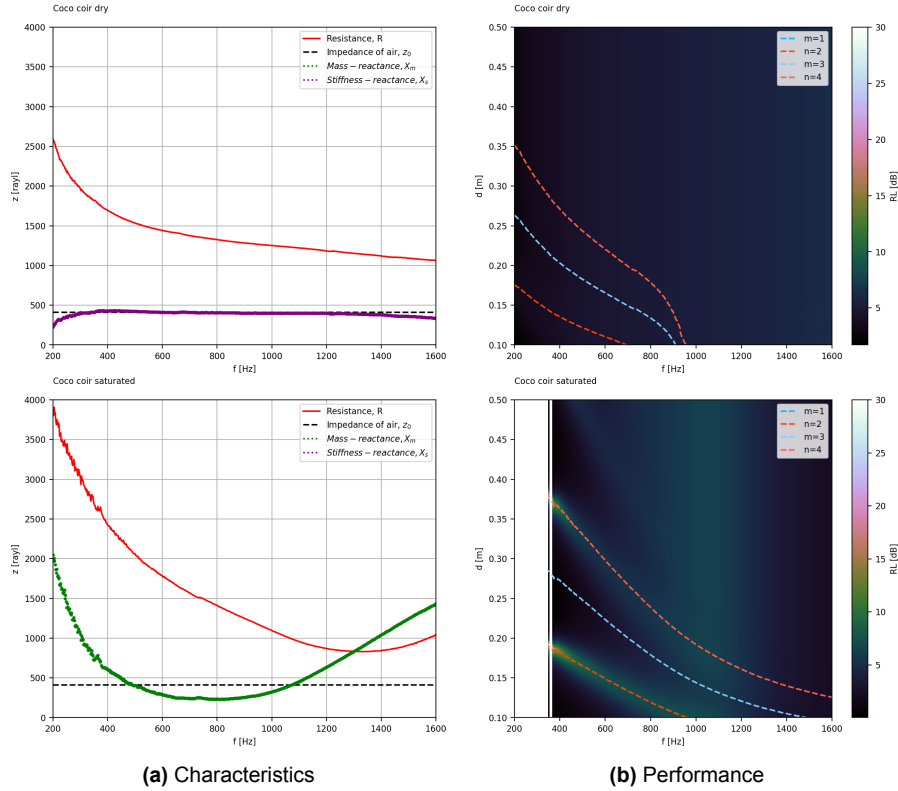
Figure 8.11: Resulting behaviour of the Coco coir

(a) Characteristics **(b)** Performance
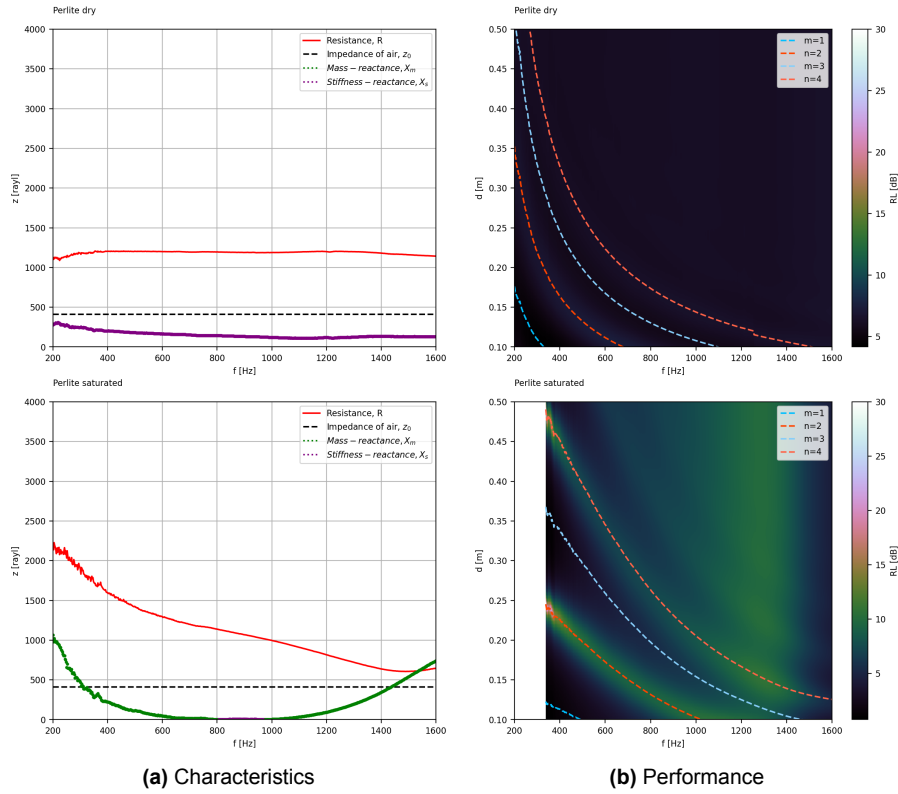
Figure 8.12: Resulting behaviour of the Perlite

(a) Characteristics **(b)** Performance
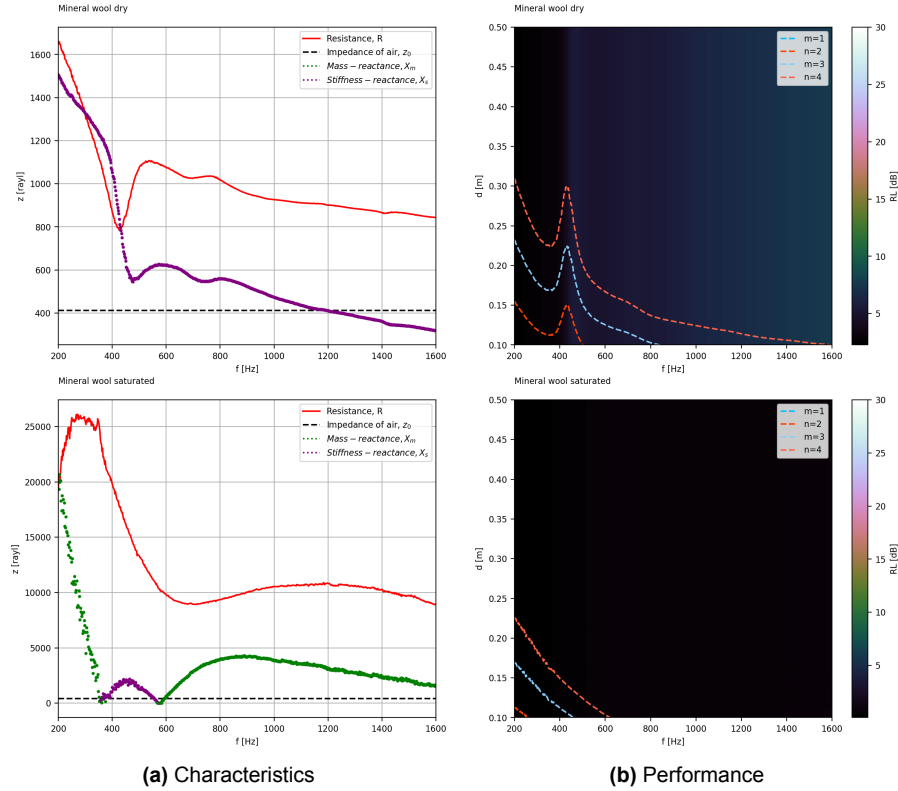
Figure 8.13: Resulting behaviour of the Mineral wool

(a) Characteristics   **(b)** Performance
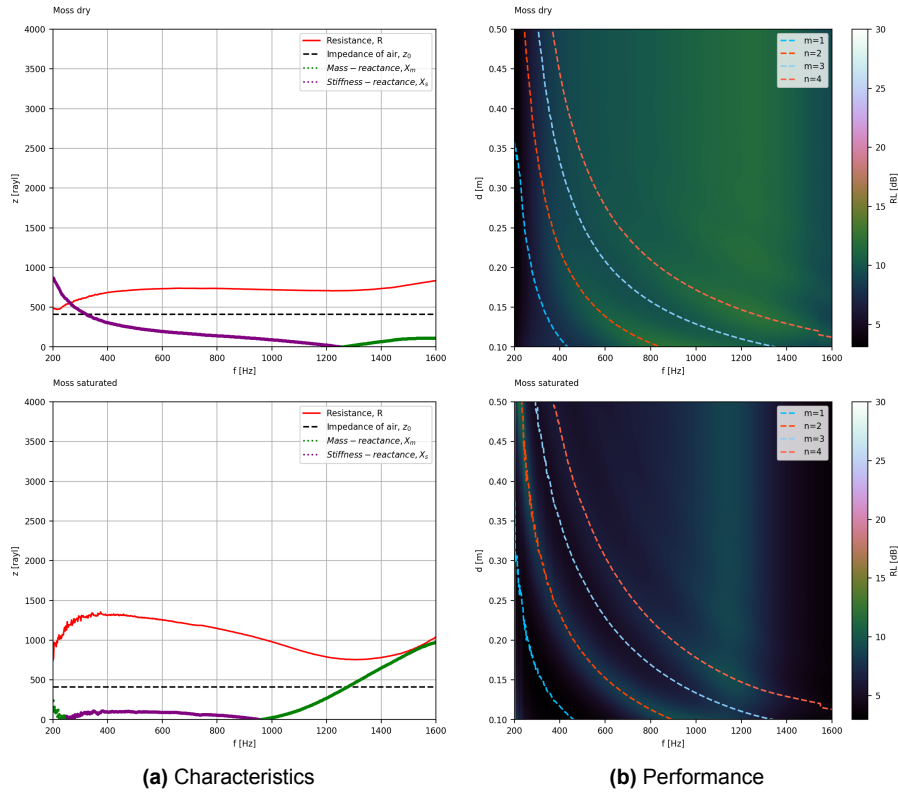
Figure 8.14: Resulting behaviour of the Moss

(a) Characteristics   **(b)** Performance
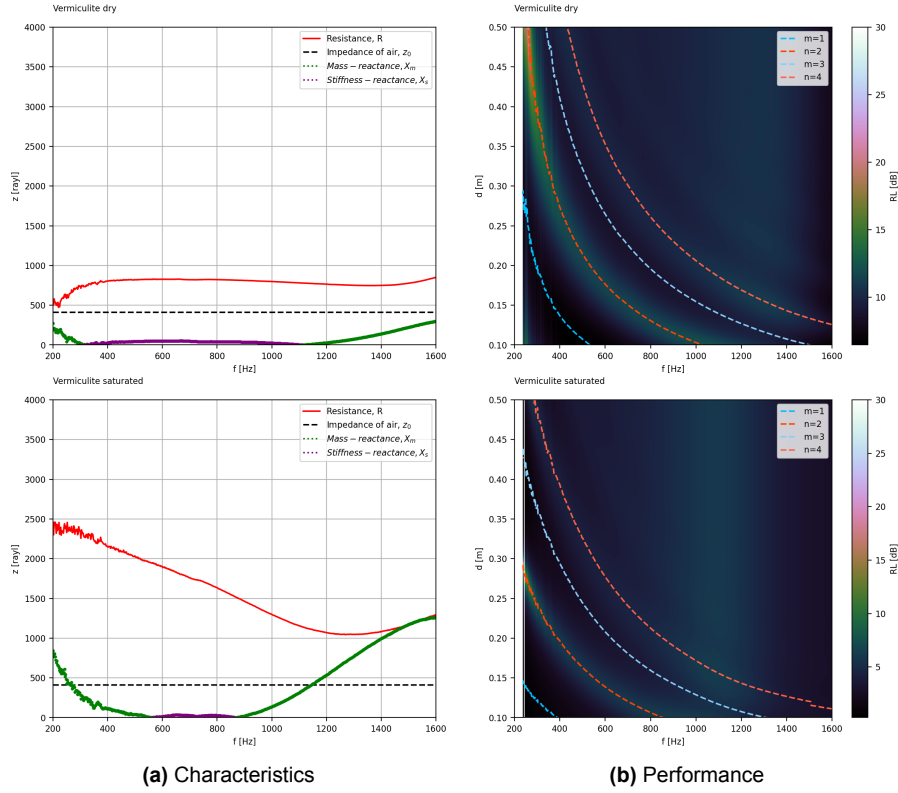
Figure 8.15: Resulting behaviour of the Vermiculite

8.2. Verdict

In the conducted analysis, the individual LWS components were evaluated under the air-layer-air boundary condition. Consequently, it becomes apparent that the performance metric, RL, utilized in this assessment, cannot be extrapolated to other boundary conditions. In essence, this implies that universal conclusions regarding the RL performance of individual LWS components cannot be derived from this analysis alone. The primary reason behind this limitation lies in the reliance of RL performance on impedance fluctuations as waves traverse diverse boundaries. Within the air-layer-air configuration, the observations indicated that when the reactance of the LWS component closely aligns with that of air, the transmission line maintains a relatively consistent profile throughout the system, thereby yielding higher return loss. However, under alternative boundary conditions like the air-layer-rigid wall setup, RL performance undergoes significant deviations due to pronounced impedance disparities, leading to disruption in transmission line consistency. Moreover, in the context of multilayer-boundary systems, the transmission line's behaviour becomes notably ambiguous, further complicating the assessment.

Another significant limitation of this analysis pertains to the understanding of how complex impedance characteristics — resistance and reactance — are influenced by the structural changes in LWS components. For instance, plants exhibit highly complex structures with varying leaf dimensions, stems, and other features that integrally influence characteristics. For example, the Heuchera plant displayed very different characteristics compared to other leafy plants. Unfortunately, it is challenging to delineate why these differences occur. Additionally, it must be noted that the derived characteristics are based on measurements followed by theoretical simplifications, which may introduce significant uncertainties and affect the validity of the results. Moreover, in the current analysis, observed changes in complex impedance with alterations in substrate state were based on visual assessments of water retention and drainage performance of test samples. While these observations provided some insights and identified implied relationships, they cannot be deemed conclusive.

Consequently, the intricate structures of both foliage and substrates make it challenging to pinpoint the exact factors influencing the derived characteristics. Therefore, a more thorough investigation at the microscale level is necessary to rigorously validate the hypotheses presented in the current analysis and provide a scientific explanation of the underlying mechanisms. Furthermore, it is essential to note that characteristic impedance and derived wavenumber work in tandem, as these parameters are interconnected and part of the transfer matrix method. Rigidly considering only one parameter may not provide a complete understanding of the system's behaviour.

In conclusion, achieving an accurate estimation of the multi-layer VGS system's performance necessitates a comprehensive approach that extends beyond the mere assessment of individual component parameters or their behaviour within specific boundaries. The transmission of waves through the system's transmission line is inherently complex, influenced not only by impedance matching between layers but also by factors such as attenuation (the imaginary part of the complex wavenumber) and phase constant (the real part of the complex wavenumber) within the various layers. These variables dictate the phase of waves upon encountering boundaries, thereby directly impacting their phase information upon reflection or transmission. Consequently, these intricate dynamics play a pivotal role in shaping the ultimate RL performance of the system.

9

Discussion

The primary objective of this section is to explore the potential advantages, limitations, or comparisons of the methods utilized in the empirical study with those employed by other researchers or alternative approaches. The main questions raised that will be discussed:

- In what ways does the current study compare to the research conducted by Attal, Dubus, et al. (2021)?
- What are alternative impedance tube measurement setups and techniques that could be considered?
- What is the primary limitation of impedance tube measurements in the context of the current study?
- Was it feasible to conduct measurements using an impedance tube in the current study, and if not, what alternative measurement techniques could have been applied?
- What alternative approaches exist for deriving effective properties using empirical models?

Each question will be addressed in its respective section, following the same order as listed.

9.1. Motivation

The current study was inspired by the works of E. Attal and his team, specifically their studies published in 2019 and 2020 (Attal, Côté, Shimizu, & Dubus, 2019; Attal, Dubus, et al., 2021). Their primary goal was to optimize a multi-layer VGS structure, including substrate and foliage, to minimize backward noise reflection and forward transmission from the wall. Their research objectives were based on a theoretical model — the TMM — which enabled them to optimize a VGS structure to improve both return and transmission losses. This approach involved creating 3D efficiency mappings to determine the optimal thicknesses of the VGS layers for maximum effectiveness.

Thus, it can be stated that the current study is a continuation of their work. The main differences highlighted in the approaches are twofold. First, the current study tested a wider range of components, whereas their studies only considered perlite and coco coir as substrates, and Japanese spindle (*Euonymus japonicus*) as foliage. Second, to derive the effective values of the components, both studies used impedance tube measurements, but with different measurement setups and methods. Attal and his team used the three-microphone two-load method with a custom impedance tube featuring an inner diameter of 192 mm, resulting in different derivation techniques for the effective parameters. Their measurement setup and effective parameters derivation technique are described in Section 9.2.

Consequently, the main aim of the current study was to use a conventional impedance tube measurement setup to make the VGS optimization method more widespread and applicable. By employing the standardized two-microphone method (NEN-EN-ISO 10534-2:2023, 2023), the current study aims to make the approach more accessible and easier to replicate.

9.2. Alternative Impedance Tube Measurement Methods

In NEN-EN-ISO 10534-2:2023 (2023), Annex F notes that when available, the three-microphone method or the four-microphone method is preferred for estimating the intrinsic (effective) parameters of materials. These methods are scheduled for standardization in ISO 10534-3 and ISO 10534-4; however, as of the

due date of the current study, these standards have not yet been published. It is estimated that these standards will be based on the methodology already presented by the American Society for Testing and Materials (ASTM) in standard ASTM E2611-19 (ASTM International, 2019).

The ASTM E2611-19 standard outlines the procedure for measuring sound transmission through materials using an impedance tube and four microphones (ASTM International, 2019). This standard involves determining the acoustic transfer matrix. The primary method detailed in the standard is referred to as the four-microphone one-load (4M1L) technique. As illustrated in Figure 9.1, this method requires a specialized impedance tube setup. A sound source, typically a loudspeaker, is positioned at one end of the tube, while an anechoic termination, made of a thick porous material, is placed at the opposite end to minimize sound wave reflections back into the tube. To achieve this, materials like glass fiber are often used in wedge or pyramidal shapes to absorb sound effectively. The test sample is mounted in the center of the tube. When plane waves (A) hit the sample, some waves are reflected (B) back toward the sound source, some are absorbed by the sample, and others pass through (C) to the receiving section of the tube. The waves that transmit through the sample then encounter the end of the receiving tube, where they are either reflected (D) or leave the tube. Each microphone measures the pressures, which are then used to calculate the pressure amplitudes of the plane waves (Cox & D'Antonio, 2017). With the amplitudes determined, the pressures and velocities at both the front and rear of the test sample can be evaluated.
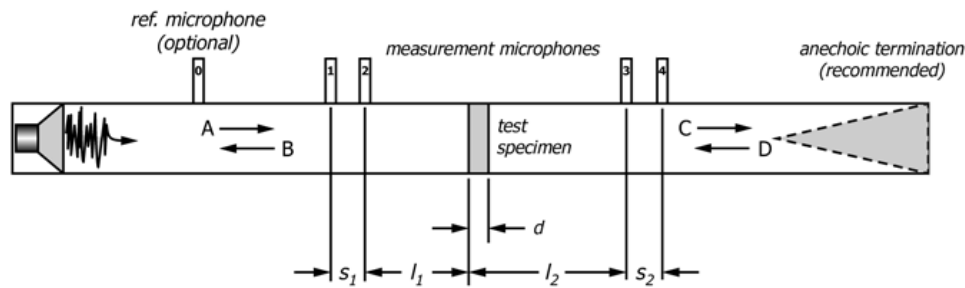
Figure 9.1: Impedance tube configuration for the 4M1L and 3M2L method measurements
Note. From *Standard Test Method for Normal Incidence Determination of Porous Material Acoustical Properties Based on the Transfer Matrix Method* by ASTM International (2019), Copyright 2019 by ASTM International.

In essence, the wave transmission phenomena is expressed using the matrix formulation in Eq.5.13. However, this standardized formulation provides only two equations, yet it entails four unknowns (T_{11}, T_{12}, T_{21}, and T_{22}). Therefore, a solution is possible only if the material is perfectly symmetrical and reciprocal, satisfying the conditions $T_{11}T_{22} - T_{12}T_{21} = 1$ and $T_{11} = T_{22}$. However, to address more realistic materials, ASTM E2611-19 employs the four-microphone two-load (4M2L) method. This method involves performing measurements with two different terminations — one with an anechoic (or rigid) end and the other with an open end. By conducting these two sets of measurements under different termination conditions, sufficient independent equations are generated to determine the matrix elements accurately (Cox & D'Antonio, 2017).

In addition to the 4M1L and 4M2L methods mentioned, Salissou, Panneton, and Doutres (2012) proposed an alternative measurement configuration based on the older ASTM E2611-09 standard (preceding E2611-19). This configuration employs three microphones and two loads as distinct air cavities (3M2L). The primary advantage of the 3M2L method is that it requires only four transfer function measurements to derive the transfer matrix for any test samples. For comparison, 4M1L needs at least three, and 4ML2 at least six. The measurement setup involves a slightly modified classical impedance tube, where the third microphone is flush-mounted on a movable hard termination, as depicted in Figure 9.2. An air cavity is added downstream of the sample. The 3M2L method was used by Attal et al. (2019) and Attal, Dubus, et al. (2021). The foundation for the 3M2L method was initially established for a measurement configuration where the porous sample is placed against a rigid termination, with the third microphone flush-mounted to the same termination (Doutres, Salissou, Atalla, & Panneton, 2010).

The alternative impedance tube measurement methods operate on the principle of directly deriving the transfer matrix elements (T_{11}, T_{12}, T_{21}, and T_{22}). This approach enables the combination of the obtained
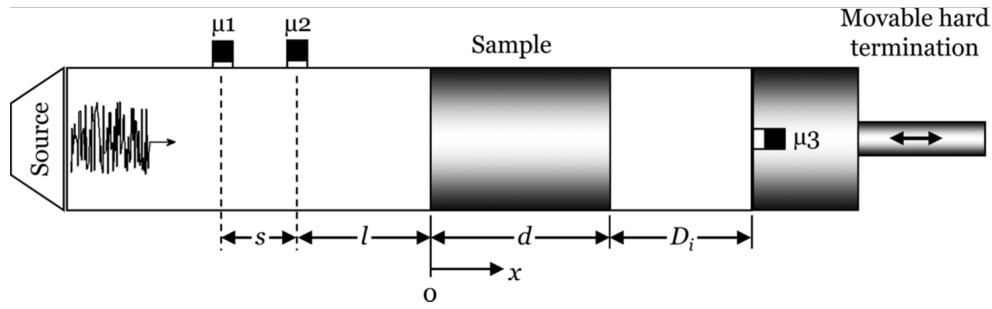
Figure 9.2: Impedance tube configuration for the 3M2L method measurements
Note. From "Complement to standard method for measuring normal incidence sound transmission loss with three microphones," by Salissou et al. (2012), *The Journal of the Acoustical Society of America*, Copyright 2012 by Acoustical Society of America.

transfer matrix to be related to the general formulation for sound propagation through an equivalent fluid impedance layer, as depicted in Eq.9.1. From this relationship, material properties such as wavenumber (Eq.9.2) and characteristic impedance (Eq.9.3) can be derived (Cox & D'Antonio, 2017). Essentially, these methods can be viewed as the inverse of the approach employed in the current study. While the current method requires determining effective values first to be inserted into the transfer matrix, these alternative methods allow for the derivation of the effective values directly from the transfer matrix.

$$\begin{bmatrix} T_{11} & T_{12} \\ T_{21} & T_{22} \end{bmatrix} = \begin{bmatrix} \cos(kd) & jz_c \sin(kd) \\ j\frac{1}{z_c}\sin(kd) & \cos(kd) \end{bmatrix} \tag{9.1}$$

$$k = \frac{1}{d}\cos^{-1}(T_{11}) \tag{9.2}$$

$$z_c = \sqrt{\frac{T_{12}}{T_{21}}} \tag{9.3}$$

9.3. Key Constraint of Impedance Tube Measurements

The primary limitation of impedance tube measurements, compared to reverberation chamber and free-field methods, is their restriction to normal incidence. In practical situations, acoustic waves impact a structure from multiple angles. As a consequence, solely measuring normal incidence coefficients, such as surface impedance, absorption, and reflection coefficients, can be deceptive.

This limitation may not affect **locally reacting materials**, as their surface impedance remains constant regardless of the angle at which a plane wave encounters them (NEN-EN-ISO 10534-2:2023, 2023). However, these materials' absorption and reflection coefficients can still vary based on the angle of incidence. Locally reacting materials in acoustics, such as those with straight, unconnected pores like homogeneous honeycomb structures, are designed to allow sound waves to penetrate deeply into the material before attenuation occurs. When sound pressure acts at a specific point on the material surface, it does not influence neighbouring points, meaning that sound reflection and absorption are confined to that point only.

In contrast, when pores are interconnected, the sound field within one pore can be influenced by the sound pressure above another pore (Dragonetti & Romano, 2017). This interconnectedness results in extended reactions within the material, leading to non-locally reactive behaviour. Consequently, the sound wave can propagate in various directions within the material. This results in the surface impedance of **non-locally reacting materials** varying depending on the angle of incidence.

When the speed of sound within a material is significantly lower than in free air, refraction causes the wave inside the material to propagate almost perpendicular to the material's surface, aligning with Snell's law (Cox & D'Antonio, 2017). This characteristic defines the surface of the material as **locally reacting**, as the surface impedance remains consistent regardless of the angle of the incident wave. This

simplification is advantageous, enabling the assumption of normal propagation in multilayered absorbents, thereby greatly simplifying evaluation. Additionally, it facilitates treating porous materials as equivalent fluids, given that only longitudinal waves are observed in fluid bulk (Allard, 1993).

However, LWS components, particularly foliage and mineral wool, despite their lower speed of sound compared to air, possess a complex structure, rendering them anisotropic and resulting in rather extended reacting surface behaviour. The inherent randomness of plants naturally results in an anisotropic layer, whereas mineral wool demonstrates high anisotropy due to its fibre arrangement in layers (Cox & D'Antonio, 2017). Therefore, simplifying them as locally reacting is considered divergent from real-world conditions. On the other hand, loose substrates, characterized by small and randomly placed particles, demonstrate relatively isotropic behaviour on a macroscale, allowing them to be considered semi-locally reacting.

As a result, due to the very complex nature of LWS components, they are considered mostly non-locally reacting. As noted in NEN-EN-ISO 10534-2:2023 (2023), for non-locally acting materials, there is no direct correlation between sound absorption coefficients measured with an impedance tube using ISO 10534 and those in a diffuse sound field using ISO 354 (NEN-EN-ISO 354:2003, 2003). NEN-EN-ISO 10534-2:2023 (2023) suggests that for such non-locally reacting materials, impedance tube measurements can be employed to determine the intrinsic properties of the material, as demonstrated in the current study. Subsequently, a characterization can be conducted, followed by the computation of a diffuse sound field simulation, e.g. FEM (Dragonetti & Romano, 2017).

Certainly, evaluating the LWS performance in real settings proves challenging with the current method. There is a necessity for further studies utilizing methods like FEM and BEM simulations or even more sophisticated approaches to address the oblique incidence performance of LWSs. However, such considerations are beyond the scope of the current study. Nevertheless, it can be generally asserted that for the main objective of the current study — to provide a quick estimation tool for arbitrary LWS configurations in early design stages — this approach can provide valuable decision-making insights.

9.4. Possible Alternatives to Impedance Tube Measurements

Impedance tube measurements present both advantages and challenges, particularly regarding their suitability for relatively small sample sizes compared to other measurement techniques. While sample size might not significantly impact the geometrical properties of various absorber materials, it posed a notable issue in testing LWS components in the current study:

- **Loose soil test samples:** The measured characteristics of loose soil in its natural environment (in situ) are significantly influenced by the level of soil compaction, which proves challenging to accurately reproduce when the same soil sample is subjected to impedance tube testing (Horoshenkov et al., 2013). As a consequence, the variability in results can be quite substantial.

- **Foliage test samples:** Measuring plant characteristics presents challenges, as evidenced in Figure 7.7, where the morphology of most plants was altered upon insertion into the impedance tube. For example, Horoshenkov et al. (2013) emphasized the importance of densely arranging leaves in the sample holder to minimize the influence of plant height and leaf stem length on tortuosity. This arrangement ensures that the path length for acoustic wave propagation through the plant is primarily controlled by the leaf angle. The densely packed foliage in the current study necessitated the use of fabric to create a reference surface. However, this compromised the angles of the front leaves. Furthermore, limitations in tube diameter also played a role in altering the angles of the remaining leaves. To address this issue, Attal et al. (2019) suggested employing an impedance tube with a significantly larger diameter than the sample heterogeneities (leaves).

Overall, it can be argued that conventional impedance tube measurement setups can distort results representative of real-life conditions for testing LWS components. Ideally, a method that accommodates larger sample sizes should be used. Larger samples enable LWS components to be accurately modelled as isotropic and homogeneous due to the ratio between sample size and sample heterogeneities. Reverberation chamber measurements, as per NEN-EN-ISO 354:2003 (2003), have limitations as they only allow for the derivation of absorption coefficient and not impedance. Consequently, one suitable method is deemed the two-microphone free-field measurement (Champoux, Nicolas, & Allard, 1988), which can be considered an extension of the impedance tube method (Cox & D'Antonio, 2017). A significant advantage of this method is its capability to measure oblique incidences.

The setup for two-microphone free-field measurements requires an anechoic or hemi-anechoic environment. In this configuration, a large absorbent sample is exposed to plane waves emitted by a loudspeaker positioned at a specific angle relative to the surface, as illustrated in Figure 9.3. Two microphones, placed at specific distances from the surface and with particular spacing, capture the reflected sound waves. The frequency limits discussed for the impedance tube, both lower and upper, in relation to microphone spacing, continue to be applicable. This also extends to the positioning of the microphones relative to the sample to ensure the capture of only plane waves. The microphone positions should have the same displacement in the horizontal plane but vary in height in the vertical plane.
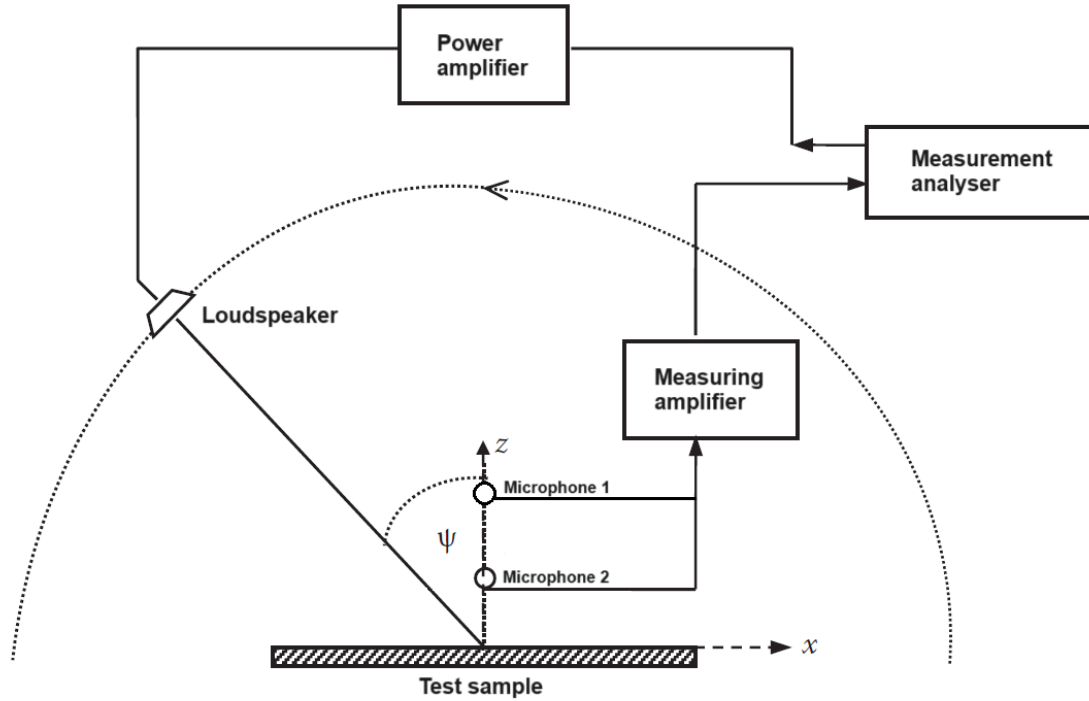
Figure 9.3: Schematic setup for two-microphone free-field measurement
Note. From *Acoustic absorbers and diffusers : Theory, Design and Application* (3rd ed. p. 100) by Cox and D'Antonio (2017), *Taylor & Francis*, Copyright 2017 by Taylor & Francis.

As a consequence, the transfer function measurement principle used in the impedance tube can be directly applied to the free-field case (Section 6.1). Specifically, Eq.6.7 can be revised to derive Eq.9.4. The surface impedance can then be calculated using Equation 6.13.

$$r = \frac{-H_{12} \cdot e^{j(kx_1)\cos(\psi)} + e^{j(kx_2)\cos(\psi)}}{H_{12} \cdot e^{-j(kx_1)\cos(\psi)} - e^{-j(kx_2)\cos(\psi)}} \tag{9.4}$$

Where: ψ = Angle of incidence (see Figure 9.3)

The primary limitation of this approach is that, ideally, the sample size should be infinite (Cox & D'Antonio, 2017). However, in practice, the sample is always finite, introducing the issue of edge diffraction. At low frequencies, edge diffraction causes the reflected wave to lose its plane-wave characteristics, making simple theoretical models ineffective. A general guideline is that the lower frequency limit occurs when half a wavelength spans the sample's smallest dimension. Therefore, samples usually need to cover several square meters. Additionally, as the angle of incidence increases, edge diffraction effects become more pronounced at higher frequencies, making it challenging to measure at very large angles without significantly larger samples.

As a result, for future research with similar objectives to current studies, it is recommended to use (two-microphone) free-field measurements instead of impedance tube measurements.

9.5. Alternative Approaches For Deriving Effective Properties

In the current study, the effective properties of the LWS components for the TMM were initially derived through impedance tube measurements, wherein their normal-incidence surface impedance was determined, followed by the application of mathematical methods to derive the characteristic impedance and wavenumber. However, other methods exist that do not rely on impedance measurements and are instead semi-empirical in deriving effective properties (Jiménez et al., 2021). These models attempt to account for the fact that porous frames have a much more complex structure than fluids. Therefore, they must consider the structural properties of the porous frame, in addition to the visco-thermal properties of the saturating fluid. Such models, however, require (numerous) input parameters to account for the majority of the physics involved in the visco-thermal processes within porous frames.

The most fundamental and simplest model of porous materials is the one-parameter model proposed by Delany and Bazley (D&B) (Delany & Bazley, 1970; Jiménez et al., 2021). This model requires only one parameter — flow resistivity — to estimate the effective properties of the materials. As described in Section 4.2, flow resistivity refers to the resistance encountered by airflow within a given thickness of material and serves as an indicator of air permeability through porous substances. Flow resistivity can be obtained based on the ISO 9053:1991 (1991) standard.

A refinement of the D&B model was carried out by Miki to correct non-physical behavior of the effective properties in the low-frequencies (Jiménez et al., 2021; Miki, 1990). It is recommended to use Miki's model instead of the D&B. Examples of where Miki's model was utilized to derive the effective properties of LWS components, such as foliage and substrates, were presented by Horoshenkov et al. (2013). However, in order to accurately predict the acoustic absorption behaviour of LWS components, two more input parameters — porosity and tortuosity — were introduced, resulting in a total of three parameters. The latter parameters could be measured directly. Nevertheless, due to limitations in measuring LWS components, Horoshenkov et al. (2013) proposed a formula to theoretically relate the effective tortuosity of a plant to the dominant angle of leaf orientation.

Furthermore, there are more complex models, such as the Johnson-Champoux-Allard (JCA) model, which require additional input parameters (Jiménez et al., 2021). However, this complexity does not necessarily guarantee increased accuracy, as many input parameters must be derived via measurements. The JCA model, for instance, involves five parameters (Champoux & Allard, 1991). Initially, the model is based on expressions for dynamic effective density and bulk modulus. The input parameters for these expressions include porosity, tortuosity, flow resistivity, and the thermal and viscous characteristic lengths. From the dynamic effective density and bulk modulus, the effective wavenumber and characteristic acoustic impedance of the porous material can be obtained. Additionally, the JCA model was extended by Lafarge (Lafarge, Lemarinier, Allard, & Tarnow, 1997), resulting in the Johnson-Champoux-Allard-Lafarge (JCAL) model. This extended model introduces one more additional parameter: static thermal permeability.

As a result, it can be inferred that all these semi-empirical models strive to elucidate the mechanisms underlying the observed acoustic attenuation in impedance tube experiments. Consequently, the methodology adopted in the current study — measuring test sample properties via impedance tube — can be deemed appropriate. The captured complex wave propagation behaviour within the test samples effectively diminishes the imprecision associated with estimating the materials' structure and the corresponding mechanism of visco-thermal losses.

Part III

Developmental Study: Optimization Tool

10

Performance Metric

The primary objective of this study is to develop a decision-support tool for stakeholders to assess the acoustical performance of arbitrary VGS designs. This tool, in addition to providing information on the performance of VGS in mitigating urban noise, will also serve as a framework for quantifying the broader environmental and monetary impacts of VGS. This objective is crucial, as Chapter 3 underscores the importance of having a clear performance metric to effectively guide the design and implementation of VGS. Such a metric is essential for stakeholders to estimate the costs and benefits associated with VGSs as a noise abatement measure and to evaluate VGSs sustainability in terms of their impact on human health and well-being.

European Environment Agency (2010) provides guidelines for quantifying the health and well-being impacts of noise. As noted in Section 1.1, the exposure of residents (population) to noise is characterized using noise level indicators such as L_{den} and L_{night}. Noise maps help to illustrate how the population is distributed across these noise levels. The relationship between noise levels and their impact in outcomes (endpoints) on health and well-being is well-established through extensive research. This information is reflected in exposure-response curves, which help determine the proportion of the population exposed to each category of endpoints (based on severity). Thereafter, the results can be converted to a health-based population indicator - DALY (Disability-Adjusted Life Years). DALY is used to estimate the health burden caused by the loss of healthy life-years due to adverse health effects associated with excessive noise exposure, such as sleep disturbance, cardiovascular diseases, and mental health impacts. By converting noise mitigation benefits, such as those provided by VGSs, into DALY, stakeholders can quantitatively evaluate and compare different noise abatement strategies within the framework of LCA focusing on human health impacts.

Similarly, a CBA of different noise abatement strategies, including VGS, can be conducted by accounting for the proportion of the population exposed to each noise level (European Environment Agency, 2010). It is found that properties exposed to higher noise levels will have a lower market value than similar buildings exposed to lower noise levels. Correspondingly, the hedonic pricing method, which translates the effects of noise on human health and well-being into monetary terms as a function of property value depreciation due to noise, can be used. The effectiveness of the implemented measures is evaluated by comparing the monetary benefits of the strategies — measured as the difference in hedonic property prices between baseline and abatement scenarios — with their corresponding investment costs (Lopez, Adams, & Walker, 2024).

As a result, the acoustic performance of VGSs in urban noise mitigation can be estimated at the district, neighbourhood, or street scale according to the noise mapping methodology established in CNOSSOS-EU (Kephalopoulos et al., 2012). This methodology requires that during simulations, reflections on vertical obstacles (e.g. building façades and noise barriers) are addressed using image sources. This approach necessitates inputting the absorption coefficient of the vertical surface in 1/3 octave bands. If this information is known, the L_{den} and L_{night} can be determined, allowing for LCA or CBA to be conducted for the selected noise exposure area.

The simulation process for urban noise levels is labour-intensive. Therefore, validating input information beforehand is crucial for ensuring its optimality. While detailed data on absorption performance in 1/3 octave bands can be informative, it may be challenging for stakeholders from diverse backgrounds to interpret.

In contrast, the weighted absorption coefficient simplifies assessment by providing a single averaged value that represents the overall sound absorption performance of VGSs across various frequencies. This coefficient, calculated according to ISO 11654 (NEN-EN-ISO 11654:1997, 1997), also determines the absorption class of the VGS. For instance, a VGS with a weighted sound absorption coefficient of 0.9 absorbs 90% of sound energy and belongs to class A. Similarly, coefficients ranging from 0.8 to 0.85 correspond to class B, 0.6 to 0.75 to class C, 0.33 to 0.55 to class D, and 0.15 to 0.25 to class E. By focusing on this overarching metric, stakeholders can simplify the process of design selection or optimization and facilitate clearer comparisons of the performance of different designs and noise abatement materials available on the market.

Despite this reasoning, the main performance metric used in the empirical study to evaluate VGS design on urban noise mitigation was RL. Understanding how different VGS configurations affect RL across frequencies allows stakeholders to develop more effective VGS solutions tailored to minimizing reflection power and explaining certain absorption behaviours of the designs. Return loss serves as a technical baseline that complements both qualitative and quantitative assessments of VGS performance.

<div align="right">11</div>

Backend Development of the Tool

The tool is designed to model the absorption properties of multilayer rigidly-backed VGS systems within air-VGS-wall boundary conditions. This boundary condition is set because VGS-s are typically installed on impervious walls, e.g. masonry or concrete facades, ensuring no transmission problem. The acoustic impedance at the VGS interface with the surrounding medium (air at 20°C) is considered $z_0 = 413.3$ Rayl. At the rear of the VGS, a rigid boundary condition $v_x = 0$ is applied.

A schematic flowchart illustrating the backend programming of the tool, including functions, their corresponding functionalities, and the sequence of execution, is depicted in Page 103. The core of the tool is encapsulated in the MAIN functions. Table 11.1 lists these MAIN functions and their respective references.

MAIN functions execution principle: The data processing procedure detailed in Section 7.3 facilitates the derivation of effective values for VGS components. These values are stored in designated binary files, which serve as inputs for the simulation tool. Specific functions are implemented to extract and read these files. Upon receiving user input through the GUI, extrinsic variables such as chosen components and layer thicknesses are defined. Subsequently, the developed code executes the functions based on equations established in the theoretical framework presented in Chapter 5. Notably, the outputs are frequency-dependent, spanning from 200 Hz to 1600 Hz at 2 Hz intervals. To align with NEN-EN-ISO 11654:1997 (1997), a dedicated function iterates through predefined center frequencies of 1/3 octave bands to calculate the average absorption coefficient for each band. After that, functions adhere to the step-by-step procedure specified in ISO 11654.

<div align="center">

Table 11.1: References for MAIN Functions

</div>

Function Name	Corresponding Eq. in Chapter 5	Corresponding Section in NEN-EN-ISO 11654:1997 (1997)
calc_T_for_d()	5.16	-
T_total()	5.17	-
RL_total()	5.19, 5.20, 5.22	-
abs_total()	5.21	-
practical_abs()	-	4.1
abs_weighted()	-	4.2, 4.3
determine_absorption_class()	-	Annex B

Tool.py

Input GUI Functions

- `load_variables()` — Loads previous input values.
- `save_variables()` — Saves current input variables.
- `update_layer_activness()` — Updates activation status of layers. → Calls `save_variables()`
- `update_layer_selection()` — Updates selected plant and substrate options. → Calls `save_variables()`
- `update_substrate_state()` — Updates the state of the substrate. → Calls `save_variables()`
- `update_substrate_thickness()` — Updates the thickness of the substrate layer. → Calls `save_variables()`
- `update_plant_thickness()` — Updates the thickness of the plant layer. → Calls `save_variables()`
- `update_cavity_thickness()` — Updates the thickness of the cavity layer. → Calls `save_variables()`

`input_interface()`

- Calls `load_variables()`
- Sets up Tkinter root window and configures styles.
- Calls `fig_scheme_opening()`.
- **Creates activation checkbuttons:**
  - `plant_checkbutton`: Activate/deactivate plant layer. → Calls `update_activness()`.
  - `substrate_checkbutton`: Activate/deactivate substrate layer. → Calls `update_activness()`.
  - `cavity_checkbutton`: Activate/deactivate cavity layer. → Calls `update_activness()`.
- **Crates dropdown menu:**
  - `plant_menu`: for selecting plant type → Calls `update_selection()`.
  - `substrate_menu`: for selecting substrate type → Calls `update_selection()`.
- **Creates radiobuttons:**
  - `dry_button` for selecting dry state. → Calls `update_state()`.
  - `saturated_button` for selecting saturated state. → Calls `update_state()`.
- **Creates sliders:**
  - `plant_slider`: for adjusting Foliage layer thickness. → Calls `update_plant_thickness()`.
  - `substrate_slider`: for adjusting Substrate layer thickness. → Calls `update_substrate_thickness()`.
  - `cavity_slider`: for adjusting Cavity thickness. → Calls `update_cavity_thickness()`.
- **Creates button**
  - `update_button`: to close the GUI and apply changes when clicked.

MAIN Functions

- `check()` — Prints the status of various global variables from `input_interface()`.
- `extract_filepaths()` — Extracts file paths for effective data from a given folder path.
- `load_eff_values()` — Loads effective data from the file paths.
- `calc_T_for_d()` — Calculates transfer matrices of the layers.
- `T_total()` — Calculates the total transfer matrix of the specified system configuration.
- `RL_total()` — Calculates reflection coefficients and return loss values based on the total transfer matrix.
- `abs_total()` — Calculates absorption coefficients based on reflection coefficients.
- `abs_to_third_octave_bands()` — Calculates third-octave band absorption coefficients from wide-band frequency range absorption values.
- `practical_abs()` — Calculates practical full octave band absorption coefficients (ISO 11654).
- `abs_weighted()` — Calculates weighted sound absorption at 500 Hz and determines shape indicators (ISO 11654).
- `determine_absorption_class()` — Determines the absorption class based on the weighted sound absorption (ISO 11654).

Figures Functions

- `fig_scheme_opening()` — Generates a figure displaying the matrix scheme with all layers activated.
- `fig_scheme()` — Generates a figure displaying the matrix scheme based on global variables from `input_interface()`.
- `fig_RL()` — Generates a figure displaying the frequency-dependent return loss (RL) values plotted against frequencies.
- `fig_abs()` — Generates a figure displaying the one-third-octave band sound absorption coefficients plotted against frequencies.
- `fig_ISO11654()` - NOT DIRECTLY ACTIVATED — Generates a figure displaying the practical sound absorption coefficients and the shifted reference curve according to ISO 11654.

Output GUI Functions

`output_interface()`

- Creates a new top-level GUI window for displaying simulation output.
- Configures grid layout for the frames.
- **First Frame**
  - Calls `fig_scheme()`
  - Adds global parameters display.
- **Second Frame**
  - Adds a heading and text for parameters according to ISO 11654.
  - Calls `fig_abs()`
- **Third Frame**
  - Calls `fig_RL()`

User Guide

This user guide aims to demonstrate the practical application of the tool by creating a possible configuration of the VGS. Specifically, for the demonstration is considered VersiWall GM module developed by Elmich, depicted in Figures 2.8 and 7.1. The module depth is 15 cm. This module supports various loose substrates, with Perlite chosen as an example. Additionally, a foliage layer of Ajuga reptans, 10 cm thick, is considered.

Figure 12.1 illustrates the pop-up GUI that appears when running the Python code. This window displays a schematic representation of the VGS transfer matrices configuration under rigid-backing conditions. It is possible, however, to include or exclude specific layers in the designed VGS configuration. Additionally, the substrate saturation state can be chosen. Currently, the substrate state is set to dry and the cavity layer is disabled, while all other parameters are inserted as described.
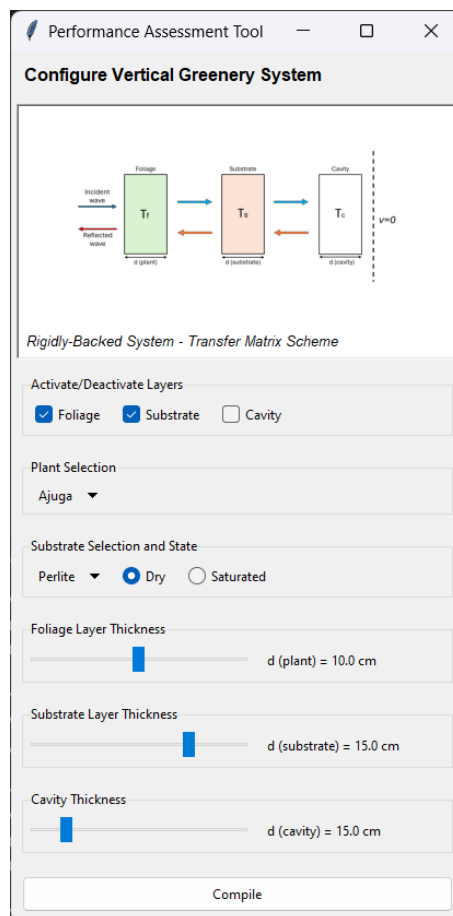
Figure 12.1: Pop-up window: input parameters

After configuring the VGS, the code runs in the background, and another pop-up window is displayed, as depicted in Figure 12.2(a). This window shows the schematic representation of the configured system in the Transfer Matrix Scheme, along with the set parameters. It includes the frequency-dependent RL performance, as well as parameters according to ISO 11654.

When rerunning the code, the previous input values remain, allowing users to modify the system step by step until the desired performance is reached. For example, Figure 12.2(b) depicts the output for a configured VGS where all the initial dimensions are left untouched, while a cavity of 15 cm is added. Figure 12.2(c) shows the system's performance when the saturation state is enabled. Finally, Figure 12.2(d) illustrates the VGS configuration with the initial dimensions, a saturated substrate state, and an added 15 cm cavity.

In Figure 12.3, the VGS configuration remains the same, except that Perlite has been replaced by Sphagnum Moss.

In Figure 12.4, the simulation output of Sempergreen's product *Flexipanel* is depicted. Figure 7.4 provides a detailed view of the Flexipanel's substrate, where mineral wool serves as the core material with a thickness of 6 cm. For the demonstration, a foliage layer of Ajuga reptans, 10 cm thick, is considered.

(a) Dry module

(b) Dry module + Cavity

(c) Saturated module

(d) Saturated module + Cavity
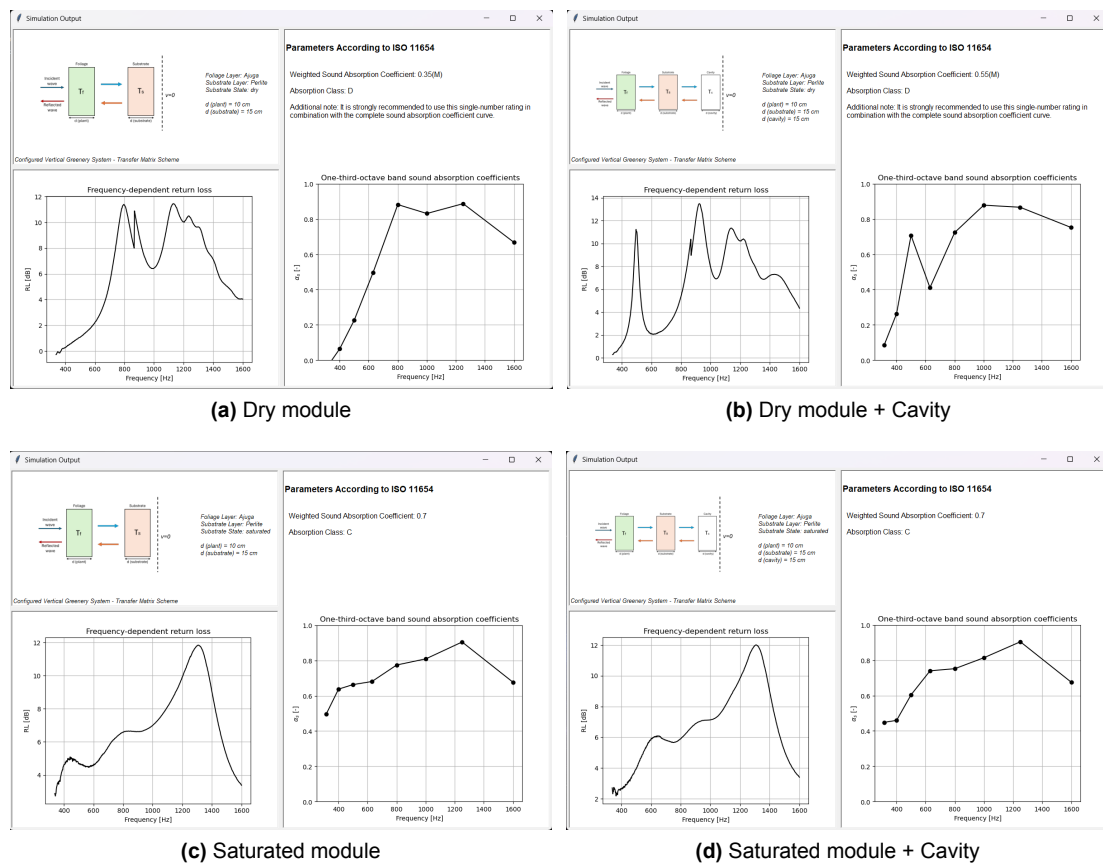
Figure 12.2: Performance of the prod. *VersiWall GM* - Plant: Ajuga, Substrate: Perlite

(a) Dry module

(b) Dry module + Cavity

(c) Saturated module

(d) Saturated module + Cavity
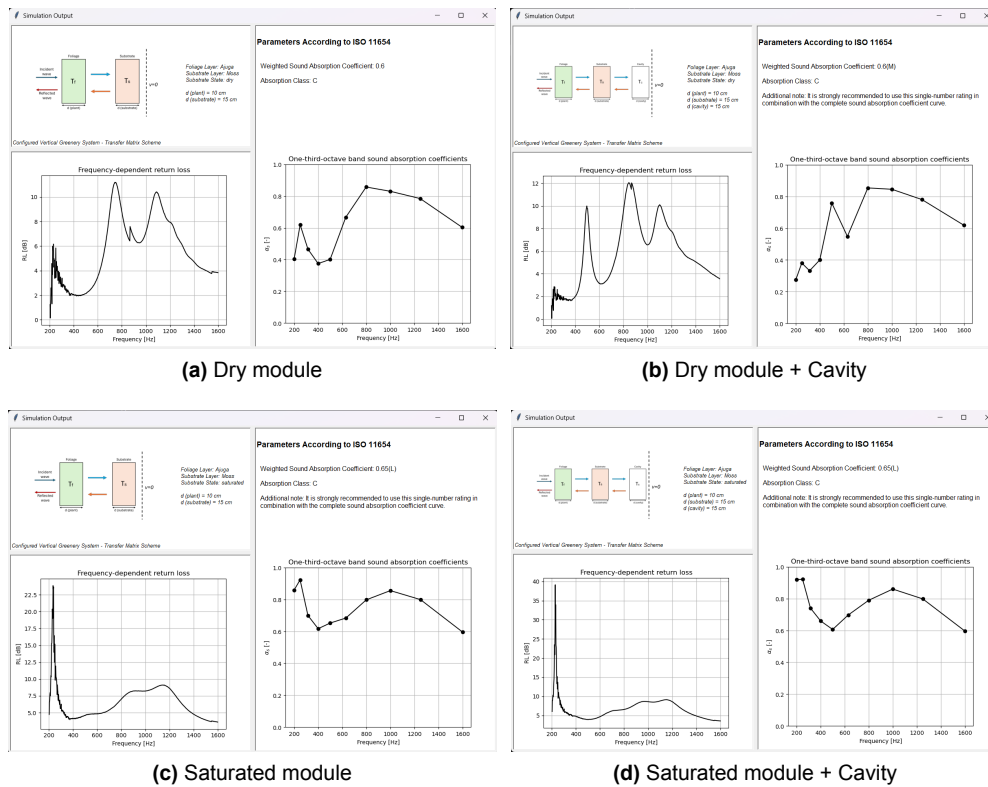
Figure 12.3: Performance of the prod.*VersiWall GM* - Plant: Ajuga, Substrate: Moss

(a) Dry module

(b) Dry module + Cavity

(c) Saturated module

(d) Saturated module + Cavity

Figure 12.4: Performance of the prod.*Flexipanel* - Plant: Ajuga, Substrate: Mineral Wool

<div style="text-align: right; font-size: 3em;">13</div>

Discussion

This section aims to clarify the tool's scope of applicability, outline practical strategies for tool utilization, propose further enhancements, and identify areas for future development. Key questions addressed include:

- How effectively can the tool's outcomes inform decision-making for urban noise mitigation?
- What are the primary practical principles for optimizing VGS designs using the current capabilities of the tool?
- What ideas exist to improve the tool's ability to depict optimal VGS designs?
- Why does the tool's cavity thickness range extend up to 1 meter?
- What are the overarching limitations of the tool in its current state that must be considered?

Each question will be addressed in its respective section, following the same order as listed.

13.1. Main Considerations

As discussed in Section 3.3, the benefits of VGS on individual buildings may diminish in significance when considering their contribution towards district, neighbourhood, or street-scale goals. Therefore, it is advisable to utilize the tool to assess VGS performance when anticipating extensive area coverage relative to the scale under consideration.

Moreover, while the tool provides performance metrics for configured VGS designs, it is crucial to note that even if a VGS exhibits favourable characteristics in terms of RL and absorption, its placement and interaction with surrounding structures can significantly impact its real-world effectiveness. Therefore, relying solely on the metrics highlighted by the tool may not fully capture the complexity of urban noise mitigation. The effec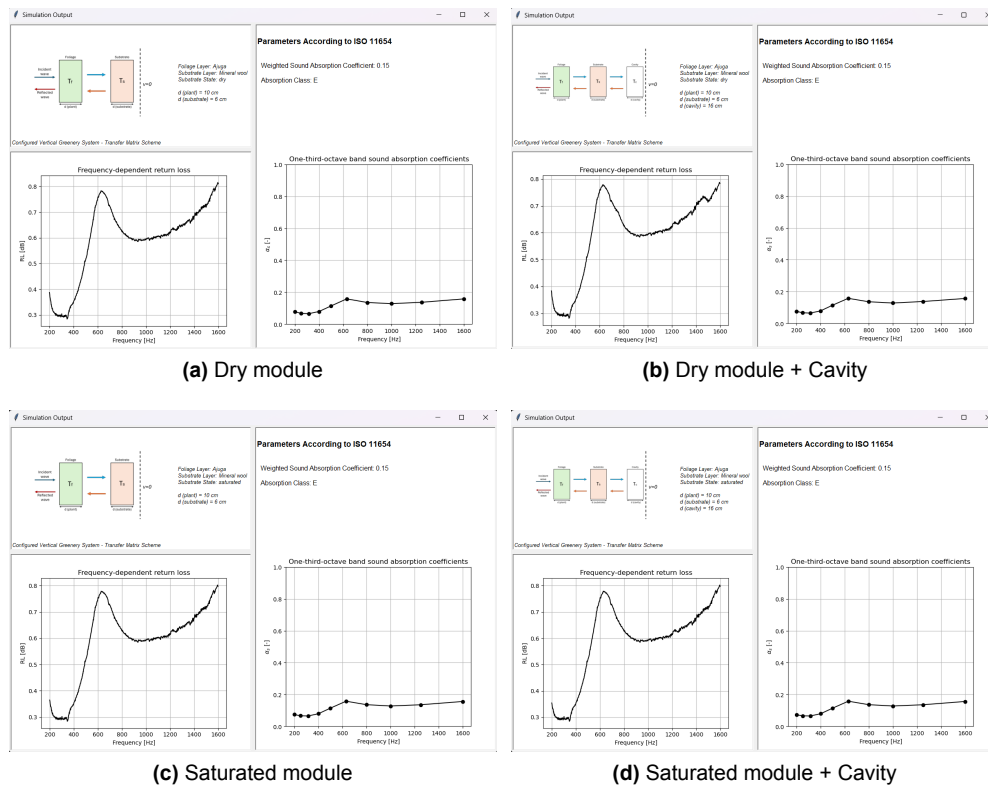tiveness of proposed VGS designs and their implementation across an urban area can only be comprehensively evaluated through simulations, as outlined in the methodology of CNOSSOS-EU (Kephalopoulos et al., 2012).

13.2. Optimization Strategies

In Chapter 8, it was concluded that optimizing VGSs based solely on the optimal thickness of individual layers under specific boundary conditions is impractical. Instead, the focus should be on understanding the interactions between these layers and the unique conditions created by their superposition. The interaction of waves with superimposed layers is intricate and influenced by complex factors inherent to each layer. Importantly, impedance matching was identified as playing a pivotal role in determining performance and providing crucial guidance.

High impedance matching or complete mismatching between VGS layers, especially when rigidly backed, results in weaker return loss. In the case of high impedance matching, the impedance change between layers is insufficient to effectively attenuate waves, leading to reduced absorption of sound energy. Conversely, in the case of complete mismatching, there are significant reflections at layer boundaries due to the large impedance differences. These reflections bounce sound waves back into the environment rather than absorbing them, further diminishing wave attenuation within the VGS. Both scenarios are

detrimental to VGS performance. Therefore, achieving the desired impedance matching is crucial for optimizing system performance.

Ideally, each successive layer of the VGS should contribute to increased return loss and improved absorption. This goal is attained by ensuring the outermost layer closely matches the impedance of air, while the inner layers offer superior sound wave attenuation with higher impedance. Gradual transitions in impedance between layers are optimal for minimizing reflections (Cox & D'Antonio, 2017). In VGS designs, achieving this typically involves using foliage layers with low flow resistivity and progressively higher resistivity for substrate layers.

However, in projects where specific foliage and substrate types are specified and impedance transitions are either too abrupt or inadequate, adjustments may be required. To enhance impedance matching in cases of abrupt impedance transitions, incorporating an intermediate layer with intermediate impedance between the foliage and substrate can be advantageous. Alternatively, in cases where impedance transitions are insufficient to provide effective sound attenuation, panel absorbers or perforated structures positioned behind the VGS can significantly enhance acoustic performance, as highlighted by Chang and Chang (2022).

13.3. Potential Optimization Algorithm

The developed tool allows the testing of various combinations of VGS components and facilitates the evaluation of optimal impedance transitions through the repeated application of transfer matrix equations. This approach is akin to a "trial-and-error method," known for its time and labour-intensive nature, highlighting the necessity for further tool enhancements to streamline user experience.

Attal, Buot de l'Epine, et al. (2021) proposed an optimization method for a conventional foliage-substrate-wall system. Based on the method of 3D mapping of RL performance of the VGS as presented in Section 8.1, they developed a methodology for detecting the optimized performance of the overall system (not individual components). They called this approach "video 3D mapping." The core idea behind video 3D mapping involves creating an interactive 3D map using the total transfer matrix of the VGS. In the total transfer matrix, the rigid wall layer maintains a constant thickness, while the substrate and foliage layers exhibit fluctuations in thickness. Correspondingly, the map illustrates the achieved return loss performance of a VGS for a specific substrate thickness, showing how performance varies with frequencies along the x-axis and with different thicknesses of the foliage layer along the y-axis. The interactive nature of this map lies in the ability to manipulate the thickness of the substrate in real-time. As the substrate thickness is adjusted, the map dynamically displays corresponding changes in the RL performance behaviour. As a result, video 3D mapping enables the identification of the optimal relationship between substrate and foliage layer thicknesses based on predefined objectives.

Inspired by this approach, the proposal aims to enhance the tool by integrating automatic optimization through a specialized algorithm. This algorithm would run in the background, calculating total transfer matrices for every frequency across various combinations of plant and substrate thicknesses within a specified range (e.g., from 5 cm to 15 cm). It would systematically evaluate these combinations to determine the optimal relationship between substrate and foliage layer thicknesses, aiming to maximize return loss within targeted frequency regions.

13.4. Cavity Implementation Guidelines

As Attal, Buot de l'Epine, et al. (2021) noted, there are generally two primary goals when optimizing VGS systems:

- To maximize return losses at lower frequencies
- To achieve as homogeneous return losses as possible across the rest of the spectrum.

However, they found that below 265 Hz, it is difficult to achieve reasonably good return loss performance. This finding is consistent with the literature (Chapter 4), which indicates that conventional VGS designs typically do not perform well below 250 Hz. Therefore, to attenuate low frequencies, the cavity between the rigid facade and the VGS could be considered.

The added cavity mechanism is discussed in Section 4.2.3. It was established that the VGS must be placed at a distance from the facade where the particle velocity maxima is formed. Therefore, the

desired cavity thickness can be derived based on Eq.13.1. Accordingly, the addition of a cavity can help attenuate only a narrow range of frequencies. Thus, the cavity thickness must be chosen to target the most bothersome frequencies.

$$d = m\frac{\lambda}{4} \tag{13.1}$$

Where: d = Optimal cavity thickness
λ = Target wavelength
m = Mode number for particle velocity maxima (1, 3, 5 ...)

In the provided examples shown in Figures 12.2 and 12.3, adding a cavity has a significant effect, particularly for dry substrates. A 15 cm cavity enhances the RL in the frequency range of 400 Hz to 600 Hz for dry perlite and moss by approximately 8-10 dB. In contrast, for saturated perlite, there is a more modest increase of around 1-2 dB. However, for saturated moss, the trend differs significantly: the added cavity enhances an existing peak in the 200-400 Hz range by about 20 dB. Despite this variation, these observations generally align with the theory described by Eq.13.1, where a quarter-wavelength cavity thickness of 15 cm corresponds to a wavelength of 0.6 meters, equivalent to 570 Hz.

However, the impact of adding a cavity on RL performance is not always substantial. This was illustrated in Figure 12.4, where a 16 cm cavity had minimal effect on RL enhancement (ca 0.02 dB) in the frequency range of 1400 Hz to 1600 Hz. This frequency range corresponds to the second particle velocity maxima interval ($m = 3$). While there was a minimal increase in RL observed for the dry substrate, the effect was fully negligible for the saturated substrate.

The variation in cavity performance between different VGS configurations can be attributed to the impedance gradient theory (Section 13.2). In the initial examples, the optimal thickness of the substrate created a desirable impedance gradient between layers, which enhanced the effectiveness of the cavity mechanism. Conversely, in the latter example, the impedance gradient between layers was relatively abrupt. From the data analysis (Chapter 8), it was evident that mineral wool has a substantially higher impedance mismatch with air. Consequently, most of the incident waves were reflected from the substrate, resulting in low RL performance of the VGS configuration, thereby rendering the cavity's overall influence negligible.

Table 13.1 highlights the central frequencies of 1/3 octave bands below 315 Hz and depicts the corresponding wavelengths with quarter-wavelength cavity thicknesses ($m = 1$). It can be seen that to address the low frequencies, the cavity thickness must be substantial. For existing buildings, accommodating these dimensions can be very challenging. However, this consideration can be incorporated into the design phase of new projects, such as integrating corridor facades (a type of double-skin facade). For instance, Figure 13.1 illustrates an example project where a GF was seamlessly integrated into a corridor facade system. This approach can similarly apply to implementing a LWS.

Table 13.1: Quarter-wavelength cavity dimensions

Frequency [Hz]	Wavelength [m]	Quarter-wavelength [m]
315	1.09	0.27
250	1.37	0.34
200	1.71	0.43
160	2.14	0.53
125	2.74	0.69
100	3.43	0.86

(a) Facade perspective from the outside   **(b)** Facade perspective from the inside

Figure 13.1: Oasia Hotel Downtown by WOHA architects in Singapore
Note. From "ArchDaily," by Bingham-Hall (2016)
(`https://www.archdaily.com/800878/oasia-hotel-downtown-woha`). Copyright 2016 by Patrick
Bingham Hall.

13.5. Current Limitations

The primary limitations of the tool developed are linked to the methods applied, and the results derived from the empirical study. The use of an impedance tube measurement method, as standardized in NEN-EN-ISO 10534-2:2023 (2023), introduced two main constraints:

Firstly, the impedance tube method is limited in its frequency range, providing reliable measurements only within the specified working frequency range (Section 6.1.1). In this study, measurements were conducted from 100 Hz to a maximum of 1600 Hz. Data processing procedure (Section 7.3) revealed that valid results are predominantly above 200 Hz. However, within this valid range, certain components show non-applicable values up to 400 Hz due to the phase unwrapping procedure discussed in Section 7.3.3. Secondly, the impedance tube method measures acoustic properties only at normal incidence, limiting the applicability of the results. This method does not consider oblique incidence or diffuse sound fields, which restricts the practical use of the measurement results.

These limitations significantly impact the derivation of the weighted absorption coefficient as specified in ISO 11654 (NEN-EN-ISO 11654:1997, 1997). According to this standard, frequency-dependent sound absorption coefficients must be derived in accordance with ISO 354 (NEN-EN-ISO 354:2003, 2003). ISO 354 specifies measurements in a diffuse sound field and defines results in 1/3 octave bands, covering central frequencies from at least 200 Hz to 5000 Hz. Consequently, the absorption coefficients derived using the impedance tube method fall short in several ways:

Firstly, the measured absorption coefficients from 200 Hz to 1600 Hz (with 2 Hz intervals) do not directly correspond to the required 1/3 octave bands. The issue arises because the 200 Hz and 1600 Hz measurements align with the centre frequencies of 1/3 octave bands, not their ranges. For computing the sound absorption coefficient for the 200 Hz 1/3 octave band, measurements between 178 Hz and 199 Hz are missing. Similarly, for the 1600 Hz 1/3 octave band, measurements between 1601 Hz and 1780 Hz are missing. Consequently, in the current study, the absorption coefficients for 1/3 octave bands are derived with these limitations in mind.

Secondly, complete coverage of 1/3 octave band absorption coefficients from 200 Hz to 5000 Hz is necessary to derive the practical sound absorption coefficient for each 1/1 octave band. This range ensures

that each 1/1 octave band includes exactly three 1/3 octave bands. However, in this study, the highest 1/3 octave band absorption coefficient derived was at 1600 Hz. Consequently, for the 2000 Hz 1/1 octave band — which includes the lower 1/3 octave band limit of 1600 Hz, centre 1/3 octave band of 2000 Hz, and upper 1/3 octave band limit of 2500 Hz —only the value at 1600 Hz is considered.

Thirdly, complete coverage of 1/3 octave band absorption coefficients from 200 Hz to 5000 Hz is necessary to derive 1/1 octave band absorption coefficients up to 4000 Hz. This is crucial because in ISO 11654, the provided reference curve covers 1/1 octave bands from 200 Hz to 4000 Hz. Due to the limitations mentioned in this study, this full range of the reference curve was not fully utilized. Therefore, the weighted sound absorption coefficients presented in the tool are incomplete and cannot be directly compared with other equivalent noise abatement measures, where single-number absorption coefficients were derived in accordance with all requirements specified in ISO 11654.

Part IV

Closure

14

Conclusion

This project has endeavoured to address critical research questions surrounding the acoustical performance and overall feasibility of VGS through the development of a robust decision-support tool. This conclusion highlights the answers to the posed research questions, synthesizes the findings, and offers insights into future research directions and practical implementations for stakeholders engaged in urban planning, architecture, and environmental management.

Sub-Question 1

How are VGSs classified, and which factors shape the selection of their components?

To address this question, the study embarked on a comprehensive exploration of VGS technologies, examining their overarching principles down to their individual components. Two main typologies were distinguished: GFs and LWSs. Various design variations were introduced and described in detail, with a specific focus on LWSs due to their complexity and potential for higher acoustic performance.

Several design factors influence the selection of LWS components. Creating a robust vegetation cover involves considering key factors such as climate suitability, sun exposure, cultivation system, maximum plant height, available root space, and competition with other plants. It is recommended to prioritize resilient species native to the climate for their ability to thrive with minimal maintenance. Evergreen plants are ideal for year-round ornamental appeal, while perennial plants ensure longevity and reduce the need for frequent replanting.

Essential properties of suitable substrate as growing media include being lightweight, highly porous, good drainage capabilities, and adequate water and nutrient-holding capacity. In LWS, the choice of growing media varies depending on the system type. Continuous systems commonly use lightweight absorbent materials such as mineral wool, geotextile, or foam. Modular systems expand options to include both inorganic materials (e.g., perlite, vermiculite, expanded clay) and organic materials (e.g., peat, coco coir, sphagnum moss), each offering distinct benefits such as structural durability, controlled nutrient supply, or moisture retention.

Sub-Question 2

What are the key sustainability challenges in the widespread adoption of VGSs, and how can these challenges be addressed?

The economic viability of LWSs hinges significantly on overcoming cost-related barriers that deter widespread adoption. Stakeholders often perceive high initial investments and ongoing life-cycle expenses — such as installation, maintenance, replacement, and potential demolition costs — as substantial hurdles. To assess the long-term economic value of LWSs, CBA serves as a crucial tool. This method compares the monetary costs and benefits throughout the system's life cycle. By quantifying benefits, stakeholders can better understand the financial feasibility and potential returns of implementing LWSs.

The most pronounced benefits of LWSs are their ecosystem services, specifically environmental benefits. To properly evaluate the long-term environmental value of LWSs, LCA serves as a crucial methodology.

LCA considers various factors, including potential reduction in noise pollution. However, conducting LCA for LWSs is complicated due to the novelty of these systems, resulting in a lack of comprehensive data and suitable models to accurately quantify the full range of benefits over their lifespans. Therefore, existing research often relies heavily on assumptions, which can introduce uncertainties that lead to scepticism and concerns about 'greenwashing' claims, where environmental benefits may be exaggerated or misrepresented.

Addressing stakeholder concerns about initial costs while emphasizing long-term savings and non-monetary advantages can significantly strengthen the case for integrating LWSs into urban development strategies. A pivotal step in this direction is to prioritize quantifying the acoustic performance of LWSs and establishing a meaningful, universal metric for evaluation. This approach empowers stakeholders to make well-informed decisions regarding optimized designs that strike a balance between environmental benefits and financial feasibility.

Sub-Question 3
What mechanisms define the acoustic performance of VGSs?

Based on an extensive literature review of empirical studies, it is evident that vegetation and substrates play crucial but distinct roles in sound absorption. Vegetation is most effective at absorbing sound above 1000 Hz (medium frequencies) but tends to scatter it at frequencies exceeding 2500 Hz (higher frequencies). In the medium frequency range, where the wavelength of the incident wave is larger than the dimensions of individual leaves, the integral foliage layer governs sound absorption. When sound waves pass through the foliage layer, they interact with leaves, stems, etc., causing sound energy to convert into heat through viscous friction and thermal conduction processes. Higher leaf area density and larger dominant leaf orientation angles increase tortuosity, leading to enhanced acoustic absorption. In the high-frequency range, where the wavelength is smaller than or equal to the leaf dimensions, individual leaves become dominant and act as vibrating plates when hit by sound pressure waves. However, the resonance velocity of a leaf is slower than the air particle velocity, resulting in rather sound energy reflection.

Substrates are critical for effective sound absorption, particularly within the 250 Hz to 1000 Hz range. All LWS substrates possess porous absorber properties, meaning they absorb and dissipate acoustic energy that passes through or interacts with their porous matrix due to visco-thermal losses. Visco-thermal dissipation mechanisms depend on the flow resistivity, porosity, tortuosity, and thickness of the layer. Higher open porosity allows more pathways for sound waves, greater tortuosity creates a longer and more irregular network, and larger pores increase surface area for deeper sound wave propagation, especially at lower frequencies. Optimal flow resistivity reduces impedance mismatch, allowing sound waves to propagate into the layer while effectively dissipating energy through visco-thermal losses. Achieving optimal thickness is crucial for the same considerations. Higher substrate saturation levels diminish acoustic absorption capacity by reducing substrate porosity, which affects all other parameters.

LWSs function effectively as porous absorbers for mid- and high-frequency sound waves, but are less effective for low-frequency sound waves. To address this limitation, enhancing the system's performance can be achieved by introducing an air cavity between the LWS and the rigid facade. Positioning the LWS at a quarter-wavelength distance from the facade, tailored to the frequency of interest, optimizes the absorption of the reflected waves from the rigid facade by effectively intercepting high-velocity particles.

Sub-Question 4
How do the proposed VGS components perform acoustically?

The following plant species native to the Dutch climate were selected: the evergreen Festuca glauca, the perennial plants Heuchera 'Cascade Dawn', Waldsteinia ternata, Bergenia cordifolia, and Ajuga reptans. For substrates, mineral wool was chosen for continuous LWS, while loose lightweight substrates were deemed suitable for modular LWS. These substrates include organic options such as coco coir, coco husk, and Sphagnum moss, as well as inorganic options like perlite and vermiculite. Additionally, heavier substrates such as expanded clay balls, popular in LWS applications, and pumice, increasingly used in green roof implementations, were considered.

The performance of individual LWS components was assessed under specific boundary conditions, with each component treated as a layer in an air-layer-air system. The RL performance of each layer was examined. Plants achieved better RL performance compared to substrates due to their superior impedance matching with air. For substrates, the RL difference between dry and saturated states was not as pronounced. The performance was highly dependent on the substrate's microstructure. For instance, substrates like perlite and coco coir, which are good at both water retention and drainage, showed better RL performance when saturated due to their closer impedance matching with air. In contrast, substrates like mineral wool, moss, and vermiculite, which have good water retention but poor drainage, exhibited greater characteristic impedance and thus worse impedance matching with air, leading to poor RL performance. Clay balls, coco husk, and pumice, with their poor water retention and good drainage, did not exhibit changes in microstructure, resulting in stable RL performance.

At higher frequency bands, the dominance of the mass-reactance component (the imaginary part of the characteristic impedance) made reflections more prevalent for both plants and substrates. For substrates, this effect became noticeable from 1400 Hz, while for plants, it was observed from 1000 Hz (up to the maximum frequency analyzed, 1600 Hz). The intricate structures of both foliage and substrates make it challenging to pinpoint the exact factors influencing these properties. Therefore, a more thorough investigation at the microscale level is necessary. It is also possible that measurement errors affected the results.

Sub-Question 5

What key metrics are essential for stakeholders to effectively assess VGS design effectiveness and make informed implementation decisions?

The weighted absorption coefficient is a crucial metric for stakeholders to effectively assess the effectiveness of VGS design in urban noise mitigation. This metric, calculated according to the ISO 11654 standard, provides a single averaged value ranging from 0 to 1 that indicates the overall sound absorption performance of VGS across frequencies. A value of 1 corresponds to full "open window" absorption, while 0 indicates full reflection from the surface. Moreover, the standard allows for the classification of VGS into specific absorption classes (A, B, C, D, or E) based on their weighted sound absorption coefficient. This metric simplifies the assessment and comparison of different VGS designs and conventional noise abatement materials, facilitating informed decisions in design selection or optimization based on their acoustic performance characteristics.

Finally, The main research question posed at the beginning of the project was:

Main Research Question

How does the TMM facilitate the quantification of the acoustic performance of VGSs?

The engineering approach in the current study involves modelling complex multi-layer LWS by breaking them down into homogeneous layers. Each layer represents specific components, such as foliage or substrate. Individual analysis of each component was conducted to evaluate how variations in thickness affect its acoustic performance under specific boundary conditions.

However, accurately assessing the effectiveness of the multi-layer LWS cannot be achieved solely through analysing individual layer parameters or their performance in specific contexts. In other words, trying to determine the optimal universal type of foliage or substrate with specific thicknesses is not feasible and is not the appropriate approach. To truly understand the behaviour of the multilayer system, one must focus exclusively on the superposition of layers and consider specific boundary conditions. Yet, the complexity of superposition's behaviour is profound, depending on the interaction of numerous intricate intrinsic variables. As a result, the most effective approach to assessing LWSs efficacy involves systematic experimentation with various component combinations. This includes varying extrinsic variables such as thicknesses of the layers to identify zones of enhanced performance potential.

A significant advancement in streamlining this approach has been the development of a tool based on the TMM. This tool facilitates estimating how complex impedance transitions between layers influence

overall acoustic performance conveniently. The tool incorporates a comprehensive material library, allowing stakeholders to leverage its capabilities based on the TMM to expedite implementation and enhance the effectiveness of VGS designs. This tool not only provides information on the performance of VGS in mitigating urban noise but also serves as a framework for quantifying the broader environmental and monetary impacts of VGS. Namely, it offers frequency-dependent inputs for further simulations that aid in quantifying the monetary and environmental performance of VGS designs.

Details on accessing the tool and its operational requirements are provided in the repository:

GitHub Repository
https://github.com/smrksn/Optimization-of-the-Vertical-Greenery-Systems

In conclusion, the developed tool significantly aids in designing optimized VGSs, yet the process remains notably labor-intensive. To address this, future research should prioritize the creation of advanced algorithms that can streamline and automate the design process, thereby improving both efficiency and accuracy. Additionally, while initial steps have been taken towards standardizing the assessment of environmental and monetary performance using the tool's outputs, further refinement and standardization are essential. By advancing these aspects, future research can greatly contribute to the promotion of sustainable practices and robust economic evaluations. This, in turn, will support the integration of environmental and financial considerations into mainstream decision-making processes, enhancing the feasibility and adoption of VGSs on a broader scale.

15

Reflection

15.1. Project-Related Insights

> 1. What is the relation between the graduation project topic, Building Technology (BT) track, and the master programme - Architecture, Urbanism and Building Sciences (AUBS)?

My graduation project on mitigating urban noise pollution is intricately related to the Building Technology track of the AUBS master's program. This research is firmly rooted in the building physics domain, emphasizing the integration of acoustical engineering with advanced technological solutions. The BT track, distinguished among other tracks within the AUBS faculty, delves deeply into fundamental sciences such as physics and technological engineering fields. This is exemplified in my project through the application of a framework rooted in linearly applied research.

The primary objective was to create a versatile tool that addresses the needs of various stakeholders, empowering them to make informed decisions in urban planning and building design. Consequently, this holistic approach not only addresses building technology but also has a direct impact on the field of architecture and urbanism by providing practical solutions to enhance living conditions in metropolitan areas. This interdisciplinary integration underscores the essence of the AUBS programme, which aims to blend architectural innovation, urban development, and building sciences to tackle contemporary urban challenges comprehensively.

> 2. How do you assess the academic and societal value, scope, and implications of your graduation project, including ethical aspects?

The academic and societal value of my graduation project, which focuses on noise pollution mitigation through the development of a decision-making tool, is significant and multifaceted.

Academic Value: From an academic perspective, my project contributes to the fields of building technology, acoustical engineering, and urban sustainability. By employing a generic model using the empirical data, my research provides a robust framework for understanding the acoustical properties of VGS. This work not only advances the scientific knowledge of VGS performance but also fills critical gaps in current methodologies for cost-benefit and life cycle assessments. The interdisciplinary approach, integrating building physics, environmental science, and programming, demonstrates the value of cross-disciplinary research in addressing complex urban issues. Additionally, the tool developed can serve as a foundation for further academic studies and widespread adoption of urban noise mitigation technologies.

Societal Value: Noise pollution is a pervasive issue in urban environments, adversely affecting the health and well-being of citizens. By providing a practical tool that stakeholders—such as urban planners, architects, and policymakers—can use to evaluate and implement VGS, my project offers a tangible solution to improve urban soundscapes and urban climate. The societal implications are broad, encompassing improved mental and physical health outcomes for individuals, enhanced quality of life in urban areas, and increased environmental sustainability. The project also promotes the aesthetic and ecological benefits of green infrastructure, contributing to more liveable and resilient cities.

Ethical Aspects: Ethically, my project addresses several key concerns. Firstly, it promotes environmental sustainability by advocating for green infrastructure, which provides various ecosystem services beyond noise reduction. Secondly, it considers social equity by aiming to improve living conditions in urban

areas, potentially benefiting underprivileged communities disproportionately affected by noise pollution. Lastly, the decision-making tool is designed to be transparent and accessible, ensuring that a wide range of stakeholders can use it to make informed decisions, thus promoting democratic and inclusive urban planning processes.

3. How do you evaluate whether the feasibility of your graduation project justifies further interest?

My graduation project focuses broadly on integrating VGSs for urban noise reduction feasibility. To assess this, it is crucial to contrast the advantages of VGSs with the limitations of traditional synthetic materials. Conventional sound-absorbing materials such as acoustic panels, foams, and specialized facade coverings are susceptible to deterioration from moisture, UV radiation, atmospheric pollutants, and microbial growth. Over time, these materials can lose their effectiveness and require costly maintenance or replacement, contributing to environmental waste and escalating project costs.

In contrast, VGSs provide a sustainable alternative with inherent durability, particularly when the plant components are carefully selected to suit specific environmental conditions. They possess natural resilience against environmental stressors with proper maintenance, and thus can maintain their acoustic properties over extended periods. Therefore, by addressing the limitations of synthetic materials and emphasizing the benefits of vegetation-based solutions, stakeholders can justify further exploration and implementation of VGSs in urban noise management projects.

15.2. Personal Insights

1. Did the research approach work out? How do you assess the value of your way of working (your approach, your used methods, used methodology)?

The main idea of my research approach was first to become well-acquainted with the topic by understanding the current state of VGS technologies. This involved conducting an extensive literature review, which was a major component of my project. I explored various VGS designs, their corresponding components, and the uncertainties in their design processes and implementation. Investigating these uncertainties was particularly important as it highlighted the gaps in sustainability assessment, superficially in widely used methods such as cost-benefit analysis and life cycle assessment.

The primary objective of the research was to integrate acoustical engineering methods, focusing primarily on addressing the uncertainty surrounding the estimation of the acoustical performance of VGSs. To tackle this, I analyzed VGS components individually in terms of their acoustical properties. This involved conducting impedance tube measurements and deriving effective acoustical parameters for each component. By inputting these effective values into the theoretical model — specifically, the TMM — it became possible to predict the acoustical performance of the multi-layered structure that constitutes a VGS. Additionally, for data analysis and the subsequent development of the decision-making tool, I employed programming techniques to automate the process. This approach ensured a systematic and efficient workflow.

Overall, all the steps in my research approach were successfully implemented. Therefore, I assess the value of my approach and methodology as highly effective, as they have led to practical and impactful outcomes in the field of building technology and urban sustainability. Nevertheless, the outcomes of the project must be validated for ease of use and applicability in real-life settings—specifically, how well it aids the decision-making process. This validation is considered a crucial aspect of further research.

2. How did you translate the feedback of your mentors into your work?

Throughout my project, I had the privilege of receiving guidance and feedback from mentors who are experts in various aspects relevant to my graduation project. These mentors were proficient in implementing acoustic design, utilizing vertical greenery technology, and conducting research on urban noise. Their feedback was instrumental in shaping the direction of my work and ensuring alignment with my objectives and research aims.

Our regular meetings, typically scheduled every 2–3 weeks, provided ample opportunity to present my progress and discuss any challenges or questions that arose. During these meetings, I actively listened to the feedback provided by my mentors and incorporated their suggestions into my work. Whether it was

refining methodologies, adjusting research focus, or considering alternative approaches, the input from my mentors helped me navigate through the complexities of my project and make informed decisions.

3. What have you learned during the graduation process?

Throughout the graduation process, I have gained invaluable insights and skills. Initially, my primary goal was to delve deeply into the principles of acoustical engineering, particularly at a fundamental level grounded in physics. This opportunity proved immensely beneficial, especially as a building technologist, where such depth of understanding is often overlooked but essential. Understanding the underlying physics bolstered my confidence in navigating the project and underscored the significance of its outcomes.

While a significant portion of the project delved into theoretical realms, seemingly distant from architectural technology, this foundational analysis was crucial. It illuminated the root causes of the issues at hand, highlighting the necessity of thorough problem analysis for effective solution generation. Through this process, I have learned the importance of approaching challenges with a comprehensive understanding, even if it means venturing into seemingly unrelated domains.

Moreover, the project allowed me to hone my research and analytical skills, particularly in synthesizing complex information and applying it practically. From conducting extensive literature reviews to performing empirical measurements and developing theoretical models, each step enhanced my abilities as a researcher and problem-solver.

References

Acoustical Society of America. (2016). *Specific Acoustic Impedance.* `https://asastandards.org/terms/specific-acoustic-impedance/`.

Acoustics - Determination of acoustic properties in impedance tubes - Part 2: Two-microphone technique for normal sound absorption coefficient and normal surface impedance (Standard). (2023). Geneva, Switzerland: International Organization for Standardization. (Nederlandse norm)

Acoustics - Determination of airflow resistance - Part 2: Alternating airflow method (Standard No. ISO 9053:1991). (1991). Geneva, Switzerland: International Organization for Standardization.

Acoustics - Measurement of Sound Absorption in a Reverberation Room (Standard). (2003). Geneva, Switzerland: International Organization for Standardization. (Nederlandse norm)

Acoustics — Sound absorbers for use in buildings — Rating of sound absorption (Standard). (1997). Geneva, Switzerland: International Organization for Standardization. (Nederlandse norm)

Alberti, V., Alonso Raposo, M., Attardo, C., Auteri, D., Ribeiro Barranco, R., Batista E Silva, F., … Zulian, G. (2019). *The future of cities* (I. Vandecasteele, C. Baranzelli, A. Siragusa, & J. Aurambout, Eds.) (No. JRC116711). Luxembourg: Publications Office of the European Union. (EUR 29752 EN) doi: 10.2760/375209

Allard, J. F. (1993). *Propagation of sound in porous media: Modelling sound absorbing materials*. Springer Netherlands. doi: 10.1007/978-94-011-1866-8

AlMakadma, H., Kei, J., Yeager, D., & Feeney, M. P. (2023). Fundamental concepts for assessment and interpretation of wideband acoustic immittance measurements. *Seminars in Hearing*, *44*(1), 17–28. doi: 10.1055/s-0043-1763293

Alves, S., Scheuren, J., & Altreuther, B. (2016). Review of recent eu funded research projects from the perspective of urban sound planning: do the results cope with the needs of europe's noise policy? *Noise Mapping*, *3*(1).

ASTM International. (2019). *Test method for normal incidence determination of porous material acoustical properties based on the transfer matrix method* (Tech. Rep.). American Society for Testing and Materials. doi: 10.1520/e2611-19

Attal, E., Buot de l'Epine, Y., Dauchez, N., & Dubus, B. (2021). Experimental investigation of the effect of moisture on the acoustic properties of lightweight substrates used in green envelopes. *Applied Acoustics*, *180*, 108108. Retrieved from `https://www.sciencedirect.com/science/article/pii/S0003682X21002012` doi: https://doi.org/10.1016/j.apacoust.2021.108108

Attal, E., Côté, N., Shimizu, T., & Dubus, B. (2019). Sound absorption by green walls at normal incidence: physical analysis and optimization. *Acta Acustica united with Acustica*, *105*(2), 301–312.

Attal, E., Dubus, B., Leblois, T., & Cretin, B. (2021). An optimal dimensioning method of a green wall structure for noise pollution reduction. *Building and Environment*, *187*, 107362. Retrieved from `https://www.sciencedirect.com/science/article/pii/S0360132320307319` doi: https://doi.org/10.1016/j.buildenv.2020.107362

Azkorra, Z., Pérez, G., Coma, J., Cabeza, L., Bures, S., Álvaro, J., … Urrestarazu, M. (2015). Evaluation of green walls as a passive acoustic insulation system for buildings. *Applied Acoustics*, *89*, 46-56. Retrieved from `https://www.sciencedirect.com/science/article/pii/S0003682X14002333` doi: https://doi.org/10.1016/j.apacoust.2014.09.010

Bakker, J., Lugten, M., & Tenpierik, M. (2023). Applying vertical greening systems to reduce traffic noise in outdoor environments: Overview of key design parameters and research methods. *Building Acoustics*, *30*(3), 315-338. Retrieved from `https://doi.org/10.1177/1351010X231171028`

Beranek, L. L. (1972). Acoustical definitions. In *American institute of physics handbook* (3rd ed., chap. 3a). McGraw-Hill.

Besir, A. B., & Cuce, E. (2018). Green roofs and facades: A comprehensive review. *Renewable and Sustainable Energy Reviews*, *82*, 915-939. Retrieved from `https://www.sciencedirect.com/science/article/pii/S1364032117313680` doi: https://doi.org/10.1016/j.rser.2017.09.106

Bianchini, R. (2016). *The Vertical Gardens of Patrick Blanc.* `https://www.verticalgardenpatrickblanc`

`.com/medias`. (Media publication retrieved from Patrick Blanc's official website on 07/02/2024)

Bingham-Hall, P. (2016). *Oasia hotel downtown / woha.* ArchDaily. Retrieved from `https://www.archdaily.com/800878/oasia-hotel-downtown-woha` (Figure retrieved 06/06/2024)

Blanco, I., Vox, G., Schettini, E., & Russo, G. (2021). Assessment of the environmental loads of green façades in buildings: a comparison with un-vegetated exterior walls. *Journal of Environmental Management*, *294*, 112927. Retrieved from `https://www.sciencedirect.com/science/article/pii/S0301479721009890` doi: https://doi.org/10.1016/j.jenvman.2021.112927

Brüel & Kjær. (2019a). *Product data. bp1039.* Retrieved from `https://www.bksv.com/doc/Bp1039.pdf` (Retrieved on 19/05/2024)

Brüel & Kjær. (2019b). *Product data. bp1870.* Retrieved from `https://www.bksv.com/doc/bp1870.pdf` (Retrieved on 19/05/2024)

Bustami, R. A., Belusko, M., Ward, J., & Beecham, S. (2018). Vertical greenery systems: A systematic review of research trends. *Building and Environment*, *146*, 226-237. Retrieved from `https://www.sciencedirect.com/science/article/pii/S0360132318306036` doi: https://doi.org/10.1016/j.buildenv.2018.09.045

Butong AB. (2020). *Peruken.* Retrieved from `https://butong.eu/project/peruken/` (Figures retrieved on 13/02/2024)

Cardinali, M., Balderrama, A., Arztmann, D., & Pottgiesser, U. (2023). Green walls and health: An umbrella review. *Nature-Based Solutions*, *3*, 100070. Retrieved from `https://www.sciencedirect.com/science/article/pii/S2772411523000228` doi: https://doi.org/10.1016/j.nbsj.2023.100070

Carl Stahl ARC GmbH. (2023). *Greencable light.* Retrieved from `https://greencable.eu/en/greencable-light/` (Figure retrieved on 08/02/2024)

Cechová, K., Kunt, M., Jebavy, M., & Kozáková, D. (2023). Assortment of plants for growing in vertical gardens of central europe. *Scientia Agriculturae Bohemica*, *54*, 1-10. doi: 10.7160/sab.2023.540101

Centre, J. R., for Environment, I., & Sustainability. (2010). *International reference life cycle data system (ilcd) handbook – general guide for life cycle assessment – detailed guidance*. Publications Office. doi: doi/10.2788/38479

Champoux, Y., & Allard, J. (1991, 08). Dynamic tortuosity and bulk modulus in air□saturated porous media. *Journal of Applied Physics*, *70*(4), 1975-1979. Retrieved from `https://doi.org/10.1063/1.349482` doi: 10.1063/1.349482

Champoux, Y., Nicolas, J., & Allard, J. (1988). Measurement of acoustic impedance in a free field at low frequencies. *Journal of Sound and Vibration*, *125*(2), 313-323. Retrieved from `https://www.sciencedirect.com/science/article/pii/0022460X88902866` doi: https://doi.org/10.1016/0022-460X(88)90286-6

Chang, L.-T., & Chang, F.-C. (2022). Study of living wall systems' (lwss) support system for improving lwss life cycle performance and noise reduction potential. *Building and Environment*, *216*, 109007. Retrieved from `https://www.sciencedirect.com/science/article/pii/S0360132322002499` doi: https://doi.org/10.1016/j.buildenv.2022.109007

Chàfer, M., Pérez, G., Coma, J., & Cabeza, L. F. (2021). A comparative life cycle assessment between green walls and green facades in the mediterranean continental climate. *Energy and Buildings*, *249*, 111236. Retrieved from `https://www.sciencedirect.com/science/article/pii/S037877882100520X` doi: https://doi.org/10.1016/j.enbuild.2021.111236

Cilaird. (2023). *Different sized pore spaces in soil.* Retrieved from `https://soil.evs.buffalo.edu/index.php/File:9FDE2B38-94FC-495B-A12B-F57898660EFC.png` (Figure retrieved 12/06/2024)

Cojocariu, M., Chelariu, E. L., & Chirută, C. (2022). Study on behavior of some perennial flowering species used in vertical systems for green facades in eastern european climate. *Applied Sciences*, *12*, 474. Retrieved from `https://www.mdpi.com/2076-3417/12/1/474` doi: 10.3390/app12010474

Colton, J. (2010). *Complex wave number.* Course webpage. Retrieved 02/05/2024, from `https://physics.byu.edu/faculty/colton/courses-phy442-winter20` (Physics 442)

Constant314. (2010). *A representation of a plane wave's electric field shown from an oblique angle.* Wikimedia Commons. Retrieved from `https://commons.wikimedia.org/w/index.php?title=File:Plane_Wave_Oblique_View.jpg` (Figure retrieved 02/05/2024)

Cortês, A., Almeida, J., Santos, M. I., Tadeu, A., de Brito, J., & Silva, C. M. (2021). Environmental performance of a cork-based modular living wall from a life-cycle perspective. *Building and Environment*, *191*, 107614. Retrieved from `https://www.sciencedirect.com/science/article/pii/S0360132321000299` doi: https://doi.org/10.1016/j.buildenv.2021.107614

Cortês, A., Tadeu, A., Santos, M. I., de Brito, J., & Almeida, J. (2021). Innovative module of expanded cork agglomerate for green vertical systems. *Building and Environment*, *188*. Retrieved from `https://www.sciencedirect.com/science/article/pii/S0360132320308283` doi: https://doi.org/10.1016/j.buildenv.2020.107461

Cox, T. J., & D'Antonio, P. (2017). Acoustic absorbers and diffusers : Theory, design and application [third edition]. *CRC Press*.

Craiyon. (2024). *Craiyon - ai model drawing images from any prompt.* Craiyon. Retrieved from `https://www.craiyon.com/` (Figure retrieved 06/06/2024)

D'Alessandro, F., Asdrubali, F., & Mencarelli, N. (2015). Experimental evaluation and modelling of the sound absorption properties of plants for indoor acoustic applications. *Building and Environment*, *94*, 913-923. Retrieved from `https://www.sciencedirect.com/science/article/pii/S0360132315300196` doi: https://doi.org/10.1016/j.buildenv.2015.06.004

Davis, M., Tenpierik, M., Ramírez, F., & Pérez, M. (2017). More than just a green facade: The sound absorption properties of a vertical garden with and without plants. *Building and Environment*, *116*, 64-72. Retrieved from `https://www.sciencedirect.com/science/article/pii/S0360132317300100` doi: https://doi.org/10.1016/j.buildenv.2017.01.010

de Bree, H.-E. (2009). *The microflown e-book.* `https://www.microflown.com/resources/e-books/e-book-the-microflown-e-book`. (Accessed on 02/05/2024)

Delany, M., & Bazley, E. (1970). Acoustical properties of fibrous absorbent materials. *Applied Acoustics*, *3*(2), 105-116. Retrieved from `https://www.sciencedirect.com/science/article/pii/0003682X70900319` doi: https://doi.org/10.1016/0003-682X(70)90031-9

Dell, A., Krynkin, A., & Horoshenkov, K. (2021). The use of the transfer matrix method to predict the effective fluid properties of acoustical systems. *Applied Acoustics*, *182*, 108259. Retrieved from `https://www.sciencedirect.com/science/article/pii/S0003682X21003534` doi: https://doi.org/10.1016/j.apacoust.2021.108259

Doutres, O., Salissou, Y., Atalla, N., & Panneton, R. (2010). Evaluation of the acoustic and non-acoustic properties of sound absorbing materials using a three-microphone impedance tube. *Applied Acoustics*, *71*(6), 506-509. Retrieved from `https://www.sciencedirect.com/science/article/pii/S0003682X10000150` doi: https://doi.org/10.1016/j.apacoust.2010.01.007

Dragonetti, R., & Romano, R. A. (2017). Errors when assuming locally reacting boundary condition in the estimation of the surface acoustic impedance. *Applied Acoustics*, *115*, 121-130. Retrieved from `https://www.sciencedirect.com/science/article/pii/S0003682X16302493` doi: https://doi.org/10.1016/j.apacoust.2016.08.024

Elmich. (2016). *National Gallery Singapore.* Retrieved from `https://elmich.com/asia/?portfolio=national-gallery-singapore` (Figures retrieved on 13/02/2024)

European Environment Agency. (2010). *Good practice guide on noise exposure and potential health effects* (Tech. Rep. No. 11/2010). Luxembourg: European Environment Agency. Retrieved from `https://www.eea.europa.eu/publications/good-practice-guide-on-noise` (Copyright © EEA, Copenhagen, 2010)

European Environmental Agency. (2022). *Decarbonising road transport—the role of vehicles, fuels and transport demand.* European Environmental Agency Copenhagen, Denmark.

European Parliament and Council. (2002). *Directive 2002/49/ec of the european parliament and of the council of 25 june 2002 relating to the assessment and management of environmental noise - declaration by the commission in the conciliation committee on the directive relating to the assessment and management of environmental noise* (Tech. Rep. No. L 189). Brussels: Official Journal.

Fahy, F. (2001). 7 - sound absorption and sound absorbers. In F. Fahy (Ed.), *Foundations of engineering acoustics* (p. 140-180). London: Academic Press. Retrieved from `https://www.sciencedirect.com/science/article/pii/B9780122476655500084` doi: https://doi.org/10.1016/B978-012247665-5/50008-4

Fernández-Cañero, R., Pérez Urrestarazu, L., & Perini, K. (2018). Chapter 2.1 - vertical greening systems: Classifications, plant species, substrates. In G. Pérez & K. Perini (Eds.), *Nature based strategies for urban and building sustainability* (p. 45-54). Butterworth-Heinemann. Retrieved from `https://www.sciencedirect.com/science/article/pii/B9780128121504000045` doi: https://doi.org/10.1016/B978-0-12-812150-4.00004-5

Field, C., & Fricke, F. (1998). Theory and applications of quarter-wave resonators: A prelude to their use for attenuating noise entering buildings through ventilation openings. *Applied Acous-*

tics, *53*(1), 117-132. Retrieved from `https://www.sciencedirect.com/science/article/pii/S0003682X97000352` doi: https://doi.org/10.1016/S0003-682X(97)00035-2

Gemeente Amsterdam. (2021). *Geluidskaart 2021.* Retrieved from `https://maps.amsterdam.nl/geluid/` (Interactive Map. Screenshot made on 06/06/2024)

Green Wall SG. (2018). *Green facades, also known as 'green screens' are created by growing climbing plants on a support structure. this can be done either by installing a climbing frame or allowing the plant to climb directly on the wall.* Facebook. Retrieved from `https://www.facebook.com/photo/?fbid=494667257611024&set=pb.100063650810262.-2207520000` (Figure retrieved on 08/02/2024)

Greenworks. (2016). *Variety of vertical gardens.* Retrieved from `https://greenworks.se/variety-of-vertical-gardens/` (Figure retrieved on 13/02/2024)

Guillaume, G., Gauvreau, B., & L'Hermite, P. (2015). Numerical study of the impact of vegetation coverings on sound levels and time decays in a canyon street model. *Science of The Total Environment*, *502*, 22-30. Retrieved from `https://www.sciencedirect.com/science/article/pii/S0048969714012911` doi: https://doi.org/10.1016/j.scitotenv.2014.08.111

Herrero Durá, I., Cebrecos Ruiz, A., García Raffi, L., & Romero-García, V. (2019). Matrix formulation in acoustics: The transfer matrix method. *Modelling in Science Education and Learning*, *12*(2), 153-164. doi: 10.4995/msel.2019.12148

Hindle, R. L. (2012). A vertical garden: origins of the vegetation-bearing architectonic structure and system (1938). *Studies in the History of Gardens & Designed Landscapes*, *32*(2), 99-110. doi: 10.1080/14601176.2011.653535

Horoshenkov, K., Khan, A., & Benkreira, H. (2013, 05). Acoustic properties of low growing plants. *The Journal of the Acoustical Society of America*, *133*(5), 2554-2565. Retrieved from `https://doi.org/10.1121/1.4798671` doi: 10.1121/1.4798671

Horoshenkov, K., Khan, A., Benkreira, H., Mandon, A., & Rohr, R. (2011, 01). The effect of moisture and soil type on the acoustical properties of green noise control elements. *Proceedings of Forum Acusticum*, 845-849.

Howard, D. M., & Angus, J. (2017). *Acoustics and psychoacoustics* (5th ed.). Routledge. doi: 10.4324/9781315716879

Jim, C. (2015). Greenwall classification and critical design-management assessments. *Ecological Engineering*, *77*, 348-362. Retrieved from `https://www.sciencedirect.com/science/article/pii/S0925857415000348` doi: https://doi.org/10.1016/j.ecoleng.2015.01.021

Jiménez, N., Groby, J.-P., & Romero-García, V. (2021). The transfer matrix method in acoustics. In N. Jiménez, O. Umnova, & J.-P. Groby (Eds.), *Acoustic waves in periodic structures, metamaterials, and porous media: From fundamentals to industrial applications* (pp. 103–164). Cham: Springer International Publishing. Retrieved from `https://doi.org/10.1007/978-3-030-84300-7_4` doi: 10.1007/978-3-030-84300-7_4

Joosten, H., & Couwenberg, J. (2008, 01). Peatlands and carbon. *Assessment on Peatlands, Biodiversity and Climate Change*, 99-117.

Julinova, P., & Beckovsky, D. (2019). Perspectives of moss species in urban ecosystems and vertical living-architecture: A review. *Advances in Engineering Materials, Structures and Systems: Innovations, Mechanics and Applications*, 2370–2375.

Jørgensen, L., Dresbøll, D. B., & Thorup-Kristensen, K. (2014). Root growth of perennials in vertical growing media for use in green walls. *Scientia Horticulturae*, *166*, 31-41. Retrieved from `https://www.sciencedirect.com/science/article/pii/S0304423813006341` doi: https://doi.org/10.1016/j.scienta.2013.12.006

Jørgensen, L., Thorup-Kristensen, K., & Dresbøll, D. B. (2018). Against the wall—root growth and competition in four perennial winter hardy plant species grown in living walls. *Urban Forestry & Urban Greening*, *29*, 293-302. Retrieved from `https://www.sciencedirect.com/science/article/pii/S1618866716304290` (Wild urban ecosystems: challenges and opportunities for urban development) doi: https://doi.org/10.1016/j.ufug.2017.12.012

Kephalopoulos, S., Paviotti, M., & Anfosso-Lédée, F. (2012). *Common noise assessment methods in europe (cnossos-eu)* (No. 25379 EN). Luxembourg: Publications Office of the European Union. (TP 281, 21027-Ispra (VA), Italy)

Koruk, H. (2021, 04). Assessment of the measurement and prediction methods for the acoustic properties of natural fiber samples and evaluation of their properties. *Journal of Natural Fibers*. doi: 10.1080/15440478.2021.1907835

Kuttruff, H. (2007). *Acoustics: An introduction* (1st ed.). CRC Press.

Lacasta, A., Penaranda, A., Cantalapiedra, I., Auguet, C., Bures, S., & Urrestarazu, M. (2016). Acoustic evaluation of modular greenery noise barriers. *Urban Forestry & Urban Greening*, *20*, 172-179. Retrieved from `https://www.sciencedirect.com/science/article/pii/S1618866716300528` doi: https://doi.org/10.1016/j.ufug.2016.08.010

Lacasta, A., Peñaranda, A., & Cantalapiedra, I. (2018). Chapter 3.9 - green streets for noise reduction. In G. Pérez & K. Perini (Eds.), *Nature based strategies for urban and building sustainability* (p. 181-190). Butterworth-Heinemann. Retrieved from `https://www.sciencedirect.com/science/article/pii/B9780128121504000173` doi: https://doi.org/10.1016/B978-0-12-812150-4.00017-3

Lafarge, D., Lemarinier, P., Allard, J. F., & Tarnow, V. (1997, 10). Dynamic compressibility of air in porous structures at audible frequencies. *The Journal of the Acoustical Society of America*, *102*(4), 1995-2006. Retrieved from `https://doi.org/10.1121/1.419690` doi: 10.1121/1.419690

Larner, D. J., & Davy, J. L. (2014). The prediction of the complex characteristic acoustic impedance of porous materials..

Liu, P., & Chen, G. (2014). Chapter three - application of porous metals. In P. Liu & G. Chen (Eds.), *Porous materials* (p. 113-188). Boston: Butterworth-Heinemann. Retrieved from `https://www.sciencedirect.com/science/article/pii/B9780124077881000034` doi: https://doi.org/10.1016/B978-0-12-407788-1.00003-4

Living Green Walls. (2020). *Living Green Walls.* Retrieved from `https://livinggreenwalls.co.za/2017/08/09/living-green-walls-vertipockets-going-green-just-became-even-easier/` (Figures retrieved on 13/02/2024)

Lopez, M., Adams, M., & Walker, T. R. (2024). Cost-benefits analysis of noise abatement measures in the port of halifax, nova scotia, canada. *Transportation Research Interdisciplinary Perspectives*, *24*, 101057. Retrieved from `https://www.sciencedirect.com/science/article/pii/S2590198224000435` doi: https://doi.org/10.1016/j.trip.2024.101057

Lunain, D., Ecotiere, D., & Gauvreau, B. (2016, August). In-situ evaluation of the acoustic efficiency of a green wall in urban area. In *Internoise 2016, 45th International Congress and Exposition of Noise Control Engineering* (p. pp. 6592-6601). HAMBOURG, Germany: Institute of Noise Control Engineering - INCE. Retrieved from `https://hal.science/hal-01382576` (Internoise 2016, 45th International Congress and Exposition of Noise Control Engineering, HAMBOURG, ALLEMAGNE, 21-/08/2016 - 24/08/2016)

Lyon, R. H. (1974). Role of multiple reflections and reverberation in urban noise propagation. *The Journal of the Acoustical Society of America*, *55*(3), 493–503.

López-Rodríguez, G., Pérez-Esteban, J., Ruiz-Fernández, J., & Masaguer, A. (2016). Behavior and evolution of sustainable organic substrates in a vertical garden. *Ecological Engineering*, *93*, 129-134. Retrieved from `https://www.sciencedirect.com/science/article/pii/S0925857416302476` doi: https://doi.org/10.1016/j.ecoleng.2016.05.020

Manso, M., & Castro-Gomes, J. (2015). Green wall systems: A review of their characteristics. *Renewable and Sustainable Energy Reviews*, *41*, 863-871. doi: https://doi.org/10.1016/j.rser.2014.07.203

Manso, M., Castro-Gomes, J. P., Marchacz, M., GÓrski, M., Dulak, L., & Zuchowski, R. (2017). Acoustic evaluation of a new modular system for green roofs and green walls. *Architecture, Civil Engineering, Environment*, *10*(1), 99–108. Retrieved from `https://doi.org/10.21307/acee-2017-023`

Manso, M., Teotónio, I., Silva, C. M., & Cruz, C. O. (2021). Green roof and green wall benefits and costs: A review of the quantitative evidence. *Renewable and Sustainable Energy Reviews*, *135*, 110111. Retrieved from `https://www.sciencedirect.com/science/article/pii/S1364032120304020` doi: https://doi.org/10.1016/j.rser.2020.110111

Martens, M., Severens, P., Van Wissen, H., & Van Der Heijden, L. (1985). Acoustic reflection characteristics of deciduous plant leaves. *Environmental and Experimental Botany*, *25*(3), 285-292. Retrieved from `https://www.sciencedirect.com/science/article/pii/0098847285900139` doi: https://doi.org/10.1016/0098-8472(85)90013-9

Martensson, L., Fransson, A., & Emilsson, T. (2016). Exploring the use of edible and evergreen perennials in living wall systems in the scandinavian climate. *Urban Forestry & Urban Greening*, *15*, 84-88. Retrieved from `https://www.sciencedirect.com/science/article/pii/S161886671500179X` doi: https://doi.org/10.1016/j.ufug.2015.12.001

Martins, A. M. T., & de Campos, I. D. (2019). From the horizontal garden to the vertical garden: An architectural and environmental perspective of the "green" element. *IOP Conference Series: Materials*

Science and Engineering, *471*. doi: 10.1088/1757-899X/471/7/072022

Miki, Y. (1990). Acoustical properties of porous materials-modifications of delany-bazley models-. *Journal of the Acoustical Society of Japan (E)*, *11*(1), 19-24. doi: 10.1250/ast.11.19

MMA Architectural Systems Ltd. (2020). *The Shires.* Retrieved from `https://jakob.co.uk/projects/view/the-shires/` (Figure retrieved on 08/02/2024)

MMA Architectural Systems Ltd. (2021). *Drapers' Gardens.* Retrieved from `https://jakob.co.uk/projects/view/drapers-garden/` (Figure retrieved on 08/02/2024)

Morillas, J. M. B., Gozalo, G. R., González, D. M., Moraga, P. A., & Vílchez-Gómez, R. (2018). Noise pollution and urban planning. *Current Pollution Reports*, *4*(3), 208–219.

Natuur & Milieuteam Zuid. (2017). *Verkiezing fraaiste groene gevels in zuid.* Retrieved from `https://nmtzuid.nl/album/verkiezing-fraaiste-groene-gevels-in-zuid-2017/` (Figure retrieved on 08/02/2024)

Nilsson, M. E., Klæboe, R., Bengtsson, J., Forssén, J., Hornikx, M., van der Aa, B., … Hong, J. Y. (2013). Novel solutions for quieter and greener cities.. Retrieved from `https://api.semanticscholar.org/CorpusID:106810979`

Novintiss Society. (2019). *Living wall maintenance and set-up: Mounting, watering and maintenance.* Retrieved from `https://www.vertiss.net/mur-vegetal-entretien-mise-en-oeuvr?lang=en` (Figures retrieved on 13/02/2024)

of California Museum of Paleontology, U. (1999). *Morphology of the sphagnopsida.* Retrieved from `https://ucmp.berkeley.edu/plants/bryophyta/sphagnomm.html` (Retrieved on 19/05/2024)

Ogut, O., Tzortzi, N. J., & Bertolin, C. (2022). Vertical green structures to establish sustainable built environment: A systematic market review. *Sustainability*, *14*, 12349. doi: 10.3390/su141912349

Oliphant, T. E., & et al. (2020). *Numpy documentation: numpy.unwrap.* `https://numpy.org/doc/stable/reference/generated/numpy.unwrap.html`. (Accessed: May 21, 2024)

Ottelé, M., Perini, K., & Haas, E. (2014). 19 - life cycle assessment (lca) of green façades and living wall systems. In F. Pacheco-Torgal, L. Cabeza, J. Labrincha, & A. de Magalhães (Eds.), *Eco-efficient construction and building materials* (p. 457-483). Woodhead Publishing. Retrieved from `https://www.sciencedirect.com/science/article/pii/B9780857097675500194` doi: https://doi.org/10.1533/9780857097729.3.457

Palumbo, D. L., Jones, M. G., Klos, J., & Park, J. (2004). Improvements to the two-thickness method for deriving acoustic properties of materials. In *Noise-con 2004summer meeting and exposition.*

Perini, K., & Ottelé, M. (2014). Designing green facades and living wall systems for sustainable constructions. *International Journal of Design & Nature and Ecodynamics*, *9*(1), 31–46.

Perini, K., Ottelé, M., Haas, E., & Raiteri, R. (2011). Greening the building envelope, facade greening and living wall systems. *Open Journal of Ecology*, *1*, 1–8. doi: 10.4236/oje.2011.11001

Peris, E., & et al. (2020). Environmental noise in europe - 2020. *European Environmental Agency*, *1*, 104.

Perlite. (2024). Retrieved from `https://www.mindat.org/min-52649.html` (Mindat ID: 52649. Retrieved on 19/05/2024)

Pluke. (2012). *Diagram showing physical manifestation of a sound wave through air from a speaker to a human ear.* Wikimedia Commons. Retrieved from `https://commons.wikimedia.org/w/index.php?title=File:CPT-sound-physical-manifestation.svg&oldid=844688536` (Figure retrieved 02/05/2024)

Pouliot, R., Hugron, S., & Rochefort, L. (2015). Sphagnum farming: A long-term study on producing peat moss biomass sustainably. *Ecological Engineering*, *74*, 135-147. Retrieved from `https://www.sciencedirect.com/science/article/pii/S0925857414005436` doi: 10.1016/j.ecoleng.2014.10.007

Pudelska, K., & Miroslaw, A. (2015). The richness of plants in art nouveau gardens. *Acta Agrobotanica*, *68*(2).

Pumice. (2024). Retrieved from `https://www.mindat.org/min-48576.html` (Mindat ID: 48576. Retrieved on 19/05/2024)

Pérez, G., Coma, J., Barreneche, C., de Gracia, A., Urrestarazu, M., Burés, S., & Cabeza, L. F. (2016). Acoustic insulation capacity of vertical greenery systems for buildings. *Applied Acoustics*, *110*, 218-226. Retrieved from `https://www.sciencedirect.com/science/article/pii/S0003682X16300731` doi: https://doi.org/10.1016/j.apacoust.2016.03.040

Pérez, G., Coma, J., & Cabeza, L. F. (2018). Chapter 3.7 - vertical greening systems for acoustic insulation and noise reduction. In G. Pérez & K. Perini (Eds.), *Nature based strategies for urban*

and building sustainability (p. 157-165). Butterworth-Heinemann. Retrieved from `https://www.sciencedirect.com/science/article/pii/B978012812150400015X` doi: https://doi.org/10.1016/B978-0-12-812150-4.00015-X

Pérez-Urrestarazu, L., Fernández-Cañero, R., Campos-Navarro, P., Sousa-Ortega, C., & Egea, G. (2019). Assessment of perlite, expanded clay and pumice as substrates for living walls. *Scientia Horticulturae*, *254*, 48-54. Retrieved from `https://www.sciencedirect.com/science/article/pii/S0304423819303358` doi: https://doi.org/10.1016/j.scienta.2019.04.078

Radić, M., Brković Dodig, M., & Auer, T. (2019). Green facades and living walls—a review establishing the classification of construction types and mapping the benefits. *Sustainability*, *11*, 4579. Retrieved from `https://doi.org/10.3390/su11174579` doi: 10.3390/su11174579

Raji, B., Tenpierik, M. J., & van den Dobbelsteen, A. (2015). The impact of greening systems on building energy performance: A literature review. *Renewable and Sustainable Energy Reviews*, *45*, 610-623. Retrieved from `https://www.sciencedirect.com/science/article/pii/S1364032115000994` doi: https://doi.org/10.1016/j.rser.2015.02.011

Reyhani, M., Santolini, E., Tassinari, P., & et al. (2023). Environmental assessment of design choices of green walls based for materials combination and plants. *International Journal of Life Cycle Assessment*, *28*, 1078–1091. doi: 10.1007/s11367-023-02181-x

Reyhani, M., Santolini, E., Torreggiani, D., & Tassinari, P. (2022). Assessing the environmental performance of plastic-based and felt-based green wall systems in a life-cycle perspective. *Science of The Total Environment*, *822*, 153648. Retrieved from `https://www.sciencedirect.com/science/article/pii/S0048969722007409` doi: https://doi.org/10.1016/j.scitotenv.2022.153648

Riley, B. (2016). The state of the art of living walls: Lessons learned. *Building and Environment*, *114*, 219-232. Retrieved from `https://www.sciencedirect.com/science/article/pii/S0360132316305108` doi: https://doi.org/10.1016/j.buildenv.2016.12.016

Romanova, A., Horoshenkov, K. V., & Hurrell, A. (2019). An application of a parametric transducer to measure acoustic absorption of a living green wall. *Applied Acoustics*, *145*, 89-97. Retrieved from `https://www.sciencedirect.com/science/article/pii/S0003682X18305504` doi: https://doi.org/10.1016/j.apacoust.2018.09.020

Rosasco, P. (2018). Chapter 4.4 - economic benefits and costs of vertical greening systems. In G. Pérez & K. Perini (Eds.), *Nature based strategies for urban and building sustainability* (p. 291-306). Butterworth-Heinemann. Retrieved from `https://www.sciencedirect.com/science/article/pii/B9780128121504000276` doi: https://doi.org/10.1016/B978-0-12-812150-4.00027-6

Rowe, T., Poppe, J., Buyle, M., Belmans, B., & Audenaert, A. (2022). Is the sustainability potential of vertical greening systems deeply rooted? establishing uniform outlines for environmental impact assessment of vgs. *Renewable and Sustainable Energy Reviews*, *162*, 112414. Retrieved from `https://www.sciencedirect.com/science/article/pii/S1364032122003227` doi: https://doi.org/10.1016/j.rser.2022.112414

Ruiz, S., Hallett, P. D., & Or, D. (2023). Bioturbation—physical processes. In M. J. Goss & M. Oliver (Eds.), *Encyclopedia of soils in the environment (second edition)* (Second Edition ed., p. 100-114). Oxford: Academic Press. Retrieved from `https://www.sciencedirect.com/science/article/pii/B9780128229743001804` doi: https://doi.org/10.1016/B978-0-12-822974-3.00180-4

Salah, G. M., & Romanova, A. (2021). Life cycle assessment of felt system living green wall: Cradle to grave case study. *Environmental Challenges*, *3*, 100046. Retrieved from `https://www.sciencedirect.com/science/article/pii/S2667010021000251` doi: https://doi.org/10.1016/j.envc.2021.100046

Salisbury, A., Blanusa, T., Bostock, H., & Perry, J. (2023). Careful plant choice can deliver more biodiverse vertical greening (green façades). *Urban Forestry & Urban Greening*, *89*, 128118. Retrieved from `https://www.sciencedirect.com/science/article/pii/S1618866723002893` doi: https://doi.org/10.1016/j.ufug.2023.128118

Salissou, Y., Panneton, R., & Doutres, O. (2012). Complement to standard method for measuring normal incidence sound transmission loss with three microphones. *The Journal of the Acoustical Society of America*, *131*(3), EL216-EL222. Retrieved from `https://doi.org/10.1121/1.3681016` doi: 10.1121/1.3681016

Scamoni, F., Scrosati, C., Depalma, M., & Barozzi, B. (2022). Experimental evaluations of acoustic properties and long-term analysis of a novel indoor living wall. *Journal of Building Engineering*, *47*, 103890. Retrieved from `https://www.sciencedirect.com/science/article/pii/S2352710221017484` doi: https://doi.org/10.1016/j.jobe.2021.103890

SemperGreenwall. (2023). *On what kind of rear walls can you mount a living wall?* Retrieved from `https://sempergreenwall.com/news/on-what-kind-of-rear-walls-can-you-mount-a-living-wall/` (Figure retrieved on 13/02/2024)

SemperGreenwall. (2024a). *Flexipanel.* Retrieved from `https://sempergreenwall.com/nl/flexipanel/` (Figures retrieved on 13/02/2024)

SemperGreenwall. (2024b). *Plantenlijst sempergreenwall outdoor mix assortiment.* PDF. Retrieved from `https://sempergreenwall.com/nl/downloads/`

SingularGreen. (2015). *EcoBin Vertical Garden.* Retrieved from `https://www.singulargreen.com/en/ecobin-system/` (Figures retrieved on 13/02/2024)

SingularGreen. (2021). *Vertical gardens for interior and exterior; F+P System.* Retrieved from `https://www.singulargreen.com/sistema-fp-cold/` (Figures retrieved on 13/02/2024)

Smith, C. D., & Parrott, T. L. (1983). Comparison of three methods for measuring acoustic properties of bulk materials. *Journal of the Acoustical Society of America*, *74*, 1577-1582.

Stollberg, M., & von Birgelen, A. (2023). Vertical plants: Plant design of living walls – evaluation of 34 perennials in a textile based living wall over a three years experiment. *Frontiers in Horticulture*, *2*. Retrieved from `https://www.frontiersin.org/articles/10.3389/fhort.2023.1091026` doi: 10.3389/fhort.2023.1091026

Susorova, I. (2015). 5 - green facades and living walls: vertical vegetation as a construction material to reduce building cooling loads. In F. Pacheco-Torgal, J. Labrincha, L. Cabeza, & C.-G. Granqvist (Eds.), *Eco-efficient materials for mitigating building cooling needs* (p. 127-153). Oxford: Woodhead Publishing. Retrieved from `https://www.sciencedirect.com/science/article/pii/B9781782423805000054` doi: https://doi.org/10.1016/B978-1-78242-380-5.00005-4

Teotónio, I., Silva, C. M., & Cruz, C. O. (2021). Economics of green roofs and green walls: A literature review. *Sustainable Cities and Society*, *69*, 102781. Retrieved from `https://www.sciencedirect.com/science/article/pii/S2210670721000731` doi: https://doi.org/10.1016/j.scs.2021.102781

Thipsorn, M. (2022). *Close up of nature view green leaf on white isolated background under sunlight with copy space using as background natural plants landscape, ecology cover concept.* Retrieved from `https://www.vecteezy.com/photo/7360323-close-up-of-nature-view-green-leaf-on-white-isolated-background-under-sunlight-with-copy-space-using-as-background-natural-plants-landscape-ecology-cover-concept` (Figure retrieved 12/06/2024)

Thomazelli, R., Caetano, F. D. N., & Bertoli, S. R. (2017, 05). Acoustic properties of green walls: Absorption and insulation. *Proceedings of Meetings on Acoustics*, *28*(1), 015017. Retrieved from `https://doi.org/10.1121/2.0000426` doi: 10.1121/2.0000426

Utsuno, H., Tanaka, T., Fujikawa, T., & Seybert, A. F. (1989). Transfer function method for measuring characteristic impedance and propagation constant of porous materials. *Journal of the Acoustical Society of America*, *86*, 637-643.

Van Renterghem, T., Hornikx, M., Forssen, J., & Botteldooren, D. (2013). The potential of building envelope greening to achieve quietness. *Building and Environment*, *61*, 34-44. Retrieved from `https://www.sciencedirect.com/science/article/pii/S036013231200323X` doi: https://doi.org/10.1016/j.buildenv.2012.12.001

Vermiculite. (2024). Retrieved from `https://www.mindat.org/min-4170.html` (Mindat ID: 4170. Retrieved on 19/05/2024)

Weinmaster, M. (2009). Are Green Walls as "Green" as They Look? An Introduction to the Various Technologies and Ecological Benefits of Green Walls. *Journal of Green Building*, *4*(4), 3-18. Retrieved from `https://doi.org/10.3992/jgb.4.4.3` doi: 10.3992/jgb.4.4.3

WHO. (2010). *Noise.* Fact sheet. Retrieved from `https://www.who.int/europe/news-room/fact-sheets/item/noise` (World Health Organization Regional Office for Europe)

Wolfe, J., & Hatsidimitris, G. (1991). *Acoustic compliance, inertance and impedance.* Presented at Physclips. Retrieved from `https://www.animations.physics.unsw.edu.au/jw/compliance-inertance-impedance.htm#L`

Wong, N. H., Kwang Tan, A. Y., Tan, P. Y., Chiang, K., & Wong, N. C. (2010). Acoustics evaluation of vertical greenery systems for building walls. *Building and Environment*, *45*(2), 411-420. Retrieved from `https://www.sciencedirect.com/science/article/pii/S0360132309001632` (1st International Symposium on Sustainable Healthy Buildings) doi: https://doi.org/10.1016/j.buildenv.2009.06.017

Yan, F., Shen, J., Zhang, W., Ye, L., & Lin, X. (2022). A review of the application of green walls in the acoustic field. *Building Acoustics*, *29*(2), 295-313. Retrieved from `https://doi.org/10.1177/`

1351010X221096789 doi: 10.1177/1351010X221096789

Yang, H.-S., Kang, J., & Cheal, C. (2013, 05). Random-incidence absorption and scattering coefficients of vegetation. *Acta Acustica united with Acustica*, *99*, 379-388. doi: 10.3813/AAA.918619
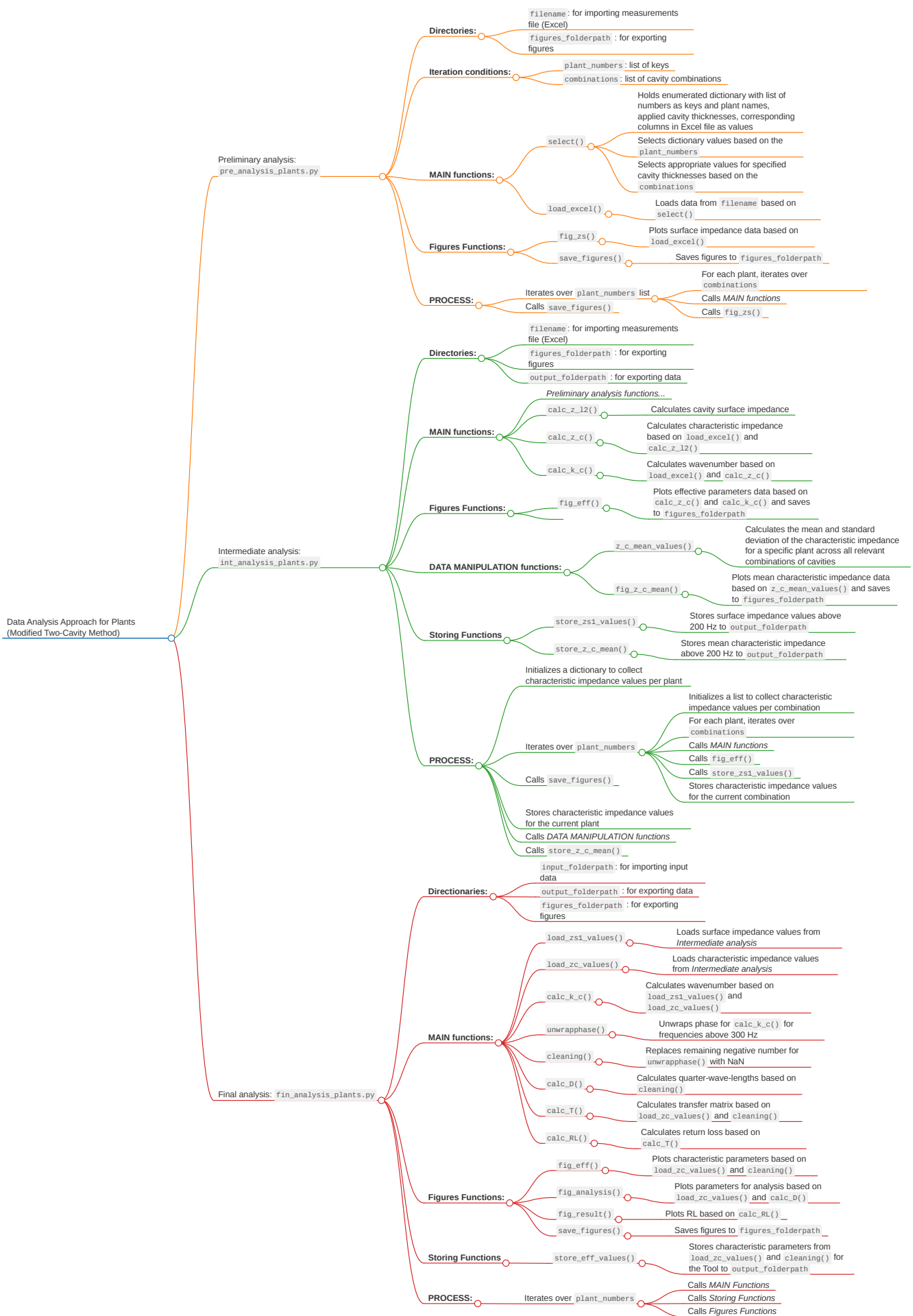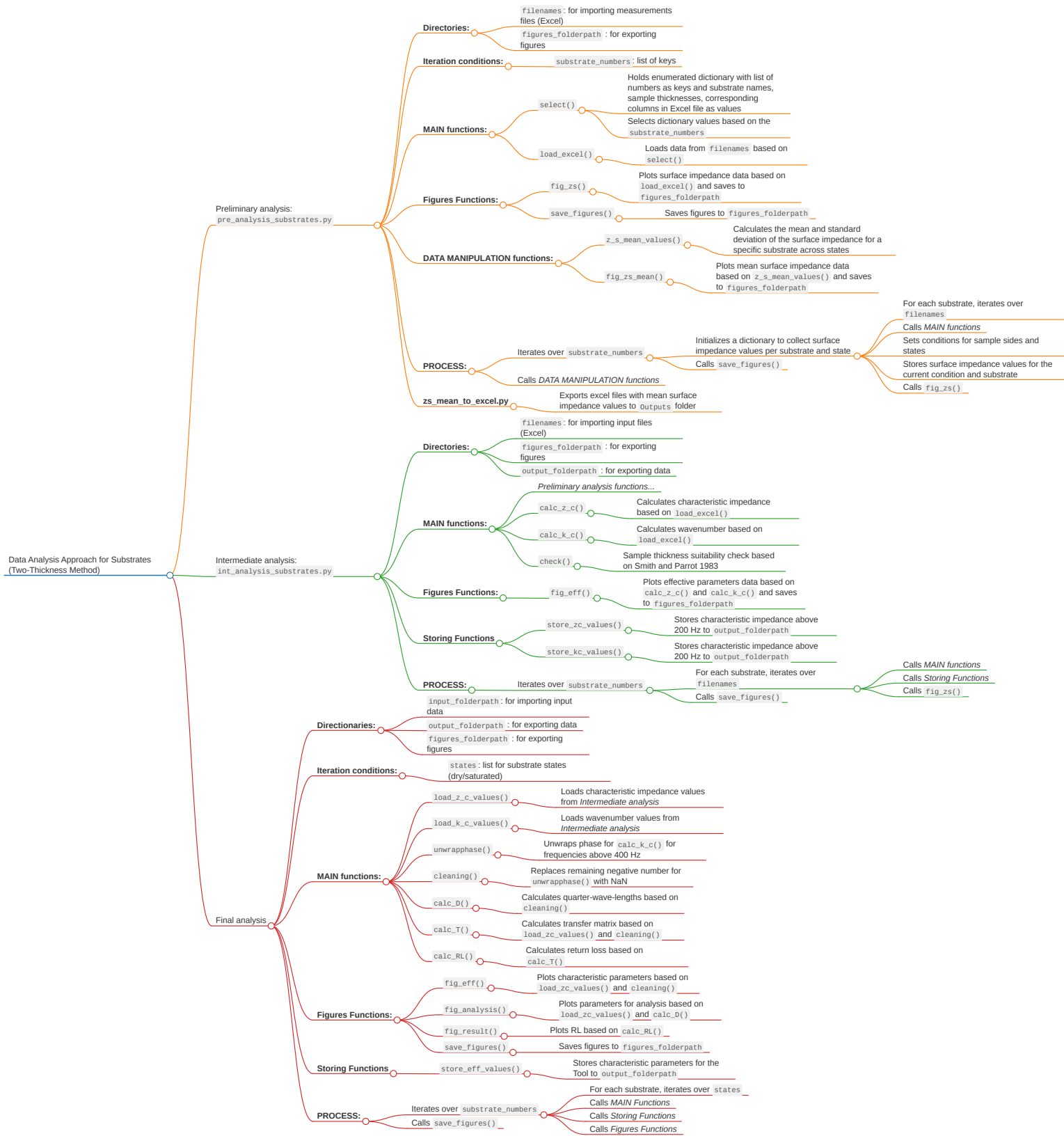
A

Data Processing Procedure

The data processing scripts are available:

GitHub Repository
https://github.com/smrksn/Optimization-of-the-Vertical-Greenery-Systems

The scripts provided facilitate the derivation of complex effective parameters from impedance tube measurements (ISO 10534-2). These scripts guide through a structured data processing procedure divided into three phases: preliminary, intermediate, and final. Each phase of the workflow for plants (Page 130) and substrates (Page 131) test samples is clearly defined to ensure a systematic approach to deriving accurate results from the measurement data.

Data Analysis Approach for Plants (Modified Two-Cavity Method)

Preliminary analysis: `pre_analysis_plants.py`

Directories:
- `filename`: for importing measurements file (Excel)
- `figures_folderpath`: for exporting figures

Iteration conditions:
- `plant_numbers`: list of keys
- `combinations`: list of cavity combinations

MAIN functions:
- `select()` — Holds enumerated dictionary with list of numbers as keys and plant names, applied cavity thicknesses, corresponding columns in Excel file as values
  - Selects dictionary values based on the `plant_numbers`
  - Selects appropriate values for specified cavity thicknesses based on the `combinations`
- `load_excel()` — Loads data from `filename` based on `select()`

Figures Functions:
- `fig_zs()` — Plots surface impedance data based on `load_excel()`
- `save_figures()` — Saves figures to `figures_folderpath`

PROCESS:
- Iterates over `plant_numbers` list
  - For each plant, iterates over `combinations`
  - Calls *MAIN functions*
  - Calls `fig_zs()`
- Calls `save_figures()`

Intermediate analysis: `int_analysis_plants.py`

Directories:
- `filename`: for importing measurements file (Excel)
- `figures_folderpath`: for exporting figures
- `output_folderpath`: for exporting data

MAIN functions:
- *Preliminary analysis functions...*
- `calc_z_l2()` — Calculates cavity surface impedance
- `calc_z_c()` — Calculates characteristic impedance based on `load_excel()` and `calc_z_l2()`
- `calc_k_c()` — Calculates wavenumber based on `load_excel()` and `calc_z_c()`

Figures Functions:
- `fig_eff()` — Plots effective parameters data based on `calc_z_c()` and `calc_k_c()` and saves to `figures_folderpath`

DATA MANIPULATION functions:
- `z_c_mean_values()` — Calculates the mean and standard deviation of the characteristic impedance for a specific plant across all relevant combinations of cavities
- `fig_z_c_mean()` — Plots mean characteristic impedance data based on `z_c_mean_values()` and saves to `figures_folderpath`

Storing Functions:
- `store_zs1_values()` — Stores surface impedance values above 200 Hz to `output_folderpath`
- `store_z_c_mean()` — Stores mean characteristic impedance above 200 Hz to `output_folderpath`

PROCESS:
- Initializes a dictionary to collect characteristic impedance values per plant
- Iterates over `plant_numbers`
  - Initializes a list to collect characteristic impedance values per combination
  - For each plant, iterates over `combinations`
  - Calls *MAIN functions*
  - Calls `fig_eff()`
  - Calls `store_zs1_values()`
  - Stores characteristic impedance values for the current combination
- Calls `save_figures()`
- Stores characteristic impedance values for the current plant
- Calls *DATA MANIPULATION functions*
- Calls `store_z_c_mean()`

Final analysis: `fin_analysis_plants.py`

Directionaries:
- `input_folderpath`: for importing input data
- `output_folderpath`: for exporting data
- `figures_folderpath`: for exporting figures

MAIN functions:
- `load_zs1_values()` — Loads surface impedance values from *Intermediate analysis*
- `load_zc_values()` — Loads characteristic impedance values from *Intermediate analysis*
- `calc_k_c()` — Calculates wavenumber based on `load_zs1_values()` and `load_zc_values()`
- `unwrapphase()` — Unwraps phase for `calc_k_c()` for frequencies above 300 Hz
- `cleaning()` — Replaces remaining negative number for `unwrapphase()` with NaN
- `calc_D()` — Calculates quarter-wave-lengths based on `cleaning()`
- `calc_T()` — Calculates transfer matrix based on `load_zc_values()` and `cleaning()`
- `calc_RL()` — Calculates return loss based on `calc_T()`

Figures Functions:
- `fig_eff()` — Plots characteristic parameters based on `load_zc_values()` and `cleaning()`
- `fig_analysis()` — Plots parameters for analysis based on `load_zc_values()` and `calc_D()`
- `fig_result()` — Plots RL based on `calc_RL()`
- `save_figures()` — Saves figures to `figures_folderpath`

Storing Functions:
- `store_eff_values()` — Stores characteristic parameters from `load_zc_values()` and `cleaning()` for the Tool to `output_folderpath`

PROCESS:
- Iterates over `plant_numbers`
  - Calls *MAIN Functions*
  - Calls *Storing Functions*
  - Calls *Figures Functions*

Data Analysis Approach for Substrates (Two-Thickness Method)

Preliminary analysis: `pre_analysis_substrates.py`

- **Directories:**
  - `filenames`: for importing measurements files (Excel)
  - `figures_folderpath`: for exporting figures
- **Iteration conditions:**
  - `substrate_numbers`: list of keys
- **MAIN functions:**
  - `select()`: Holds enumerated dictionary with list of numbers as keys and substrate names, sample thicknesses, corresponding columns in Excel file as values. Selects dictionary values based on the `substrate_numbers`
  - `load_excel()`: Loads data from `filenames` based on `select()`
- **Figures Functions:**
  - `fig_zs()`: Plots surface impedance data based on `load_excel()` and saves to `figures_folderpath`
  - `save_figures()`: Saves figures to `figures_folderpath`
- **DATA MANIPULATION functions:**
  - `z_s_mean_values()`: Calculates the mean and standard deviation of the surface impedance for a specific substrate across states
  - `fig_zs_mean()`: Plots mean surface impedance data based on `z_s_mean_values()` and saves to `figures_folderpath`
- **PROCESS:**
  - Iterates over `substrate_numbers`: Initializes a dictionary to collect surface impedance values per substrate and state. Calls `save_figures()`
    - For each substrate, iterates over `filenames`
    - Calls *MAIN functions*
    - Sets conditions for sample sides and states
    - Stores surface impedance values for the current condition and substrate
    - Calls `fig_zs()`
  - Calls *DATA MANIPULATION functions*
- **`zs_mean_to_excel.py`**: Exports excel files with mean surface impedance values to `Outputs` folder

Intermediate analysis: `int_analysis_substrates.py`

- **Directories:**
  - `filenames`: for importing input files (Excel)
  - `figures_folderpath`: for exporting figures
  - `output_folderpath`: for exporting data
- **MAIN functions:**
  - *Preliminary analysis functions...*
  - `calc_z_c()`: Calculates characteristic impedance based on `load_excel()`
  - `calc_k_c()`: Calculates wavenumber based on `load_excel()`
  - `check()`: Sample thickness suitability check based on Smith and Parrot 1983
- **Figures Functions:**
  - `fig_eff()`: Plots effective parameters data based on `calc_z_c()` and `calc_k_c()` and saves to `figures_folderpath`
- **Storing Functions:**
  - `store_zc_values()`: Stores characteristic impedance above 200 Hz to `output_folderpath`
  - `store_kc_values()`: Stores characteristic impedance above 200 Hz to `output_folderpath`
- **PROCESS:**
  - Iterates over `substrate_numbers`: For each substrate, iterates over `filenames`. Calls `save_figures()`
    - Calls *MAIN functions*
    - Calls *Storing Functions*
    - Calls `fig_zs()`

Final analysis

- **Directionaries:**
  - `input_folderpath`: for importing input data
  - `output_folderpath`: for exporting data
  - `figures_folderpath`: for exporting figures
- **Iteration conditions:**
  - `states`: list for substrate states (dry/saturated)
- **MAIN functions:**
  - `load_z_c_values()`: Loads characteristic impedance values from *Intermediate analysis*
  - `load_k_c_values()`: Loads wavenumber values from *Intermediate analysis*
  - `unwrapphase()`: Unwraps phase for `calc_k_c()` for frequencies above 400 Hz
  - `cleaning()`: Replaces remaining negative number for `unwrapphase()` with NaN
  - `calc_D()`: Calculates quarter-wave-lengths based on `cleaning()`
  - `calc_T()`: Calculates transfer matrix based on `load_zc_values()` and `cleaning()`
  - `calc_RL()`: Calculates return loss based on `calc_T()`
- **Figures Functions:**
  - `fig_eff()`: Plots characteristic parameters based on `load_zc_values()` and `cleaning()`
  - `fig_analysis()`: Plots parameters for analysis based on `load_zc_values()` and `calc_D()`
  - `fig_result()`: Plots RL based on `calc_RL()`
  - `save_figures()`: Saves figures to `figures_folderpath`
- **Storing Functions:**
  - `store_eff_values()`: Stores characteristic parameters for the Tool to `output_folderpath`
- **PROCESS:**
  - Iterates over `substrate_numbers`: Calls `save_figures()`
    - For each substrate, iterates over `states`
    - Calls *MAIN Functions*
    - Calls *Storing Functions*
    - Calls *Figures Functions*

A.1. Preliminary Data Analysis Outcomes

### A.1.1. Measured surface impedances of the plant samples with varying backing conditions

Figure A.1: Frequency-dependent surface impedance of the Ajuga reptans test sample
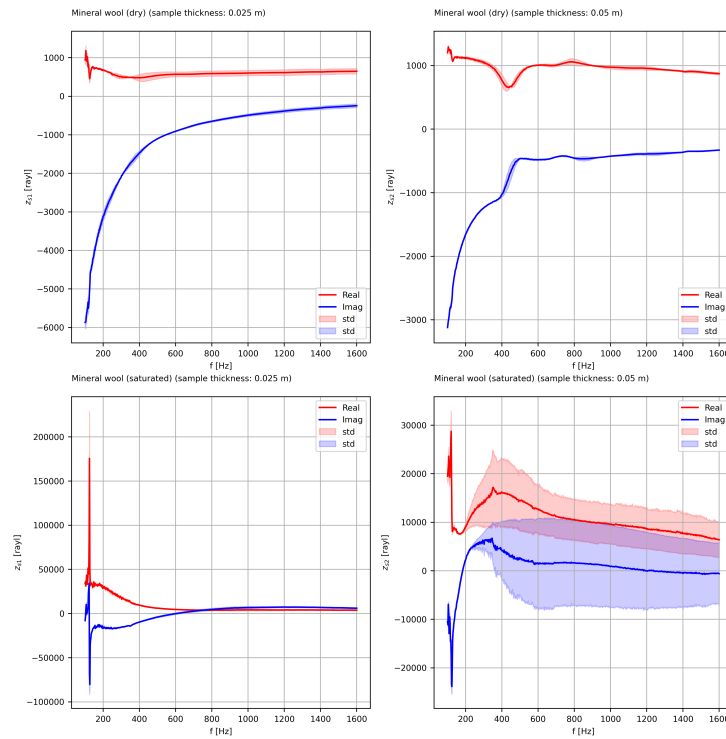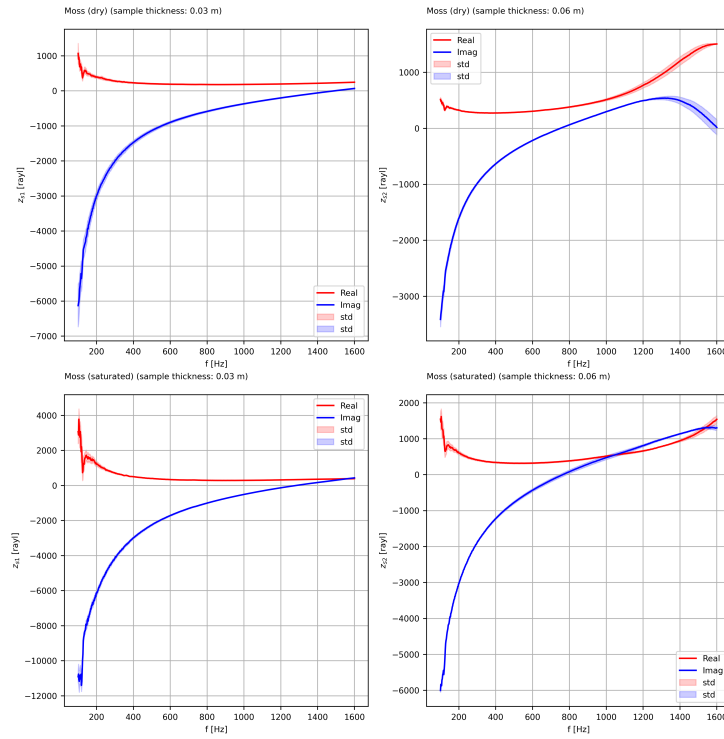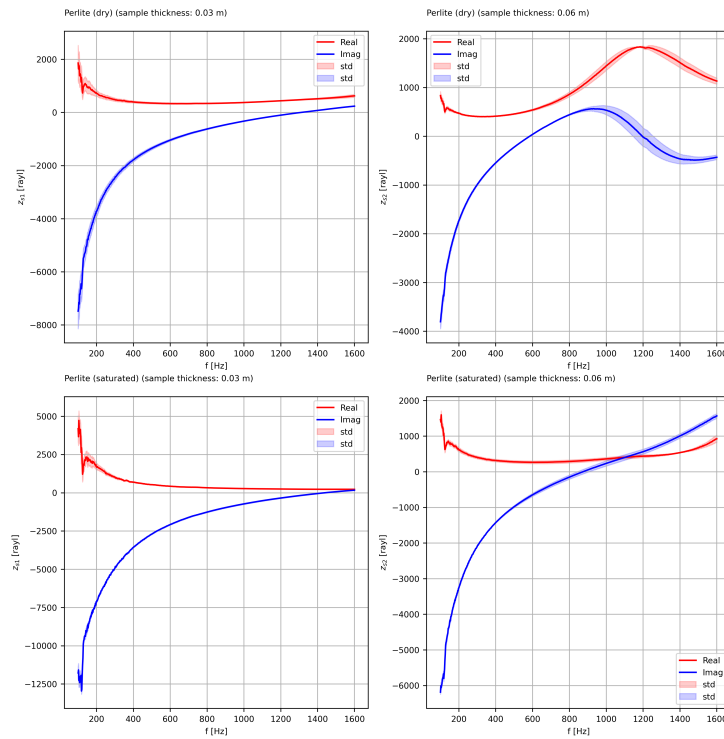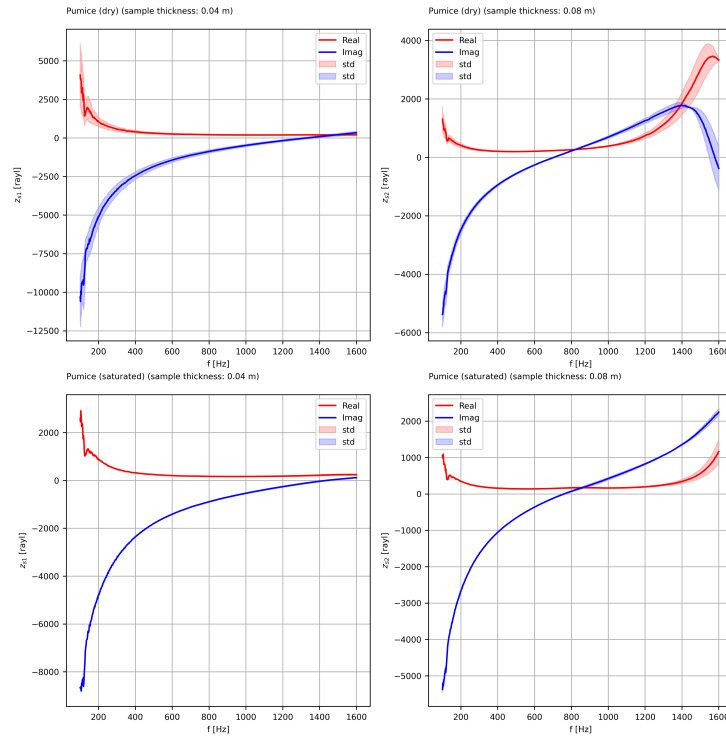
Figure A.2: Frequency-dependent surface impedance of the Bergenia cordifolia test sample

Figure A.3: Frequency-dependent surface impedance of the Festuca glauca test sample

Figure A.4: Frequency-dependent surface impedance of the Heuchera 'Cascade Dawn' test sample
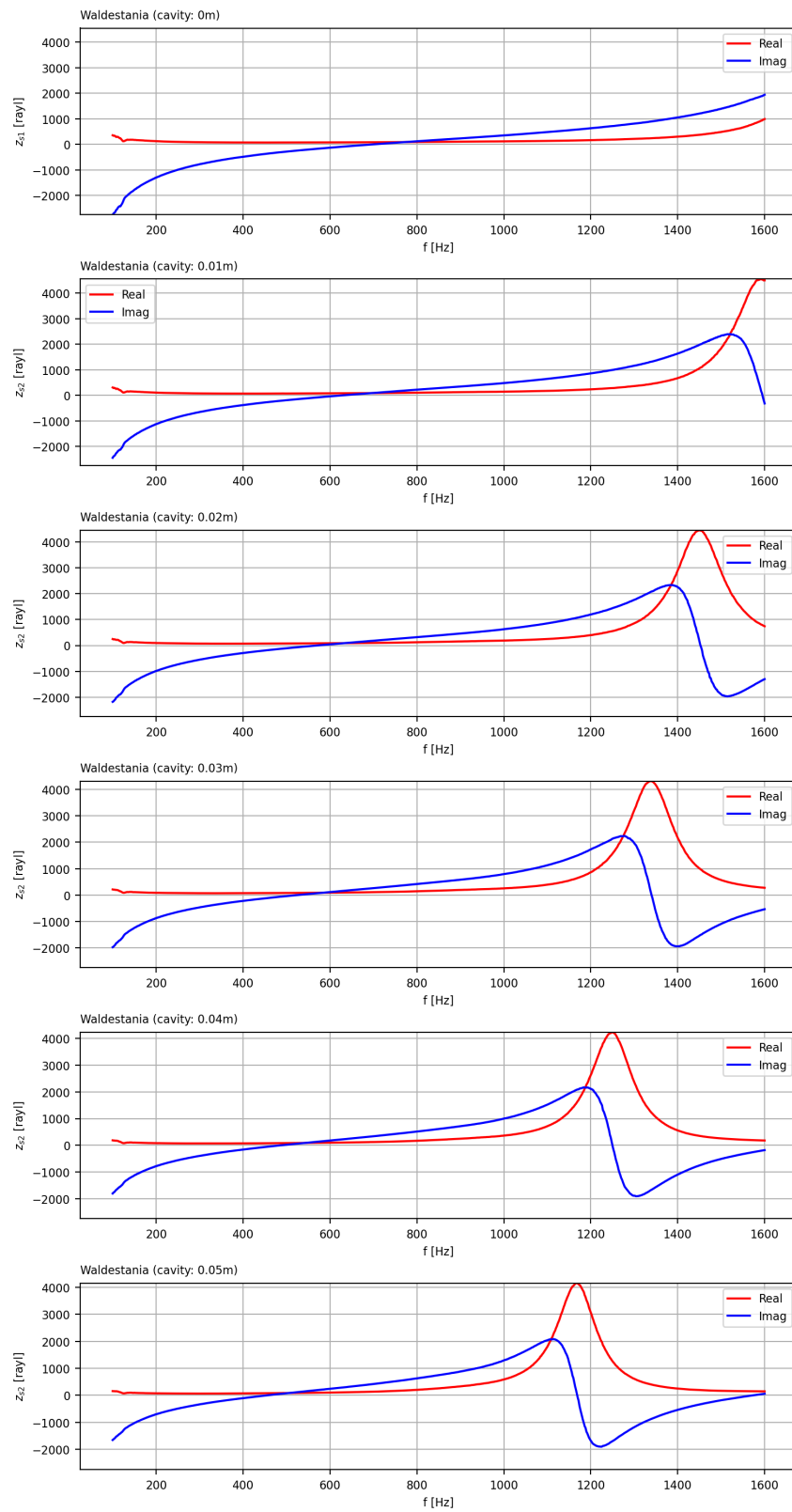
Figure A.5: Frequency-dependent surface impedance of the Waldestania ternata test sample

A.1.2. Measured surface impedances of the substrate samples with varying thicknesses
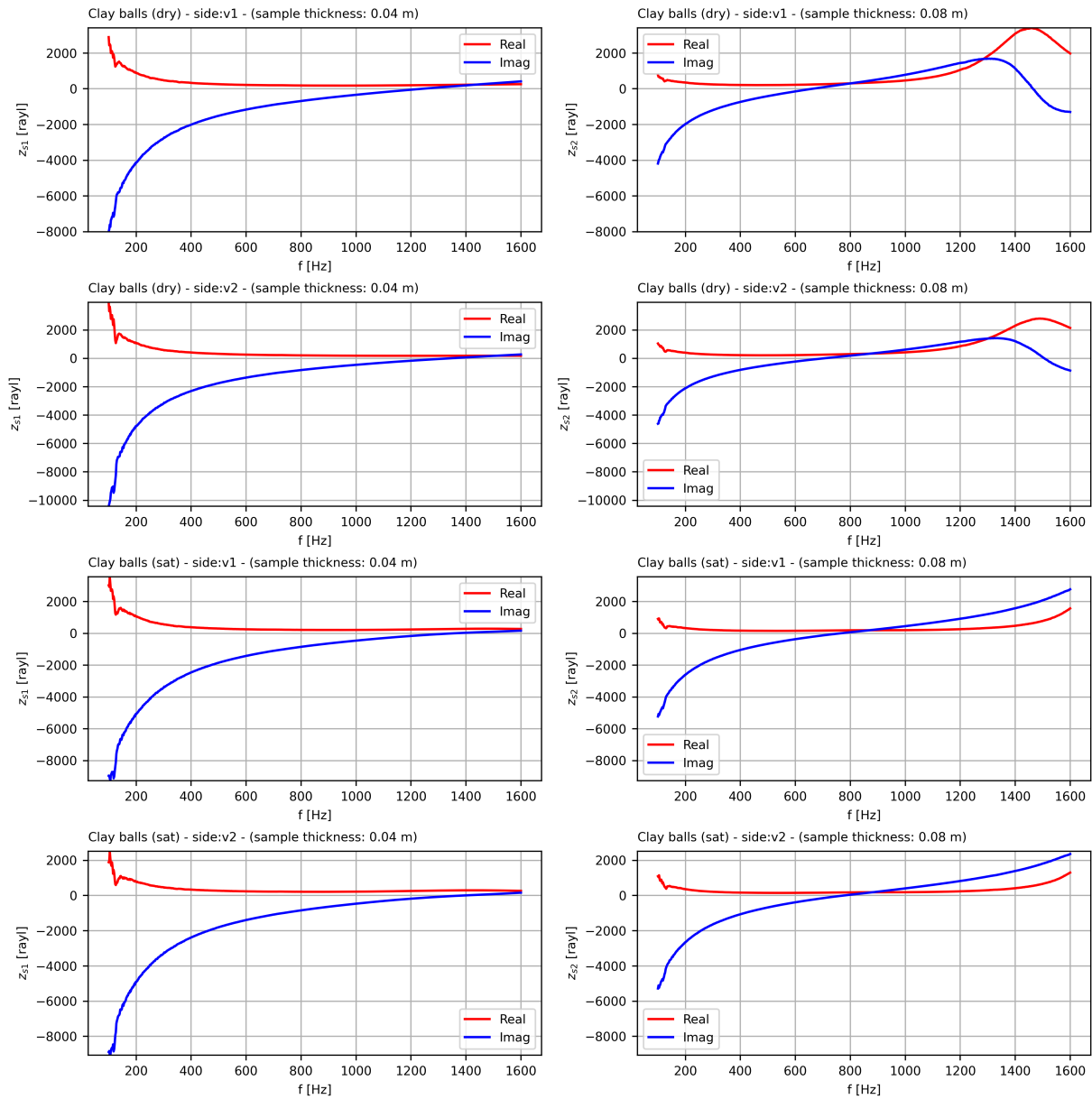
Figure A.6: Frequency-dependent surface impedance of the clay balls test sample
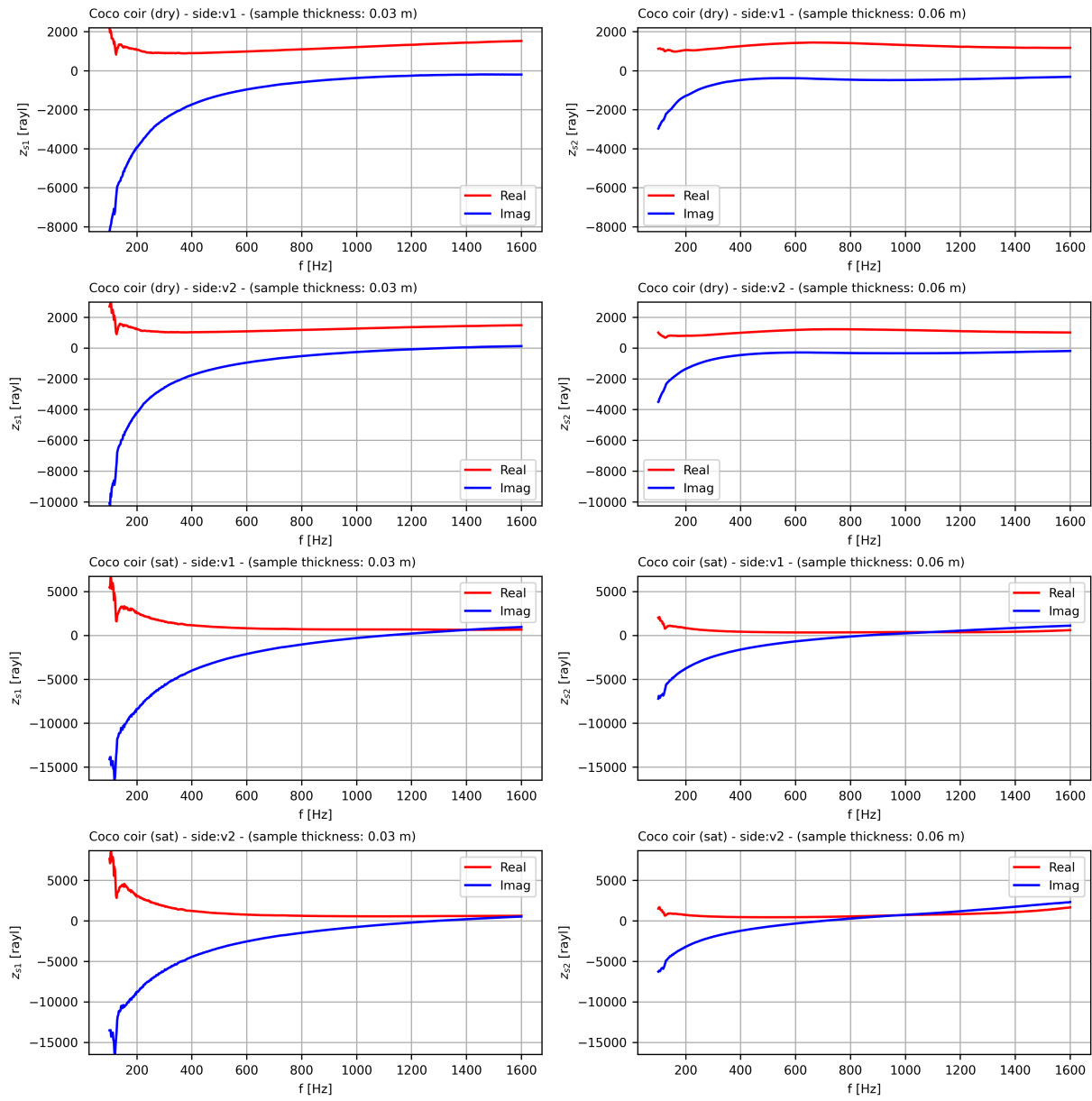
Figure A.7: Frequency-dependent surface impedance of the coco coir test sample
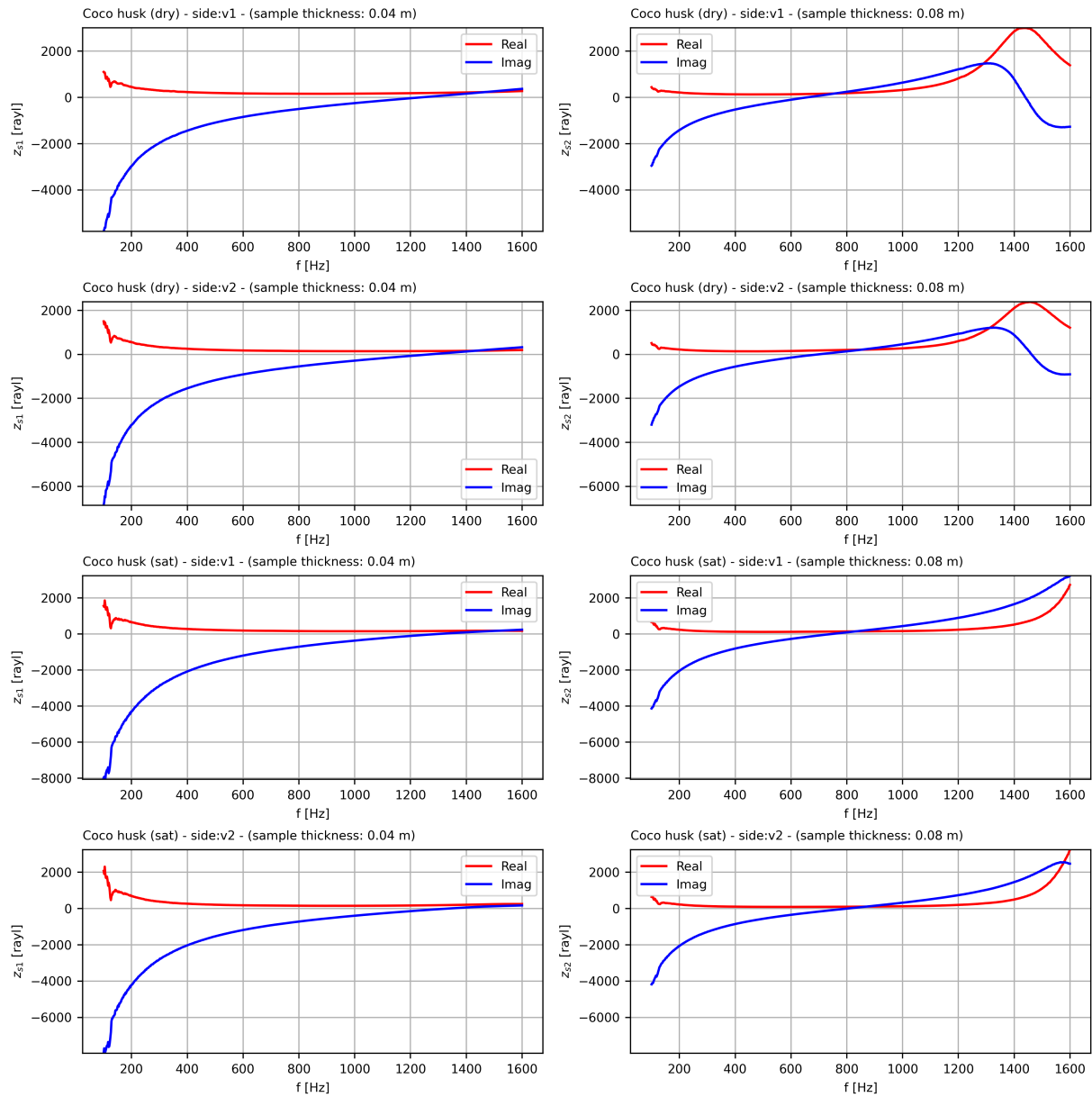
Figure A.8: Frequency-dependent surface impedance of the coco husk test sample
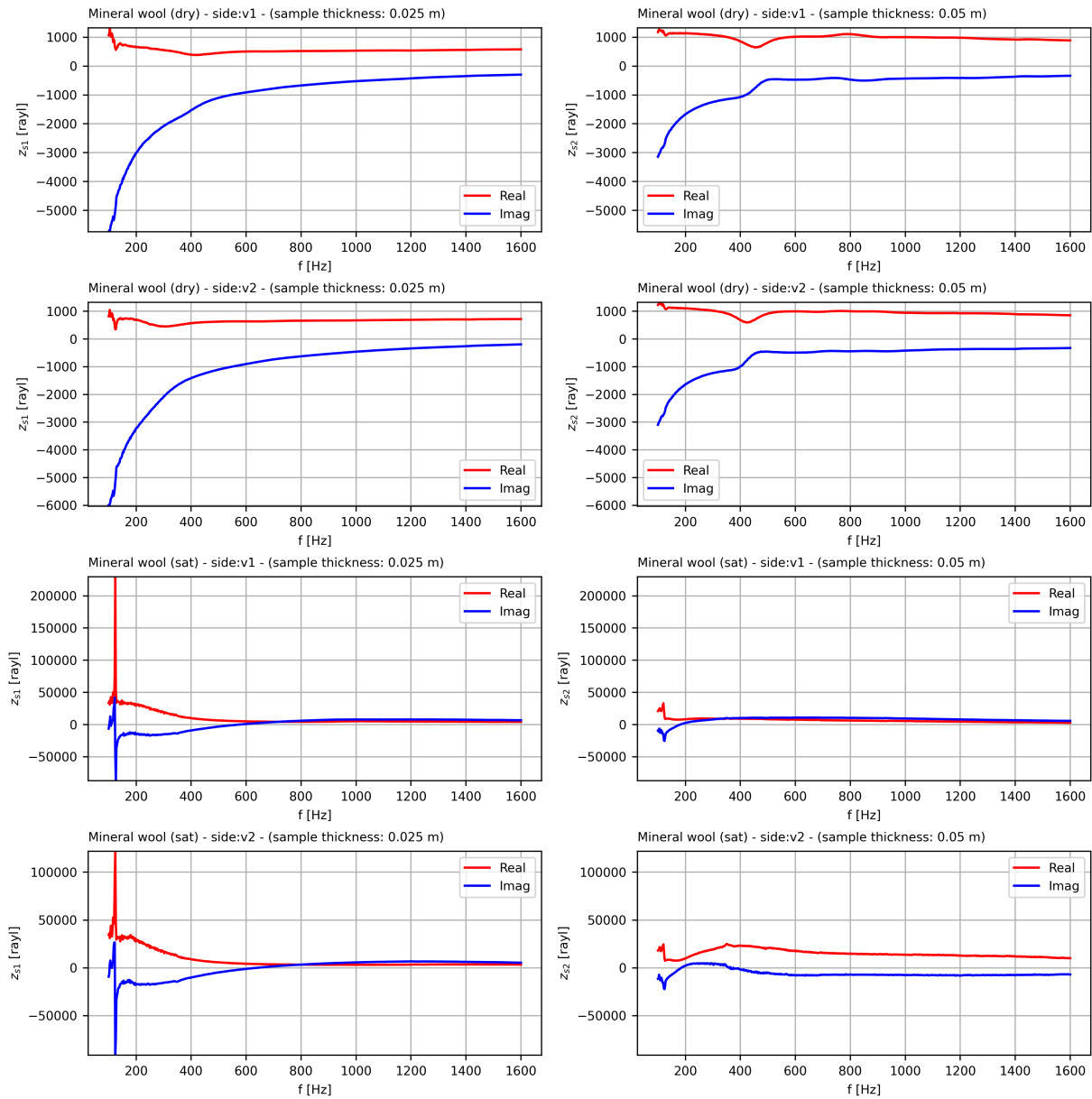
Figure A.9: Frequency-dependent surface impedance of the mineral wool test sample
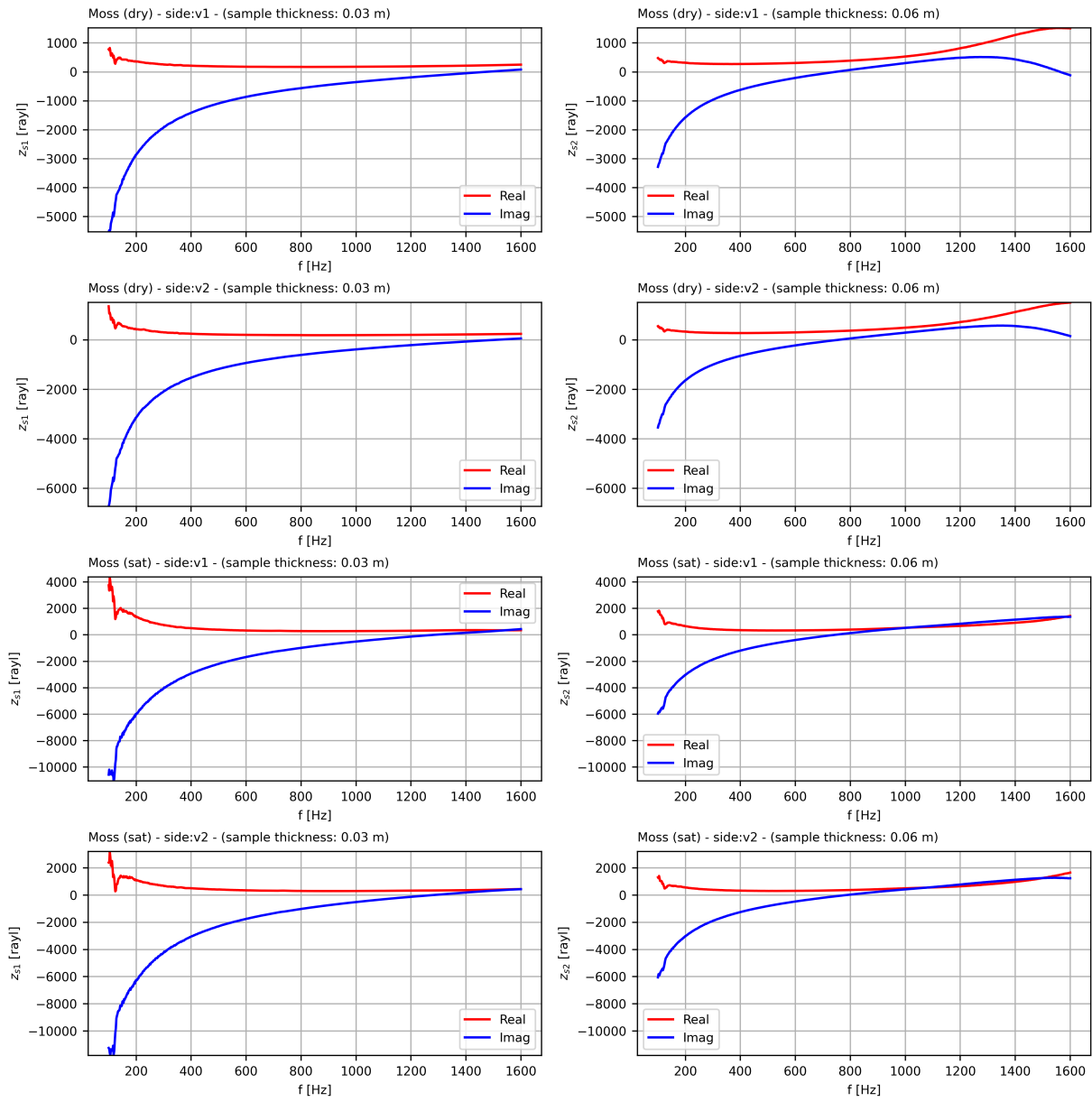
Figure A.10: Frequency-dependent surface impedance of the moss test sample
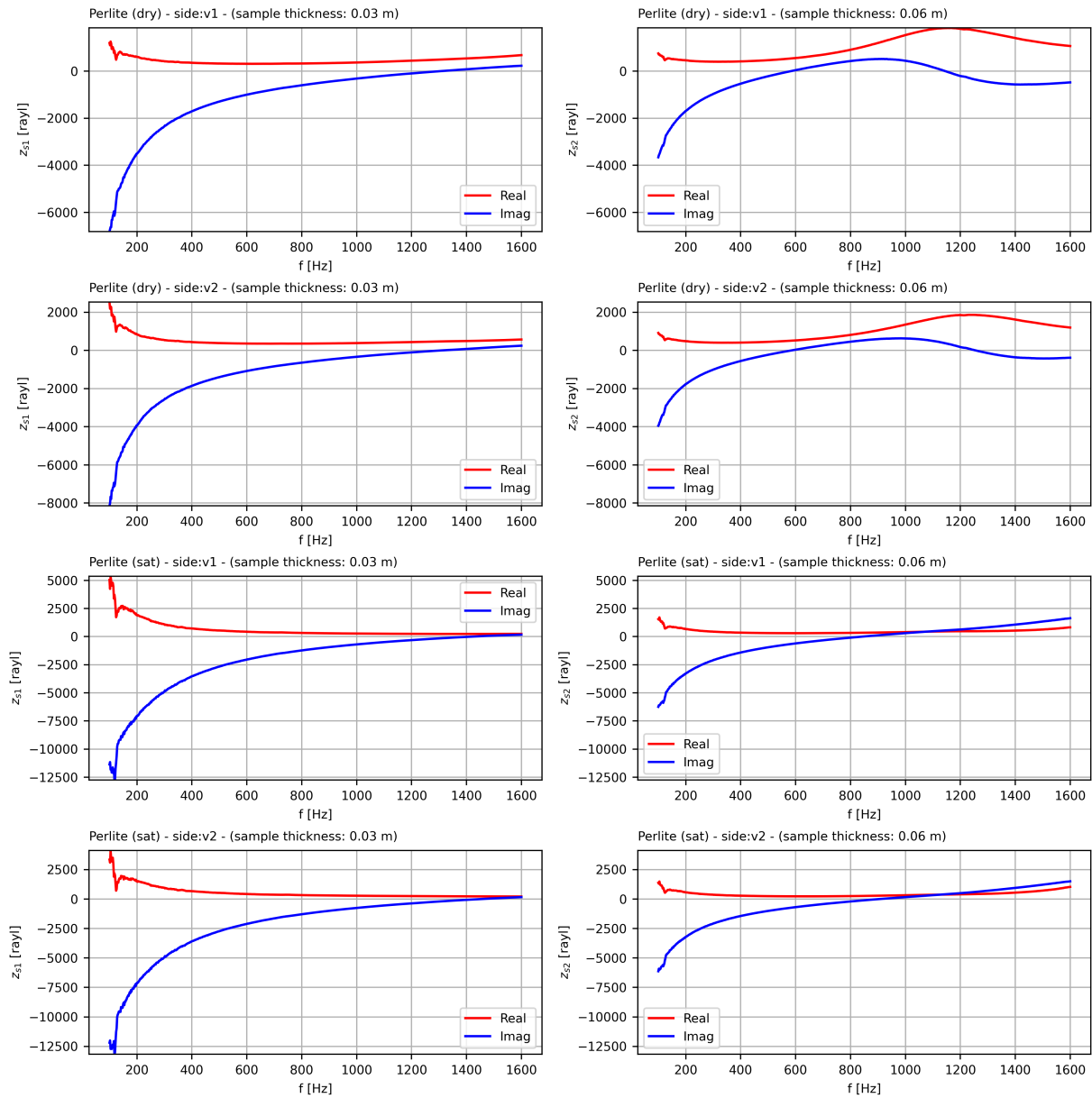
Figure A.11: Frequency-dependent surface impedance of the perlite test sample
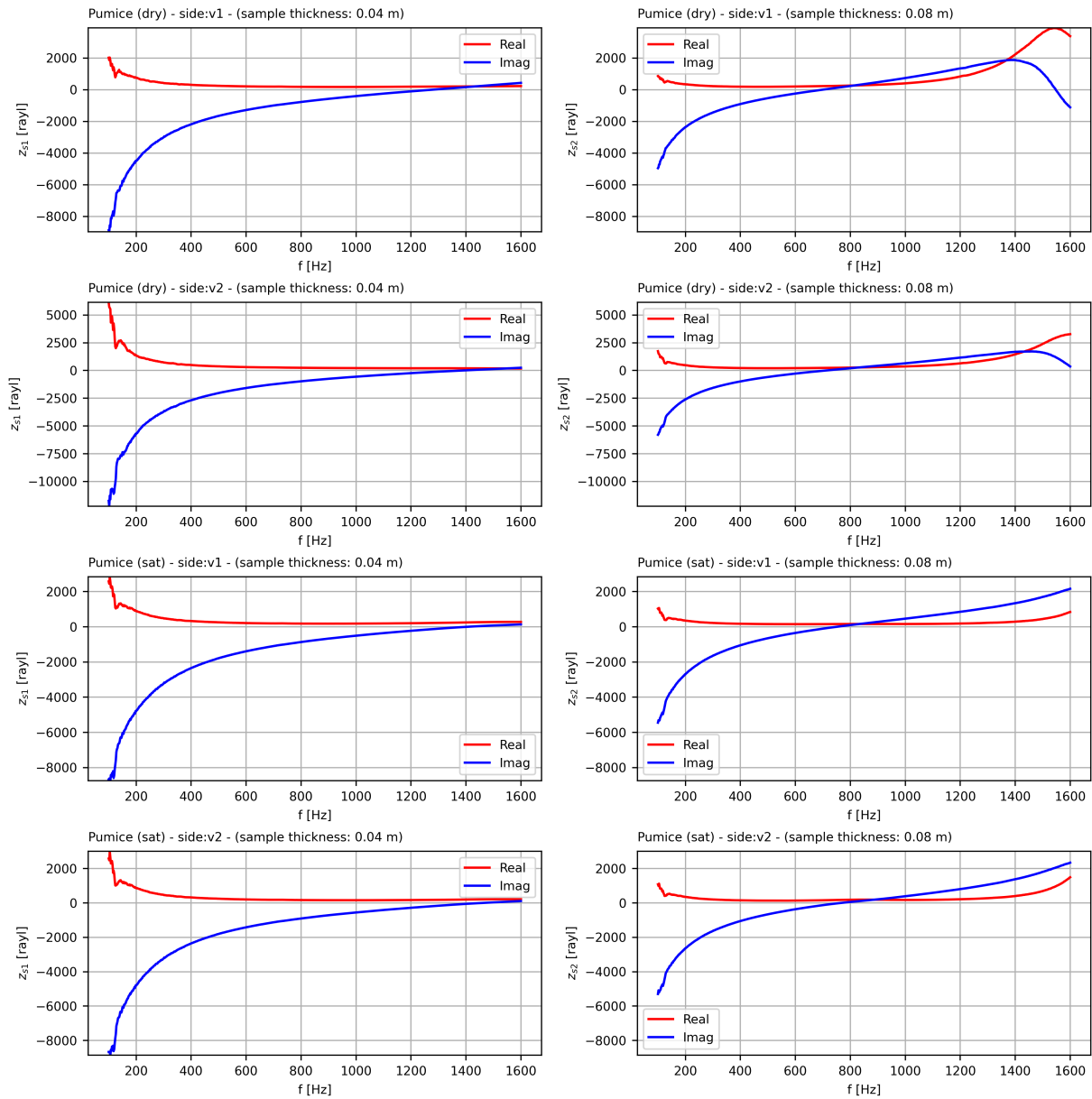
Figure A.12: Frequency-dependent surface impedance of the pumice test sample
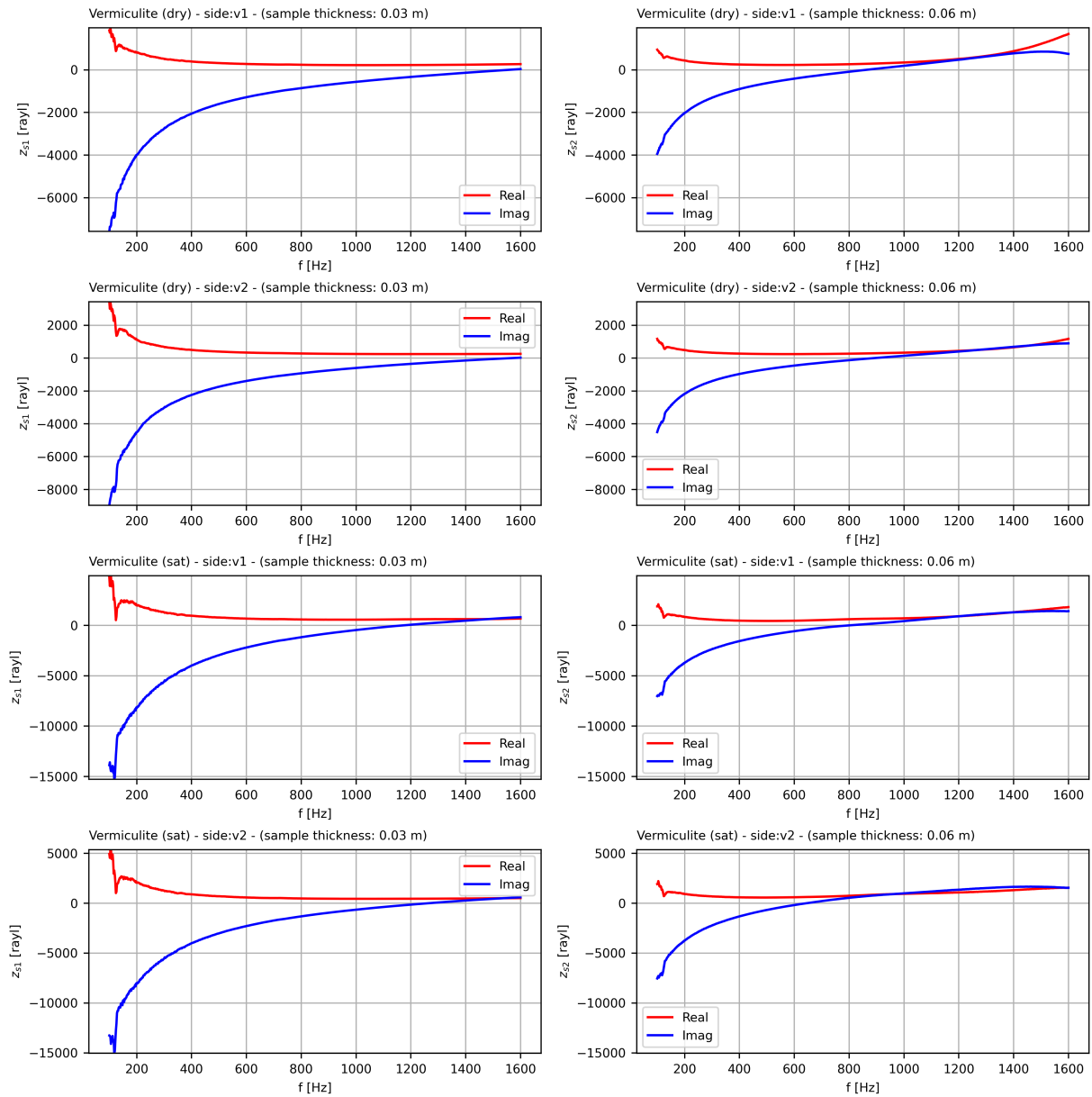
Figure A.13: Frequency-dependent surface impedance of the vermiculite test sample

A.1.3. Mean surface impedance of the substrates
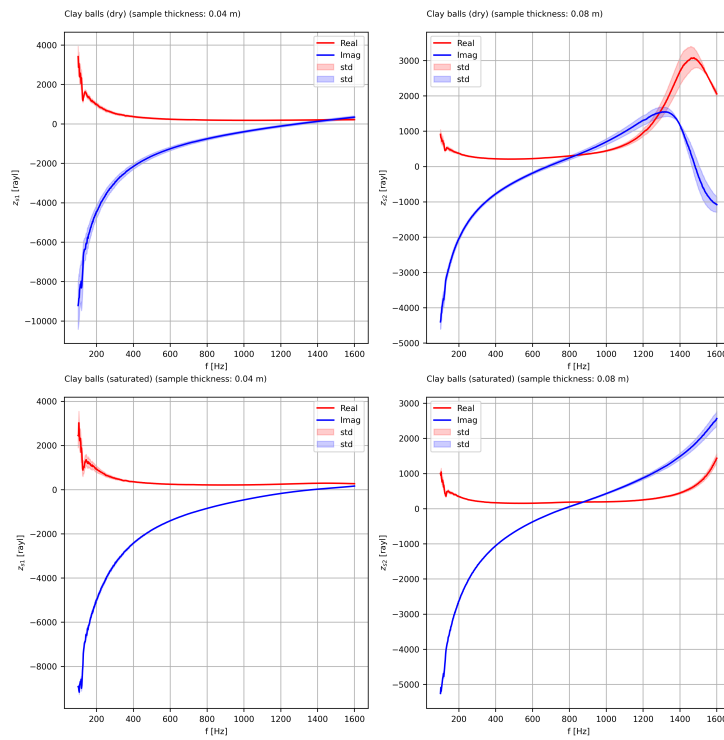
Figure A.14: Frequency-dependent mean surface impedance of the clay balls test sample
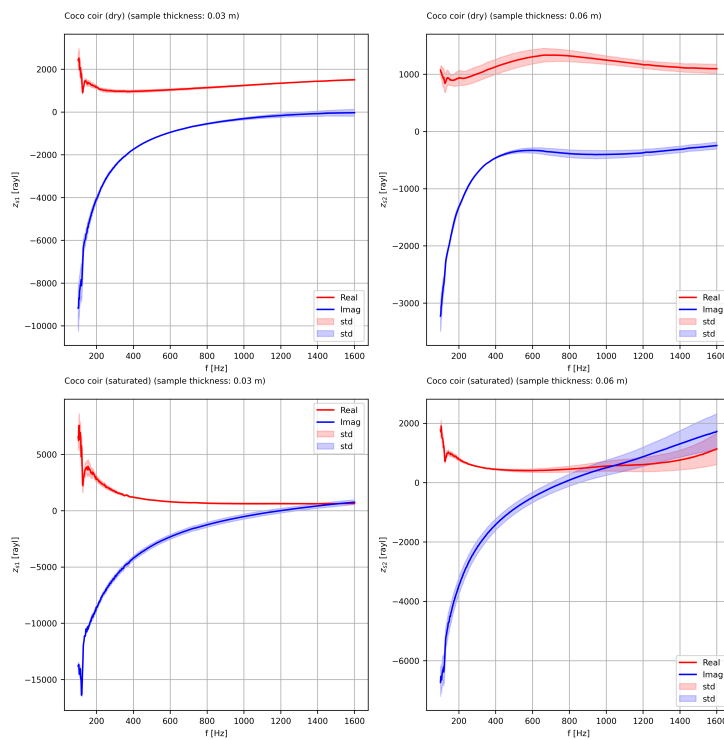
Figure A.15: Frequency-dependent mean surface impedance of the coco coir test sample
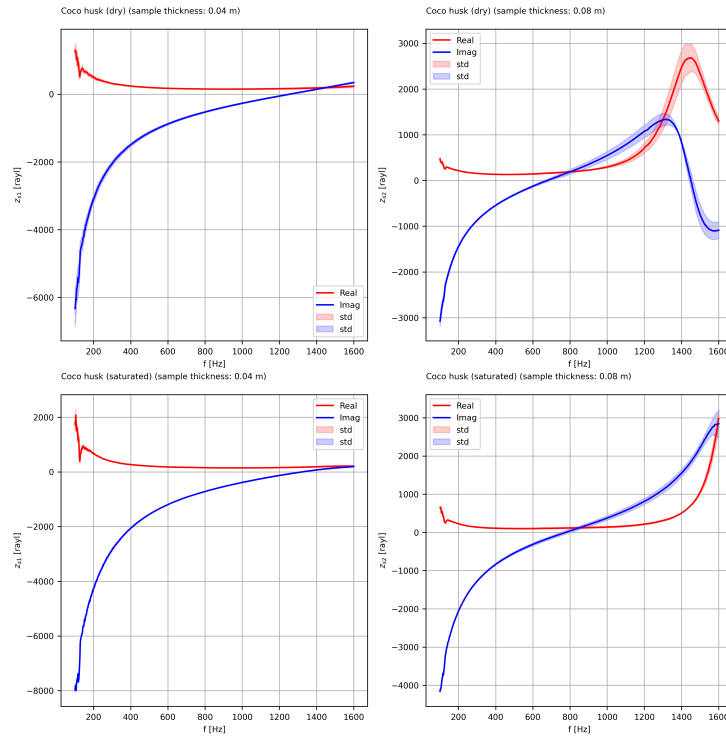
Figure A.16: Frequency-dependent mean surface impedance of the coco husk test sample

Figure A.17: Frequency-dependent mean surface impedance of the mineral wool test sample

Figure A.18: Frequency-dependent mean surface impedance of the moss test sample

Figure A.19: Frequency-dependent mean surface impedance of the perlite test sample

Figure A.20: Frequency-dependent mean surface impedance of the pumice test sample
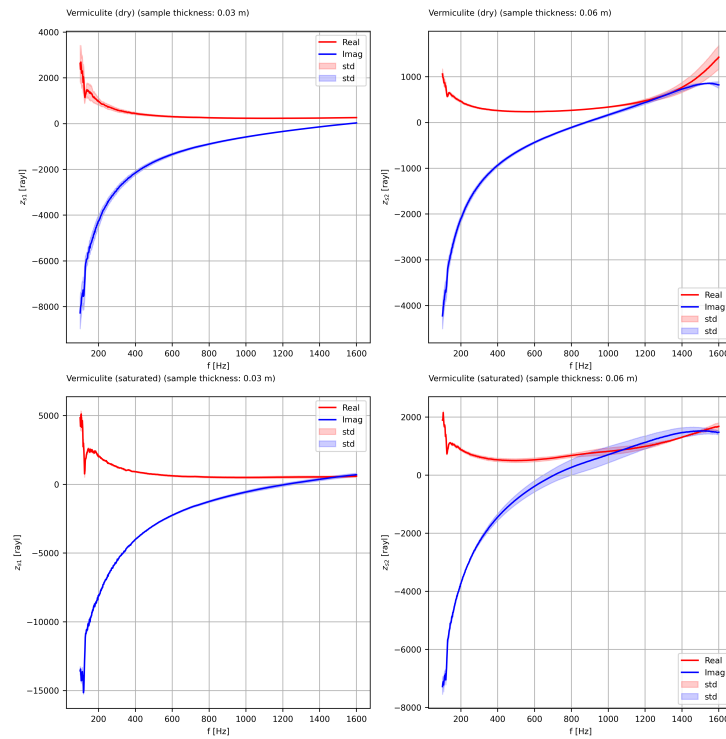
Figure A.21: Frequency-dependent mean surface impedance of the vermiculite test sample

A.2. Intermediate Data Analysis Outcomes
A.2.1. Effective parameters of the plants based on the modified two-cavity method
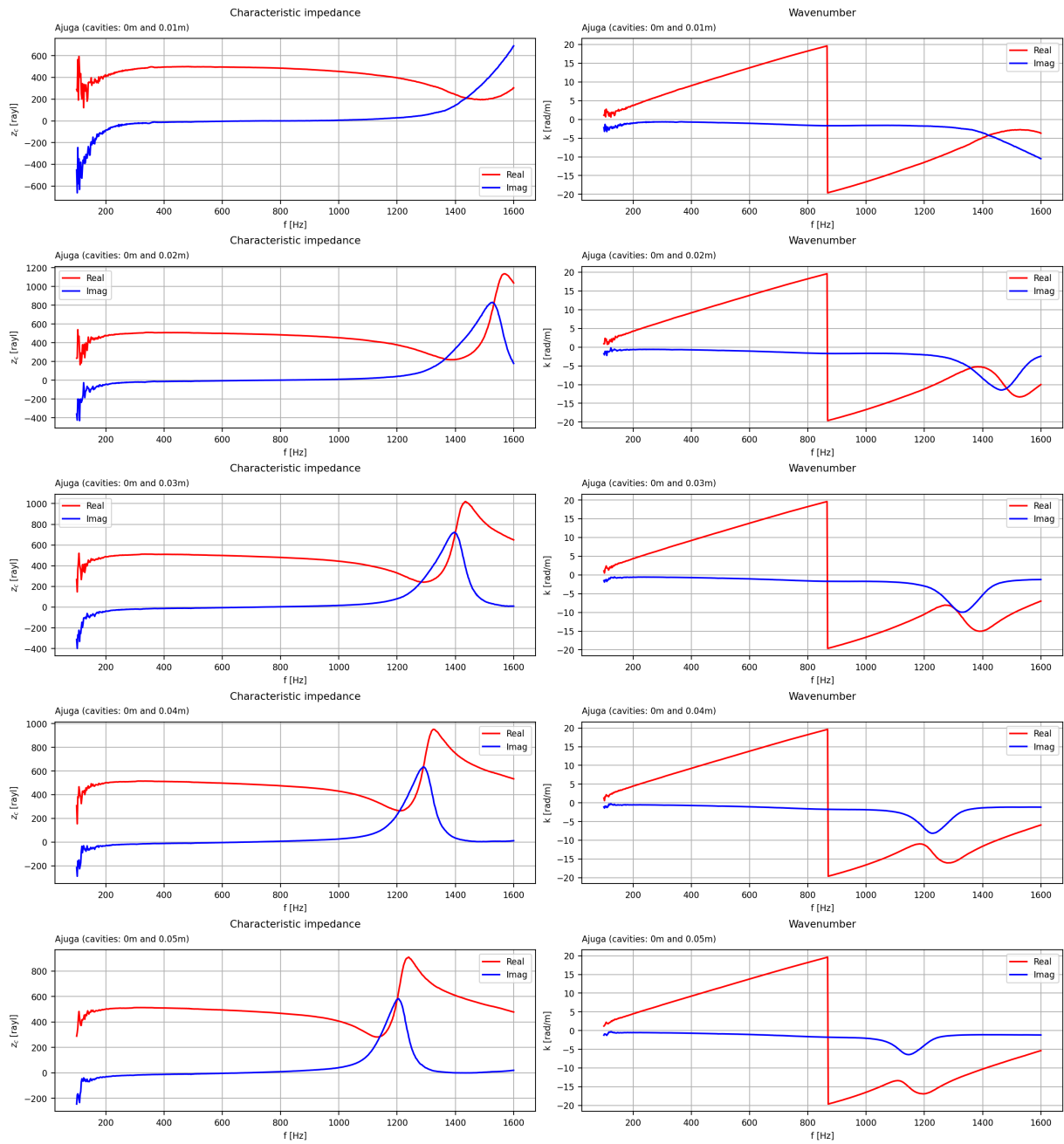
Figure A.22: Frequency-dependent (unprocessed) effective parameters of Ajuga reptans
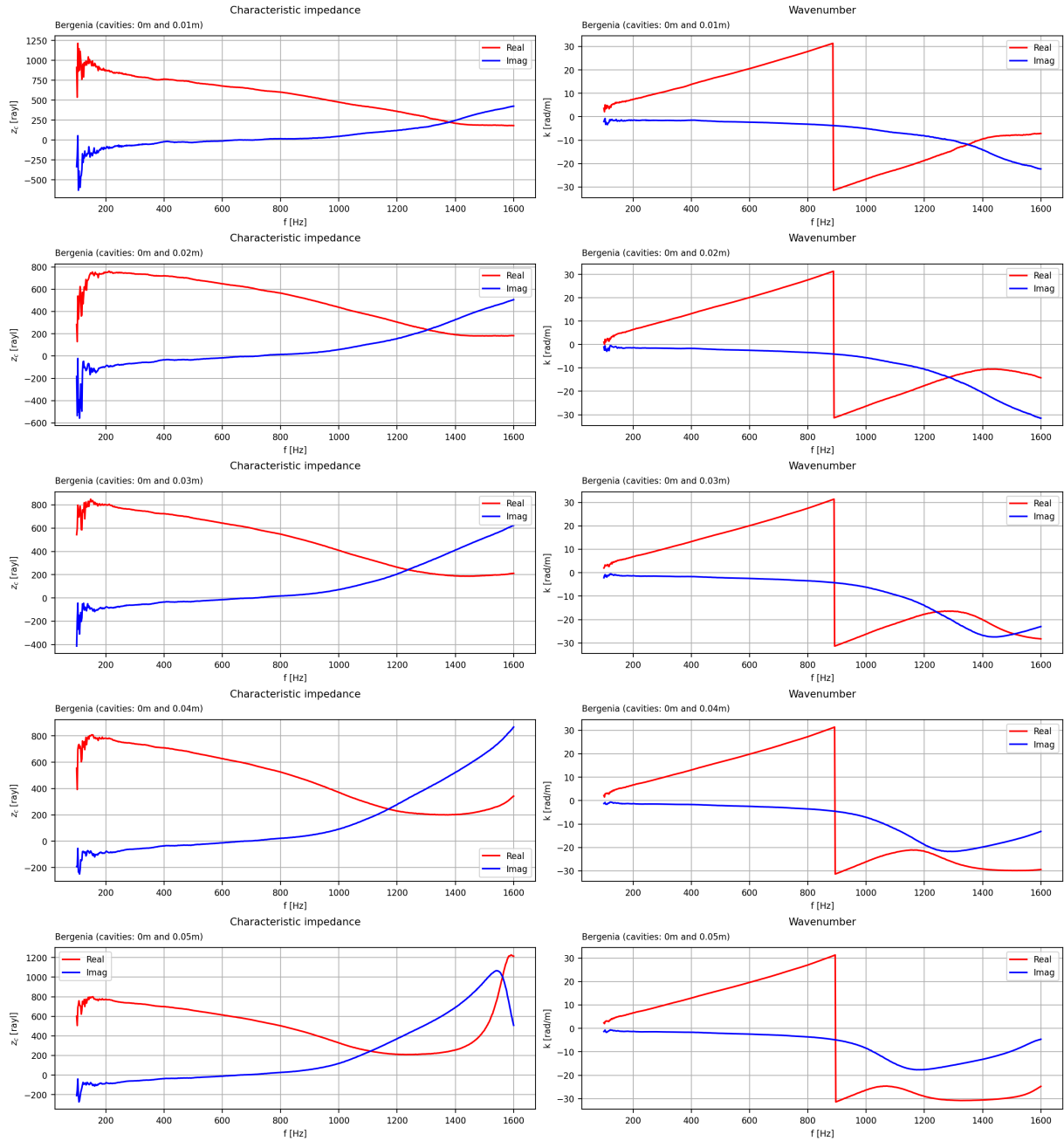
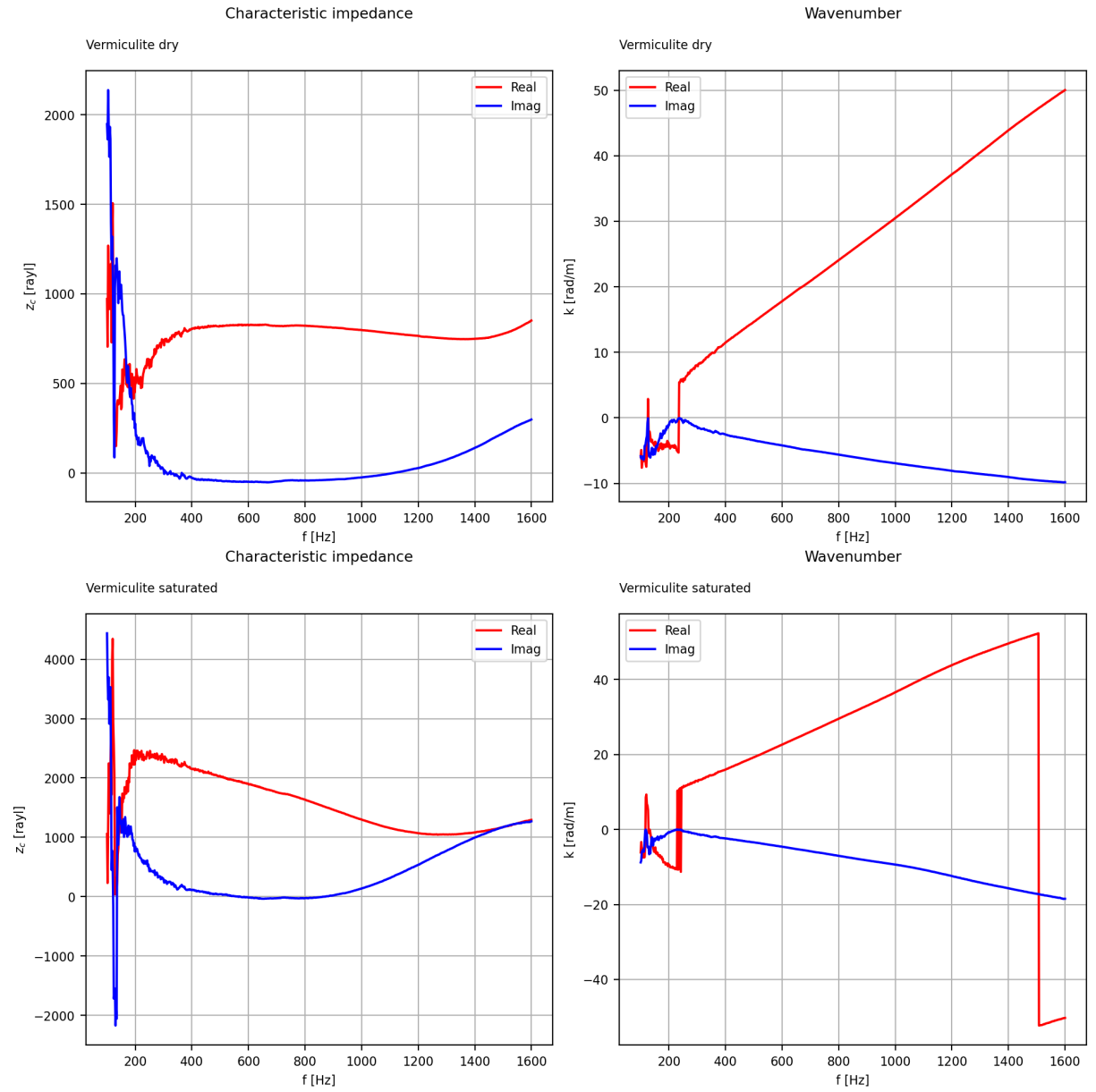**Figure A.23:** Frequency-dependent (unprocessed) effective parameters of Bergenia cordifolia
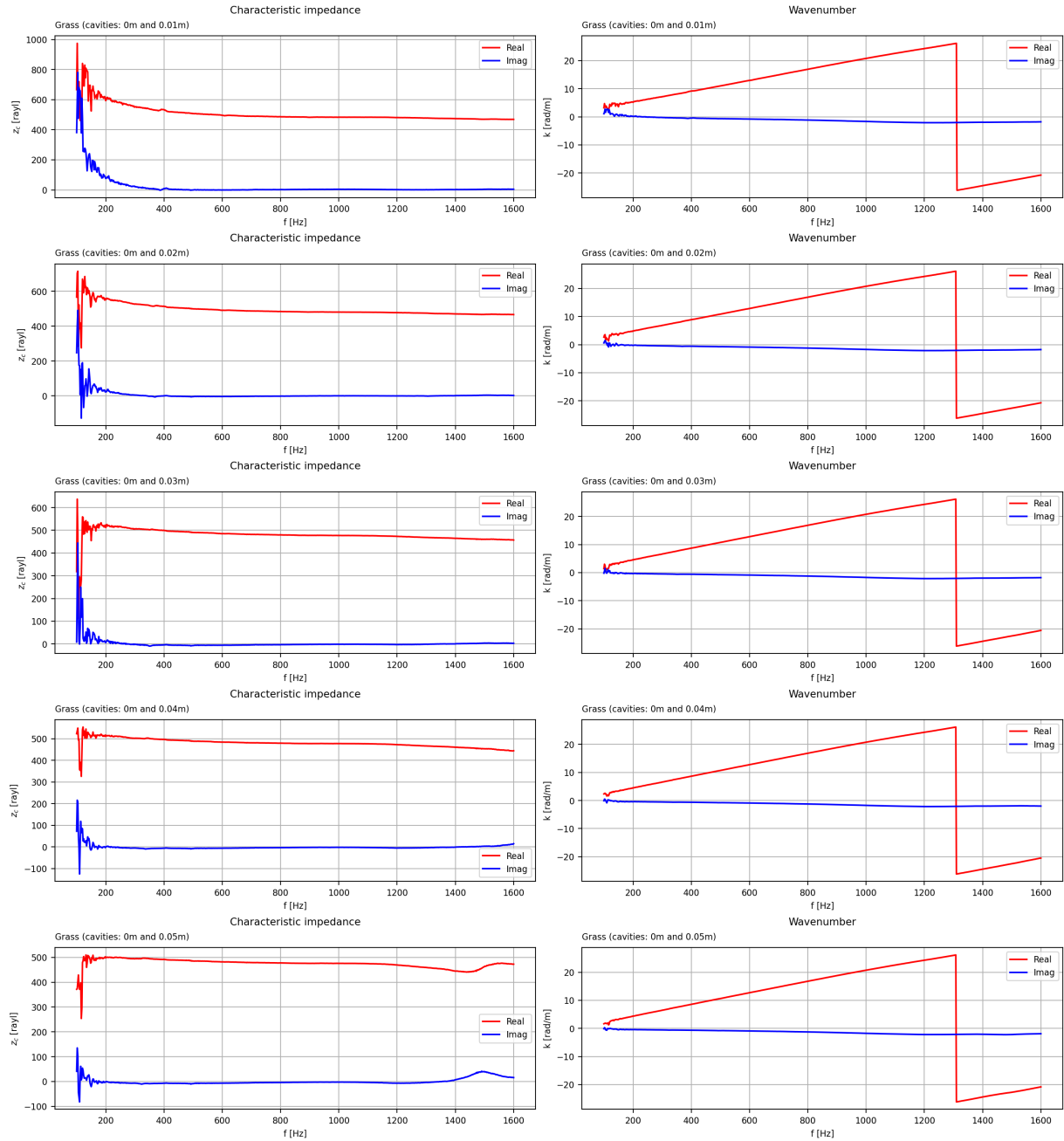
Figure A.24: Frequency-dependent (unprocessed) effective parameters of Festuca glauca
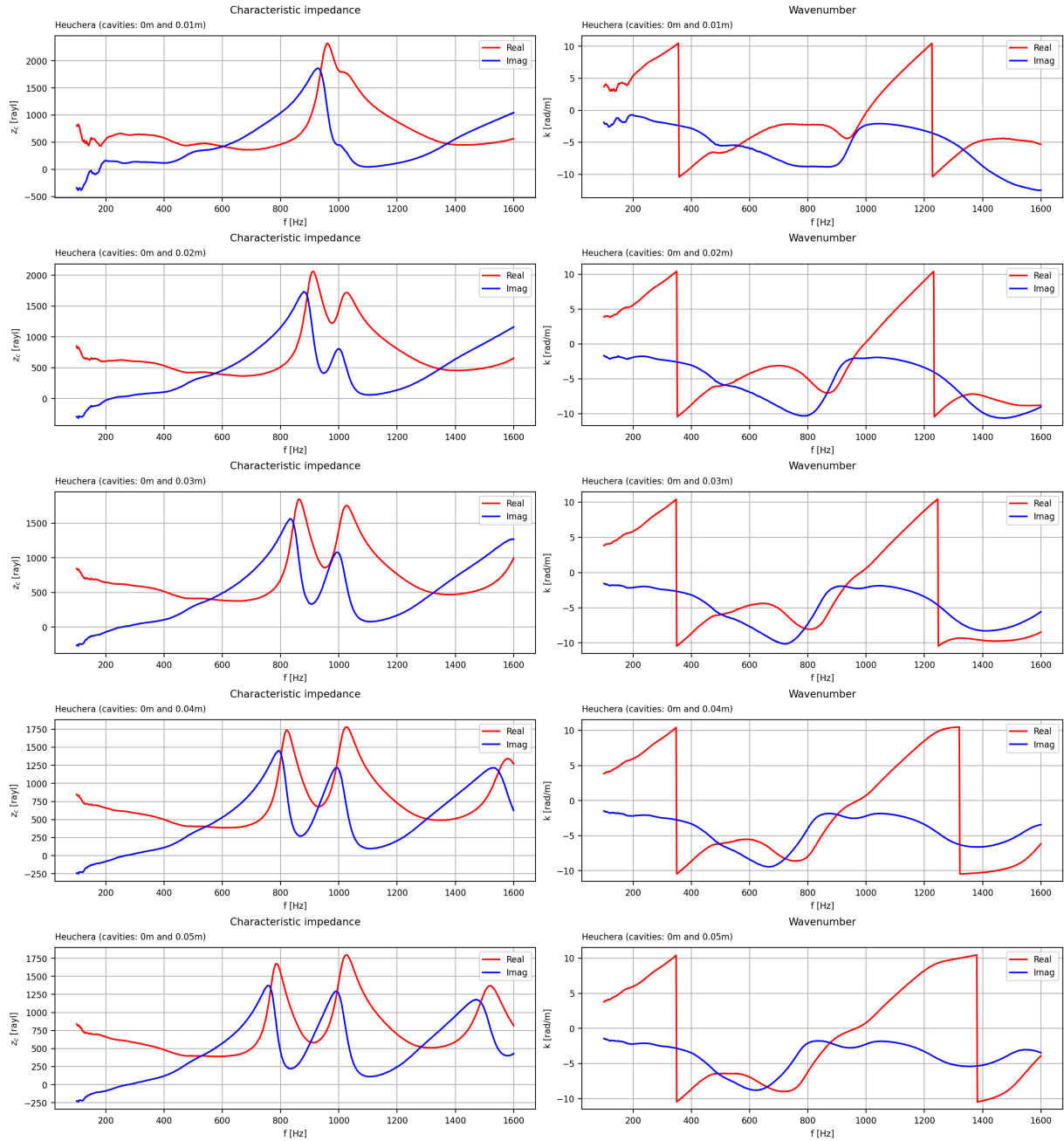
Figure A.25: Frequency-dependent (unprocessed) effective parameters of Heuchera 'Cascade Dawn'
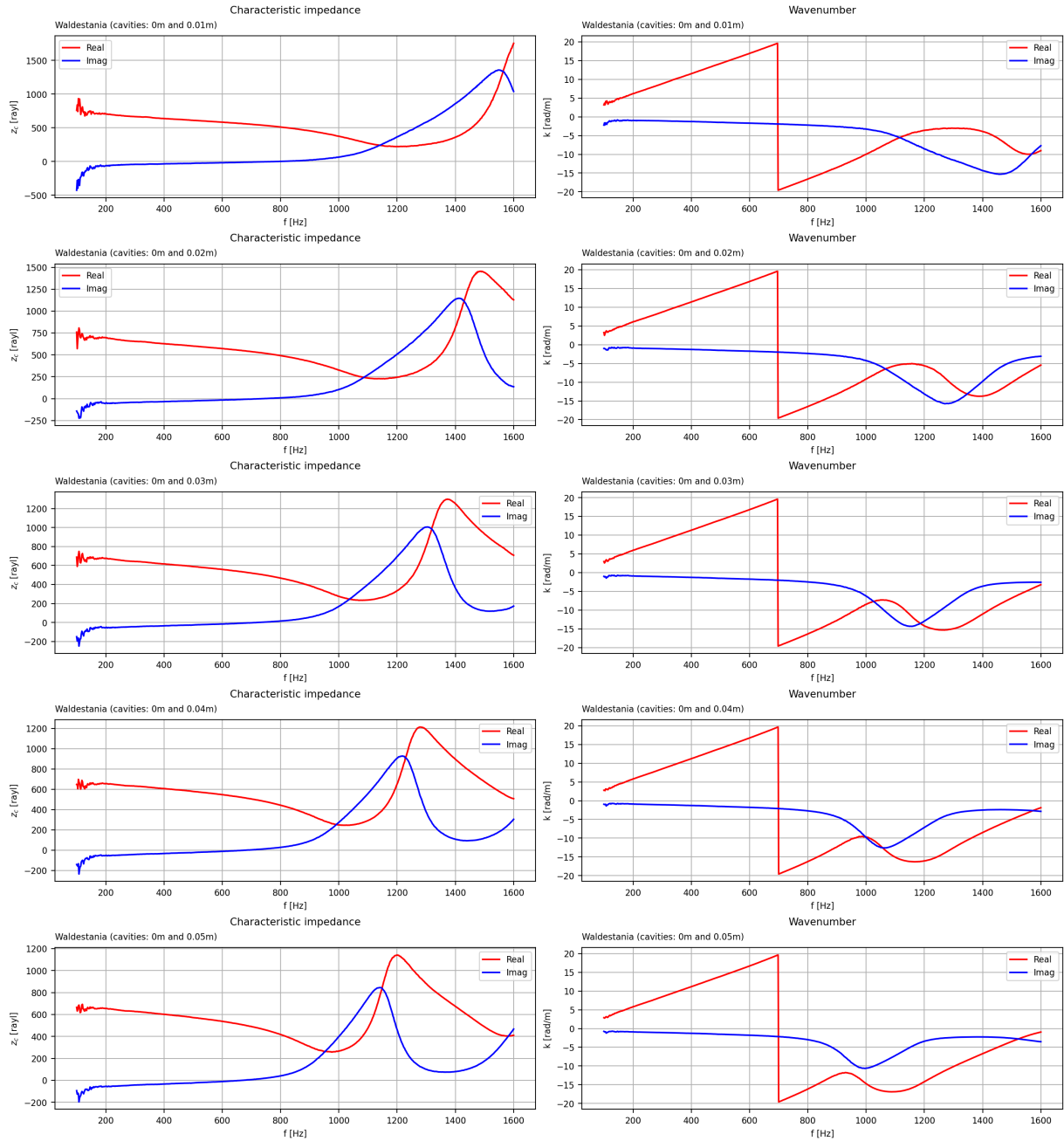
Figure A.26: Frequency-dependent (unprocessed) effective parameters of Waldestania ternata

A.2.2. Mean characteristic impedance of the plants
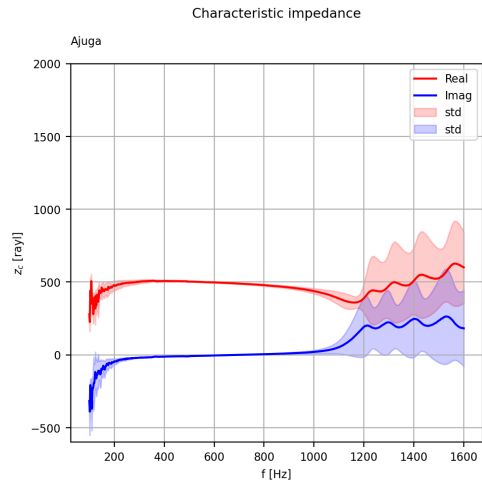
Figure A.27: Frequency-dependent (unprocessed) mean characteristic impedance of Ajuga reptans
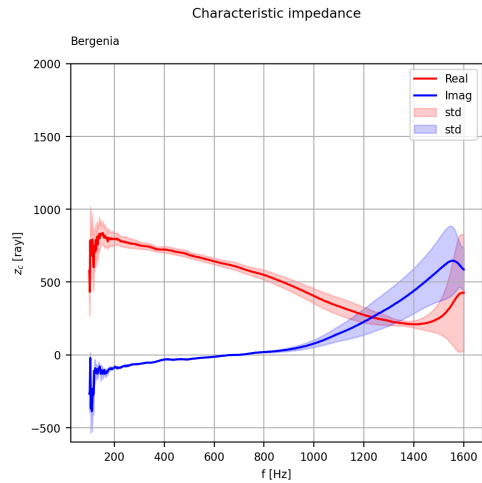
Figure A.28: Frequency-dependent (unprocessed) mean characteristic impedance of Bergenia cordifolia
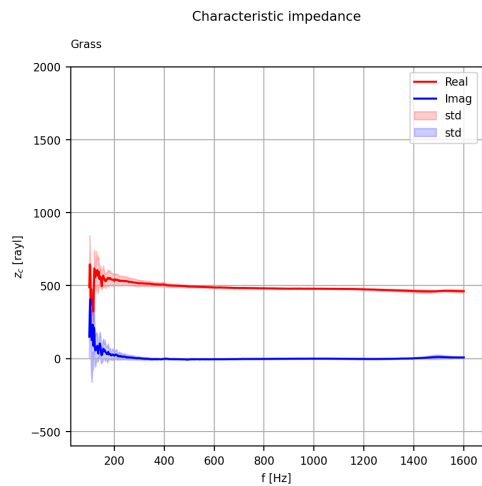
Figure A.29: Frequency-dependent (unprocessed) mean characteristic impedance of Festuca glauca
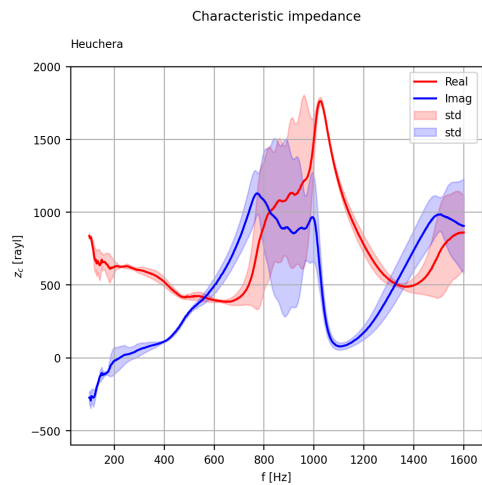
Figure A.30: Frequency-dependent (unprocessed) mean characteristic impedance of Heuchera 'Cascade Dawn'
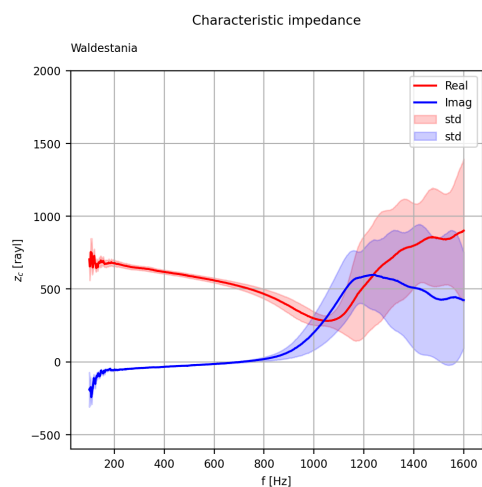
Figure A.31: Frequency-dependent (unprocessed) mean characteristic impedance of Waldestania ternata

A.2.3. Effective parameters of the substrates based on the two-thickness method
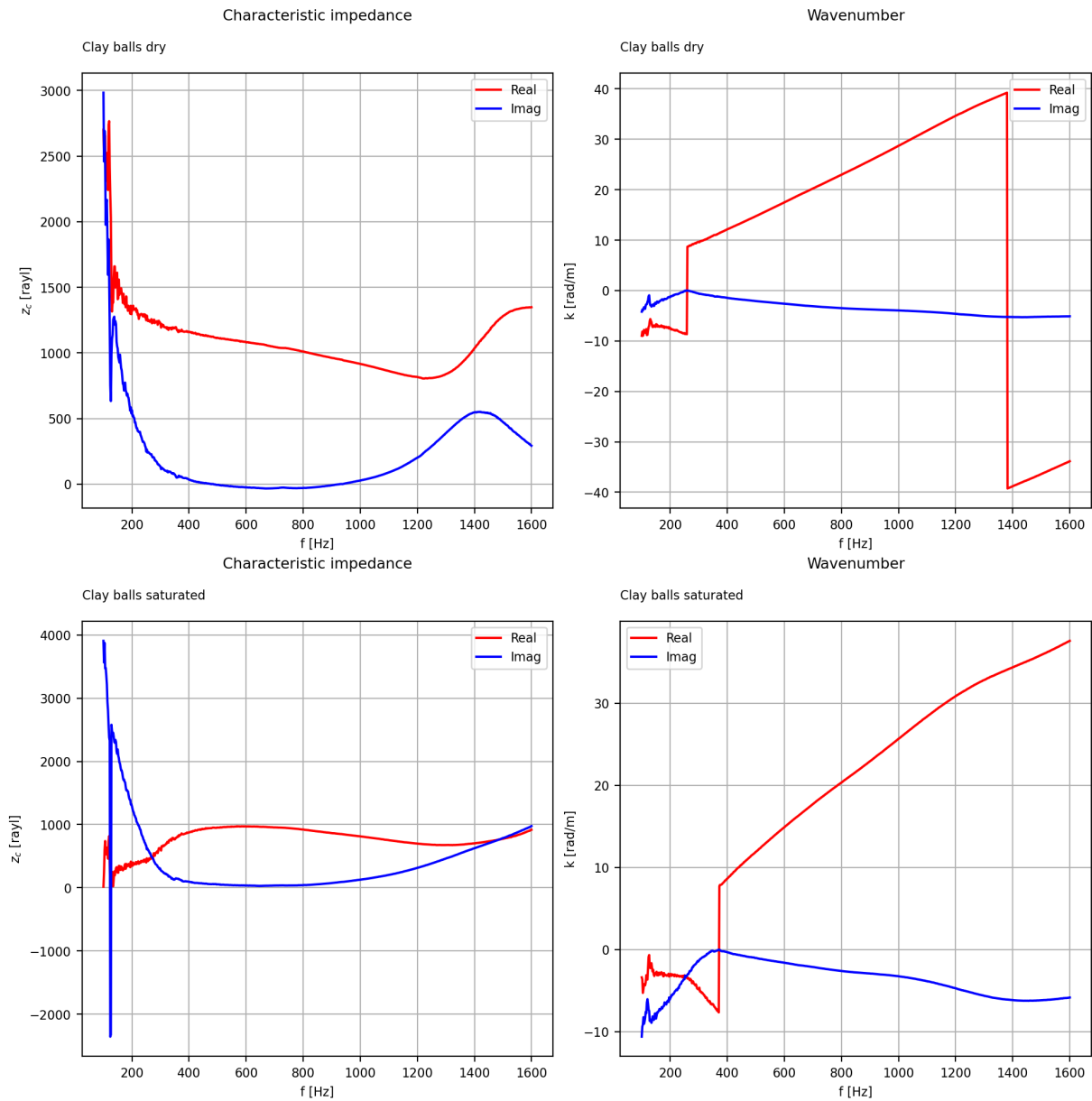
Figure A.32: Frequency-dependent (unprocessed) effective parameters of clay balls
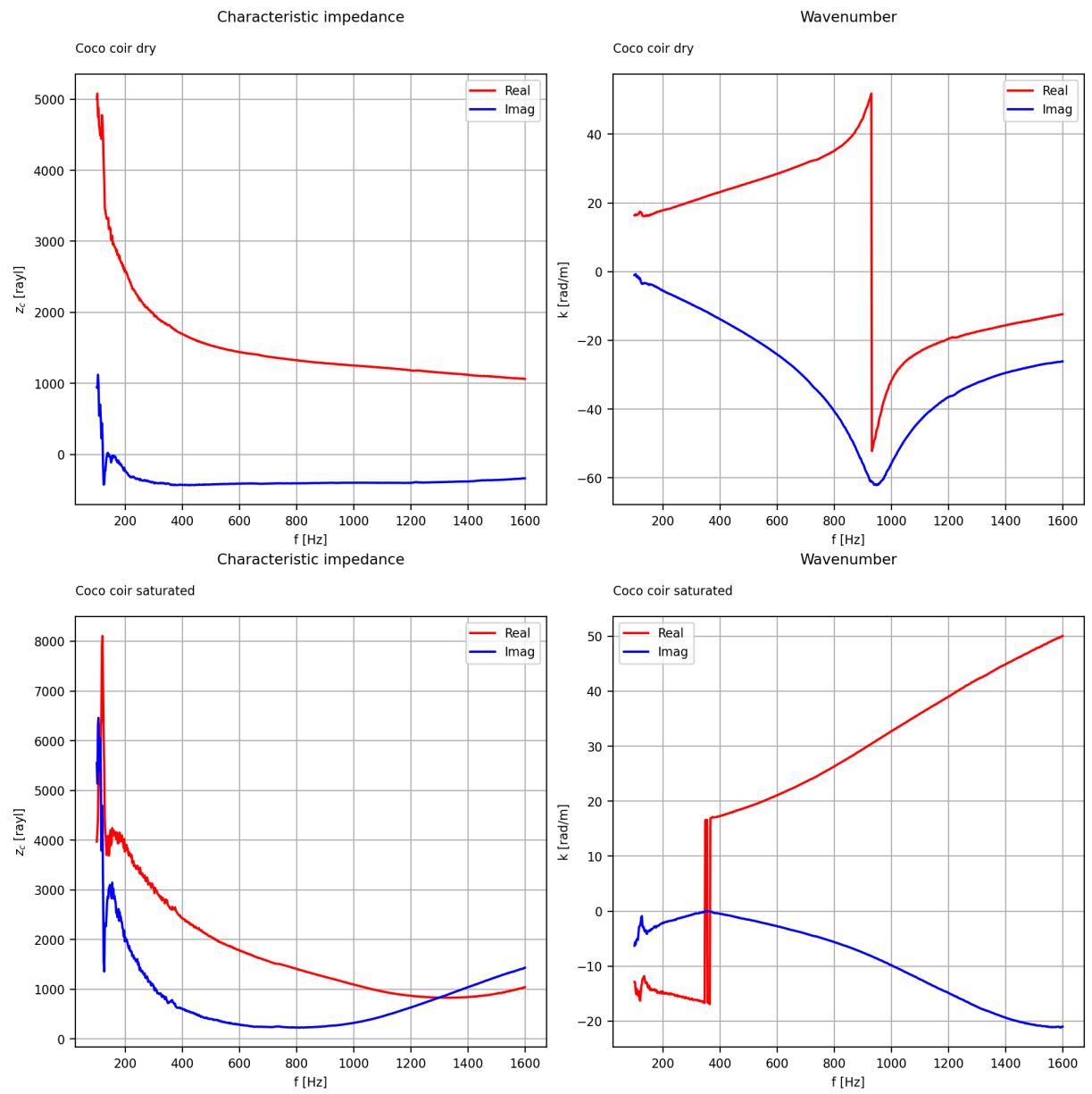
Figure A.33: Frequency-dependent (unprocessed) effective parameters of coco coir
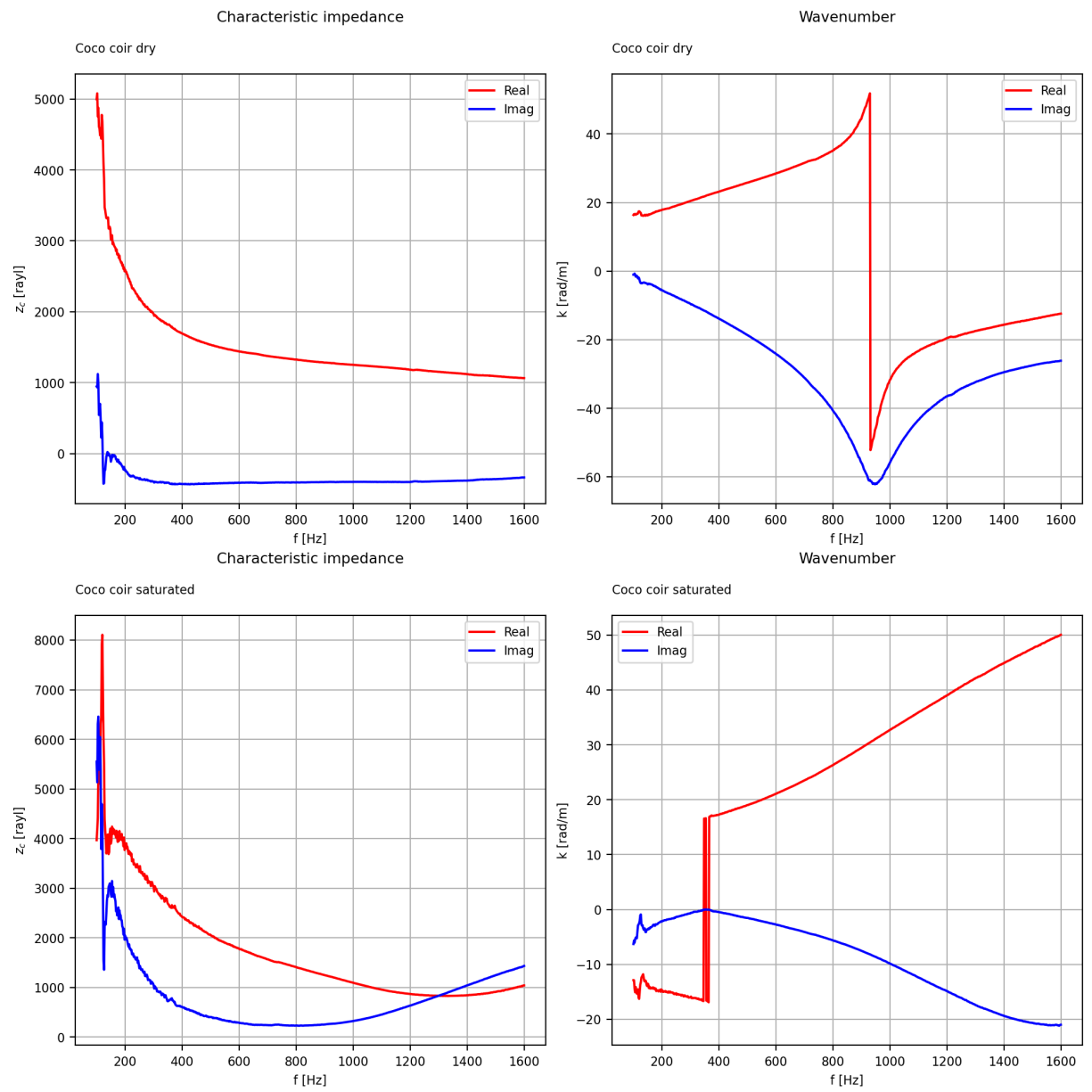
Figure A.34: Frequency-dependent (unprocessed) effective parameters of coco husk
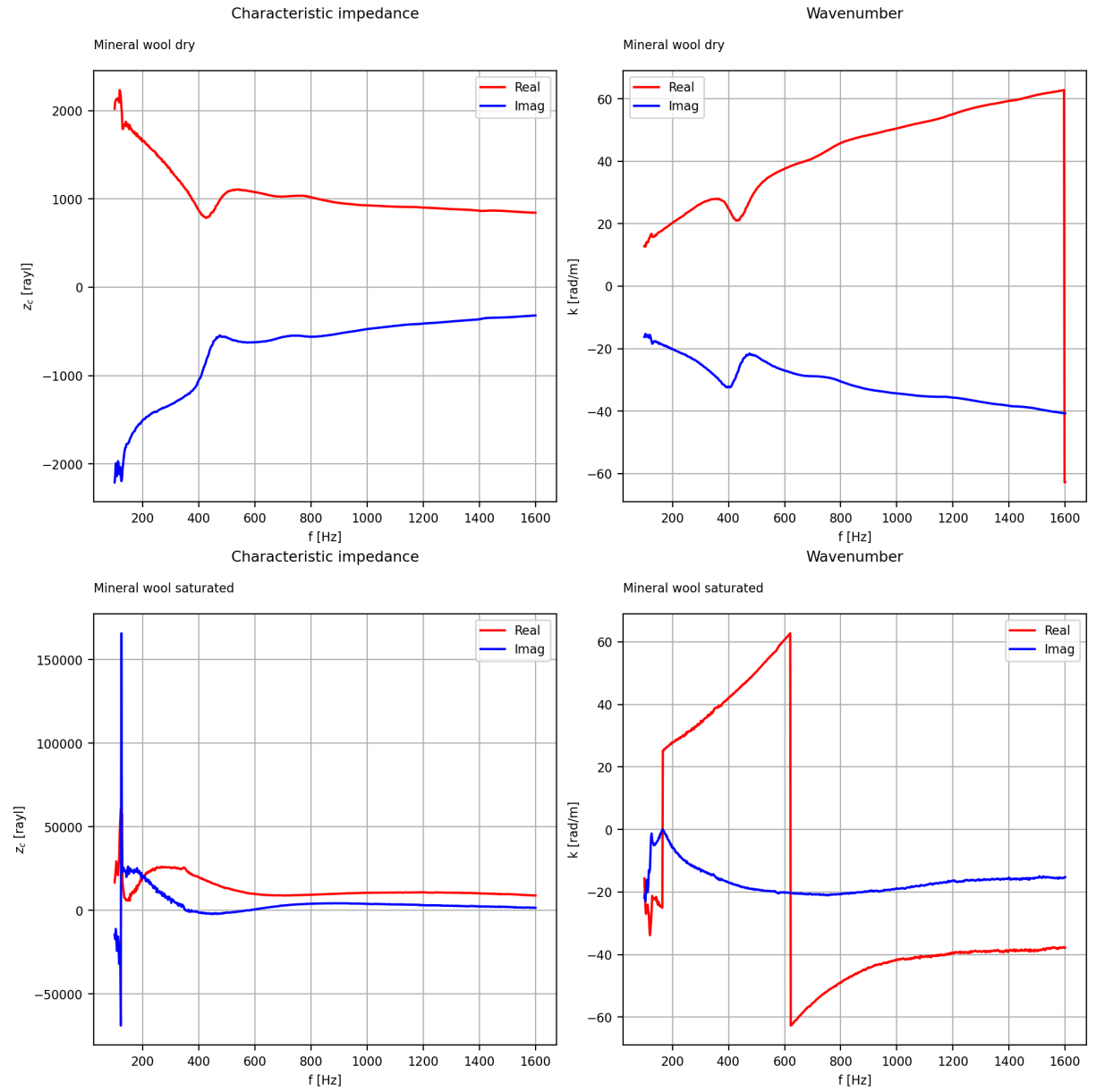
Figure A.35: Frequency-dependent (unprocessed) effective parameters of mineral wool
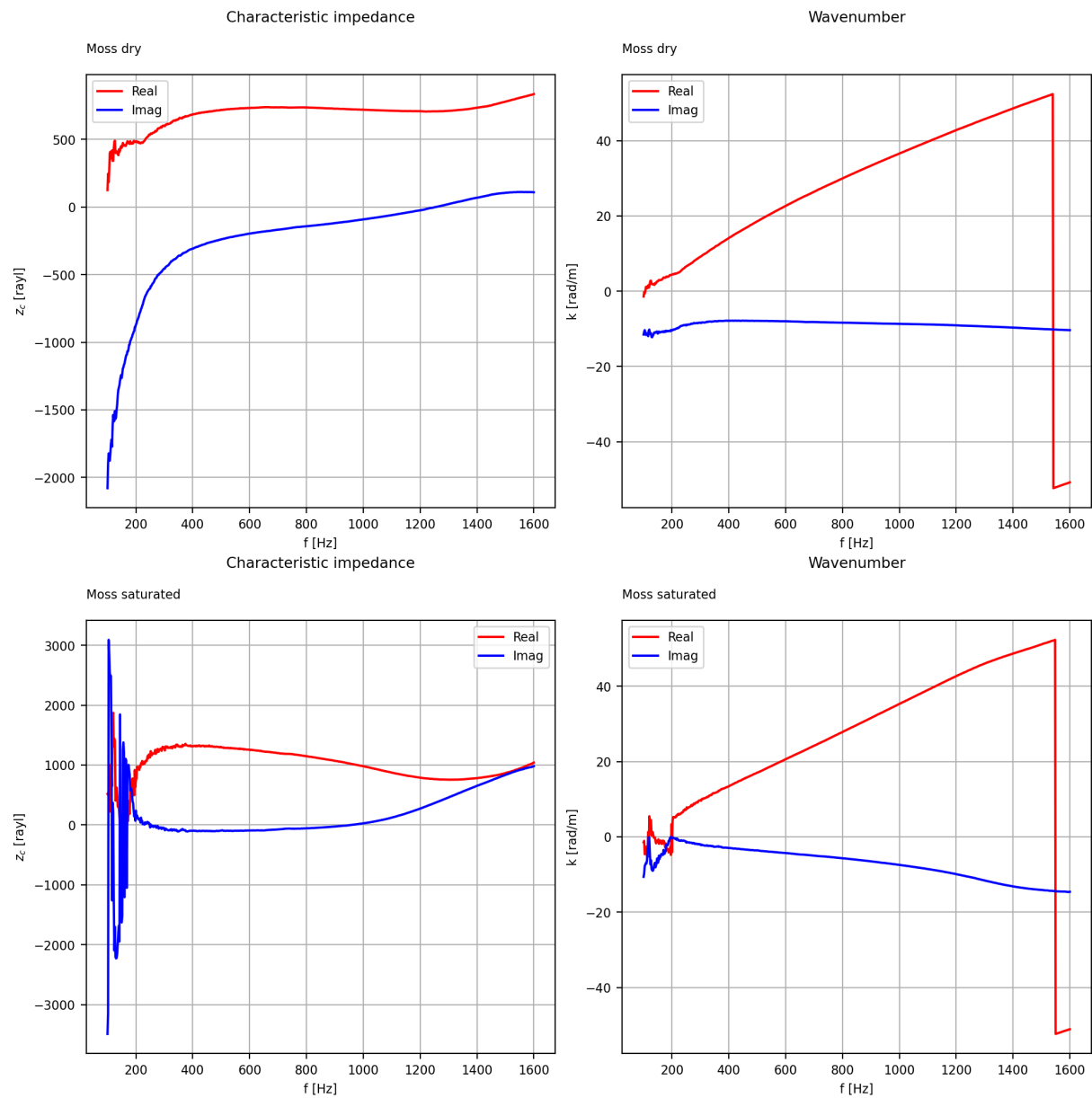
Figure A.36: Frequency-dependent (unprocessed) effective parameters of moss
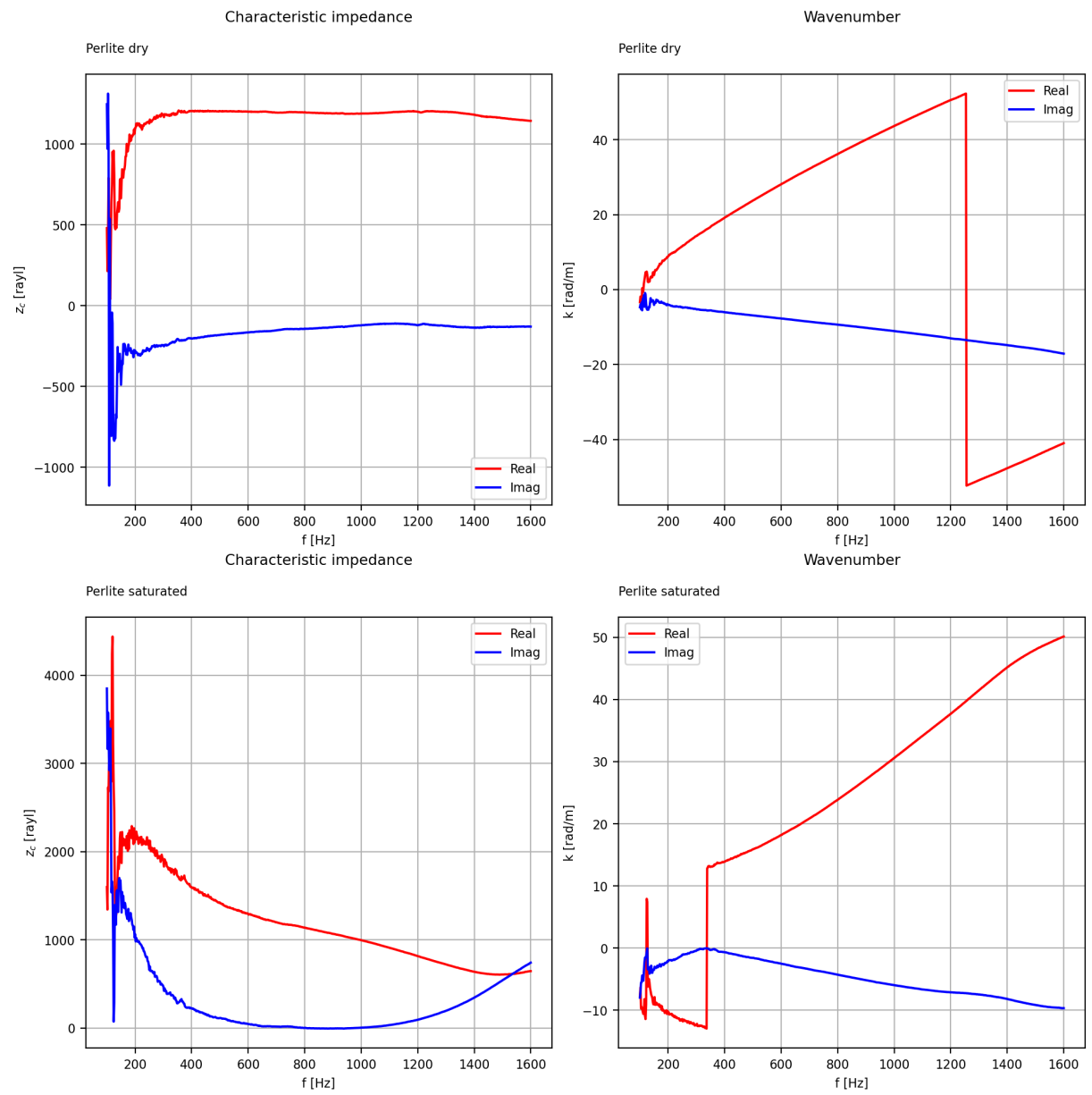
Figure A.37: Frequency-dependent (unprocessed) effective parameters of perlite
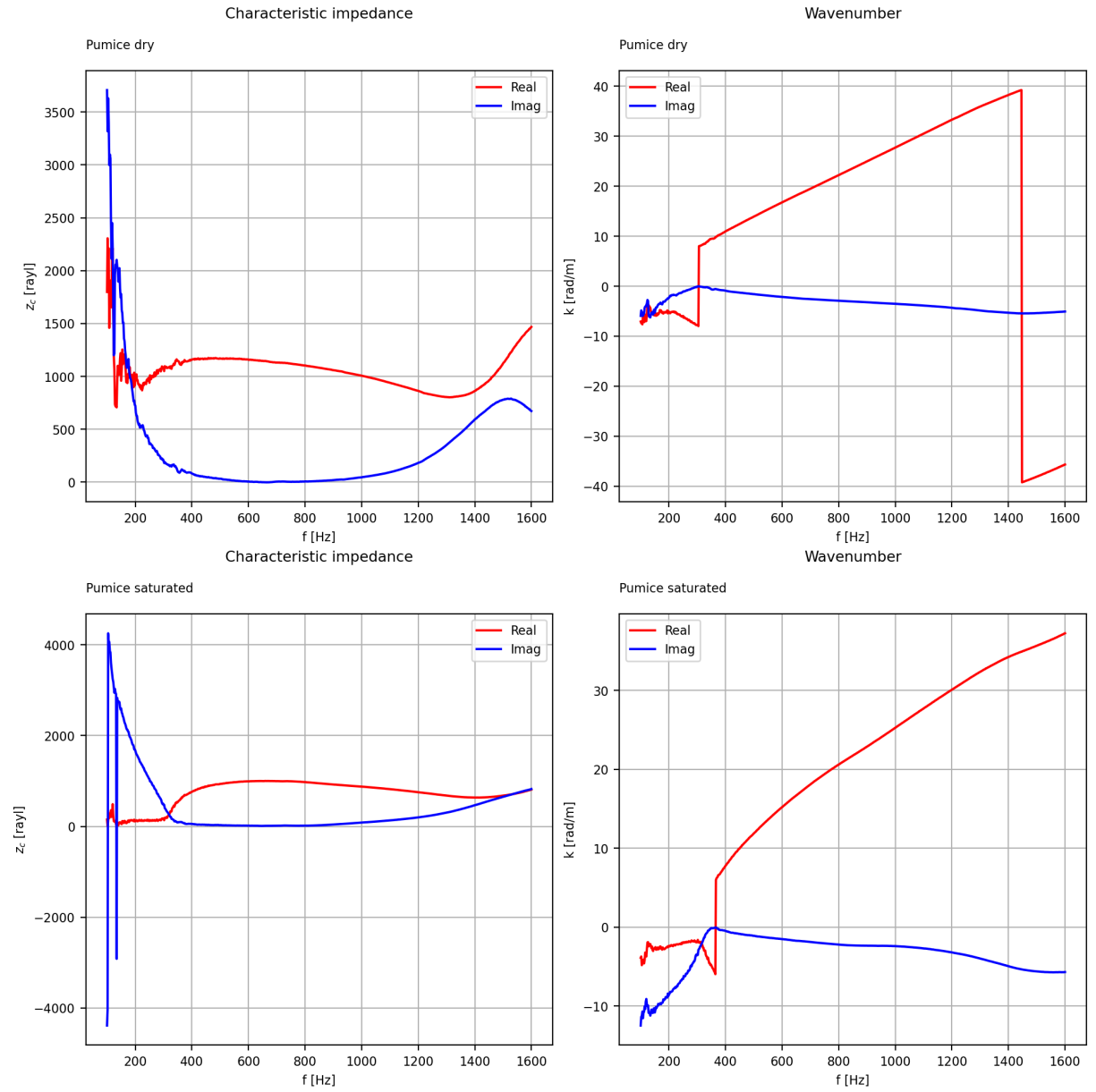
Figure A.38: Frequency-dependent (unprocessed) effective parameters of pumice

Figure A.39: Frequency-dependent (unprocessed) effective parameters of vermiculite

A.3. Final Data Analysis Outcomes
A.3.1. Processed effective parameters of the plants
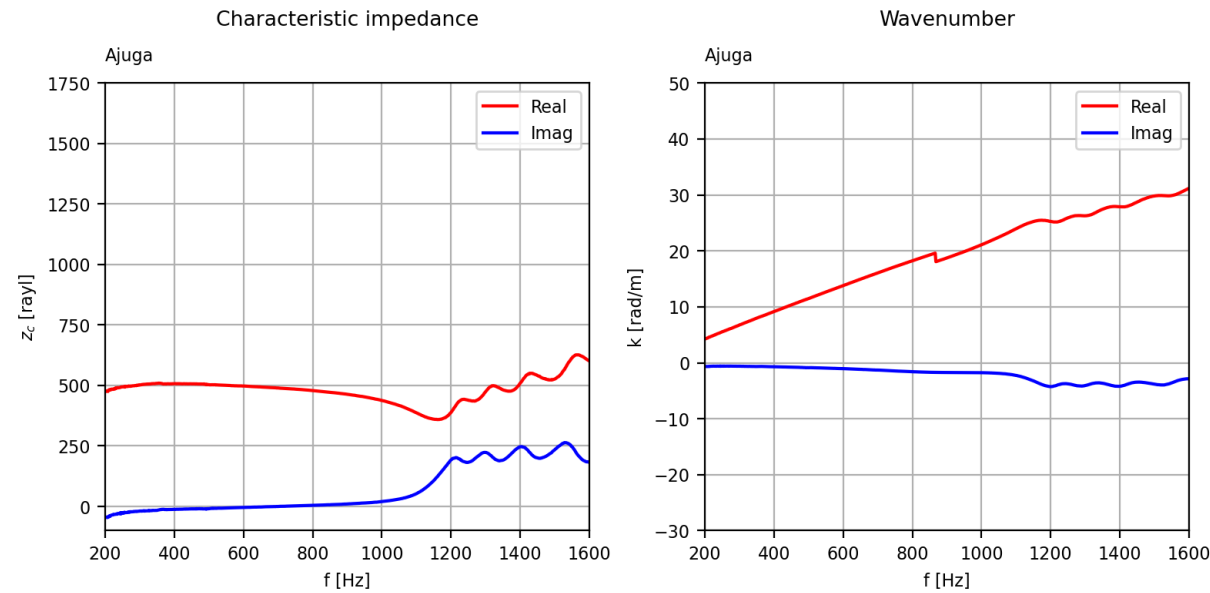
Figure A.40: Frequency-dependent effective parameters of Ajuga reptans
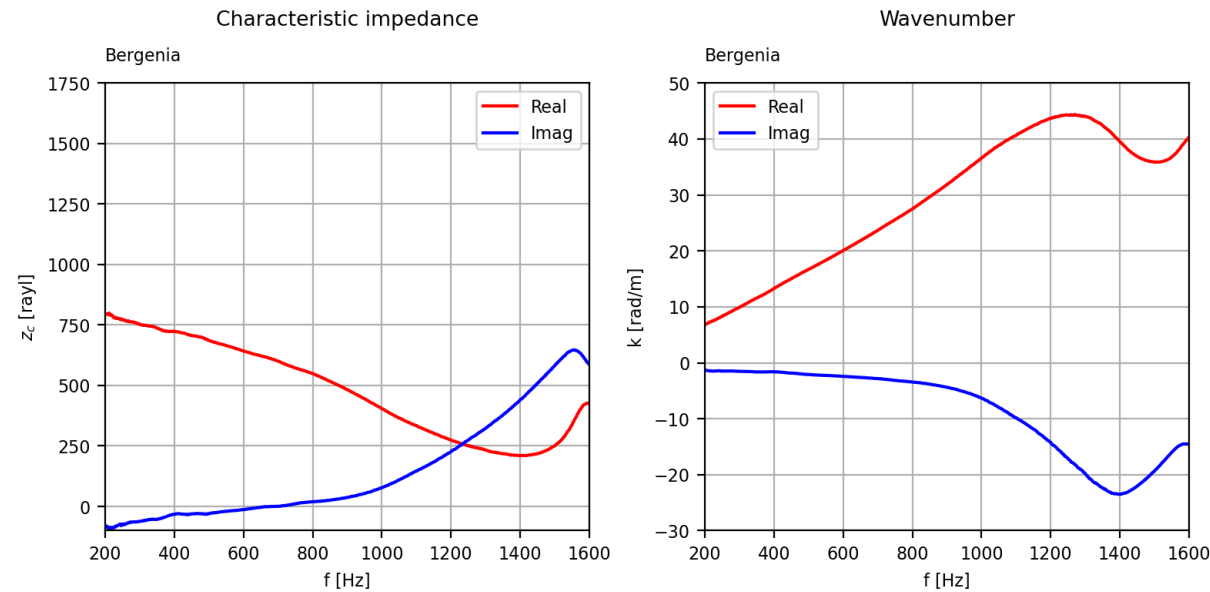
Figure A.41: Frequency-dependent effective parameters of Bergenia cordifolia
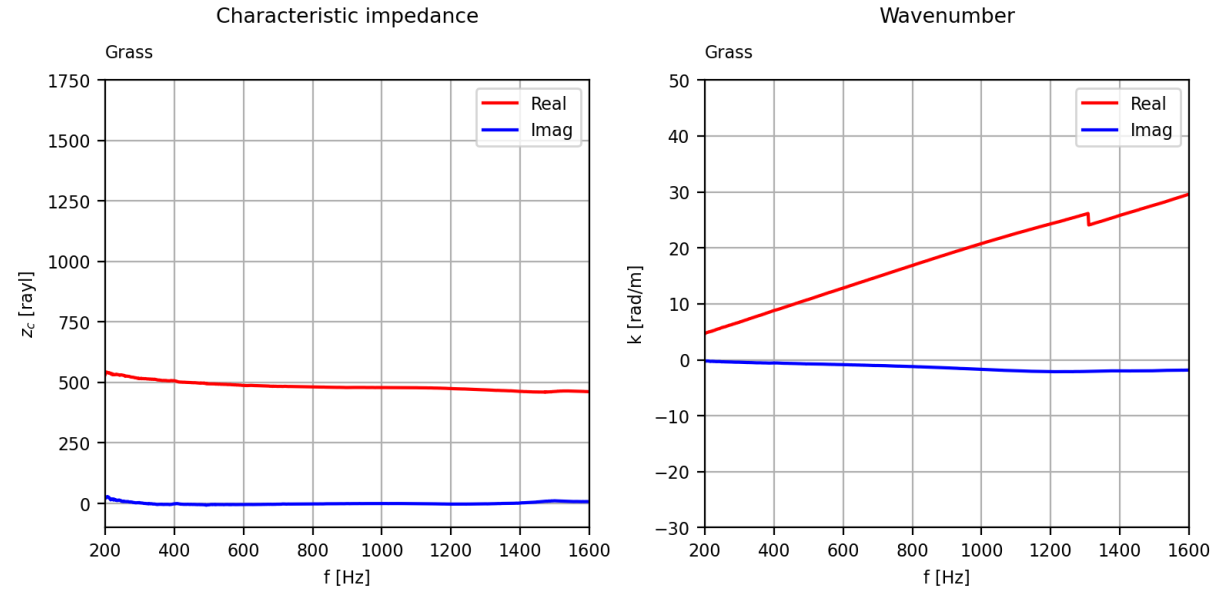
Figure A.42: Frequency-dependent effective parameters of Festuca glauca
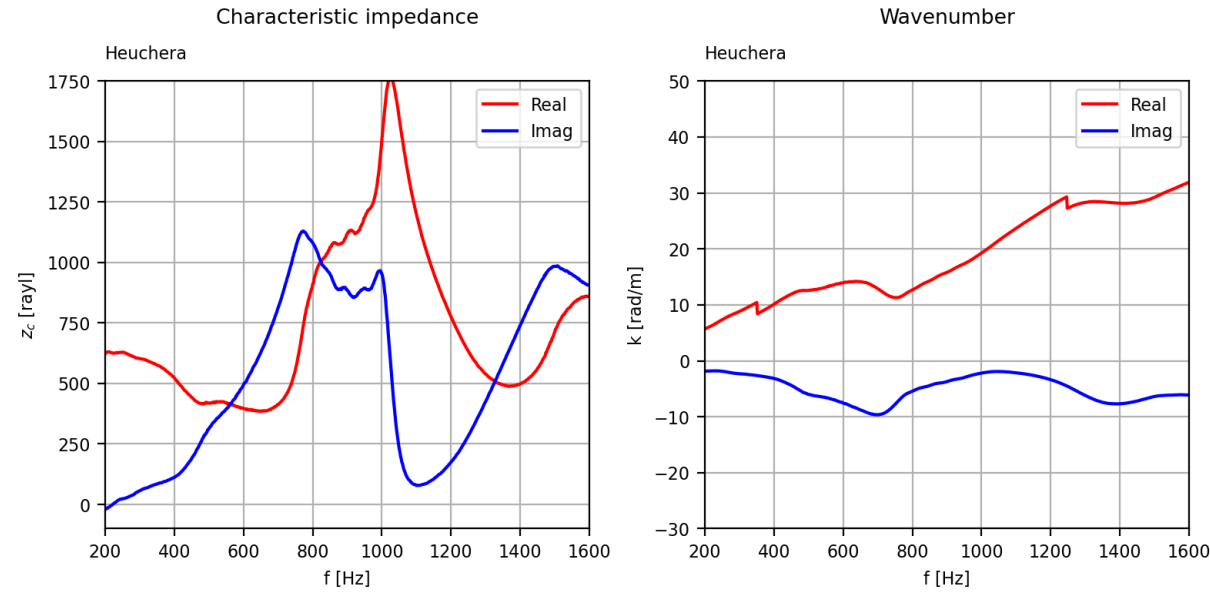
Figure A.43: Frequency-dependent effective parameters of Heuchera 'Cascade Dawn'

Characteristic impedance

Wavenumber
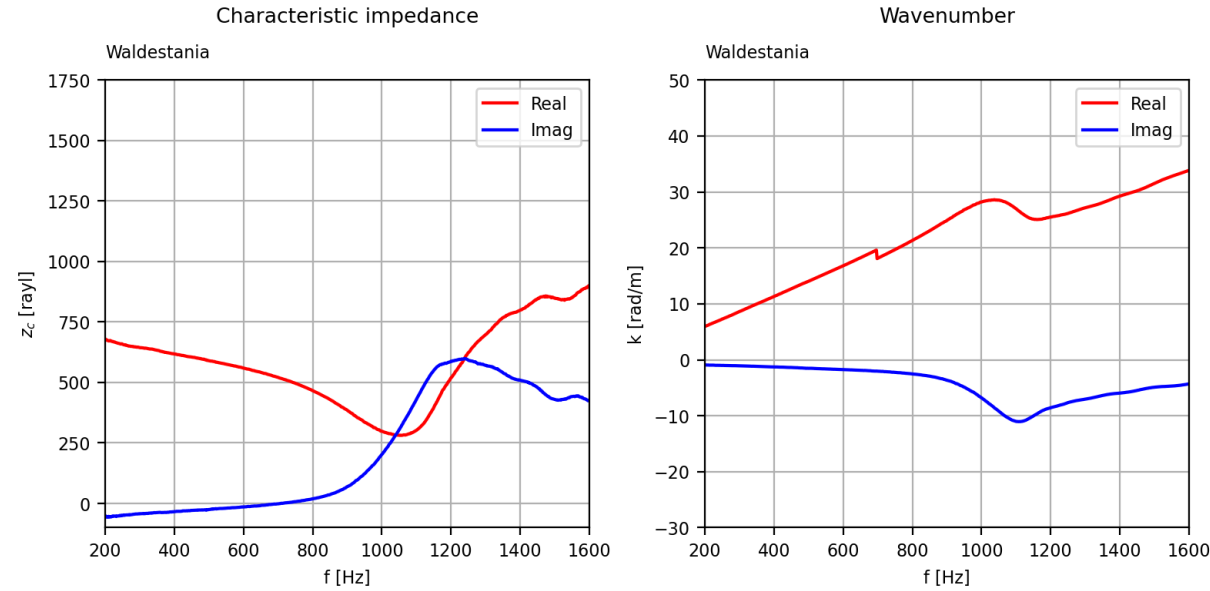
Figure A.44: Frequency-dependent effective parameters of Waldestania ternata

A.3.2. Processed effective parameters of the substrates
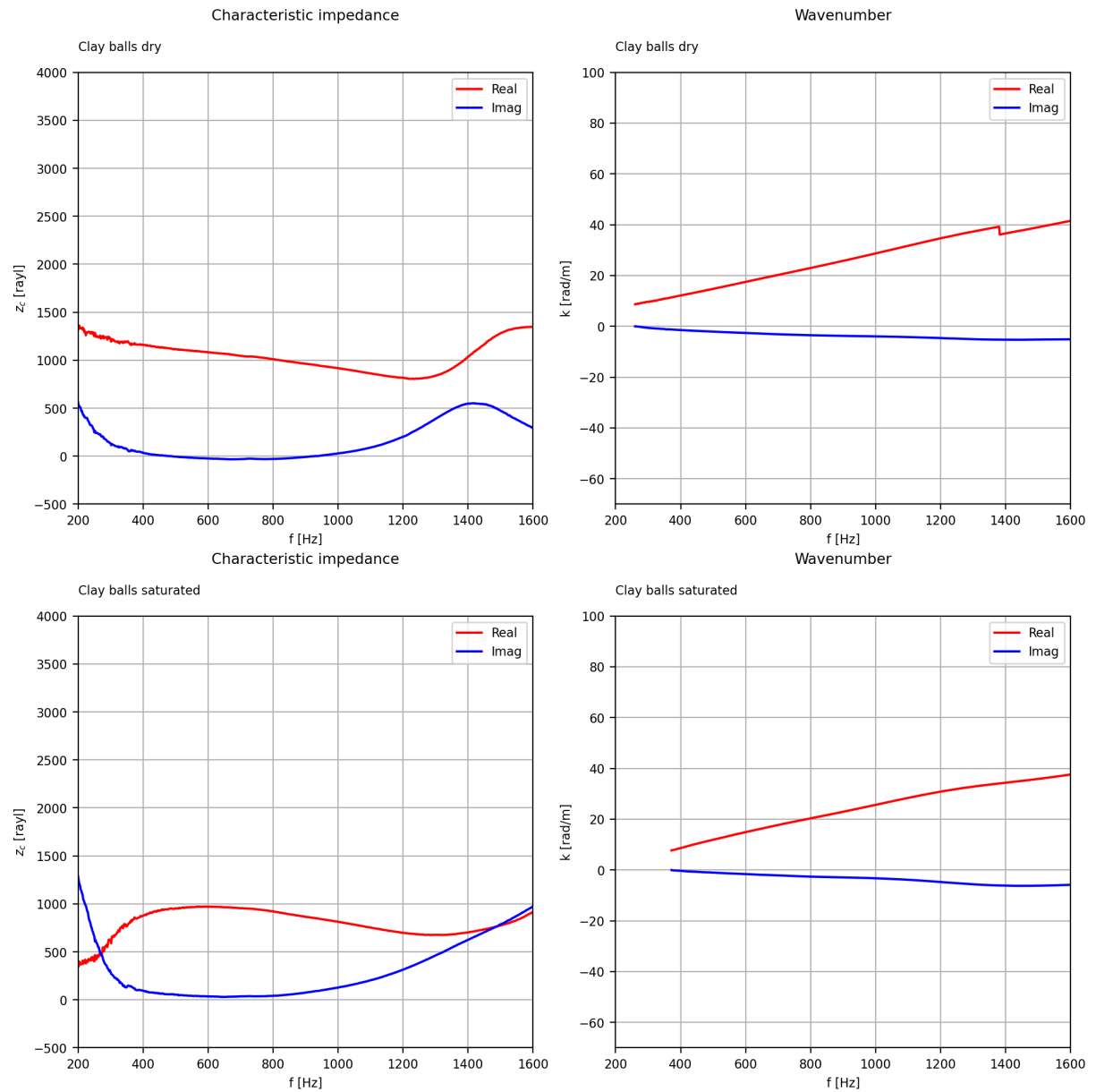
Figure A.45: Frequency-dependent effective parameters of clay balls
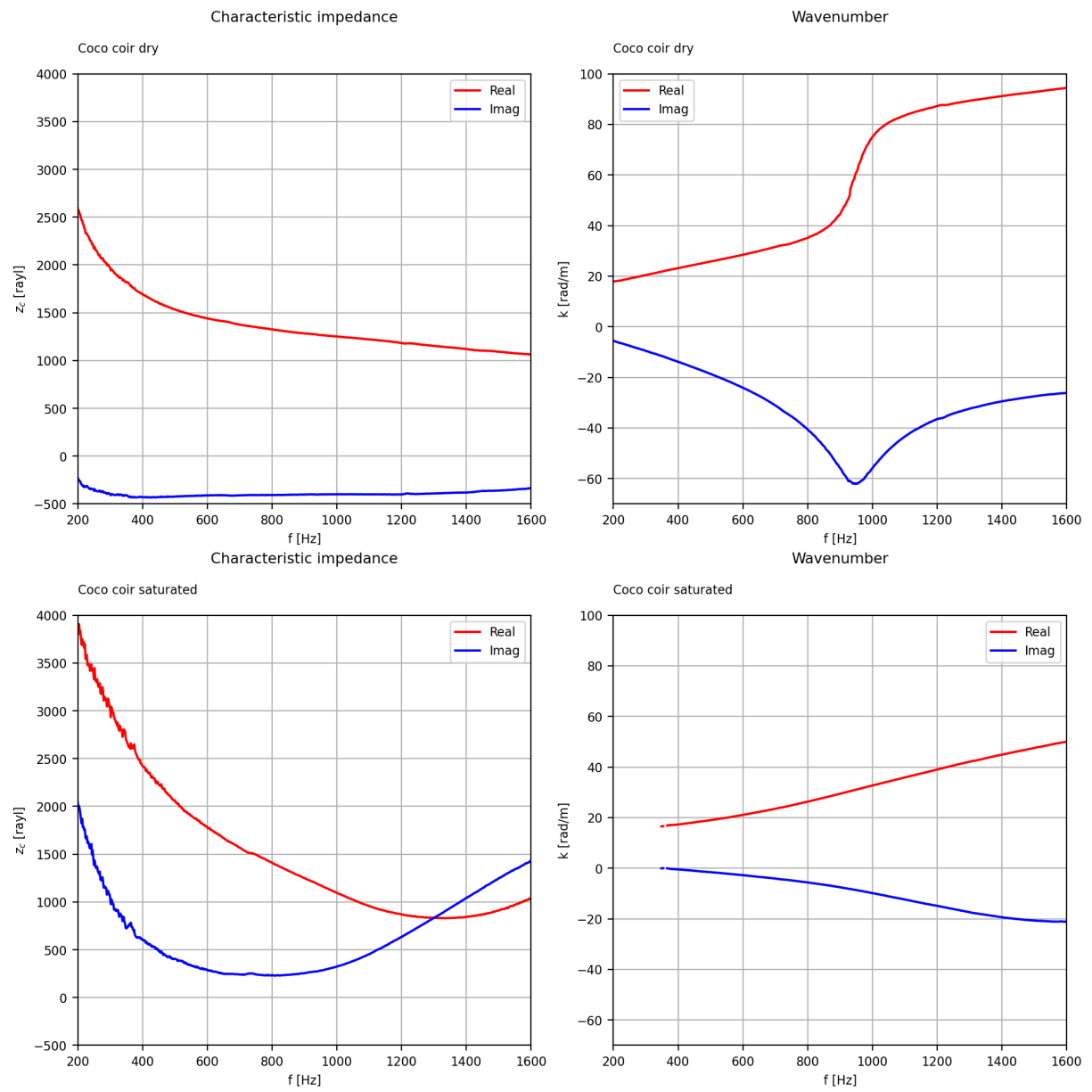
Figure A.46: Frequency-dependent effective parameters of coco coir
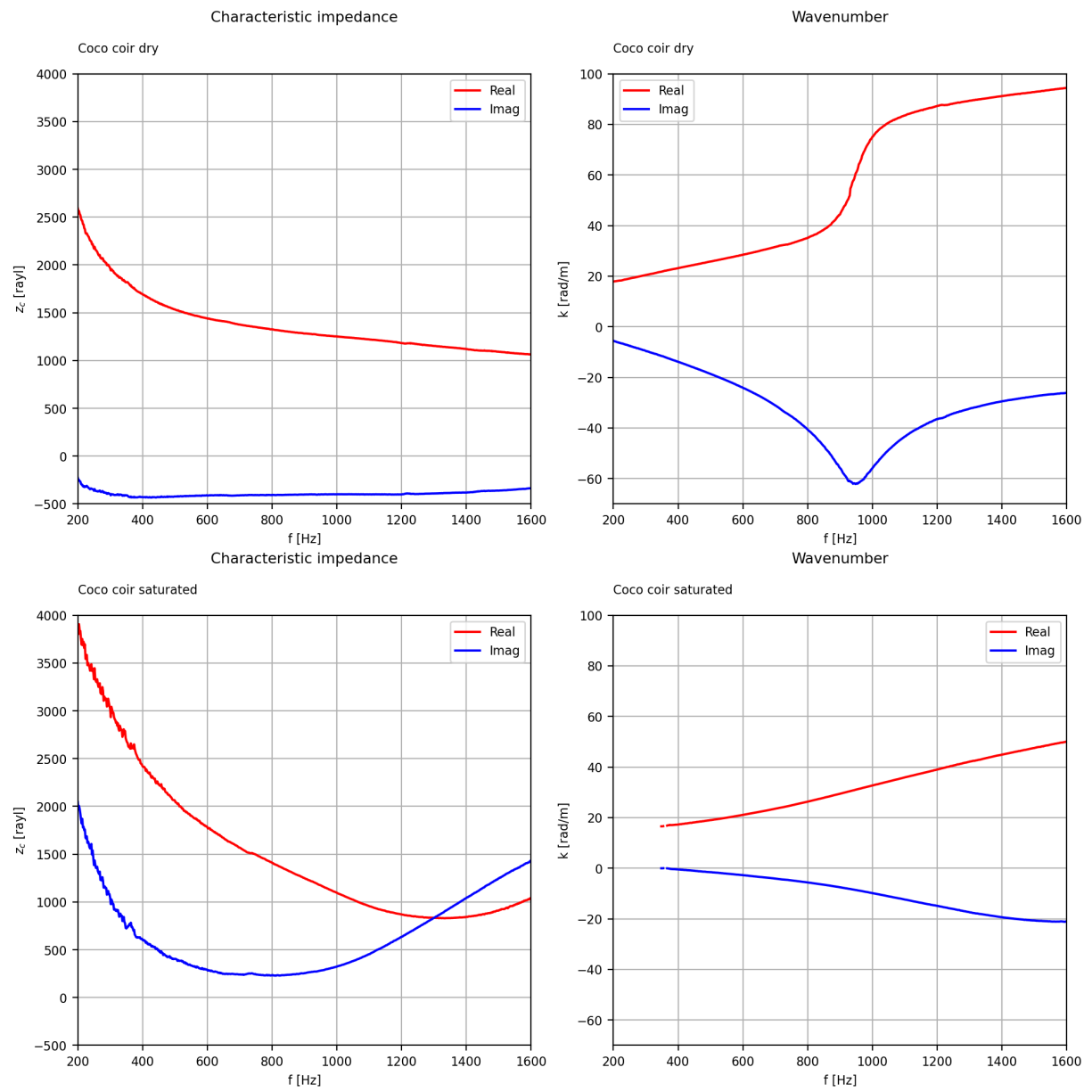
Figure A.47: Frequency-dependent effective parameters of coco husk
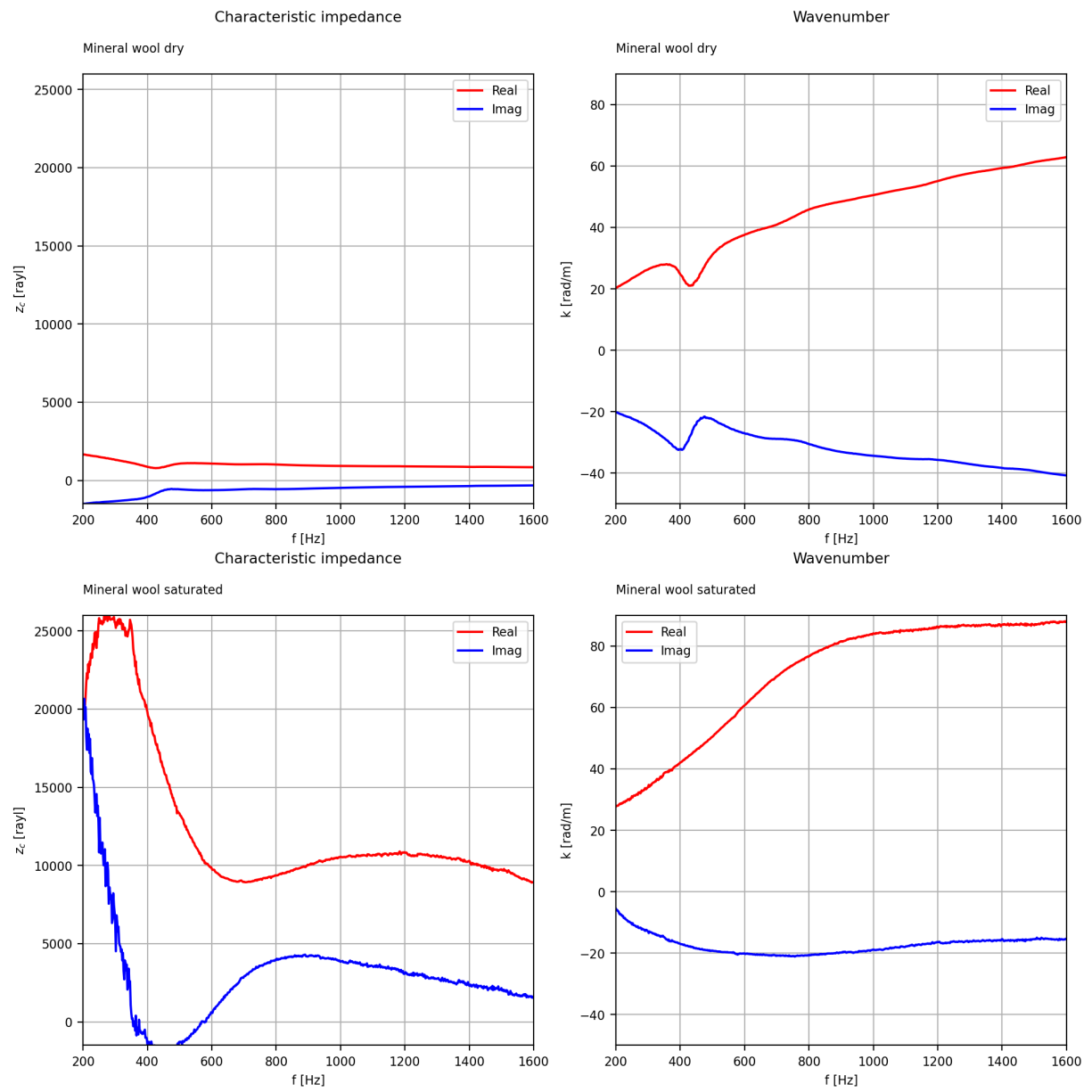
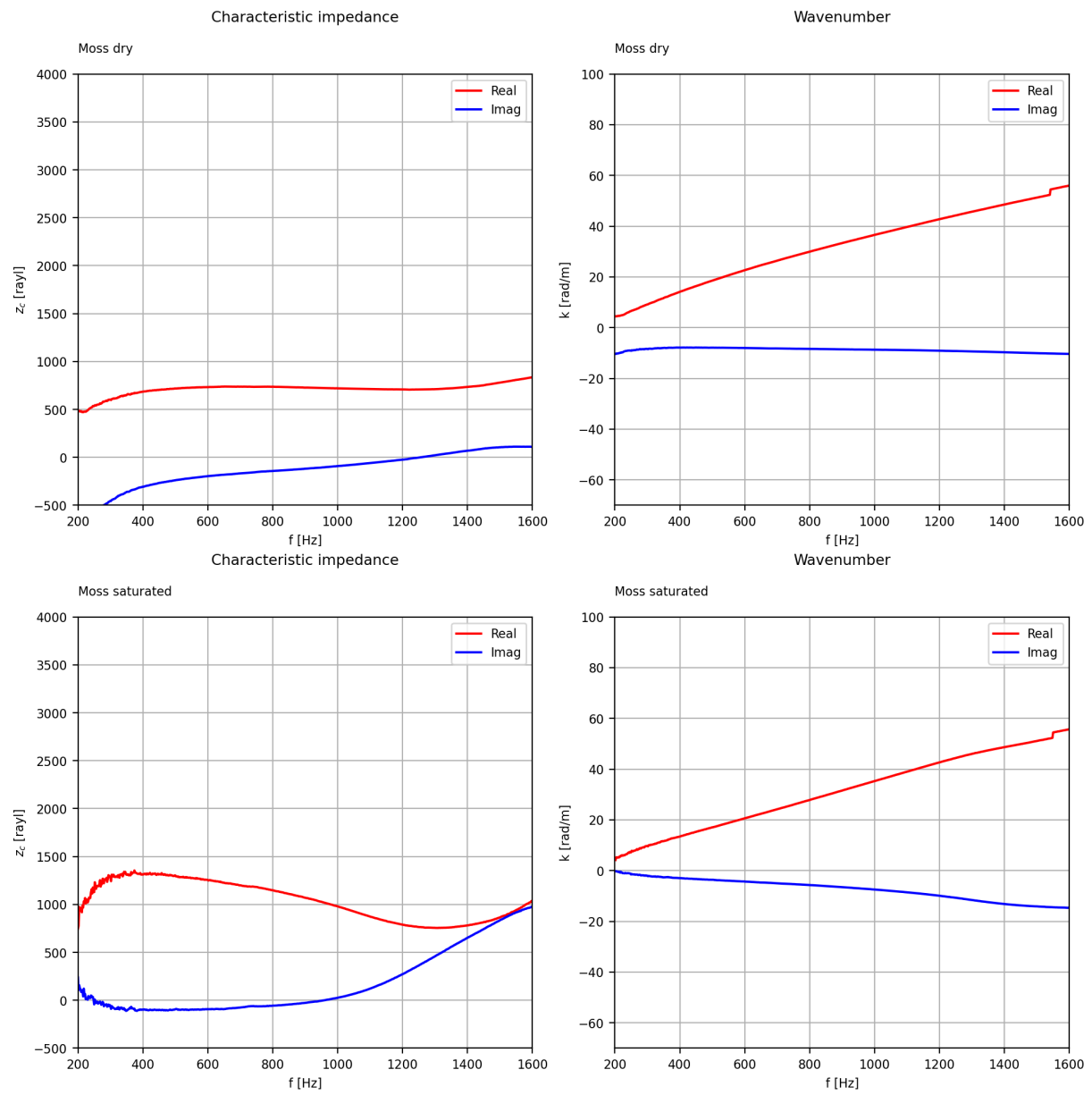**Figure A.48:** Frequency-dependent effective parameters of mineral wool

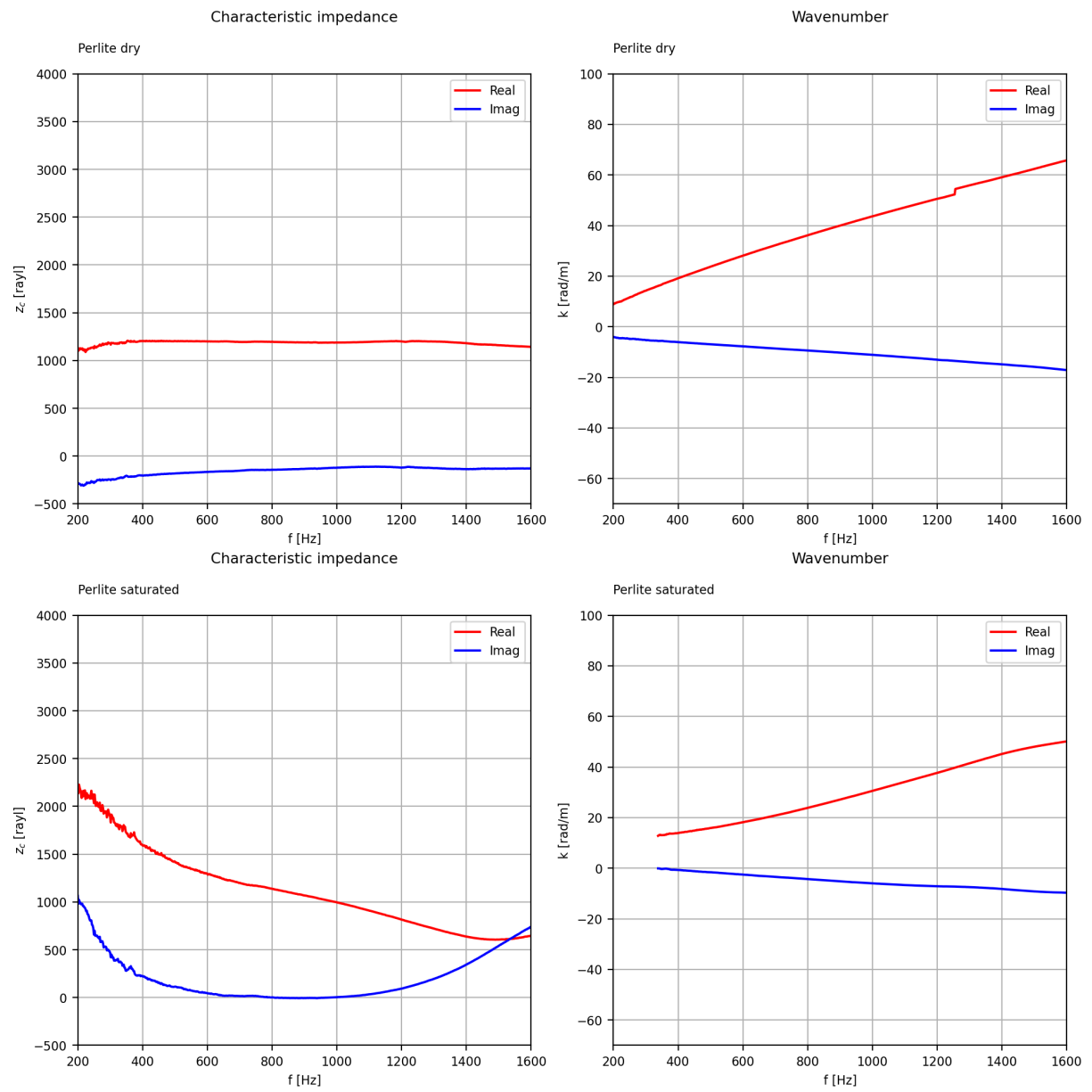**Figure A.49:** Frequency-dependent effective parameters of moss

Figure A.50: Frequency-dependent effective parameters of perlite
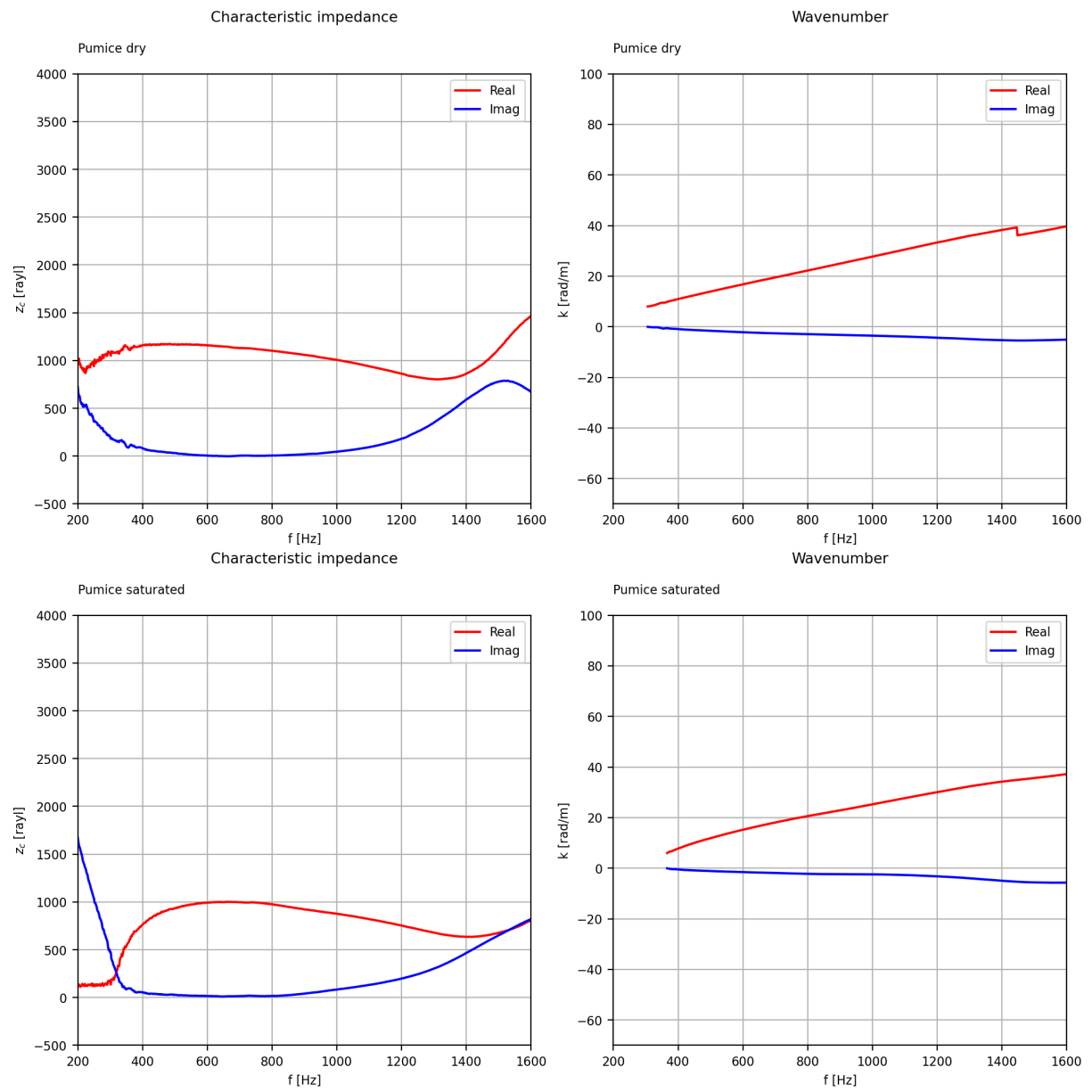
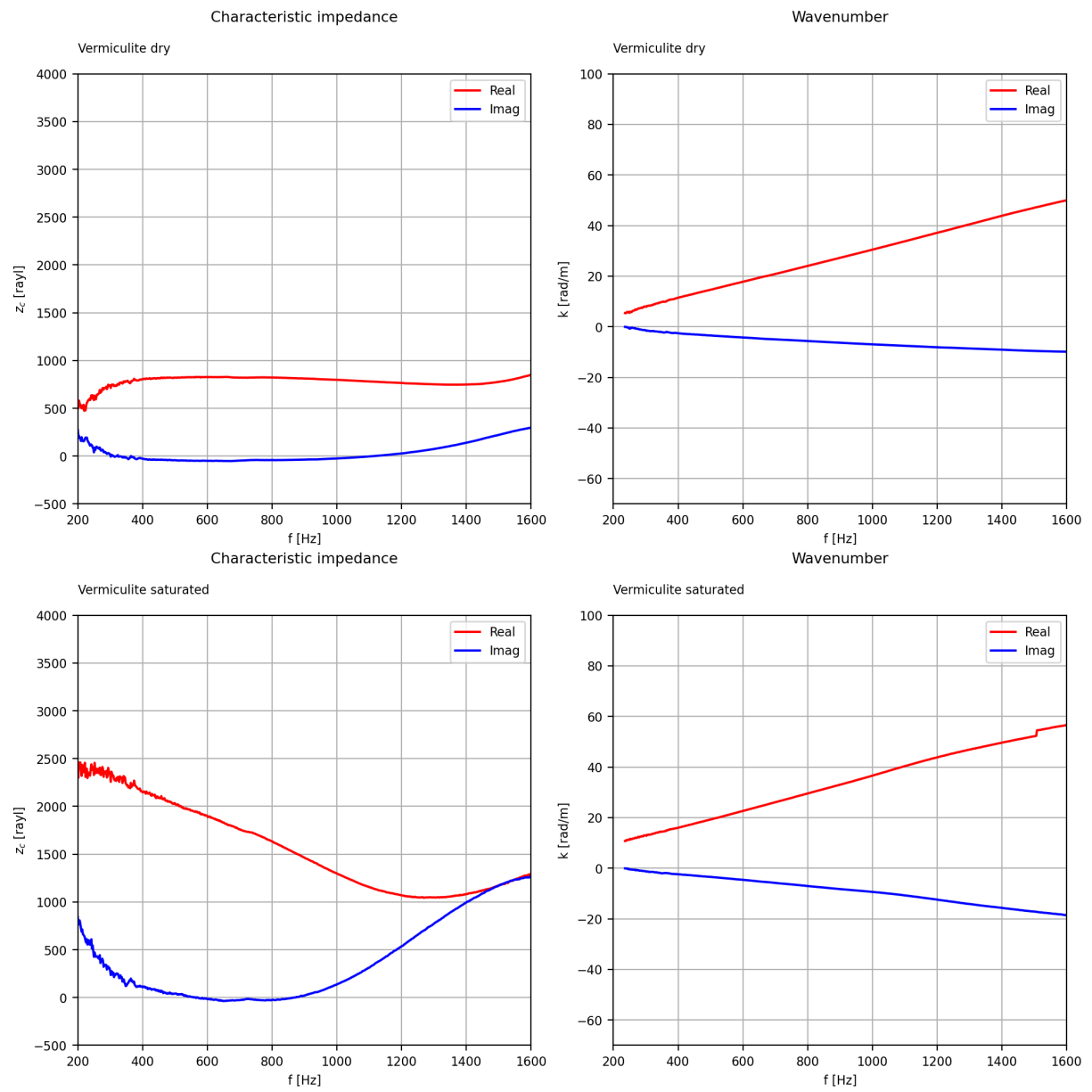**Figure A.51:** Frequency-dependent effective parameters of pumice

Figure A.52: Frequency-dependent effective parameters of vermiculite